



**HAL**  
open science

# Geometry of surfaces :from the estimation of local differential quantities to the robust extraction of global differential features

Marc Pouget

► **To cite this version:**

Marc Pouget. Geometry of surfaces :from the estimation of local differential quantities to the robust extraction of global differential features. Mathematics [math]. Université Nice Sophia Antipolis, 2005. English. NNT: . tel-00102998

**HAL Id: tel-00102998**

**<https://theses.hal.science/tel-00102998>**

Submitted on 3 Oct 2006

**HAL** is a multi-disciplinary open access archive for the deposit and dissemination of scientific research documents, whether they are published or not. The documents may come from teaching and research institutions in France or abroad, or from public or private research centers.

L'archive ouverte pluridisciplinaire **HAL**, est destinée au dépôt et à la diffusion de documents scientifiques de niveau recherche, publiés ou non, émanant des établissements d'enseignement et de recherche français ou étrangers, des laboratoires publics ou privés.

UNIVERSITE DE NICE–SOPHIA ANTIPOLIS – UFR Sciences  
Ecole Doctorale STIC

# THÈSE

pour obtenir le titre de **Docteur en Sciences**

**de l'UNIVERSITE de Nice–Sophia Antipolis**

Discipline : Mathématiques appliquées et applications des mathématiques

présentée et soutenue le 2 Décembre 2005 par

**Marc POUGET**

## **Geometry of surfaces : from the estimation of local differential quantities to the robust extraction of global differential features**

Thèse dirigée par **Frédéric CAZALS** et préparée à l'INRIA Sophia Antipolis, projet GEOMETRICA

### **Rapporteurs :**

**M. Jean-Marie MORVAN, Professeur (Lyon)**  
**M. Konrad POLTHIER, Directeur de recherche (Berlin)**

### **Jury :**

**M. Nicholas AYACHE, Directeur de recherche INRIA, Président du jury**  
**M. Frédéric CAZALS, Chargé de recherche INRIA, Directeur de thèse**  
**M. Peter GIBLIN, Professeur (Liverpool)**  
**M. Jean-Marie MORVAN, Professeur (Lyon)**  
**M. Sylvain PETITJEAN, Chargé de recherche LORIA**  
**M. Konrad POLTHIER, Directeur de recherche (Berlin)**  
**M. Jean-Philippe THIRION, Quantificare, Membre invité**



UNIVERSITE DE NICE–SOPHIA ANTIPOLIS – UFR Sciences  
Ecole Doctorale STIC

# THÈSE

pour obtenir le titre de **Docteur en Sciences**

**de l'UNIVERSITE de Nice–Sophia Antipolis**

Discipline : Mathématiques appliquées et applications des mathématiques

présentée et soutenue le 2 Décembre 2005 par

**Marc POUGET**

## **Géométrie des surfaces : de l'estimation des quantités différentielles locales à l'extraction robuste d'éléments caractéristiques globaux**

Thèse dirigée par **Frédéric CAZALS** et préparée à l'INRIA Sophia Antipolis, projet GEOMETRICA

### **Rapporteurs :**

**M. Jean-Marie MORVAN, Professeur (Lyon)**  
**M. Konrad POLTHIER, Directeur de recherche (Berlin)**

### **Jury :**

**M. Nicholas AYACHE, Directeur de recherche INRIA, Président du jury**  
**M. Frédéric CAZALS, Chargé de recherche INRIA, Directeur de thèse**  
**M. Peter GIBLIN, Professeur (Liverpool)**  
**M. Jean-Marie MORVAN, Professeur (Lyon)**  
**M. Sylvain PETITJEAN, Chargé de recherche LORIA**  
**M. Konrad POLTHIER, Directeur de recherche (Berlin)**  
**M. Jean-Philippe THIRION, Quantificare, Membre invité**



# Remerciements

Je tiens à remercier en premier lieu Frédéric Cazals, mon directeur de thèse, pour sa disponibilité et sa motivation communicative. Je remercie les rapporteurs et les membres du jury d'avoir accepté de relire avec attention ce document.

Un grand merci à tous les membres de l'équipe Géométrica pour leur accueil, leur aide et leur soutien pendant ces trois années passées à Sophia. Merci également à tout ceux avec qui j'ai pu travailler en particulier dans les équipes Coprain, Galaad et Salsa.

Enfin, je remercie Nelly et ma famille qui me soutiennent et me permettent de garder confiance en moi.

"– Vous savez, me dit-il, les Vikings qui avaient sillonné les mers et découvert l'Amérique, c'est un mythe allégorique. Les vrais Vikings sont ceux qui traversent des océans d'angoisse et découvrent des terres nouvelles. Vous êtes un Viking, Rodolphe. Il m'appelait Rodolphe parce qu'il me connaissait déjà.

– Qu'est-ce qu'il y a de vrai à découvrir?

– Les seules réponses possibles ce sont les questions, Maurice. Les vrais Vikings, ce sont les questions. Les réponses, c'est ce que les Vikings se chantent pendant la traversée pour se donner du courage."

*Pseudo, Emile Ajar.*

À la mémoire de Laurent.

"Je ne savais pas encore que l'incompréhension va toujours plus loin que tout le savoir, plus loin que le génie, et que c'est toujours elle qui a le dernier mot. Le regard de mon frère est beaucoup plus près de la vérité qu'Einstein."

*Pseudo*, Romain Gary.





# Contents

<b>1</b>	<b>Thesis overview</b>	<b>13</b>
1.1	Geometry of surfaces . . . . .	13
1.1.1	Surface representations . . . . .	13
1.1.2	Geometry and topology of surfaces : smooth versus discrete . . . . .	14
1.2	Estimation geometric properties : local and global aspects . . . . .	16
1.2.1	Estimation of local differential quantities . . . . .	16
1.2.2	Estimation of global differential properties, the example of ridges . . . . .	17
1.2.3	Applications . . . . .	18
1.3	Outline and contributions . . . . .	19
1.3.1	Differential Topology and Geometry of Smooth Embedded Surfaces: Selected Topics . . . . .	19
1.3.2	Estimating Differential Quantities using Polynomial fitting of Osculating Jets . . . . .	19
1.3.3	Topology driven algorithms for ridge extraction on meshes . . . . .	20
1.3.4	The implicit structure of ridges of a smooth parametric surface . . . . .	20
1.3.5	Topologically certified approximation of umbilics and ridges on polynomial parametric surfaces . . . . .	21
<b>2</b>	<b>Résumé de la thèse</b>	<b>23</b>
2.1	Géométrie des surfaces . . . . .	23
2.1.1	Représentations de surfaces . . . . .	23
2.1.2	Géométrie et topologie des surfaces: lisse versus discret . . . . .	24
2.2	Estimation des propriétés géométriques: aspects locaux et globaux . . . . .	26
2.2.1	Estimation des quantités différentielles locales . . . . .	28
2.2.2	Estimation des propriétés différentielles globales, l'exemple des ridges . . . . .	28
2.2.3	Applications . . . . .	30
2.3	Plan de la thèse et contributions . . . . .	30
2.3.1	Topologie et géométrie différentielles des surfaces lisses plongées: éléments choisis . . . . .	30
2.3.2	Estimation des quantités différentielles par ajustement polynomiale des jets osculateurs . . . . .	30
2.3.3	Algorithmes guidés par la topologie pour l'extraction des ridges sur un maillage . . . . .	31
2.3.4	La structure implicite des ridges d'une surface paramétrée . . . . .	32
2.3.5	Approximation topologique certifiée des ombilics et des ridges d'une surface polynomiale paramétrée . . . . .	32
2.4	Conclusion . . . . .	32
<b>3</b>	<b>Differential Topology and Geometry</b>	<b>37</b>
3.1	Introduction . . . . .	37
3.1.1	Motivations for a geometric and topological analysis . . . . .	37
3.1.2	Chapter overview . . . . .	38
3.2	The Monge form of a surface . . . . .	38
3.2.1	Generic surfaces . . . . .	38
3.2.2	The Monge form of a surface . . . . .	38
3.3	Umbilics and lines of curvature, principal foliations . . . . .	40
3.3.1	Classification of umbilics . . . . .	40
3.3.2	Principal foliations . . . . .	41
3.4	Contacts of the surface with spheres, Ridges . . . . .	42
3.4.1	Distance function and contact function . . . . .	43

3.4.2	Generic contacts between a sphere and a surface . . . . .	43
3.4.3	Contact points away from umbilics . . . . .	44
3.4.4	Contact points at umbilics . . . . .	46
3.4.5	Umbilic classification in the complex plane . . . . .	47
3.4.6	Summary of the global picture of ridges and umbilics on a generic surface . . . . .	48
3.4.7	Illustrations . . . . .	49
3.5	Medial axis, skeleton, ridges . . . . .	50
3.5.1	Medial axis of a smooth surface . . . . .	50
3.5.2	Medial axis and ridges . . . . .	51
3.6	Topological equivalence between embedded surfaces . . . . .	52
3.6.1	Homeomorphy, isotopy, ambient isotopy . . . . .	52
3.6.2	Geometric conditions for isotopy . . . . .	53
3.7	Conclusion . . . . .	54
<b>4</b>	<b>Estimating Differential Quantities</b>	<b>55</b>
4.1	Introduction . . . . .	55
4.1.1	Estimating differential quantities . . . . .	55
4.1.2	Contributions and chapter overview . . . . .	56
4.2	Geometric pre-requisites . . . . .	56
4.2.1	Curves and surfaces, height functions and jets . . . . .	56
4.2.2	Interpolation, approximation and related variations . . . . .	58
4.2.3	Contributions revisited . . . . .	59
4.3	Numerical pre-requisites . . . . .	59
4.3.1	Interpolation . . . . .	59
4.3.2	Least square approximation . . . . .	60
4.3.3	Numerical Issues . . . . .	60
4.4	Surfaces . . . . .	61
4.4.1	Problem addressed . . . . .	61
4.4.2	Polynomial fitting of the height function . . . . .	62
4.4.3	Influence of normal accuracy on higher order estimates . . . . .	64
4.5	Plane Curves . . . . .	65
4.5.1	Problem addressed . . . . .	65
4.5.2	Error bounds for the interpolation . . . . .	65
4.6	Algorithm . . . . .	66
4.6.1	Collecting $N$ neighbors . . . . .	66
4.6.2	Solving the fitting problem . . . . .	66
4.6.3	Retrieving differential quantities . . . . .	67
4.7	Experimental study . . . . .	67
4.7.1	Convergence estimates on a graph . . . . .	67
4.7.2	Illustrations . . . . .	68
4.8	Conclusion . . . . .	74
<b>5</b>	<b>Ridge extraction on meshes</b>	<b>75</b>
5.1	Introduction . . . . .	75
5.1.1	Ridges of a smooth surface . . . . .	75
5.1.2	Previous work . . . . .	76
5.1.3	Contributions and chapter overview . . . . .	77
5.2	Ridge topology and orientation issues . . . . .	77
5.2.1	Problem addressed . . . . .	77
5.2.2	Orientation and crossings . . . . .	78
5.2.3	Gaussian extremality . . . . .	78
5.2.4	Acute rule . . . . .	79
5.3	A generic algorithm . . . . .	79
5.3.1	Compliant triangulations . . . . .	79
5.3.2	Generic algorithm . . . . .	80
5.4	A Heuristic to process a triangle mesh . . . . .	82
5.4.1	Computing the Monge coefficients using polynomial fitting . . . . .	82

5.4.2	Detection of umbilics and patches . . . . .	82
5.4.3	Processing edges outside umbilic patches . . . . .	83
5.4.4	Tagging ridge segments . . . . .	83
5.5	Filtering sharp ridges and crest lines . . . . .	84
5.6	Illustration . . . . .	85
5.7	Conclusion . . . . .	87
<b>6</b>	<b>The implicit structure of ridges</b>	<b>91</b>
6.1	Introduction . . . . .	91
6.1.1	Contributions and chapter overview . . . . .	91
6.1.2	Notations . . . . .	91
6.2	Manipulations involving the Weingarten map of the surface . . . . .	92
6.2.1	Principal curvatures. . . . .	92
6.2.2	Principal directions. . . . .	93
6.3	Implicitly defining ridges . . . . .	93
6.3.1	Problem . . . . .	93
6.3.2	Method outline . . . . .	94
6.3.3	Precisions of vocabulary . . . . .	94
6.3.4	Implicit equation of ridges . . . . .	94
6.3.5	Singular points of $\mathcal{P}$ . . . . .	96
6.4	Implicit system for turning points and ridge type . . . . .	97
6.4.1	Problem . . . . .	97
6.4.2	Method outline . . . . .	97
6.4.3	System for turning points . . . . .	98
6.5	Polynomial surfaces . . . . .	99
6.5.1	About $W$ and the vector fields . . . . .	99
6.5.2	Degrees of expressions . . . . .	100
6.5.3	An example . . . . .	100
6.6	Maple computations . . . . .	100
6.6.1	Principal directions, curvatures and derivatives . . . . .	100
6.6.2	Ridges . . . . .	101
6.6.3	Turning points . . . . .	103
6.7	Conclusion . . . . .	104
<b>7</b>	<b>Topology of ridges on polynomial parametric surfaces</b>	<b>105</b>
7.1	Introduction . . . . .	105
7.1.1	Previous work . . . . .	105
7.1.2	Contributions and chapter overview . . . . .	105
7.2	Notations . . . . .	106
7.3	The implicit structure of ridges, and study points . . . . .	106
7.3.1	Implicit structure of the ridge curve . . . . .	106
7.3.2	Study points and zero dimensional systems . . . . .	107
7.4	Note on methods for approximating implicit plane curves . . . . .	107
7.4.1	Marching cubes and relatives . . . . .	108
7.4.2	Interval analysis . . . . .	108
7.4.3	Restricted Delaunay diagrams . . . . .	108
7.4.4	Using Morse theory . . . . .	108
7.5	Some Algebraic tools for our method . . . . .	109
7.5.1	Zero dimensional systems . . . . .	109
7.5.2	Univariate root isolation . . . . .	109
7.5.3	About square-free polynomials . . . . .	110
7.6	On the difficulty of approximating algebraic curves . . . . .	110
7.7	Certified topological approximation . . . . .	112
7.7.1	Output specification . . . . .	112
7.7.2	Method outline . . . . .	113
7.7.3	Step 1. Isolating study points . . . . .	114
7.7.4	Step 2. Regularization of the study boxes . . . . .	115

7.7.5	Step 3. Computing regular points in study fibers . . . . .	115
7.7.6	Step 4. Adding intermediate rational fibers . . . . .	115
7.7.7	Step 5. Performing connections . . . . .	116
7.8	Certified plot . . . . .	116
7.9	Illustrations . . . . .	117
7.9.1	Certified topology for ridges in generic position . . . . .	117
7.9.2	Certified plot . . . . .	118
7.10	Conclusion . . . . .	122
7.11	Appendix: Algebraic pre-requisites . . . . .	123
7.11.1	Gröbner bases . . . . .	123
7.11.2	Zero-dimensional systems . . . . .	124
7.11.3	The Rational Univariate Representation . . . . .	125
7.11.4	From formal to numerical solutions . . . . .	126
7.11.5	Signs of polynomials at the roots of a system . . . . .	126
<b>8</b>	<b>Conclusion</b>	<b>127</b>

# Chapter 1

## Thesis overview

### 1.1 Geometry of surfaces

Our perception of the physical world around us can be captured by the surfaces of objects. We have intuitive notions of smoothness or curvature of surfaces. In mathematics, surfaces appear as ideal objects which have been studied by classical smooth analysis for centuries. Surfaces are ubiquitous in applications such as scientific computations and simulations, computer aided design, medical imaging, visualization or computer graphics. For instance, in virtual reality, a scene is usually modeled with objects described by their boundary surfaces. In geometric computer processing, surfaces have to be described as discrete objects and many different discretizations are used. These applications require some knowledge of the surfaces processed: their topology, as well as local and global descriptions from differential geometry.

Applied geometry, at the crossroads of mathematics and computer sciences, aims at defining concepts, methods and algorithms for geometrical problems encountered in experimental sciences or engineering. On one hand, mathematics contribute with classical differential topology and geometry, as well as with combinatorial methods on discrete objects. On the other hand, computer science comes with discrete data structures, algorithms and complexity analysis.

With the constant improvements of technology, more and more complex shapes can be processed. Real time simulation and visualization are a great benefit to science and industry. Acquisition systems now generate huge rough data sets that need to be structured and processed. As powerful as computer processing can be, it has its own constraints and limitations : representations are discrete and computations are done with limited numerical precision. Hence the mathematical objects cannot be discretized naively. Interval analysis or computer algebra are some of the new tools able to certify basic computations. At a higher level, there is a real need to develop models of shapes rich enough to define equivalents of the smooth properties, but with the constraints of a computer processing. This implies a better understanding between the smooth and discrete worlds. On one way, how can one transfer informations from a smooth to a discrete object? On the other way, how can one retrieve information of a smooth object from a discrete representation? The final aim is the conception of certified algorithms in the sense that the results come with approximation guarantees.

As surfaces are the object of our study, we first list several ways they are encoded for theoretical analysis as well as for computer processing. Second, we introduce discrete topological and geometrical literature and discuss the relationship between the smooth and discrete worlds.

#### 1.1.1 Surface representations

Smooth surfaces are described either explicitly by a parameterization  $f : \mathbb{R}^2 \longrightarrow \mathbb{R}^3$  or implicitly as a level set  $\{p \in \mathbb{R}^3, F(p) = 0\}$  with  $F : \mathbb{R}^3 \longrightarrow \mathbb{R}$ . The differential quantities are computed straightforwardly in both cases, but each model has its own advantages and drawbacks. For instance, an implicit representation can model arbitrary topology whereas a parametric surface always has the trivial topology of its domain. On the other hand, modeling a surface with multiple parametric patches offers more flexibility.

Discrete representations related to surfaces such as graphs or simplicial complexes are usual objects of combinatorial or simplicial topology. In experimental sciences, discrete data result from measurements. For some specific processing, a smooth object can be discretized. Hence there is a need to develop data structures to encode

and process these discrete data. For discrete surface representation one can roughly distinguish the three following cases.

Piecewise linear surfaces or meshes are given by a set of points and a list of facets. Such representations are widely used in the computer graphics community. These representations are also the basic level for subdivision surfaces used in graphic modeling.

Point clouds acquired by scanning a real object or by sampling any other surface representation can be considered as a representation of a surface. Methods have been developed to render such data, but most of the time a reconstruction is further computed. The two major categories of such algorithms are Delaunay based methods providing a mesh, or implicit fitting methods providing an implicit representation. Another reason to switch to an alternative representation is that point clouds acquired with scanners come with noise and redundant information.

Volumetric data acquired by tomography are frequent in medical imaging. For these data, an implicit representation is computed and sometimes a mesh describing a level set is extracted with a marching cube or related technique.

### 1.1.2 Geometry and topology of surfaces : smooth versus discrete

In the smooth case, differential geometry and topology enable a rich description of surfaces from metric properties (geodesics, area, Gauss curvature) to extrinsic ones (normal field, principal curvatures, principal foliations, ridges). Morse theory and more generally singularity theory also enable the study of functions and vector fields defined on surfaces.

For discrete objects, these classical differential properties are not defined. On the other hand, discrete objects have combinatorial properties that allow algorithmic approaches to be applied. The challenges are to take advantage of this duality smooth/discrete, to study topology and geometry with efficient methods. It is not easy to classify the methods where discrete and differential concepts interfere. We propose in the following three main categories. First, from discrete data a smooth model can be constructed locally or globally, then differential concepts are obviously defined through the model. Second, a theory on discrete objects can be explored with analogs of the smooth concepts aiming at recovering classical smooth results in a purely discrete setting. Third, as a converse to the first point, one can discretize a smooth model for further processing with discrete methods.

#### From discrete data to a smooth model

For a discrete surface given as a mesh or a point cloud, one can fit locally or globally the data with a smooth surface. Differential quantities are then defined through these fits. With a global fitting, the initial discrete data can even be discarded afterwards. Examples in this category are implicit fitting with radial basis functions [LF99], moving least square surfaces given as stationary points of a map [Lev03, AK04] or simply local explicit fitting by bivariate polynomials [Pet01]. For volumetric data on regular 3D grids typical in medical imaging, convolution with Gaussian functions enable to define surfaces as level sets and compute their derivatives straightforwardly [MBF92]

Applications include simple visualization of the surface with ray tracing using surface normals, computation of curvatures or extraction of higher order differential features. For data acquired with a scan of a real object, the fit is a more compact representation avoiding redundancy.

In practice, these methods are applied to data that do not come from a smooth well defined object. As a consequence there is no possible theoretical validation of the results. The evaluation of the method is rather in terms of efficiency of the algorithm. Local fittings are usually faster than global ones requiring large linear systems to be solved. From a theoretical point a view, a method can be evaluated with synthetic data sampled on a smooth surface. In this setting, one can compare the differential quantities of the original surface against those of the fitted surface. The numerical accuracy may be expressed with error bounds or with order of convergence, if a notion of convergent sequence of discretizations is defined. Asymptotic estimates for the normal and the Gauss curvature of a sampled surface for several methods are given in [MW00]. These results are refined for the second fundamental form in [CSM03] or for higher order quantities in [CP05a].

#### Discrete differential topology and geometry

Discrete objects such as meshes have a combinatorial structure and also carry geometric information. The combinatorial structure can be represented by a simplicial or cell complex. The geometrical information given by the vertex positions enables the definition of a metric and even in a non obvious way discrete notions of normals or curvatures. Consequently, regarding topology a mesh has well defined properties and questions on homology, homeomorphism or isotopy can be addressed. Regarding geometry, there is no unique theory but several approaches aiming at defining analogs of the smooth properties.

On a mesh viewed as a simplicial complex, homology theory is well defined. For example, the Betti numbers can be computed and the well known Euler formula holds. Adding some geometric ingredients such as the lengths of edges leads to combinatorial optimization problems. For example, in [CdVL05], an algorithm to compute shortest loops in a given homotopy class is given. In [For98], *combinatorial differential topology* is defined as the application of the standard concepts of differential topology, such as vector fields and their corresponding flows to the study of simplicial complexes. A discrete Morse function is defined as a real valued function on simplices of any dimension with constraints between adjacent simplices. Finding a Morse function with the least number of critical points [LLT03] is rather a combinatorial question. In more geometrical applications, it is not straightforward to define a Morse function from given values on vertices or on faces such that the associated Morse-Smale decomposition respects our geometrical intuition [CCL03].

The domain of *discrete differential geometry* aims at preserving some structure present in the smooth theory while defining concepts in a purely discrete setting. For example, one may define Gaussian curvature in such a way that the Gauss-Bonnet theorem remains valid. Many contributions have been done in this domain.

Straightest geodesics [PS98] are defined so that there is a unique solution to the initial value problem for discrete geodesics. Applications are the parallel transport of vectors and discrete Runge-Kutta integration for vector fields on meshes. Discrete minimal surfaces and harmonic functions [PP93] are obtained through the discretization of the Dirichlet energy. Applications are smoothing or denoising of surfaces with discrete differential operators [DMSB00].

Discrete equivalents of integrability properties of differential equations are presented in [BS05] for surfaces represented by lattices. Surprisingly, this point of view also enables a better understanding of the similarities present in the smooth setting. An application is discrete complex analysis and circle packings.

Geometric measure theory is also a way to unify the smooth and discrete aspects [Fed59, Mor]. Based upon the normal cycle and restricted Delaunay triangulations, an estimate for the second fundamental form of a surface is developed in [CSM03].

A more geometrical than combinatorial approach of Morse theory [Ban67, EHZ01] applies to functions linearly interpolated from values on vertices. A “simulation of differentiability paradigm” guides the construction of a complex with the same structural form as a smooth Morse-Smale decomposition. In applications, to deal with noisy measurements and retain most relevant informations at different levels of details, the notion of persistence is introduced [ELZ00].

The development of a coherent discrete theory independent of the smooth one may be the final achievement and can be evaluated by its effectiveness in applications. It may also be desirable to formalize the links between both settings. When a notion of convergence of a sequence of discrete surfaces to a smooth surface is defined, one naturally expects also convergence of some properties of the sequence to the smooth surface ones. The first problem is to precisely characterize the required topology and conditions on the discrete sequence. Examples of non-convergence are the surface area of a mesh which may not converge to that of the discretized surface (for example the *lampion de Schwarz* in [MT02]), or the angular defect at a vertex of a triangulation which usually does not provide any information on the Gauss curvature of the underlying smooth surface [BCM03]. Conditions for convergence of the surface area of a mesh and its normal vector field versus those of a smooth surface are considered in [MT02, HPW05]. Convergence in a measure sense of the second fundamental form of a surface is proved [CSM03].

#### **Discretization : from a smooth model to a discrete one**

From a smooth model it is sometimes desirable to derive a discrete representation for further processing such as visualization (de Casteljau’s algorithm for Bezier surfaces), simulation with finite element methods (FEM) or registration. Several properties are required for a discretization : it should be a good approximation of the smooth object for some criterion, optimized for memory and easy to compute. The discretization conditions are guided by the properties of the smooth model and the constraints of the post processing.

A basic problem is to mesh a level set of a smooth function with the guaranty that the topology is not modified. Several methods exist for a non singular surface using sampling and restricted Delaunay triangulation [BO03], Morse theory [BCSV04] or interval analysis [PV04]. In the restricted case of a polynomial surface, computer algebra can also handle singular surfaces [MT05a]. In addition, other geometrical properties of the surface can be considered. In [AB99], an error bound is proved on the normal estimate to a smooth surface sampled according to a criterion involving the skeleton. The approximation of the area, the normal field and the unfolding with a triangulation is conducted in [MT02].

Finding a mesh with the minimum number of elements and minimizing a criterion such as Hausdorff distance or  $L^p$  distance is addressed in [D’A91]. To generate a mesh for a FEM, the size and the shape of each element is optimized according to the PDE problem to be solved [She02a].



## 1.2 Estimation geometric properties : local and global aspects

Geometry of smooth or discrete surfaces can be described either by local properties or global ones. Local differential properties are the tangent plane (at the first order), the principal directions and curvatures (at the second order, see Fig. 1.3), or higher order coefficients. In the smooth case, all this information is encoded in the Taylor expansion of the function whose graph locally defines the surface in a given coordinate system. We call a *jet* such a Taylor expansion and Fig. 1.1 illustrates this local approximation. Global differential properties usually refer to loci of points having a prescribed differential property. Examples such loci are lines of curvature, parabolic lines (where the Gauss curvature vanishes Fig. 1.2), ridges (lines of extremal curvature) or the medial axis (centers of maximal spheres included in the complement of the surface in  $\mathbb{R}^3$ ). Hence local information is required to be able to generate global information.

In the present work, we first investigate estimation of local differential properties of any order. Then we study a global differential object on surfaces : the set of lines of extremal curvature, called ridges.

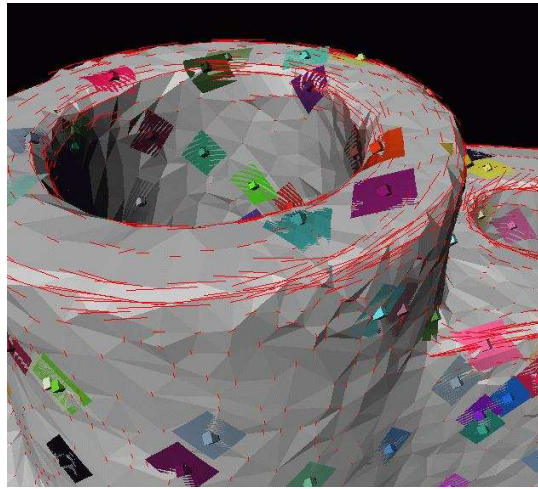


Figure 1.1: The graph of jets around some vertices of a mesh are local approximation of the surface (see chap. 4).



Figure 1.2: The parabolic curves on the Apollo of Belvedere drawn by Felix Klein (from [Koe90]).

### 1.2.1 Estimation of local differential quantities

While local differential quantities are well defined and easy to compute on smooth surfaces, they are not well defined for discrete surfaces. When defining a method to estimate differential quantities on a discrete surface, a way to evaluate the method is to compare the results obtained on some discretizations of a given smooth surface and the actual values for this smooth surface. The sensitivity of the method with respect to the properties and the

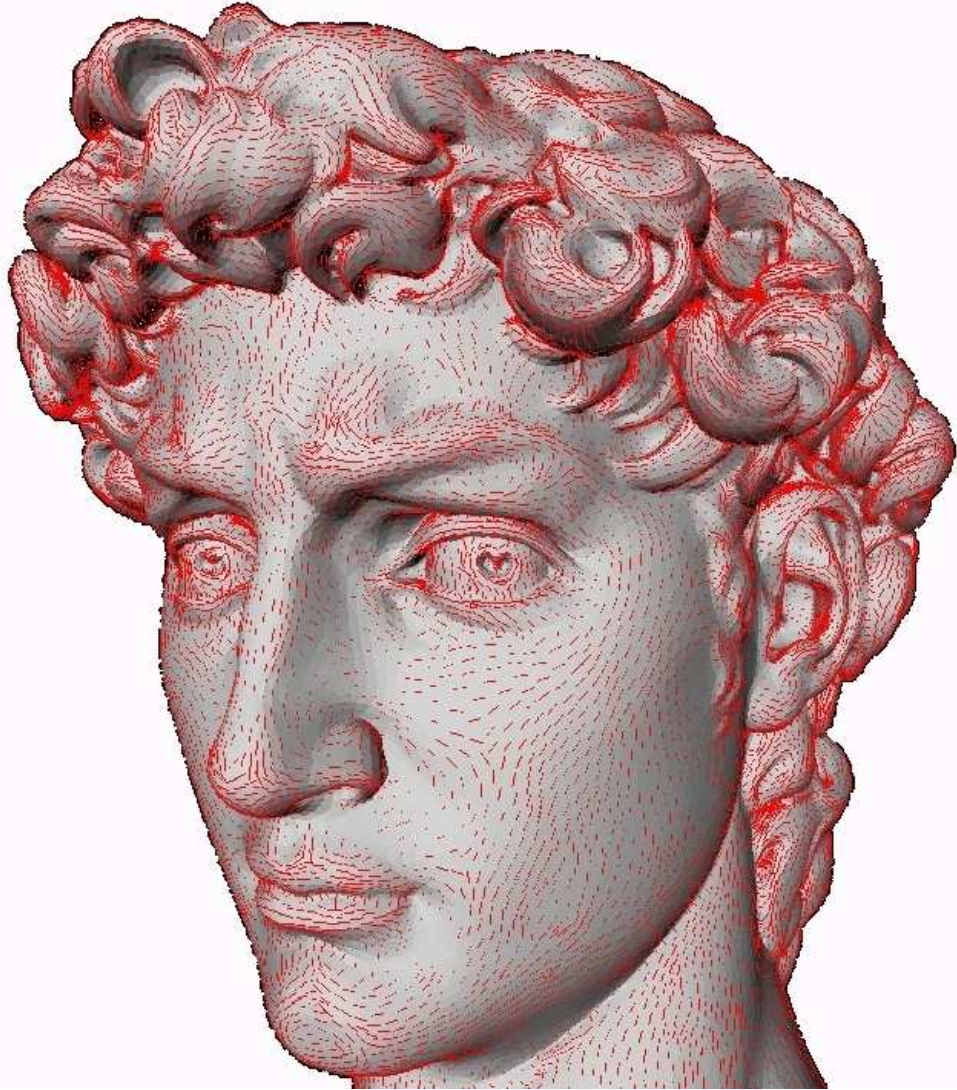


Figure 1.3: Michelangelo's David: principal directions associated with  $k_{max}$  scaled by  $k_{min}$  (see chap. 4).

quality of the discretizations can be analyzed. The convergence of the estimated values to the correct ones can also be specified for some sequence of discretizations. The development of algorithms providing such guarantees has been subject to intense research [Pet01], and recent advances provide guarantees either point-wise (see chapter 4) or in the geometric measure theory sense [CSM03]. It is worth noting that some widely used methods such as the angular defect for the Gauss curvature do not provide convergent estimations as demonstrated in [BCM03].

### 1.2.2 Estimation of global differential properties, the example of ridges

Estimating global differential loci needs reliable point-wise estimates, but in addition, imposes to respect (global) topological constraints. These difficulties are tangible from a practical perspective, and only few algorithms are able to report global differential patterns with some guarantee. For example, reporting the homotopy type of the medial axis has only been addressed quite recently [CL05], but problems involving homeomorphy or isotopy are more demanding.

We focused in our work on lines of *extremal* curvature on a surface, called ridges. In terms of topological guarantees, we wish to report isotopic approximations. To get acquainted with extrema of curvature, first consider the case of plane curves. Points where the curvature is extremal are called vertices, the set of centers of osculating circles is the focal curve and, the centers of circles tangent in two places to the curve is called the symmetry set. These objects are related : the border points of the symmetry set (centers of circles for which the two tangent points coincide) are the singularities of the focal curve, and the circles centered at these points touch the curve

at vertices. For example, Fig. 1.4 shows the focal curve of an ellipse which has four cusps corresponding to the four vertices. For surfaces, one can define a focal surface for each principal curvature and the same properties hold. The equivalent of vertices of a curve are lines on the surface corresponding to contact points with spheres centered on the singularities of the focal surfaces. These lines called ridges of a surface also has an alternative characterization : they consists of the points where one of the principal curvatures has an extremum along its curvature line. Denoting  $k_1$  and  $k_2$  the principal curvatures —we shall always assume that  $k_1 \geq k_2$ , a ridge is called blue (red) if  $k_1$  ( $k_2$ ) has an extremum. Moreover, a ridge is called *elliptic* if it corresponds to a maximum of  $k_1$  or a minimum of  $k_2$ , and is called *hyperbolic* otherwise. Ridges on an ellipsoid are displayed on Fig. 1.5 and 1.6. Fig. 1.7, displaying a subset of the ridges on the David's head, illustrates how these lines enhance the sharpest features of a model. Ridges witness extrema of principal curvatures and their definition involves derivatives of curvatures, whence third order differential quantities. Moreover, the classification of ridges as elliptic or hyperbolic involves fourth order differential quantities, so that the precise definition of ridges requires  $C^4$  differentiable surfaces.

Ridges were mentioned in 1904 by A. Gullstrand, Nobel Prize for Physiology and Medicine, for his work in optics where fourth order differential quantities were necessary to explain the accommodation of the eye lens [Por01]. More recently, singularity theory allowed a precise setting to describe ridges and umbilics as special points on these lines.

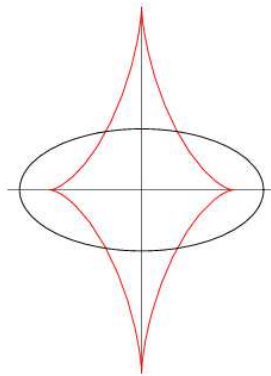


Figure 1.4: Focal curve (red) of an ellipse

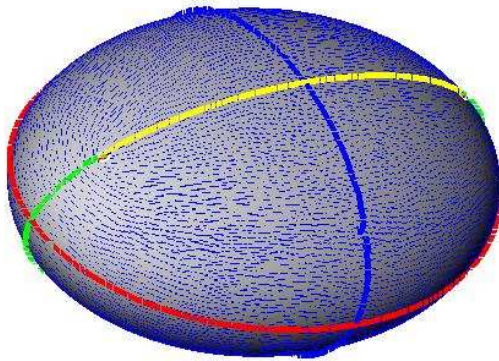


Figure 1.5: Umbilics, ridges, and principal blue foliation on the ellipsoid (see chap. 3).

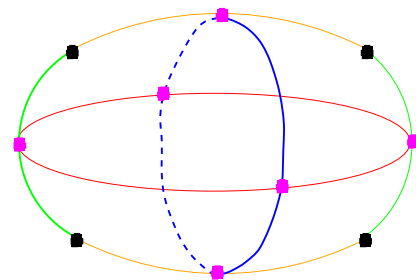


Figure 1.6: Schematic view of the umbilics and the ridges (see chap. 3).

### 1.2.3 Applications

For many applications, estimating first and second order differential quantities, that is the tangent plane and curvature-related quantities, is sufficient. In computer graphics, shading algorithms require the normal vector field. Gauss and mean curvatures are commonly used for surface segmentation, the mean curvature vector can be used for smoothing or denoising of surfaces. However, higher order local properties and global ones are also more and more frequent. The lines of curvature are used for surface remeshing with quad elements [ACSD<sup>+</sup>03]. The topology of vector and tensor fields helps scientific visualization [DH94]. The medial axis or skeleton is used for surface reconstruction [AB99, BC01]. The extraction of ridges is applied to the registration of medical images



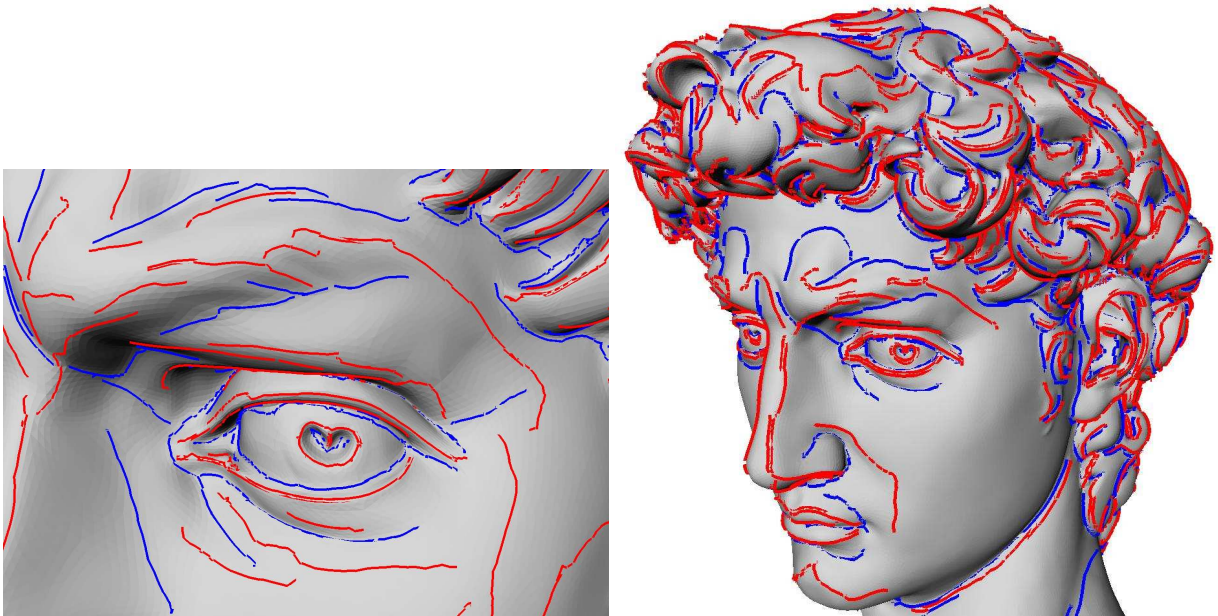


Figure 1.7: Filtered crest lines on a 380k pts model (see chap. 5).

[MLD94, Fid97, PAT00], surface segmentation [SF04], face recognition [HGY<sup>+</sup>99] or compression of polygonal surfaces [WB01].

### 1.3 Outline and contributions

This thesis addresses topics of surface geometry from local estimation to global extraction of differential characteristics. Discrete surfaces given by point clouds or meshes as well as smooth parametric surfaces are considered. We put the stress upon the development of algorithms providing estimations whose accuracies are analyzed. We also provide algorithms for the extraction of global features with guaranteed topology.

Chapter 3 is a survey of smooth surface geometry including all the notions needed in the sequel. Chapter 4 addresses the estimation of local differential geometry on sampled surfaces. The following chapters are devoted to the global approximation of ridges on a generic surface. First, the case of surfaces given by a mesh is analyzed in chapter 5. Second, the implicit structure of ridges is worked out for a general parametric surface in chapter 6. Third, computer algebra methods are developed to compute the topology of ridges for a polynomial parametric surface (chapter 7).

#### 1.3.1 Differential Topology and Geometry of Smooth Embedded Surfaces: Selected Topics

Chapter 3 surveys mathematical notions and results scattered over several sources. As a prerequisite for the development of algorithms for the manipulation of surfaces, we propose a concise overview of core concepts from differential geometry applied to smooth embedded surfaces. Basics of singularity theory and contact between surfaces are introduced to enable the definition of ridges. In particular we recall the classification of umbilics and the geometry of ridges as chapters 5 to 7 are dedicated to algorithms extracting these features. The connection between ridges and the medial axis is analyzed. At last, topological notions of homeomorphy and isotopy are discussed for embedded surfaces. This work has been accepted for publication in the International Journal of Computational Geometry and Applications [CP05b].

#### 1.3.2 Estimating Differential Quantities using Polynomial fitting of Osculating Jets

Chapter 4 addresses the point-wise estimation of differential properties of a smooth surface in 3D from a mesh or a point cloud. The method consists of fitting the local representation of the manifold using a jet with either interpolation or approximation. A jet is a truncated Taylor expansion, and the incentive for using jets is that they

encode all local geometric quantities —such as normal, curvatures, extrema of curvature. The main contribution of this chapter is to recast the problem of estimating differential properties into a problem of classical numerical analysis. Since the proposed method consists of performing polynomial fitting, connections with the questions of interpolation and approximation are discussed. Regarding polynomial interpolation fitting of differential properties for a surface, our results are closely related to [MW00, Lemma 4.1]. In that article, a degree two interpolation is used and analyzed. We generalize this result for arbitrary degrees, with interpolation and approximation. Approximation orders of the method are proved for the estimation of any order differential quantity of the surface. In particular estimations of normal, curvatures and derivatives of curvatures are provided and will be used for the algorithms of the next chapter on ridge extraction. More precisely, given a parameter  $h$  measuring the sampling step, the main result is the following (see theorem 12) :

**Theorem. 1** *A polynomial fitting of degree  $n$  estimates any  $k^{\text{th}}$ -order differential quantity to accuracy  $O(h^{n-k+1})$ . In particular:*

- *the coefficients of the first fundamental form and the unit normal vector are estimated with accuracy  $O(h^n)$ , and so is the angle between the normal and the estimated normal.*
- *the coefficients of the second fundamental form and the shape operator are approximated with accuracy  $O(h^{n-1})$ , and so are the principal curvatures and directions (as long as they are well defined, i.e. away from umbilics).*

An algorithm to process point clouds or meshes is described and the implementation for meshes confirms the expected asymptotic convergence results. A conference version of this work has been published in the proceedings of the Symposium on Geometric Processing 2003 and a journal version in Computer Aided Geometric Design [CP05a].

### 1.3.3 Topology driven algorithms for ridge extraction on meshes

Chapter 5 addresses the problem of ridge extraction for a surface given as a mesh and we make two contributions. First, for a generic smooth surface, the aim is the description of the topology of ridges from a mesh discretizing the surface. Surprisingly, no method developed so far to report ridges from a mesh approximating a smooth surface comes with a careful analysis, which entails that one does not know whether the ridges are reported in a coherent fashion. We present a careful analysis of the orientation issues arising when one wishes to report the ridges associated to the two principal curvatures separately. The analysis highlights the subtle interplay between ridges, umbilics, and curvature lines. Finally, sampling conditions and a certified algorithm are given to report umbilics and the correct topology of ridges on the mesh. The sampling conditions require a dense enough mesh such that (a) umbilics are isolated in patches, and outside these patches (b) a local orientation of the principal directions is possible, and (c) an edge is intersected by a single ridge. As these conditions are not constructive, a heuristic algorithm is proposed. This algorithm is implemented and uses the estimator of differential quantities provided by chapter 4. Figures 1.8 and 1.9 prove the correctness of the algorithm for a Bezier surface whose ridges topology is known (see chapter 7).

Second, for a mesh which is not the approximation of a smooth surface, a filtering method allows the extraction of a subset of these lines. This subset, which has already been considered in medical imaging, can be used for characterization, registration and matching of surfaces. Figure 1.10 illustrates the efficiency of our filtering technique to capture significant features.

### 1.3.4 The implicit structure of ridges of a smooth parametric surface

Chapter 6 provides a theoretical contribution to the analysis of the global structure of ridges. The surface is given by a parameterization and ridges are sought in the parametric domain. As all previous works have to resort to local orientations of the principal directions of curvature to define ridges, they were unable to give a global description of the ridge curve. Using an idea introduced in [Thi96] to turn around these orientation difficulties, and a fine analysis of the Weingarten endomorphism, we derive the implicit equation of ridges. We also derive zero dimensional systems coding the singularities of this curve : one or three ridge umbilics and purple points (see Fig. 1.11). This classification of singularities is compared to the classical one obtained with contact theory in [Por01]. Finally, similar computations with the second derivatives of curvatures lead to the definition of another implicit curve whose intersections with the ridge curve identify the so-called turning points. A turning point is a point on a ridge where the curvature extremum changes from maximum to minimum. In conclusion, we derive both the global structure of the ridge curve and the local classification of its singularities.

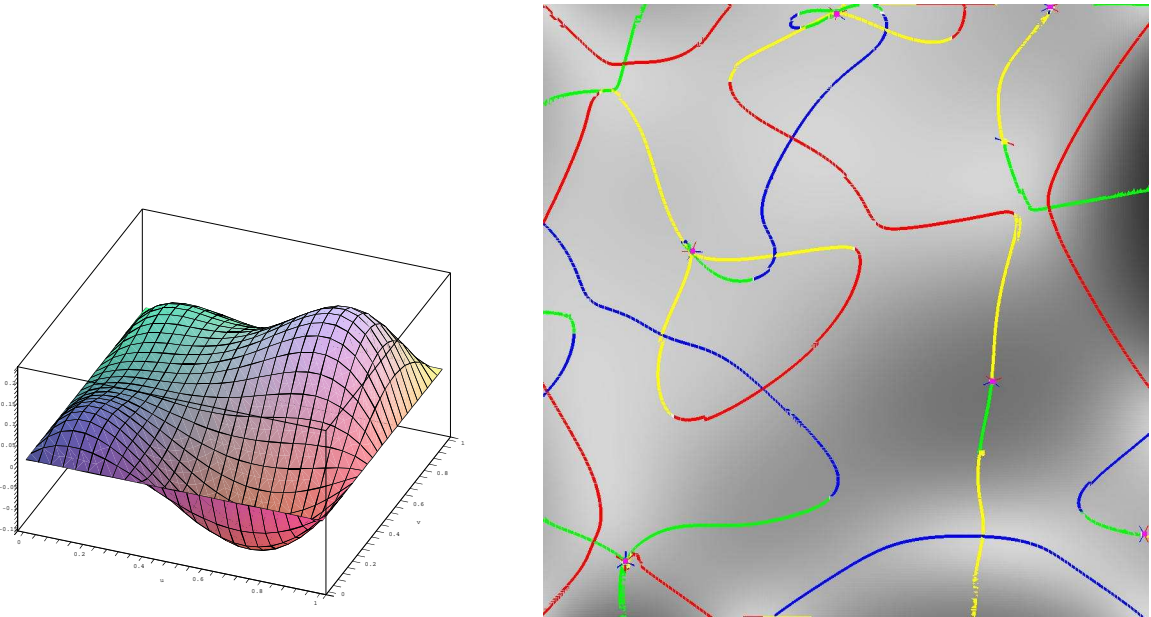


Figure 1.8: A (4,4) degree Bezier surface (left), its ridges and umbilics on a triangulated model (60k points), view from above (right)

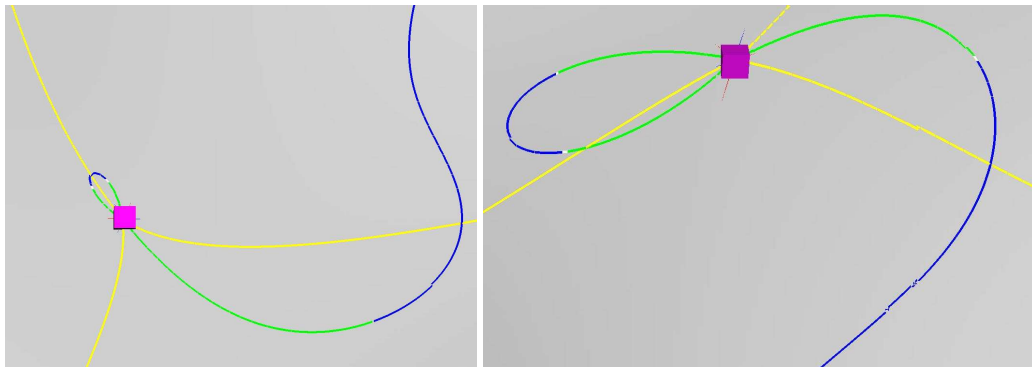


Figure 1.9: Zoom view on two 3-ridge umbilics

### 1.3.5 Topologically certified approximation of umbilics and ridges on polynomial parametric surfaces

Chapter 7 uses results of the previous chapter for the special case of a polynomial parametric surface. Indeed, for a polynomial parametric surface, the above mentioned equations are polynomial as well. An algorithm to compute the topology of the ridge curve is developed. The difficulty is that even for low degree surfaces, the polynomial defining the ridges is of rather high degree, more than 10 times the degree of the surface. Hence classical methods of computational algebra, based on the cylindrical algebraic decomposition [GVN02], are not effective. The contribution is to exploit as far as possible the geometry of the problem to be able to produce an efficient and still certified algorithm. The method uses rational univariate representations of zero dimensional systems to locate the singularities in the parametric domain. One of the main advantage of this method is that it only requires roots isolation of univariate polynomial with *rational* coefficients.

If the complexity of the surface prevents the computation of the topology of ridges, we also provide a plot at any fixed resolution of the ridge curve. Examples are provided to demonstrate the efficiency of the methods.

Results of chapters 6 and 7 have been obtained in collaboration with Jean-Charles Faugère and Fabrice Rouillier of the SALSA project, specialists of computer algebra. This work has been presented at the poster session of the Symposium on Geometric Processing 2005 and at the workshop on Computational Methods for Algebraic Spline Surfaces II.

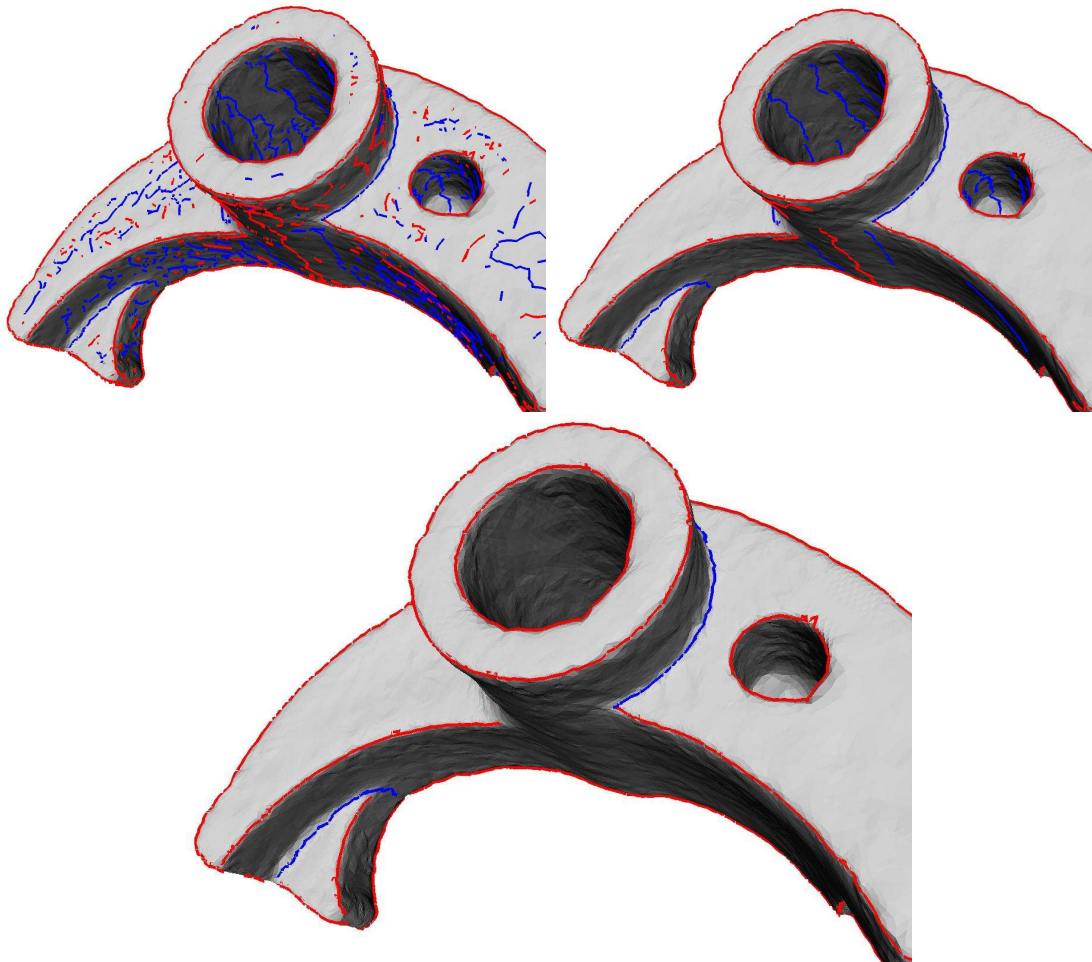


Figure 1.10: Mechanical part (37k pts): (a) All crest lines, (b) crests filtered with the strength (state of the art) and (c) crests filtered with our sharpness criterion. Notice that any point on a flat or cylindrical part lies on two ridges, so that the noise observed on the top two Figs. is unavoidable. It is however easily filtered out with the sharpness on the bottom figure.

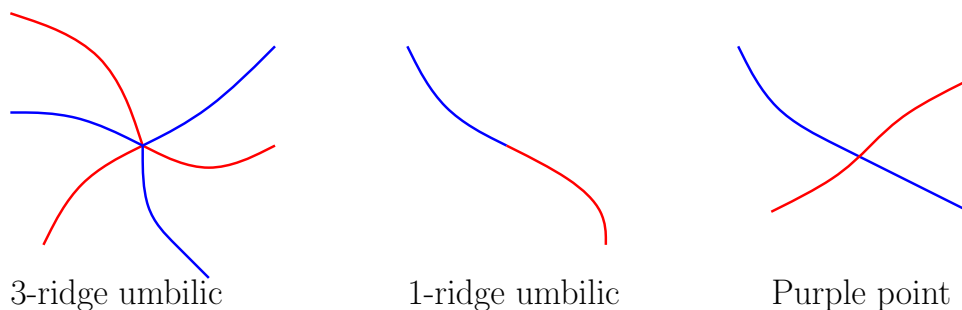


Figure 1.11: Singularities of the ridge curve : red and blue curves distinguish extrema of the two principal curvatures. (left and middle) There are two types of umbilics with one or three curves passing through and changing color at the umbilic. (right) A crossing of a blue and a red ridge is called a purple point.



## Chapter 2

# Résumé de la thèse

### 2.1 Géométrie des surfaces

La perception de notre environnement peut être décrite par les surfaces des objets qui nous entourent. Nous avons des notions intuitives de régularité ou de courbure d'une surface. En mathématiques, les surfaces apparaissent comme des objets idéalisés qui sont étudiés depuis des siècles. Les surfaces sont omniprésentes dans les applications telles que le calcul scientifique et la simulation, la conception assistée par ordinateur, l'imagerie médicale, la visualisation ou l'informatique graphique. Par exemple, en réalité virtuelle, une scène est souvent composée de surfaces décrivant le bord des objets. Lors du traitement de la géométrie par ordinateur, les surfaces doivent être décrites de manière discrète et il existe différentes discrétisations possibles. Les applications nécessitent une connaissance des surfaces traitées: leur topologie, ainsi que des descriptions locales et globales issues de la géométrie différentielle.

La géométrie appliquée, à la croisée des mathématiques et de l'informatique, a pour objectif la définition de concepts, méthodes et algorithmes pour la résolution de problèmes géométriques qui se posent en sciences expérimentales ou en ingénierie. D'une part, les mathématiques apportent la géométrie et la topologie différentielles classiques, ainsi que des méthodes combinatoires sur des objets discrets. D'autre part, l'informatique apporte des structures des données discrètes, des algorithmes ainsi que l'analyse de complexité.

Grâce aux progrès technologiques incessants, des formes de plus en plus complexes peuvent être traitées. La simulation et la visualisation en temps réel sont d'un grand intérêt pour la science et l'industrie. Les systèmes d'acquisition actuels génèrent des ensembles de données brutes gigantesques qui nécessitent d'être structurés et analysés. Aussi puissant que puisse être le traitement informatique, il faut tenir compte de ses propres contraintes et limitations: les représentations sont discrètes et les calculs sont faits avec une précision numérique limitée. Ainsi, les objets mathématiques ne peuvent être discrétisés naïvement. L'analyse par intervalles ou le calcul algébrique formel font partie des nouveaux outils capables de certifier les opérations de base. A un niveau plus élevé, il y a un réel besoin de développer des modèles de formes suffisamment riches pour pouvoir définir des équivalents des propriétés lisses, mais adaptés aux contraintes du traitement informatique. Tout ceci plaide pour une meilleure compréhension des interactions entre les mondes lisse et discret. D'une part, comment transférer de l'information d'un objet lisse à un objet discret? D'autre part, comment analyser les propriétés d'un objet lisse à partir d'une représentation discrète? Le but final est la conception d'algorithmes certifiés, au sens où le résultat vient avec des garanties d'approximation.

Puisque les surfaces sont les objets de notre étude, premièrement, nous listons différentes représentations utilisées pour une analyse théorique ainsi que pour les besoins d'un traitement informatique. Deuxièmement, nous proposons une introduction aux travaux en topologie et géométrie discrète, et discutons les relations entre les mondes lisse et discret.

#### 2.1.1 Représentations de surfaces

Les surfaces lisses sont décrites ou bien explicitement par une paramétrisation  $f : \mathbb{R}^2 \rightarrow \mathbb{R}^3$  ou implicitement par un ensemble de niveau  $\{p \in \mathbb{R}^3, F(p) = 0\}$  avec  $F : \mathbb{R}^3 \rightarrow \mathbb{R}$ . Les quantités différentielles sont calculables de façon directe dans les deux cas, mais chaque modèle possède ses avantages et inconvénients propres. Par exemple, une représentation implicite peut avoir une topologie arbitraire. D'un autre point de vue, modéliser une surface avec plusieurs paramétrisations offre plus de flexibilité.



Des représentations discrètes en lien avec les surfaces, telles que les graphes ou les complexes simpliciaux sont des objets usuels en combinatoire ou topologie. En sciences expérimentales, les données discrètes proviennent de mesure. Pour les besoins d'un traitement particulier, un objet lisse peut être discrétisé. Ainsi, il est nécessaire de développer des structures de données pour coder et traiter ces données discrètes. En ce qui concerne les représentations discrètes de surfaces, nous pouvons grossièrement distinguer les trois cas suivants.

Les surfaces linéaires par morceaux, ou maillages, sont donnés par un ensemble de points et une liste de faces. De telles représentations sont largement utilisées dans la communauté de l'informatique graphique. Ces représentations sont également à la base des surfaces de subdivisions.

Les nuages de points obtenus en scannant un objet réel ou en échantillonnant une autre représentation peuvent être considérés comme des modèles de surfaces. Des méthodes spécifiques ont été développées pour la visualisation de telles données, mais dans la plus part des cas, une reconstruction est calculée. Il existe deux grandes classes d'algorithmes de reconstruction basés sur la triangulation de Delaunay, lesquels calculent un maillage, ou basés sur une approximation implicite lesquels calculent une représentation implicite de la surface. Une autre motivation pour passer à une représentation alternative s'explique par la présence de bruit et la redondance d'information contenue dans les nuages de points acquis avec un scanner.

Les données volumiques acquises par tomographie sont fréquentes en imagerie médicale. Dans ce cas, une représentation implicite est calculée, et parfois un maillage décrivant un ensemble de niveau est extrait avec un algorithme de "marching cube" ou une technique similaire.

### 2.1.2 Géométrie et topologie des surfaces: lisse versus discret

Dans le cas lisse, la géométrie et la topologie différentielles permettent une description riche des surfaces allant des propriétés métriques (géodésiques, aires, courbure de Gauss) aux propriétés extrinsèques (champs des vecteurs normaux, courbures principales, feuilletage principaux, lignes d'extrêmes de courbure). La théorie de Morse et plus généralement la théorie des singularités permettent également l'étude de fonctions ou de champs de vecteurs définis sur les surfaces.

Pour des objets discrets, ces propriétés différentielles discrètes ne sont pas définies. D'un autre côté, les objets discrets ont des propriétés combinatoires qui permettent une approche algorithmique. L'enjeu est donc de tirer partie de cette dualité lisse versus discret. Il n'est pas facile de classer les méthodes où interfèrent des concepts discrets et différentiels. Nous proposons une analyse en distinguant trois catégories principales. Premièrement, à partir de données discrètes, un modèle lisse peut être construit localement ou globalement, ainsi les concepts différentiels sont bien définis sur le modèle et simplement transférés. Deuxièmement, une théorie sur les objets discrets peut être explorée avec des analogues des concepts lisses, cherchant à retrouver des résultats de la théorie lisse tout en restant purement dans le domaine discret. Troisièmement, à l'opposé du premier point, nous pouvons discrétiser un modèle lisse pour le traiter ensuite avec des méthodes discrètes.

#### Des données discrètes à un modèle lisse.

Pour une surface discrète donnée par un maillage ou un nuage de points, nous pouvons ajuster localement ou globalement une surface lisse sur ces données. Les quantités différentielles sont alors définies par l'intermédiaire de ces ajustements. Lors d'un ajustement global, les données discrètes initiales pourront même être abandonnées pour ne garder que l'ajustement. Nous trouvons dans cette catégorie les représentations implicites avec des fonctions à base radiale [LF99], les "moving least square surfaces" définies par l'ensemble des points fixes d'un fonction [Lev03, AK04] ou simplement des ajustements locaux explicites par des polynômes bivariés [Pet01]. Pour des données volumiques sur des grilles régulières 3d, une convolution avec des fonctions gaussiennes permet de définir des surfaces comme ensembles de niveau et de calculer leurs dérivées directement [MBF92].

Parmi les applications, citons la visualisation de surfaces par lancer de rayons utilisant les normales, le calcul des courbures ou l'extraction d'éléments caractéristiques différentiels d'ordre supérieur. Pour des données acquises grâce à un scanner à partir d'un objet réel, l'ajustement est une représentation plus compacte évitant la redondance.

En pratiques, ces méthodes sont appliquées à des données ne provenant pas d'un objet lisse bien défini. Ceci implique qu'il n'y a donc pas de validation possible des résultats obtenus. L'évaluation de ces méthodes se fait plutôt en terme d'efficacité de l'algorithme. Les ajustements locaux sont en général plus rapides que les globaux nécessitant la résolution de systèmes linéaires de grande taille. D'un point de vue théorique, une évaluation est possible en considérant des données artificielles échantillonnées sur une surface lisse connue. Dans ce cas, nous pouvons comparer les quantités différentielles de la surface originale avec celles que nous calculons sur son ajustement. La précision numérique s'exprime alors avec des bornes d'erreurs, ou des ordres de convergence si une notion de convergence d'une suite de discrétisation est définie. Des estimations asymptotiques de la normale et de

la courbure de Gauss sont données dans [MW00]. Ces résultats sont généralisés pour la seconde forme fondamentale dans [CSM03] ou pour des quantités d'ordre supérieur dans [CP05a].

### Topologie et géométrie différentielles discrètes.

Les objets discrets tels que les maillages possèdent une structure combinatoire ainsi des informations géométriques. La structure combinatoire peut être représentée par un complexe simplicial ou cellulaire. L'information géométrique donnée par la position des sommets permet la définition d'une métrique, ainsi que de façon indirecte et non canonique des définitions discrètes de normales et de courbures. Par conséquent, concernant la topologie, un maillage a des propriétés bien définies et les problèmes classiques d'homologie, d'homéomorphie ou d'isotopie sont bien posés. Concernant la géométrie, il n'y a pas de théorie unique mais différentes approches visant à définir des analogues des concepts lisses.

Sur un maillage considéré comme un complexe simplicial, la théorie de l'homologie est bien définie. Par exemple, les nombres de Betti peuvent être calculés et la formule d'Euler qui les relie est valide. En ajoutant un peu de géométrie, comme la longueur des arêtes, des problèmes d'optimisation combinatoire apparaissent. Par exemple, [CdVL05] fournit un algorithme de calcul d'un cycle de longueur minimal dans une classe d'homotopie donnée. Dans [For98], la *topologie différentielle combinatoire* est définie comme l'application des concepts classiques de topologie différentielle, comme les champs de vecteurs et leurs flots, pour l'étude des complexes simpliciaux. Une fonction de Morse discrète est une fonction à valeurs réelles définie sur les simplexes avec des contraintes entre les simplexes adjacents. Trouver une fonction de Morse avec le minimum de points critiques [LLT03] est un problème combinatoire. Pour des applications dans un cadre plus géométrique, il n'est pas aisé de définir une fonction de Morse à partir de valeurs sur les sommets ou les faces de sorte que la décomposition de Morse-Smale associée soit en accord avec notre intuition géométrique [CCL03].

La *géométrie différentielle discrète* a pour but de préserver des structures présentes dans la théorie lisse tout en définissant ses concepts dans un cadre purement discret. Par exemple, la courbure de Gauss sera définie de sorte qu'un équivalent discret du théorème de Gauss-Bonnet soit valide. De nombreuses contributions ont été faites dans ce domaine relativement récent.

Les "straightest geodesics" [PS98] sont définies de sorte que le problème à valeur initiale fixée pour les géodésiques discrètes ait une solution unique. Cette formulation permet la définition du transport parallèle de vecteurs et d'une méthode discrète d'intégration de Runge-Kutta sur des maillages. Les surfaces minimales et les fonctions harmoniques discrètes [PP93] sont obtenues par discrétisation de l'énergie de Dirichlet. Parmi les applications, nous pouvons citer le lissage ou débruitage de surfaces avec des opérateurs différentiels discrets [DMSB00].

Des équivalents discrets des propriétés d'intégrabilité des équations différentielles sont présentés dans [BS05] pour des surfaces représentées par des réseaux. De façon surprenante, ce point de vue permet également une meilleure compréhension des similarités présentes dans le cadre lisse. Une des applications est l'analyse complexe discrète et les pavages circulaires.

La théorie géométrique de la mesure est un moyen d'unifier les aspects lisse et discret [Fed59, Mor]. A partir du cycle normal et de la triangulation de Delaunay restreinte, une estimation de la seconde forme fondamentale d'une surface est développée dans [CSM03].

Une approche plus géométrique que combinatoire de la théorie de Morse [Ban67, EHZ01] s'applique aux fonctions définies par interpolation linéaire de valeurs aux sommets d'un maillage. Un paradigme de "simulation de la différentiabilité" guide la construction d'un complexe ayant les mêmes propriétés structurelles qu'une décomposition de Morse-Smale classique. Dans les applications, pour gérer les imprécisions des mesures et ne retenir que les informations les plus pertinentes à différents niveaux de détails, une notion de persistance est introduite [ELZ00].

Le développement d'une théorie discrète cohérente et indépendante de la théorie lisse peut être considéré comme un objectif final, et l'évaluation peut être faite en considérant son efficacité pour les applications. Il est aussi satisfaisant de vouloir formaliser les liens entre les deux aspects. Lorsqu'une notion de convergence d'une suite de surfaces discrètes vers une surface lisse est définie, la convergence de certaines propriétés de la suite vers celles de la surface lisse peut être espérée. La première difficulté est de caractériser la topologie nécessaire et les conditions sur la suite de discrétisations. Des exemples de non convergence sont l'aire d'un maillage qui peut ne pas converger vers l'aire d'une surface lisse (par exemple le lampion de Schwarz dans [MT02]), ou le défaut angulaire a un sommet d'une triangulation qui ne donne en général pas d'information sur la courbure de Gauss de la surface lisse sous-jacente [BCM03]. Des conditions pour la convergence de l'aire ou du champ de vecteur normal d'un maillage vers ceux d'une surface lisse sont considérées dans [MT02, HPW05]. La convergence au sens de la mesure, c'est à dire par intégration sur un domaine, de la seconde forme fondamentale est étudiée dans [CSM03].

### Discretisation : d'un modèle lisse vers un modèle discret.

A partir d'un modèle lisse il est souhaitable de construire une représentation discrète pour un traitement comme la visualisation (l'algorithme de de Casteljau pour les surfaces de Bézier), la simulation avec des méthodes d'éléments finis ou le recalage. Plusieurs propriétés sont attendues d'une discrétisation, elle doit approcher l'objet lisse pour un critère donné, être optimisée pour la mémoire, et peu coûteuse à calculer. Les conditions de discrétisations sont guidées par les propriétés du modèle lisse et les contraintes du traitement envisagé ultérieurement.

Un problème classique est celui du maillage d'un ensemble de niveau d'une fonction lisse garantissant de ne pas modifier la topologie. Différentes méthodes existent pour une surface non singulière utilisant l'échantillonnage et la triangulation de Delaunay restreinte [BO03], la théorie de Morse [BCSV04] ou l'analyse par intervalles [PV04]. Dans le cas particulier des surfaces polynomiales, les systèmes de calcul algébrique formel permettent aussi de traiter des surfaces singulière [MT05a]. En plus de la topologie, des garanties sur la géométrie peuvent aussi être fournies. Dans [AB99], une borne d'erreur est donnée pour l'estimation de la normale d'une surface lisse faisant intervenir le squelette. L'approximation de l'aire, le champ des normales et du dépliage à partir d'un maillage est analysée dans [MT02].

Construire un maillage avec le nombre minimum d'éléments et minimisant un critère comme la distance de Hausdorff ou une distance  $L^p$  est considéré dans [D'A91]. Pour générer un maillage adapté à une méthode d'éléments finis, la taille et la forme de chaque élément sont optimisées selon l'équation aux dérivées partielles à résoudre [She02a].

## 2.2 Estimation des propriétés géométriques: aspects locaux et globaux

La géométrie des surfaces lisses ou discrètes peut être décrite par des propriétés locales ou globales. Les propriétés différentielles globales sont le plan tangent (au premier ordre), les courbures et directions principales (au second ordre, voir Fig. 2.3), ou des coefficients d'ordres supérieurs. Dans le cas lisse, toutes ces informations sont codées dans le développement de Taylor de la fonction dont le graphe définit localement la surface dans un repère donné. Nous appelons *jet* ce développement de Taylor, la figure 2.1 illustre cette propriété d'approximation locale. Une propriété différentielle globale caractérise le lieu des points ayant une propriété différentielle locale commune. Des exemples de tels lieux sont les lignes de courbure, les lignes paraboliques (où la courbure de Gauss s'annule, Fig. 2.2), les "ridges" (lignes de courbure extrême) ou l'axe médian (centres des sphères maximales incluses dans le complémentaire de la surface dans  $\mathbb{R}^3$ ). Ainsi, la connaissance de l'information locale est un prérequis pour la génération d'informations globales.

Dans cette thèse, nous étudions, dans un premier temps, l'estimation des propriétés locales d'ordre quelconque. Puis, dans un deuxième temps, nous considérons un objet global: l'ensemble des lignes de courbure extrême ou ridges.

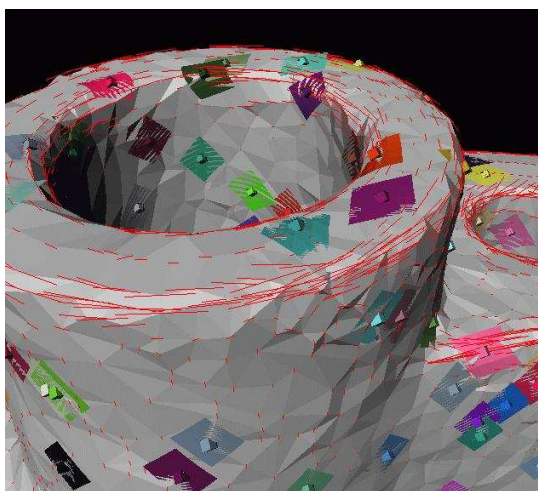


Figure 2.1: Le graphe du jet au voisinage d'un sommet d'un maillage est une approximation locale de la surface (cf. chap. 4).





Figure 2.2: Les lignes paraboliques sur l'Apollon du Belvedere dessinées par Felix Klein (cf. [Koe90]).



Figure 2.3: Le David de Michel-Ange: directions principales associées à la courbure  $k_{max}$  avec une longueur proportionnelle à  $k_{min}$  (cf. chap. 4).

### 2.2.1 Estimation des quantités différentielles locales

Alors que les quantités différentielles locales sont bien définies et simple à calculer sur des surfaces lisses, elles ne sont pas bien définies sur des surfaces discrètes. Pour une méthode donnée d'estimation des quantités différentielles à partir d'une surface discrète, une évaluation est possible en comparant les résultats obtenus sur des discrétisations d'une même surface lisse avec les vraies valeurs calculées sur la surface lisse. La précision de la méthode peut être évaluée selon les propriétés et les qualités des discrétisations. La convergence des valeurs estimées vers les vraies valeurs peut être analysée pour une suite de discrétisations. Le développement d'algorithmes spécifiant des garanties d'approximation est un sujet actif de recherche [Pet01], et des travaux récents fournissent des garanties ou bien locales (cf. chap. 4) ou au sens de la théorie de la mesure [CSM03]. Il est utile de souligner que certaines méthodes communément utilisées comme le défaut angulaire pour estimer la courbure de Gauss ne donnent pas des approximations convergentes [BCM03].

### 2.2.2 Estimation des propriétés différentielles globales, l'exemple des ridges

L'estimation de propriétés différentielles globales nécessite non seulement des estimations locales fiables, mais de plus impose de respecter des contraintes topologiques. Ces difficultés sont tangibles sur le plan pratique, et rares sont les algorithmes capables de calculer des lieux géométriques avec des garanties. Par exemple, le calcul du type d'homotopie de l'axe médian est un problème qui n'a été considéré que récemment [CL05], mais des problèmes concernant l'homéomorphie ou l'isotopie sont encore plus délicats.

Nous nous concentrons dans ce travail sur les lignes de courbure extrême sur une surface. En termes de garanties topologiques, nous souhaitons obtenir des approximations isotopes. Pour se familiariser avec les extrêmes de courbure, considérons dans un premier temps le cas des courbes planes. Les points où la courbure est extrême sont appelés les sommets, l'ensemble des centres des cercles osculateurs forment la courbe focale, et les centres des cercles tangents en deux points à la courbe est appelé l'ensemble de symétrie. Ces différents objets interagissent de la façon suivante: les points du bord de l'ensemble de symétrie (c'est à dire les centres des cercles pour lesquels les deux points de tangence avec la courbe coïncident) sont les singularités de la courbe focale, et les cercles centrés en ces points touchent la courbe en ses sommets. Par exemple, la figure 2.4 montre la courbe focale d'une ellipse qui a quatre points de rebroussement correspondant aux quatre sommets. Dans le cas des surfaces, à chacune des courbures principales est associée une surface focale dont les propriétés sont similaires. L'équivalent des sommets dans le cas d'une courbe sont des lignes sur la surface formées par les points de contacts avec les sphères centrées sur les singularités des surfaces focales. Ces lignes, appelées ridges de la surface, ont aussi la caractérisation suivante: elles sont l'ensemble des points pour lesquels une des courbures principales a un extrême le long de la ligne de courbure correspondante. Notons  $k_1$  et  $k_2$  les courbures principales —avec la convention  $k_1 \geq k_2$ , un ridge est qualifié de bleu (rouge) si  $k_1$  ( $k_2$ ) a un extrême. De plus, un ridge est appelé *elliptique* si il correspond à un maximum de  $k_1$  ou un minimum de  $k_2$ , ou *hyperbolique* dans les autres cas. Les ridges d'un ellipsoïde sont représentés sur la figure 2.5 et 2.6. La figure 2.7, présentant un sous-ensemble des ridges sur la tête du David, illustre la capacité de ces lignes à souligner les parties saillantes du modèle. Les ridges révèlent les extrêmes des courbures principales et leur définition implique les dérivées des courbures, par conséquent ce sont des quantités différentielles de troisième ordre. De plus, la classification des ridges en type elliptique et hyperbolique nécessite des quantités de quatrième ordre, donc la définition précise des ridges nécessite des surfaces de classe  $C^4$ .

Les ridges sont mentionnés en 1904 par A. Gullstrand, prix Nobel de physiologie et médecine, dans ses travaux en optique où des quantités différentielles d'ordre quatre étaient indispensables pour expliquer l'accommodation du cristallin [Por01]. Plus récemment, la théorie des singularités a permis de dégager un cadre rigoureux pour décrire les ridges et les ombilics.

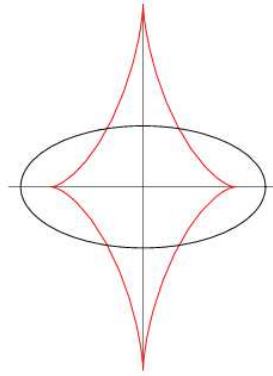


Figure 2.4: La courbe focale (en rouge) d'une ellipse

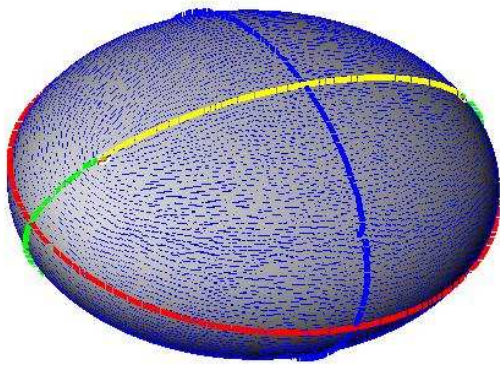


Figure 2.5: Umbilics, ridges, et feuilletage principal bleu sur un ellipsoïde (cf. chap. 3).

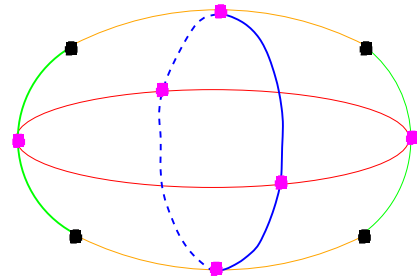


Figure 2.6: Vue schématique des ombilics et des ridges sur un ellipsoïde (cf. chap. 3).

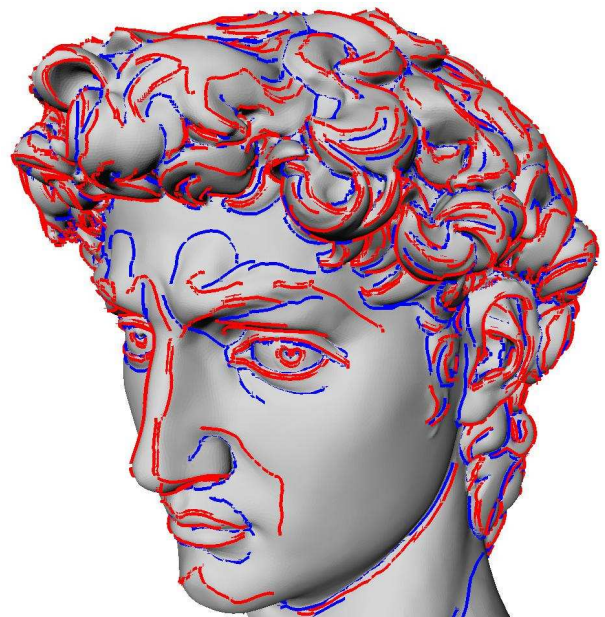
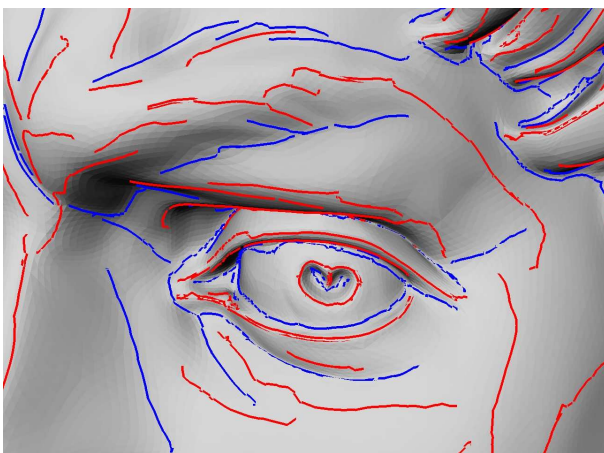


Figure 2.7: Lignes de crête filtrées sur un modèle de 380k pts (cf. chap. 5).



### 2.2.3 Applications

Pour de nombreuses applications, estimer les quantités différentielles de premier et deuxième ordre, c'est à dire la normale et les courbures, est suffisant. En informatique graphique, le champ des normales est utilisé pour les algorithmes d'éclairage. Les courbures de Gauss et moyenne sont fréquentes en segmentation, le vecteur courbure moyenne est utilisé en lissage et débruitage du surfaces. Néanmoins, des quantités d'ordre supérieur, locales ou globales apparaissent de plus en plus fréquemment. Les lignes de courbures servent pour le remaillage avec des quadrilatères [ACSD<sup>+</sup>03]. La topologie des champs de vecteurs et directions aident la visualisation scientifique [DH94]. L'axe médian ou squelette est utilisé en reconstruction de surfaces [AB99, BC01]. L'extraction des ridges s'applique au recalage d'images médicales [MLD94, Fid97, PAT00], à la segmentation [SF04], à la reconnaissance de visages [HGY<sup>+</sup>99] ou encore à la compression de surfaces polygonales [WB01].

## 2.3 Plan de la thèse et contributions

Cette thèse aborde des thèmes de géométrie des surfaces, de l'estimation locale à l'extraction de caractéristiques globales. Des surfaces données par des maillages et des nuages de points aussi bien que des surfaces lisses paramétrées sont étudiées. Nous nous concentrons sur le développement d'algorithmes générant des estimations dont la précision est analysée. Nous proposons également des algorithmes pour l'extraction de caractéristiques globales avec des garanties topologiques.

Le chapitre 3 présente un panorama de la géométrie des surfaces lisses, couvrant toutes les notions nécessaires dans la suite. Le chapitre 4 aborde l'estimation de la géométrie différentielle locale à partir de surfaces échantillonnées. Les chapitres suivants sont consacrés à l'approximation globale des ridges d'une surface générique. Premièrement, le cas d'une surface donnée par un maillage est étudié dans le chapitre 5. Deuxièmement, la structure implicite des ridges est développée pour une surface paramétrée dans le chapitre 6. Troisièmement, des méthodes de calcul algébrique formel sont adaptées pour le calcul de la topologie des ridges d'une surface polynomiale paramétrée (chap. 7).

### 2.3.1 Topologie et géométrie différentielles des surfaces lisses plongées: éléments choisis

Le chapitre 3 rassemble des notions mathématiques et des résultats dispersés dans la littérature. Comme prérequis au développement d'algorithmes pour la traitement des surfaces, nous proposons un panorama succinct de concepts de géométrie différentielle appliqués aux surfaces plongées. Une introduction à la théorie des singularités et du contact permet la définition des ridges. En particulier, nous rappelons la classification des ombilics et la géométrie des ridges puisque les chapitres 5 à 7 sont consacrés à l'extraction de ces caractéristiques. La relation entre les ridges et l'axe médian est analysée. Enfin, les notions d'homéomorphie et d'isotopie sont discutées. Ce travail a donné lieu à une publication dans le journal "International Journal of Computational Geometry and Applications" [CP05b].

### 2.3.2 Estimation des quantités différentielles par ajustement polynomiale des jets osculateurs

Le chapitre 4 aborde l'estimation locale des propriétés différentielles d'une surface en 3D à partir d'un maillage ou d'un nuage de points. La méthode consiste à ajuster le jet de la représentation locale de la variété en utilisant l'interpolation ou l'approximation. Un jet est une série de Taylor tronquée, la motivation pour utiliser les jets réside dans leur propriété de coder toutes les quantités géométriques locales —comme la normale, les courbures ou les extrêmes de courbure. La contribution principale de ce chapitre est de replacer le problème d'estimation des propriétés différentielles dans le cadre de l'analyse numérique classique. La méthode proposée utilisant l'ajustement polynomial, les relations avec les questions d'interpolation et d'approximation sont discutées. En ce qui concerne l'interpolation, nos résultats sont reliés à [MW00, Lemma 4.1]. Dans cet article, une interpolation de degré deux est utilisée et analysée. Nous généralisons ce résultat pour un degré arbitraire, ainsi que pour l'interpolation aussi bien que pour l'approximation. En particulier, des estimations des normales, des courbures et des dérivées des courbures sont données et seront utilisées dans le chapitre suivant sur l'extraction des ridges. Plus précisément, étant donné un paramètre  $h$  mesurant le pas d'échantillonnage, le résultat principal est le suivant (voir le théorème 12) :

**Theorem. 2** *Un ajustement polynomial de degré  $n$  approche une quantité différentielle de  $k^{\text{ième}}$ -ordre avec une précision en  $O(h^{n-k+1})$ . En particulier:*

- Les coefficients de la première forme fondamentale et du vecteur normal unitaire sont estimés avec une précision en  $O(h^n)$ , et il en est de même de l'angle entre la normale et la normale estimée.
- Les coefficients de la seconde forme fondamentale et de l'opérateur de Weingarten sont approchés en  $O(h^{n-1})$ , et il en est de même des courbures et directions principales (en supposant qu'elles soient bien définies, c'est à dire loin des ombilics).

Un algorithme pour traiter des nuages de points ou des maillages est décrit, et l'implémentation pour le cas des maillages confirme les résultats de convergence asymptotique attendus. Ce travail a donné lieu à une publication à la conférence "Symposium on Geometric Processing 2003" et dans le journal "Computer Aided Geometric Design" [CP05a].

### 2.3.3 Algorithmes guidés par la topologie pour l'extraction des ridges sur un maillage

Le chapitre 5 aborde le problème de l'extraction des ridges sur une surface donnée par un maillage, et nous apportons deux contributions. Premièrement, pour une surface lisse générique, le but est de décrire la topologie des ridges à partir d'un maillage discrétisant la surface. De façon surprenante, aucune des méthodes développées jusqu'à présent pour l'extraction des ridges à partir d'un maillage approchant une surface lisse ne fournit une analyse précise, ceci implique qu'il n'est pas possible de savoir si les ridges extraits ont une structure globale cohérente. Nous présentons une étude détaillée des problèmes d'orientation intervenant lors de l'extraction séparée des ridges associés à chacune des courbures principales. Cette analyse révèle les relations entre ridges, ombilics et lignes de courbure. Finalement, des conditions d'échantillonnage et un algorithme certifié sont donnés pour l'extraction des ridges sur le maillage en respectant la topologie. Les conditions d'échantillonnage mettent en évidence la nécessité de disposer d'un maillage suffisamment dense pour que (a) les ombilics soient isolés dans des régions, et pour qu'en dehors de ces régions, (b) l'orientation des direction principales soit possible localement, et (c) une arête soit intersectée par un seul ridge. Ces conditions n'étant pas constructives, un algorithme heuristique est aussi proposé. Cet algorithme est implémenté et utilise l'estimateur de quantités différentiables exposé au chapitre 4. Les figures 2.8 et 2.9 prouvent que l'algorithme calcule correctement la topologie des ridges pour une surface de Bézier dont les ridges sont connus (cf. chapitre 7).

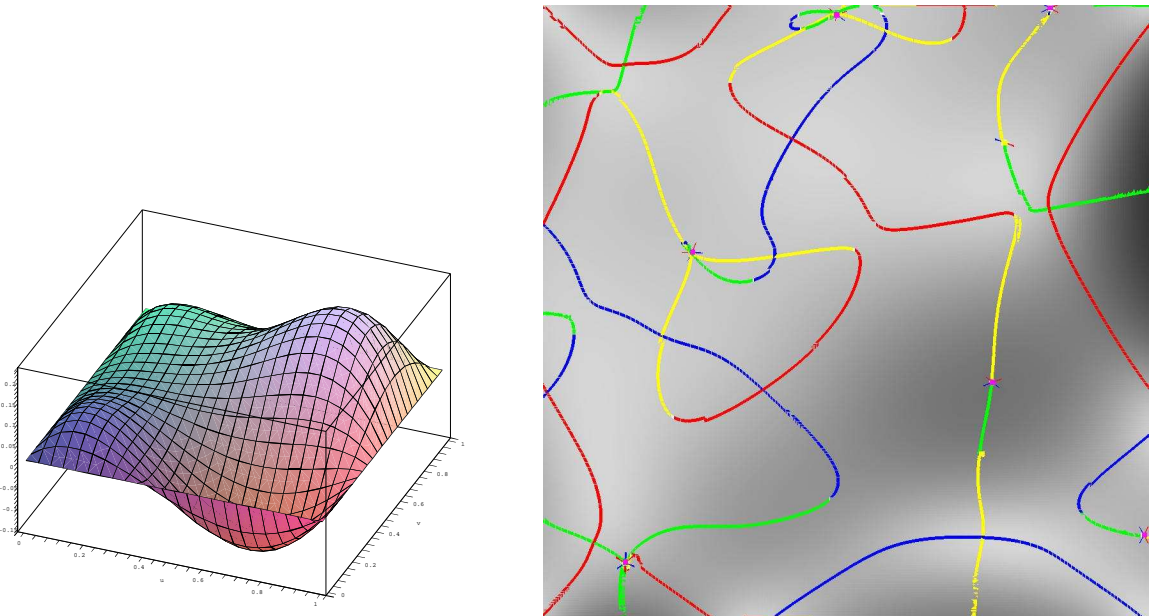


Figure 2.8: Une surface de Bézier de bi-degré (4,4) (gauche), ses ridges et ombilics sur une model triangulé (60k points), vue de dessus (droite)

Deuxièmement, pour un maillage qui n'est pas l'approximation d'une surface lisse, une méthode de filtrage permet l'extraction d'un sous ensemble de lignes. Ce sous ensemble, qui a déjà appliqué dans le domaine des images médicales, peut être utilisé pour le recalage et la comparaison de surfaces. La figure 2.10 illustre l'efficacité de notre technique de filtrage pour la mise en évidence de caractéristiques saillantes d'un model.



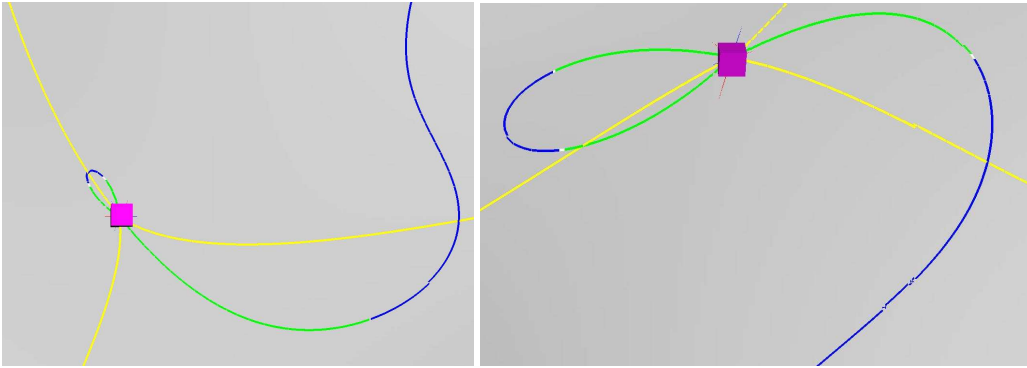


Figure 2.9: Gros plans sur deux ombilics 3-ridge de la figure 2.8

### 2.3.4 La structure implicite des ridges d’une surface paramétrée

Le chapitre 6 apporte une contribution théorique à l’analyse de la structure globale des ridges. La surface est donnée par une paramétrisation et les ridges sont calculés dans le domaine paramétrique. Devant faire appel à l’orientation locale des directions principales de courbures, les approches antérieures ne pouvaient pas définir une description globale des ridges. Reprenant une idée introduite dans [Thi96] pour contourner ces difficultés d’orientation, et une analyse précise de l’endomorphisme de Weingarten, nous déduisons l’équation implicite des ridges. Nous présentons également des systèmes d’équations codant les singularités de la courbe: ombilics un ou trois ridges et points *purples* (cf. Fig. 2.11). Cette classification est comparée à celle obtenue grâce à la théorie du contact dans [Por01]. Enfin, des calculs similaires avec les dérivées secondes des courbures conduisent à la définition d’une autre courbe implicite, dont l’intersection avec celle des ridges permet l’identification des points “turning”. Un point “turning” est un point sur un ridge où l’extrême de courbure passe de maximum à minimum. En conclusion, nous proposons une description globale des ridges ainsi qu’une analyse locale de ses singularités.

### 2.3.5 Approximation topologique certifiée des ombilics et des ridges d’une surface polynomiale paramétrée

Le chapitre 7 exploite les résultats du chapitre précédent dans le cas particulier des surfaces polynomiales paramétrées. En effet, pour une surface polynomiale, les équations précédentes sont également polynomiales. Nous développons un algorithme pour le calcul de la topologie de la courbe des ridges. La difficulté provient de la complexité de cette courbe même pour des surfaces relativement simples: le degré de la courbe est plus de dix fois plus élevé que celui de la surface. Pour une telle courbe, les méthodes classiques, basées sur la décomposition cylindrique algébrique [GVN02], ne sont pas assez performantes. Notre contribution est d’exploiter le plus possible la géométrie du problème pour proposer un algorithme performant et certifié. La méthode repose sur la représentation univariée rationnelle des systèmes polynômes de dimension zéro afin de localiser les singularités des ridges dans le domaine paramétrique. Un des principaux avantages de la méthode provient du fait qu’elle ne nécessite que l’isolation des racines de polynômes univariés à coefficients *rationnels*.

Si néanmoins, la complexité de la surface ne permet pas le calcul de la topologie des ridges, nous fournissons également une méthode de tracé à résolution fixée. L’efficacité de ces méthodes est démontrée sur des exemples.

Les résultats des chapitres 6 et 7 ont été obtenus en collaboration avec Jean-Charles Faugère et Fabrice Rouillier du projet SALSA, spécialistes de calcul algébrique formel. Ce travail a été présenté à la session de posters du “Symposium on Geometric Processing 2005” et au “workshop on Computational Methods for Algebraic Spline Surfaces II” dont la publication des actes est en cours.

## 2.4 Conclusion

Dans cette thèse, deux aspects de la géométrie des surfaces ont été abordés: l’estimation locale des propriétés différentielles, et le calcul global de la structure des ridges d’une surface lisse.

Concernant l’estimation des quantités différentielles, notre méthode utilise l’ajustement polynomial et s’applique aux maillages et aux nuages de points. Les ordres d’approximation sont les meilleurs prouvés à ce jour, et la méthode est testée avec des données échantillonnées sur des surfaces lisses. Bien que notre méthode repose sur le

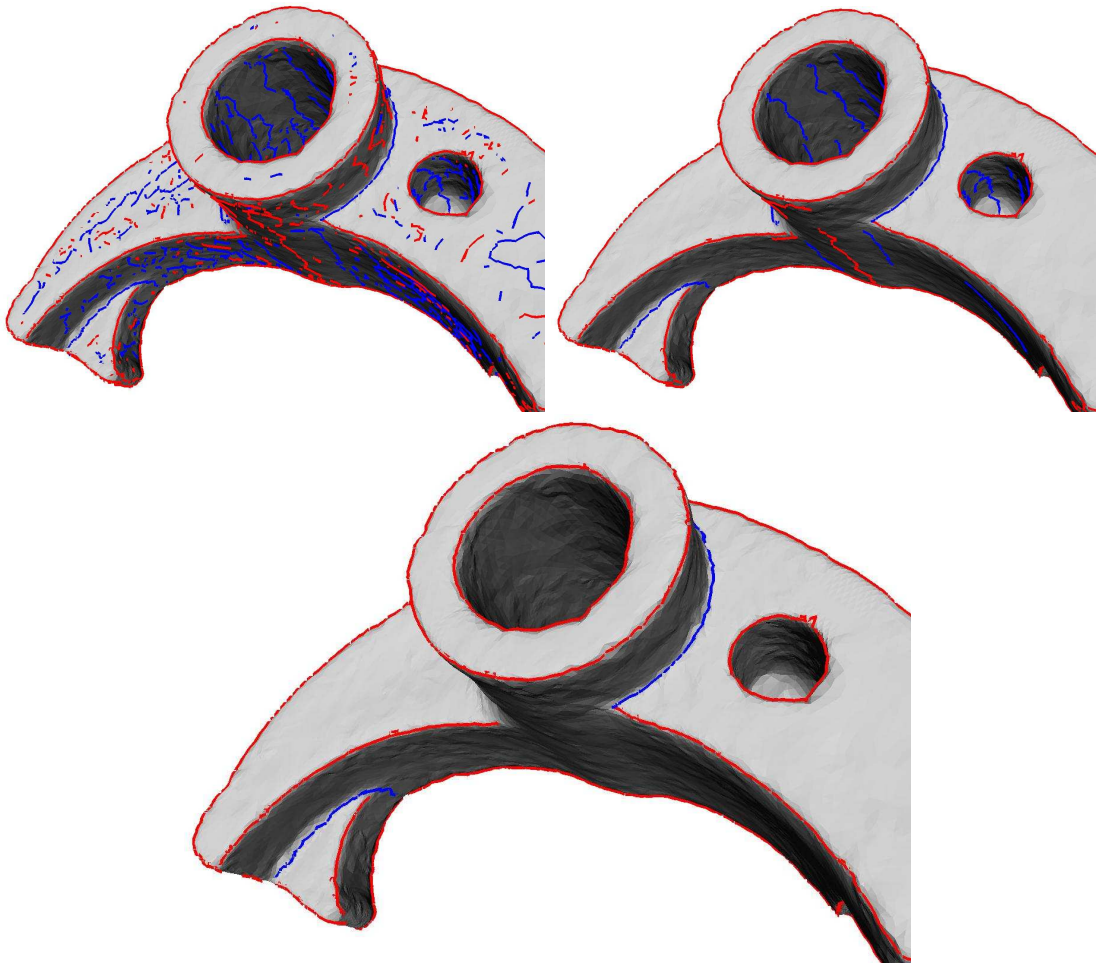


Figure 2.10: Pièce mécanique (37k pts): (a) toutes les lignes de crêtes, (b) lignes de crêtes filtrées par leur “strength” (état de l’art) et (c) lignes de crêtes filtrées par notre critère “sharpness”. Remarquez que les points dans les parties plates ou cylindriques appartiennent à deux ridges, ainsi le bruit présent sur les deux figures du haut est inévitable. Il est néanmoins aisé d’éliminer ce bruit avec le filtrage que nous proposons (figure du bas).

cadre lisse, et donc ne définit pas de concept discret, elle permet l’estimation de quantités différentielles d’ordre arbitraire. Lorsque l’approximation est conduite avec un schéma d’approximation, nous avons expérimentalement observé un comportement robuste face au bruit.

Une approche alternative au problème d’estimation à partir de données discrètes est proposée par la géométrie différentielle discrète. L’idée consiste à définir des quantités différentielles directement sur l’objet lisse et de développer une théorie discrète par analogie avec la théorie lisse. Le problème de convergence des quantités discrètes pour une suite de discrétisations peut alors être étudié. Des résultats ont été obtenus pour le champ des normales, l’aire, les géodésiques [MT02, HPW05], les courbures de Gauss ou moyenne à l’aide d’une formulation variationnelle [PP93], le tenseur de courbure dans le cadre de la théorie de la mesure [CSM03]. Toutes ces contributions s’appliquent à des maillages, et les nuages de points ne sont pas traités. Les théorèmes de convergence ne sont disponibles que pour des quantités différentielles du premier ou du second ordre.

Alors que l’intérêt pour les nuages de points s’accroît, le défi serait de comprendre dans quelle mesure la géométrie différentielle et l’analyse statistique peuvent s’appliquer. L’irrégularité de la densité d’échantillonnage, l’anisotropie et le bruit doivent être pris en compte. Par exemple, l’influence du voisinage d’un point qu’il faut considérer pour faire une estimation n’est pas bien comprise [LP05]. Une analyse de l’estimation de la normale à une surface à partir d’un nuage de points bruité est proposée dans [MN03]. Des méthodes de votes propagent l’information dans des voisinages locaux pour déterminer la pertinence de chaque information individuelle. Le vote pour la normale et le tenseur de courbure permet d’identifier le bruit et les discontinuités, et donc rend possible le traitement de surfaces lisses par morceaux [TM02].

Concernant le calcul de structures globales sur une surface, nous avons traité l’approximation topologique et

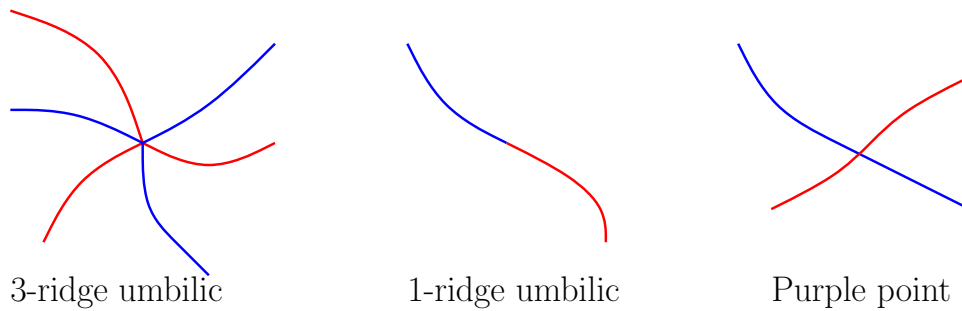


Figure 2.11: Singularités de la courbe des ridges: les courbes rouges et bleues différencient les extrêmes des deux courbures principales. (à gauche et au milieu) Il y a deux types d’ombilics traversés par une ou trois branches de ridges, chacune changeant de couleur à l’ombilic. (à droite) Le croisement d’un ridge bleu et d’un ridge rouge est appelé point *purple*.

géométrique des ridges. Deux types de données ont été considérés: un maillage discrétisant une surface lisse et une surface paramétrée.

Premièrement, pour un maillage discrétisant une surface lisse, nous présentons le premier algorithme certifié pour l’extraction des ridges d’une surface lisse avec des garanties sur la topologie. L’algorithme exploite la géométrie des ridges et des ombilics d’une surface générique, et dissocie le traitement au voisinage des ombilics du reste de la surface. L’algorithme est générique au sens où le calcul des quantités différentielles et l’isolation des ombilics sont confiés à des routines qui peuvent dépendre du type de surface discrétisé par le maillage. Pour des maillages approchant des surfaces lisses —sans pour autant avoir accès à aucune information analytique, nous fournissons des heuristiques. Pour des surfaces discrétisant des surfaces lisses dont les ridges sont connus, des exemples prouvent que notre algorithme heuristique retrouve la topologie des ridges et des ombilics. Pour des maillages reconstruits à partir de données scannées, des exemples montrent que notre algorithme retrouve des sous-ensembles des ridges comparables aux autres méthodes de l’état de l’art (qui utilisent des ajustements globaux), tout en améliorant les temps de calculs d’au moins un ordre de grandeur et en fournissant une méthode de filtrage plus performante.

Deuxièmement, pour une surface paramétrée, nous explicitons l’équation implicite de la courbe singulière codant les ridges dans le domaine paramétrique. Alors que l’analyse mathématique classique des ridges était seulement locale, nous avons maintenant une description globale. Nous analysons ses singularités et fournissons des méthodes pour les identifier. Cette formulation du problème évite les difficultés d’orientation locale des directions principales de courbure. Elle permet donc une approche globale de l’extraction des ridges d’une surface paramétrée. Finalement, ces résultats sur la structure des ridges sont utilisés dans le cas particulier des surfaces paramétrées polynomiales. Puisque les outils classiques de calcul algébrique formel ne permettent pas de traiter nos exemples de grande complexité, nous avons tiré partie de l’information géométrique fournie par l’analyse de la structure. Nous développons un algorithme spécifique basé sur les représentations univariées rationnelles des systèmes polynômiaux de dimension zéro, et sur l’isolation des racines de polynômes univariés à coefficients rationnels. Cet algorithme est le premier à calculer une approximation topologique certifiée de ridges. Une fois la topologie obtenue, une approximation géométrique plus précise peut facilement être déduite. Nous proposons également un autre algorithme qui calcule un tracé certifié à résolution fixée: les calculs sont moins coûteux, mais la topologie n’est plus garantie. Les résultats pour une surface paramétrée sont directement applicables aux surfaces de Bézier incontournable en CAO. Il est à noter que la méthode développée pour le calcul de la topologie des ridges peut être généralisée pour d’autres courbes algébriques, à partir du moment où le nombre de branches réelles passant par chaque singularité peut être calculé efficacement.

En conclusion, nous donnons plusieurs algorithmes certifiés et performants pour l’extraction des ridges. Les méthodes s’appliquent dans les cadres lisse et discret, et différents niveaux de certification sont proposés à l’utilisateur selon ses exigences.

L’intérêt pour l’analyse et le calcul de propriétés géométriques globales n’est pas nouveau. Par exemple, de nombreuses contributions existent pour la visualisation des champs de vecteurs avec des informations topologiques [DH94, Tri02]. Néanmoins, la plupart de ces contributions se restreignent à des domaines Euclidiens et ne sont pas généralisées pour des surfaces. De plus, seulement des heuristiques sont proposées, et des algorithmes avec des garanties topologiques font défaut.

Dans le cadre discret, les champs de vecteurs sont analysés avec une décomposition discrète de Hodge [PP03], ou avec une décomposition de Morse-Smale [EHZ01] via un paradigme de *simulation de la différentiabilité*. Lors

de l'analyse d'une propriété différentielle globale à partir d'une discrétisation, la première étape consiste à comprendre sa stabilité et sa généricité. Une telle approche a prouvé sa réussite pour les ridges et l'axe médian. Le calcul du type d'homotopie de l'axe médian est proposé dans [CL05] guidé par des résultats de stabilité [eRS04]. Pour les surfaces, les feuilletages des directions principales de courbure sont particulièrement intéressants, ils peuvent être utilisés pour le maillage par des quadrilatères optimisant l'approximation [ACSD<sup>+</sup>03]. Néanmoins, il n'existe pas encore de méthode pour calculer la topologie de ces feuilletages.

Dans ce contexte, la collaboration entre les communautés de mathématiques et d'informatiques est nécessaire pour modéliser et résoudre les problèmes de géométrie appliquée.



## Chapter 3

# Differential Topology and Geometry of Smooth Embedded Surfaces: Selected Topics

This chapter surveys mathematical notions and results scattered over several sources. As a prerequisite for the development of algorithms for the manipulation of surfaces, we propose a concise overview of core concepts from differential topology and geometry applied to smooth embedded surfaces.

The understanding of surfaces embedded in  $E^3$  requires local and global concepts, which are respectively evocative of differential geometry and differential topology. While the local theory has been classical for decades, global objects such as the foliations defined by the lines of curvature, or the medial axis still pose challenging mathematical problems. This duality is also tangible from a practical perspective, since algorithms manipulating sampled smooth surfaces (meshes or point clouds) are more developed in the local than the global category.

We first recall the classification of umbilics, of curvature lines, and describe the corresponding stable foliations. Next, fundamentals of contact and singularity theory are recalled, together with the classification of points induced by the contact of the surface with a sphere. This classification is further used to define ridges and their properties, and to recall the stratification properties of the medial axis. Finally, properties of the medial axis are used to present sufficient conditions ensuring that two embedded surfaces are ambient isotopic.

### 3.1 Introduction

#### 3.1.1 Motivations for a geometric and topological analysis

Sampled surfaces represented either by point clouds or meshes are ubiquitous in computer graphics, computer aided design, medical imaging, computational geometry, finite element methods or geology. Aside from the situations where a sample surface is of self-interest —e.g. in computer graphics, sampled surfaces approximating (piecewise-)smooth surfaces are essentially found in two contexts which are surface reconstruction and surface discretization. In the first category, one is given a set of sample points acquired from a scanner (medical or laser) and wishes to reconstruct (by interpolation or approximation) the continuous or (piecewise-)smooth surface which has been sampled. In the second one, a surface is given implicitly or parametrically, and one wishes to discretize it for visualization or calculation purposes. In any case, three types of properties are usually of interest when comparing a (piecewise-)smooth surface and its discretization: topological and geometric properties, local differential properties, and global differential properties.

From a topological standpoint, one expects the surfaces to be homeomorphic or even better isotopic. Example algorithms with such a guarantee are [APR03, ACDL00] in the surface reconstruction area, and [BCSV04, BO03] in the surface meshing context. Apart from these algorithms, the interested reader should consult [SP03, CCS04] where sufficient conditions on isotopy can be found. It should also be pointed out that the hypothesis under which one achieves these properties usually also yield a bound on the Hausdorff distance between the surfaces, a property of geometric nature.

Local differential properties are of two types, namely intrinsic and extrinsic. For extrinsic quantities, one wishes to guarantee that the tangent plane (at the first order), the principal directions and curvatures (at the sec-



ond order), or higher order coefficients (e.g. curvature extremality coefficients) are close. The development of algorithms providing such guarantees has been subject to intense research [Pet01], and recent advances provide guarantees either point-wise [BCM03, CP05a] or in the geometric measure theory sense [CSM03]. Although extrinsic properties are usually the properties sought, some applications care for intrinsic faithfulness. These applications are usually concerned with the question of flattening / parameterizing a surface, and the reader is referred to [MT02] for an example related to geology, together with the ensuing conditions.

At last, global differential properties usually refer to guarantees on loci of points having a prescribed differential property. Example such loci are lines of curvature, ridges, or the medial axis. Applications involving such patterns are surface remeshing [ACSD<sup>+</sup>03], scientific visualization [DH94], feature extraction [PAT00, WB01, HGY<sup>+</sup>99], or surface reconstruction [AB99, BC01] and related topics [DZ02]. Providing such guarantees faces the difficulties afore-mentioned. Not only point-wise estimates must be reliable, but they must also be connected correctly at the surface level. The difficulties are tangible from a practical perspective, and only few algorithms are able to report global differential patterns with some guarantee [CL05].

The lack of such algorithms is partly due to the fact that global differential patterns have an involved structure described in differential topology and singularity theory sources. Easing the access to these notions is the incentive of this concise survey, which deliberately focuses on selected topics related to the geometry and topology on embedded surfaces. In selecting these topics, we had to make choices and omitted the following themes: symmetry sets [BGG85]; distance functions used in analysis [Hor94], optimization [Cla97], mathematical morphology [Ser82], and geometric modeling [Lie03]; bifurcations of symmetry sets and medial axis [BG86, GK02]; differential geometry of skeletal structures [Dam04]; practical algorithms to extract medial axis [CL05].

Our presentation focuses on the geometric intuition rather than the technicalities. From a practical standpoint, we hope it will be helpful for those aiming at producing globally coherent approximations of surfaces.

### 3.1.2 Chapter overview

Following a natural trend, we successively examine differential geometric concepts of the second order (umbilics, lines of curvatures, foliations) and the third order (ridges, medial axis). To finish up, selected properties of the medial axis are used to specify the topological equivalence between embedded surfaces.

More precisely, the Monge form of a surface is recalled in section 3.2. Second order properties are presented in section 3.3 —umbilics and lines of curvature. The classification of contact points between the surface and spheres is presented in section 3.4. This classification is used in section 3.5 to recall the stratification properties of the medial axis. Finally, the topological equivalence between embedded surfaces is recalled in section 3.6, and sufficient conditions involving the medial axis are also presented.

## 3.2 The Monge form of a surface

### 3.2.1 Generic surfaces

Our focus is on generic phenomena on surfaces, and the statements presented are valid for generic surfaces only. Formally if one considers the set of all smooth surfaces  $S$  in  $E^3$  as an infinite dimensional space with a well defined topology, a property is generic if the surfaces exhibiting this property form an open dense subset. Informally this notion means that (i) a generic property remains valid if one allows random perturbations, and (ii) that every surface is arbitrary close to another for which the property holds. Due to the infinite dimension of the space of surfaces, it is not straightforward to define a topology on this set. We will consider the  $C^r$  topology ( $r \in \mathbb{N} \cup \{\infty\}$ ) on the set of all smooth oriented surfaces  $S$  embedded in the Euclidean space  $E^3$  (cf. [GS91][p.27]). A sequence  $S_n$  of surfaces converges to  $S$  in the  $C^r$  sense provided there is a sequence of real functions  $f_n$  on  $S$  such that  $S_n = (I + f_n N)(S)$ , where  $I$  is the identity of  $E^3$ ,  $N$  is the normal vector of  $S$  and  $f_n$  tends to 0 in the  $C^r$  sense. That is, for every chart  $(u, v)$  with inverse parameterization  $X$ ,  $f_n \circ X$  converges to 0 together with the partial derivatives of order  $r$ , on compact parts of the domain of  $X$ .

### 3.2.2 The Monge form of a surface

We consider an oriented surface  $S$  embedded in the Euclidean space  $E^3$ . We consider  $E^3$  given with an orthonormal basis called the world coordinate system. Another orthonormal basis is called *direct* if it is the image of the world coordinate system by a special orthogonal transformation. At any point of the surface which is not an umbilic,

principal directions are well defined, and the (non oriented) principal directions  $d_1, d_2$  together with the normal vector  $n$  define two direct orthonormal frames. If  $v_1$  is a unit vector of direction  $d_1$  then there exists a unique unit vector  $v_2$  so that  $(v_1, v_2, n)$  is direct; and the other possible frame is  $(-v_1, -v_2, n)$ . In one of these, and as long as our study is a local differential one, the surface is assumed to be given as a Monge patch at the origin [HGY<sup>+</sup>99] —with *h.o.t* standing for *higher order terms*:

$$z = \frac{1}{2}(k_1x^2 + k_2y^2) + \frac{1}{6}(b_0x^3 + 3b_1x^2y + 3b_2xy^2 + b_3y^3) \quad (3.1)$$

$$+ \frac{1}{24}(c_0x^4 + 4c_1x^3y + 6c_2x^2y^2 + 4c_3xy^3 + c_4y^4) + h.o.t \quad (3.2)$$

Occasionally, we shall refer to the cubic part  $C_M(x, y)$  as the Monge cubic, that is:

$$C_M(x, y) = b_0x^3 + 3b_1x^2y + 3b_2xy^2 + b_3y^3. \quad (3.3)$$

If the origin is not an umbilic, the principal direction  $d_1$  (resp.  $d_2$ ) associated to the principal curvature  $k_1$  (resp.  $k_2$ ) is the  $x$  (resp.  $y$ ) axis. We shall always assume that  $k_1 \geq k_2$  and we consider 'blue' (resp. 'red') something special happening with  $k_1$  (resp.  $k_2$ ). For example the blue focal surface is the set of centers of curvature associated to the blue curvature  $k_1$ . Note that a change of the normal surface orientation swaps the colors.

Away from umbilics, local analysis of the principal curvatures can be done for the Monge coordinate system and along the curvature lines. The Taylor expansion of the principal curvature  $k_1$  in the Monge coordinate system is

$$k_1(x, y) = k_1 + b_0x + b_1y + \left(\frac{c_0 - 3k_1^3}{2} + \frac{b_1^2}{k_1 - k_2}\right)x^2 \quad (3.4)$$

$$+ \left(c_1 + \frac{2b_1b_2}{k_1 - k_2}\right)xy + \left(\frac{c_2 - k_1k_2^2}{2} + \frac{b_2^2}{k_1 - k_2}\right)y^2 + h.o.t \quad (3.5)$$

The Taylor expansion of  $k_1$  (resp.  $k_2$ ) along the blue (resp. red) curvature line going through the origin and parameterized by  $x$  (resp.  $y$ ) are:

$$k_1(x) = k_1 + b_0x + \frac{P_1}{2(k_1 - k_2)}x^2 + h.o.t \quad P_1 = 3b_1^2 + (k_1 - k_2)(c_0 - 3k_1^3). \quad (3.6)$$

$$k_2(y) = k_2 + b_3y + \frac{P_2}{2(k_2 - k_1)}y^2 + h.o.t \quad P_2 = 3b_2^2 + (k_2 - k_1)(c_4 - 3k_2^3). \quad (3.7)$$

Notice also that switching from one of the two coordinate systems mentioned in introduction to the other reverts the sign of all the odd coefficients on the Monge form of the surface.

Some notions about cubics will be useful in the sequel.

**Definition. 1** A real cubic  $C(x, y)$  is a bivariate homogeneous polynomial of degree three, that is  $C(x, y) = b_0x^3 + 3b_1x^2y + 3b_2xy^2 + b_3y^3$ . Its discriminant is defined by  $\delta(C) = 4(b_1^2 - b_0b_2)(b_2^2 - b_1b_3) - (b_0b_3 - b_1b_2)^2$ .

A cubic factors as a product of three polynomials of degree one with complex coefficients, called its factor lines. In the  $(x, y)$  plane, a real factor line defines a direction along which  $C$  vanishes. The number of real factor lines depends on the discriminant of the cubic and we have

**Proposition. 1** Let  $C$  be a real cubic and  $\delta$  its discriminant. If  $\delta > 0$  then there are 3 distinct real factors, if  $\delta < 0$  there is only one real factor.

In the particular description of surfaces as Monge patches, we have a family of Monge patches with two degrees of freedom —the dimension of the manifold. A property requiring 1 (resp. 2) condition(s) on this family is expected to appear on lines (resp. isolated points) of the surface —a condition being an equation involving the Monge coefficients. A property requiring at least three conditions is not generic. As an example, ridge points (characterized by the condition  $b_0 = 0$  or  $b_3 = 0$ ) appears on lines and umbilics (the two conditions are those for a quadric to have equal roots, i.e. the coefficient of the  $xy$  term vanishes and those of  $x^2$  and  $y^2$  are equal) are isolated points. A flat umbilic, requiring the additional condition  $k_1 = 0$ , is not generic.



### 3.3 Umbilics and lines of curvature, principal foliations

This section is devoted to second order properties on a surface, and more precisely to umbilics and lines of curvature. General references are [Mor90, Por01, GS91, HGY<sup>+</sup>99, MWP96].

#### 3.3.1 Classification of umbilics

To present the classification of umbilics, let us first recall some facts about lines of curvature. On each point of the set  $S'$  defined as the surface  $S$  except its umbilics, the two principal directions are well defined and orthogonal. They define two direction fields on  $S'$ , one everywhere orthogonal to the other, so it is sufficient to study only one of these. Each principal direction field defines lines of curvature. The set of all these lines, called the principal foliation, will be studied in the next section.

**Definition. 2** *A line of curvature is an integral curve of the principal field, that is a regular curve on  $S'$  which is everywhere tangent to the principal direction and is maximal for inclusion (it contains any regular curve with this property which intersects it).*

The index of an umbilic describes the way the lines of curvature turn around the umbilic. The index of a direction field at a point is  $(1/2\pi) \int_0^{2\pi} \theta(r) dr$ , where  $\theta(r)$  is the angle between the direction of the field and some fixed direction, and the integral is taken over a small counterclockwise circuit around the point. For generic umbilics this index is  $\pm 1/2$ , this implies that the direction field is not orientable on a neighborhood of such points. As illustrated on Fig. 3.1, if one fixes an orientation of the field at a point on a circuit around an umbilic, propagating this orientation by continuity along the circuit gives the reverse orientation after one turn. In other words, there is no non vanishing continuous vector field inducing the direction field around the umbilic. The index can also be computed with the Monge cubic, this computation is point wise as opposed to the previous one, but need third order coefficients (hence it is likely to be less stable in practice). Let  $S = (b_0 - b_2)b_2 - b_1(b_1 - b_3)$ ,

- if  $S < 0$  then the index is  $-1/2$  and the umbilic is called a star,
- if  $S > 0$  then the index is  $+1/2$  and we have to do more calculations to distinguish between the so called lemon and monstar.

A finer classification is required to distinguish between the two umbilics of index  $+1/2$ . We shall need the following:

**Definition. 3** *Consider an umbilic  $p$  and denote  $T_p S$  the tangent plane of the surface at  $p$ . A limiting principal direction is a direction of  $T_p S$  which is tangent to a line of curvature which end at the umbilic.*

Limiting principal directions are related to the Jacobian cubic of the umbilic (cf. [HGY<sup>+</sup>99]):

$$J_C = B_0 x^3 + 3B_1 x^2 y + 3B_2 x y^2 + B_3 y^3 = b_1 x^3 + (2b_2 - b_0)x^2 y - (2b_1 - b_3)xy^2 - b_2 y^3. \quad (3.8)$$

The real factor lines of this form are the limiting principal directions at the umbilic. As recalled by proposition 1, the number of such directions depends on the discriminant  $U$  of  $J_C$ :

- If  $U < 0$  then there is one limiting principal direction, necessarily  $S > 0$  and the umbilic is called a lemon.
- If  $U > 0$  then there are three limiting principal directions, furthermore if  $S < 0$  the umbilic is a star else  $S > 0$  and it is called a monstar. For a monstar, the three directions are contained within a right angle and all the curvature lines in this angle end at the umbilic and form the parabolic sector of the monstar. Note that all these lines have the same tangent at the umbilic: the limiting principal direction inside the parabolic sector. For a star, only three lines of curvature end at the umbilic and the limiting directions are not contained in a right angle.

We summarize the previous discussion as follow:

**Theorem. 3** *There are three classes of generic umbilics in the  $C^3$  sense, namely Lemons, Monstar and Stars. They are distinguished by their index and the number of limiting principal directions.*

To be an umbilic requires two conditions on the Monge coefficients, this implies that the cases  $S = 0$  or  $U = 0$  are not generic umbilics. From the same argument, a generic umbilic is a non flat point: its Gaussian curvature does not vanish, and generic umbilics are isolated (cf. [Por01][p.184]).

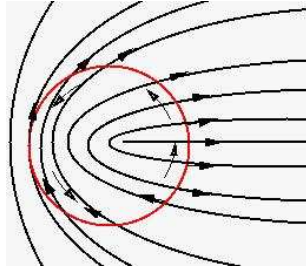


Figure 3.1: Impossibility of a global orientation around an umbilic

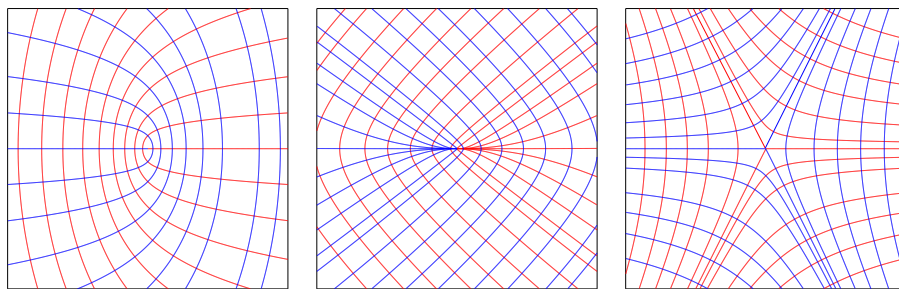


Figure 3.2: Umbilics: Lemon and Monstar of index  $+1/2$ , Star of index  $-1/2$ .

### 3.3.2 Principal foliations

Recall that the blue (resp. red) principal foliation is the set of all blue (resp. red) curvature lines defined on  $S' - S$  except its umbilics. The umbilics can be regarded as singular points for these foliations if one wishes to consider them on  $S$ . The first element required concerns the topology of a curvature line. A line of curvature  $\gamma$  is either homeomorphic to:

- an open interval  $I = (\omega_-, \omega_+)$ , then it is assumed to be oriented and parameterized by this interval. Its  $\alpha(\gamma)$  (resp.  $\omega(\gamma)$ ) limit set is the collection of limit points of sequences  $\gamma(s_n)$ , convergent in  $S$ , with  $s_n$  tending to  $\omega_-$  (resp.  $\omega_+$ ). The limit set of  $\gamma$  is the union  $\alpha(\gamma) \cup \omega(\gamma)$ .
- or to a circle, then it is called a cycle. It is hyperbolic if the differential of its Poincaré return map differs from the identity. In other words, if one orients an hyperbolic cycle, the lines of curvature can be oriented on a neighborhood of this cycle by continuity and they are all attracted or repelled on both sides of the cycle (cf. Fig. 3.3).

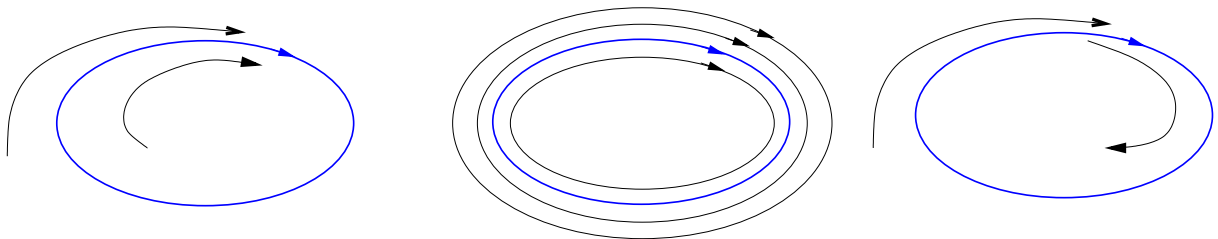


Figure 3.3: A hyperbolic cycle and two non hyperbolic ones

Special lines divide the set of all curvature lines in the vicinity of an umbilic into sectors, they are separatrices.

**Definition. 4** A separatrix is a line of curvature with an umbilic in its limit set and so that there exists arbitrarily close to that line, another line without this umbilic in its limit set.

A sector defined by two consecutive separatrices is

- hyperbolic if none of the lines in the sector have the umbilic in their limit set;
- parabolic if all curvature lines in the sector have the umbilic in their  $\alpha$  or exclusive  $\omega$  limit set;

The alternative case of an elliptic sector, if all curvature lines in the sector have the umbilic in their  $\alpha$  and  $\omega$  limit set, is not generic —cf. Nikolaev [Nik01][p.360]. Note that a separatrix is a line of curvature which ends at an umbilic, hence its tangent at this point is a limiting principal direction. But the limiting principal direction inside the parabolic sector of a monstar is not tangent to a separatrix of this umbilic —because all lines in a neighborhood have the monstar in their limit set. This explains another classification of umbilics from Darboux based on the number of separatrices. This classification rephrases the previous one: a lemon or  $D_1$  has one separatrix, a monstar or  $D_2$  has two and a star or  $D_3$  has three.

The next result [GS91][p.27] describes stable configuration of the principal foliations for smooth compact oriented surfaces embedded in  $E^3$ . A surface  $S$  is said to be  $C^r$  principal structurally stable if for every sequence  $S_n$  converging to  $S$  in the  $C^r$  sense, there is a sequence of homeomorphisms  $H_n$  from  $S_n$  onto  $S$ , which converges to the identity of  $S$ , such that, for  $n$  big enough,  $H_n$  is a principal equivalence from  $S_n$  onto  $S$ . That is  $H_n$  maps the umbilical set of  $S_n$  onto the umbilical set of  $S$ , and maps the lines of the principal foliations of  $S_n$  onto those of  $S$ .

**Theorem. 4** *Let  $\Sigma$  be the subset of smooth compact oriented surfaces which satisfies the following four conditions:*

- all the umbilic points are of type  $D_i$ ,  $i = 1, \dots, 3$ ;
- all the cycles are hyperbolic;
- the limit sets of every line of curvature are umbilics or cycles;
- all the separatrices are separatrices of a single umbilic (they cannot connect two umbilics or twice the same one being separatrices at both ends).

*Then  $\Sigma$  is open and each of its elements is principal structurally stable in the  $C^3$ -sense,  $\Sigma$  is dense in the  $C^2$ -sense.*

This theorem implies that stable principal foliations are described with the set of umbilics, cycles and the way the separatrices connect these elements. The complement of these features on the surface  $S$  then decomposes on canonical regions of two types parallel and cylindrical. On each region, the limit sets of all lines are the same: a cycle or a  $D_2$  umbilical point (through its parabolic sector). A region is parallel if there are separatrices in its boundary. If the boundary consists only of cycles then the region is cylindrical.

The topology of the surface  $S$  constrains the number and the type of umbilics. More precisely, the sum of indices of umbilics must be the Euler characteristic  $\chi(S)$  —[Spi99b][p.223]. Moreover, the principal foliation defines a bipartite graph  $G(V_1, V_2, E)$  with  $V_1$  the set of umbilics,  $V_2$  the set of cycles and parabolic sectors and  $E$  the set of separatrices. The edges connect elements of  $V_1$  to elements of  $V_2$  with the following constraints.

- A  $D_i$  umbilic has  $i$  incident edges.
- Since there is no elliptic sector, a separatrix of a  $D_2$  umbilic cannot be connected to its parabolic sector.
- The graph is embedded on the surface without intersecting the separatrices.

### 3.4 Contacts of the surface with spheres, Ridges

To classify points of a smooth surface regarding curvature properties, we first recall fundamentals from contact and singularity theory. Following [Por71, Por83, Mor90], we probe a point of the surface with a sphere centered along the normal at that point. Working out the dominant terms of the Taylor expansion of the probe function yields the classification of points desired. General references for this section are [BG92], [Por01] or [Arn92].

### 3.4.1 Distance function and contact function

A standard way to classify points on a smooth surface consists of using contact theory. Consider a portion of surface locally parameterized in a chart  $(U, p(x, y))$  with  $U \subset \mathbb{R}^2$ ,  $(x_0, y_0) \in U$  and a sphere  $C$  of center  $c$ . Denoting  $\langle, \rangle$ , the standard inner product of  $E^3$ , the contact function at the point  $p(x_0, y_0) \in S$  is the function defined by:

$$g : U \times \mathbb{R}^3 \mapsto \mathbb{R}, g((x, y), c) = \langle p(x, y), c \rangle^2 - \langle p(x_0, y_0), c \rangle^2. \quad (3.9)$$

This function is just the square distance from the surface to the center of the sphere minus the square of its radius  $r^2 = \langle p(x_0, y_0), c \rangle^2$ . The intersection points between  $S$  and  $C$  have coordinates  $(x, y, p(x, y))$  satisfying  $g(x, y) = 0$ . The philosophy of contact theory is the following. Once the center of the sphere have been chosen, the contact function is a bivariate function. Then, we wish to report the possible *normal forms* of  $g$  as a bivariate function.

Before illustrating this process, let us observe that if the center of the sphere  $C$  is not contained in the affine space defined by the contact point and the normal at the surface  $S$  there, then the intersection between  $S$  and  $C$  is transverse, which does not reveal much about  $S$  at  $p$ . Studying the nature of the contact really starts with a center aligned with the normal, and we shall see that the cases encountered actually yield a decomposition of the normal bundle<sup>1</sup> of the surface.

**Remark.** Note that if one of the principal curvatures vanishes, one can assume the center of the principal sphere is at infinity. This means that the relevant contact to be considered is that of a plane with the surface at such a point. One can find a precise description of these parabolic points in [HGY<sup>+</sup>99].

### 3.4.2 Generic contacts between a sphere and a surface

Before presenting the generic contacts, let us illustrate the process of finding the first normal form using the Morse lemma. To ease the calculations, assume that the contact point is the origin, that the surface is given in Monge form, and that the center of the sphere has coordinates  $c(0, 0, r)$ . Then, the contact function simplifies to:

$$g(x, y) = x^2 + y^2 + (z - r)^2 - r^2 = \langle pc, pc \rangle - r^2. \quad (3.10)$$

Using the Monge form of  $f$ , one gets the following expansion:

$$g(x, y) = x^2(1 - rk_1) + y^2(1 - rk_2) - \frac{r}{3}C_M(x, y) + h.o.t \quad (3.11)$$

The expansion does not contain linear terms and the origin is therefore a critical point. Moreover, if  $r \neq 1/k_1$  and  $r \neq 1/k_2$ , the critical point is non-degenerate. By the Morse lemma, the contact function rewrites as  $g = \pm x^2 \pm y^2$  up to a diffeomorphism. If the coefficients of both variables have the same sign, then the intersection between  $S$  and  $C$  reduces to point. Otherwise, the intersection consists of two curves.

The previous discussion is typical from singularity theory. Assuming  $r \neq 1/k_1$  and  $r \neq 1/k_2$ , we worked out the *normal form* of a multivariate function, thus highlighting its dominant terms. In the sequel, we shall just state and use the classification of generic singularities of the contact function. As illustrated by Morse's lemma, it is important to observe that the normal form is exact, i.e. does not hide any higher order term. We shall need the following:

**Definition. 5** Let  $f(x, y)$  be a smooth bivariate function. Function  $f$  has an  $A_k$  or  $D_k$  singularity if, up to a diffeomorphism, it can be written as:

$$\begin{cases} A_k : f = \pm x^2 \pm y^{k+1}, & k \geq 0, \\ D_k : f = \pm yx^2 \pm y^{k-1}, & k \geq 4. \end{cases} \quad (3.12)$$

The singularity is further denoted  $A_k^\pm$  or  $D_k^\pm$  if the product of the coefficients of the monomials is  $\pm 1$ .

As subsumed by this definition, an  $A_k$  singularity precludes an  $A_{k+1}$  singularity, and similarly for  $D_k$ . An important characteristic of these normal forms is their zero level set. Those of the  $A_k$  sequence are illustrated on Fig. 3.4, where the (branches of) curves are defined from  $x = \pm y^{(k+1)/2}$ . More precisely:

<sup>1</sup>The normal bundle of the surface is the three-dimensional manifold obtained by adding to each point of the surface a one-dimensional affine space defined by the pair (point, normal).

**Observation. 1** The zero level set of an  $A_0$  singularity consists of a smooth curve, and that of an  $A_{2p}$  singularity for  $p \geq 1$  of one curve having a cusp at the origin. The zero level set of an  $A_{2p-1}$  singularity consists of two tangential curves or an isolated point depending on the product of the signs of the monomials.

For a  $D_k$  singularity, since  $f = y(\pm x^2 \pm y^{k-2})$ , the line  $y = 0$  is always solution. For the other solutions, the discussion is identical to the  $A_k$  case.

**Observation. 2** The zero level set of an  $D_{2p}^+$  ( $D_{2p}^-$ ) singularity consists of one (three) curve(s). The zero level set of an  $D_{2p+1}^+$  or  $D_{2p+1}^-$  singularity consists of two curves.

The classification of generic contact points is the following [Por71, Por83]:

**Theorem. 5** The generic singularities of the contact function between a sphere and a surface are of type  $A_0, A_1, A_2, A_3, A_4, D_4$ .

The  $A_0$  contact is just the transverse intersection mentioned at the beginning of this section, and we shall not discuss it further. The others types of contacts —respectively  $A_k$  and  $D_k$ — encode properties of the surface away from umbilics and at umbilics.

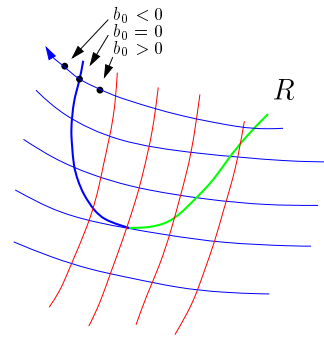
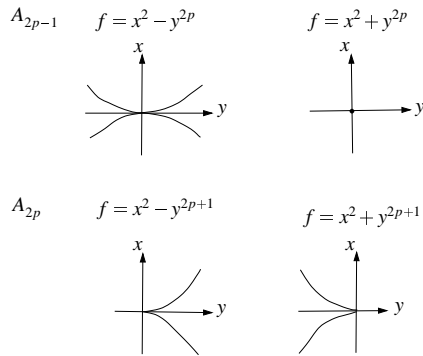


Figure 3.4: Zero level sets of the  $A_k : f = x^2 \pm y^{k+1}$  singularities

Figure 3.5: Variation of the  $b_0$  coefficient and turning point of a ridge

### 3.4.3 Contact points away from umbilics

We proceed with the discussion of the contacts away from umbilics.

**$A_1$  contact.** [ $r \neq 1/k_1, r \neq 1/k_2$ ] The origin is a non degenerate critical point. The local intersection reduces to one point if  $r$  is in the connected component of  $\mathbb{R} \setminus \{1/k_1, 1/k_2\}$  which contains 0, or is two transverse curves otherwise.

**$A_2$  contact.** [ $r = 1/k_1, b_0 \neq 0$  (or  $r = 1/k_2, b_3 \neq 0$ )] The sphere is a sphere of principal curvature, and the curvature is not an extremum by Eq. (3.6) since  $b_0 \neq 0$ . Due to the presence of terms of odd degree in the normal form, the local intersection between the sphere and the surface is not reduced to a point (cf. Fig. 3.7 and 3.8).

**$A_3$  contact.** [ $r = 1/k_1, b_0 = 0, P_1 \neq 0$  (or  $r = 1/k_2, b_3 = 0, P_2 \neq 0$ )] The sphere is a sphere of principal curvature, and the principal curvature has a local extremum since  $b_0 = 0$  and  $P_1 \neq 0$  —or  $b_0 = 3$  and  $P_2 \neq 0$ . An  $A_3$  contact defines a ridge point, but not all ridge points are  $A_3$  points —see the turning points below. Distinguishing further between  $A_3^-$  and  $A_3^+$  yields the distinction between elliptic and hyperbolic ridge points <sup>2</sup>:

- Elliptic. If  $P_1 < 0$ , the contact function has  $A_3^+$  singularity and its normal form is  $g = y^2 + x^4$ . Equivalently, the blue curvature is maximal along its curvature line. The blue sphere of curvature has a local intersection with  $S$  reduced to  $p$  (cf. Fig. 3.9).

<sup>2</sup>Elliptic and hyperbolic ridge points are called sterile and fertile by Porteous. This refers to the possibility for umbilics to appear near such ridges.

- Hyperbolic. If  $P_1 > 0$ , the contact function has an  $A_3^-$  singularity and its normal form is  $g = y^2 - x^4$ . Equivalently, the blue curvature is minimal along its line. The local intersection of the blue sphere of curvature with  $S$  is two tangential curves (cf. Fig. 3.10).

Summarizing,  $b_0 = 0, P_1 \neq 0$  defines a blue ridge point, either elliptic or hyperbolic. Similarly,  $b_3 = 0$  defines a red ridge point, whose type is specified by the sign of  $P_2$  defined by Eq. (3.7). A red ridge is elliptic if  $k_2$  is minimal ( $P_2 < 0$ ) along its curve and hyperbolic if  $k_2$  is maximal ( $P_2 > 0$ ). (Notice that in Eq. (3.7) the sign of  $P_2$  is in accordance with the negative sign of  $k_2 - k_1$ .)

Notice that the type, elliptic or hyperbolic, is independent of the surface orientation. However the sign of  $b_0$  depends on the orientation of the principal directions. The corresponding geometric interpretation when moving along a curvature line and crossing the ridge is recalled on Fig. 3.6.

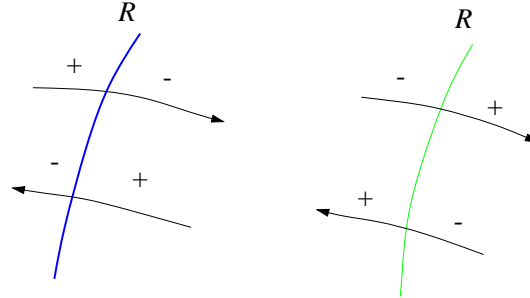


Figure 3.6: Sign changes of  $b_0$  along an oriented blue curvature line crossing a blue ridge : elliptic case (max of  $k_1$ , left), and hyperbolic case (min of  $k_1$ , right).

Ridge points are on smooth curves on the surface called ridge lines and can be colored according to the color of the points. Away from umbilics, a blue ridge can cross a red ridge at a ridge point colored blue and red that we call a purple point. A crossing of ridges of the same color is not generic.

**Remark.** When displaying ridges, we shall adopt the following conventions:

- blue elliptic (hyperbolic) ridges are painted in blue (green),
- red elliptic (hyperbolic) ridges are painted in red (yellow).

**$A_4$  contact.** [ $r = 1/k_1, b_0 = 0, P_1 = 0$  (or  $r = 1/k_2, b_3 = 0, P_2 = 0$ )] The blue curvature has a inflection along its line ( $k'_1 = k''_1 = 0$  but  $k'''_1 \neq 0$ , derivatives shall be understood as along the curvature line, cf Eq. (3.6)). As an  $A_4$  singularity, the local intersection of the blue sphere of curvature with  $S$  is a curve with a cusp at the contact point. Such a point is called a *ridge turning point*. At such a point, the ridge is tangent to the line of curvature of the same color, and the ridge changes from elliptic to hyperbolic—from a maximum to a minimum of the principal curvature.

The variation of the  $b_0$  coefficient in the neighborhood of a blue ridge and a turning point of such a ridge are illustrated on Fig. 3.5. Summarizing the previous observations, we have:

**Definition. 6** Let  $p \in S$  be a non-umbilical point, then  $p$  is a blue ridge point if one of the following equivalent conditions is satisfied:

- (i) the blue principal curvature has an extremum along the corresponding blue line of curvature,
- (ii)  $b_0 = 0$ ,
- (iii) the blue sphere of curvature has at least an  $A_3$  contact with  $S$  at  $p$ .

Notice again that a contact involves a sphere and the surface. The contact therefore provides information on the surface but also on its focal surfaces—the blue/red one assuming the sphere in contact is a principal blue/red sphere of curvature. The reader is referred to [BGG85] for local models of the focal surface at such singularities. We actually have the following:



**Observation. 3** At a ridge point, the focal surface is not regular —the center of the osculating sphere is located on a cuspidal edge of the focal surface.

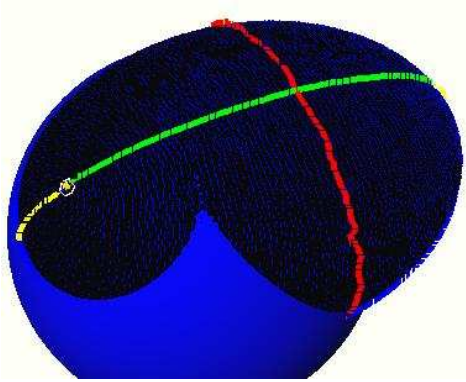


Figure 3.7:  $A_2$  contact with the blue sphere

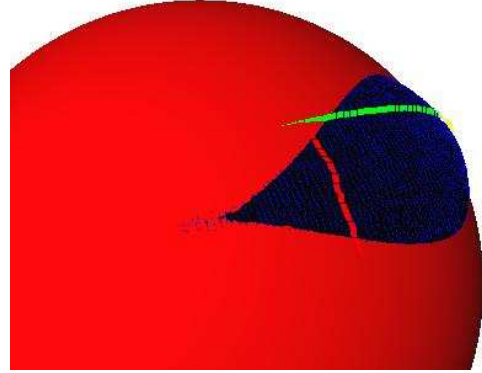


Figure 3.8:  $A_2$  contact with the red sphere

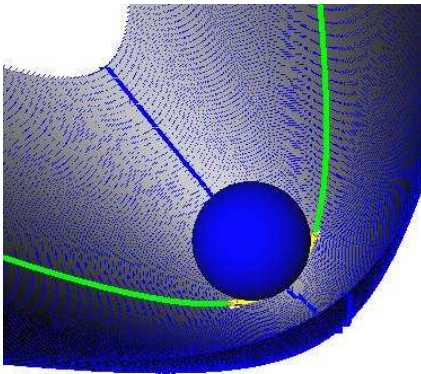


Figure 3.9:  $A_3^+$  contact of the blue sphere of curvature at a blue elliptic ridge point (on the blue curve)

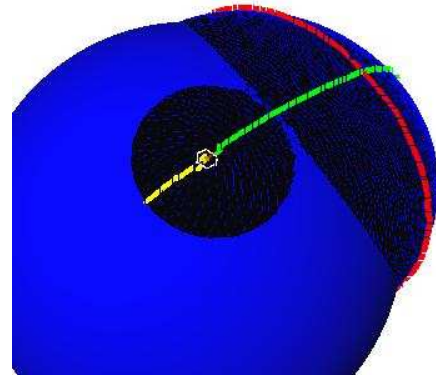


Figure 3.10:  $A_3^-$  contact of the blue sphere of curvature at a blue Hyperbolic ridge point (on the green curve)

### 3.4.4 Contact points at umbilics

Away from umbilic, the  $x$  and  $y$  coordinates of the Monge coordinate system follow the principal directions; at the umbilic there is no such canonical choice of coordinates, hence the values of  $b_0$  and  $b_3$  are not relevant and other invariants must be considered.

To see which ones, consider the contact function given by Eq. (3.11). Since  $r = 1/k_1 = 1/k_2$ , it is dominated by the cubic terms. More precisely, the singularity is generically a  $D_4^\pm$ . The number of ridges passing through the umbilic is the number of curves in the zero level set of the contact function. Hence this number reads on the normal form, and is equal to one or three as mentioned in observation 2. This fact is not intuitive and it is neither obvious that ridges pass through umbilics. A way to explain these facts is to study the gradient field  $\nabla k_1$  (the same holds for  $\nabla k_2$ ) well defined at non umbilical points. Indeed a non-umbilical blue ridge point can be seen as a point on a blue curvature line where  $\nabla k_1$  is orthogonal to the curve that is  $\langle \nabla k_1, d_1 \rangle = 0$ , or equivalently the iso-curve of  $k_1$  is tangent to the curvature line. Hence one has to study orthogonality between the two fields  $\nabla k_1$  and  $d_1$ . In section 3.3.1, it has been shown that the index of the  $d_1$  fields distinguishes stars (index  $-1/2$ ) from lemons or monstars (index  $+1/2$ ). The study of  $k_1$  and  $\nabla k_1$  shows that generically, one has the following:

- $k_1$  has a minimum, then the vector field  $\nabla k_1$  has index 1; this also implies that the umbilic is a star and that there are 3 directions in which  $\langle \nabla k_1, d_1 \rangle = 0$ ;
- there is a curve along which  $k_1 = k$  is constant passing through the umbilic, then  $\nabla k_1$  has index 0 and there is 1 direction in which  $\langle \nabla k_1, d_1 \rangle = 0$ .

The distinction between these two cases also reads on the Monge cubic  $C_M$ , its number of real factor lines is the

number of ridges, hence it depends on the sign of its discriminant  $D = \delta(C_M)$ . One can summarize the previous discussion as follows [Por01, Chap 11.6, p.191]—see also Fig. 3.12:

**Theorem. 6** *Generic umbilics are of two types:*

- *Elliptic. The Monge cubic has three different real factor lines, or equivalently the contact function has a  $D_4^-$  singularity. Three non-singular ridge branches cross at the umbilic. Moreover at the umbilic,  $k_1$  has a minimum and  $k_2$  a maximum. Such an umbilic is a star.*
- *Hyperbolic. The Monge cubic has only one real factor line, or equivalently the contact function has a  $D_4^+$  singularity. Only one non-singular ridge branch passes through the umbilic. Moreover passing through the umbilic, there is one curve along which  $k_1$  (resp.  $k_2$ ) is constant equal to  $k$ . Such an umbilic is either a lemon, a monstar or a star.*

The number of ridges is given by the number of real factors lines of the Monge cubic, but these lines are not the tangent directions to ridge lines going through the umbilic. However, these tangent directions can be computed from the Monge cubic cf. [HGY<sup>+</sup>99].

**Definition. 7** *An umbilic is called a 1-ridge (resp. 3-ridge) umbilic if there is 1 (resp. 3) non-singular ridge curve going through it.*

Generically, the discriminant  $\delta(C_M)$  of  $C_M$  does not vanish, so that  $C_M$  is either elliptic or hyperbolic. Therefore, a generic umbilic is either 1-ridge or 3-ridge.

The intersection between the surface and its osculating sphere at an umbilic is not reduced to a point (cf. Observation 2). This fact remains true close to the umbilic and in particular on ridges, so we have:

**Observation. 4** *A ridge passing through an umbilic must be hyperbolic.*

It also turns out that ridges are smooth curves crossing at umbilics and changing color there —from a minimum of  $k_1$  to a maximum of  $k_2$ . Notice that a ridge may not pass through an umbilic, then it is of a single color and changes type at each turning point if any —there is an even number of such points.

**Remark.** A finer distinction of elliptic umbilics concerns the ordering of ridge colors around the umbilic: it is called symmetrical if ridges alternate colors RBRBRB (then  $T = b_0^2 + b_3^2 + 3(b_0b_2 + b_1b_3) < 0$ ) and unsymmetrical if the ordering is RRRBBB ( $T > 0$ ). Figure 3.11 gives a schematic view of ridges at umbilics, more accurate figures can be found in [HGY<sup>+</sup>99].

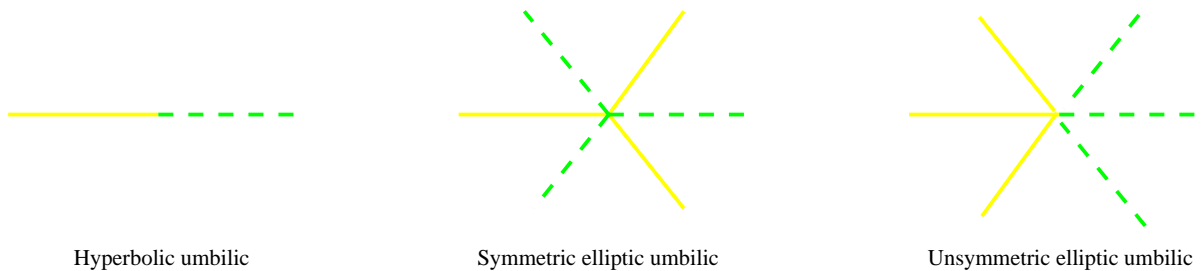


Figure 3.11: Ridges at umbilic

### 3.4.5 Umbilic classification in the complex plane

The classification of umbilics with respect to the cubic part of the Monge form of the surface can be illustrated by a diagram in the plane (Fig. 3.12). With a change of variables which corresponds to a rotation in the tangent plane and noting  $\zeta = x + iy$  the cubic form  $b_0x^3 + 3b_1x^2y + 3b_2xy^2 + b_3y^3$  becomes  $Re(\zeta^3 + \omega\zeta^2\bar{\zeta})$  for some complex number  $\omega$ . Then umbilics are parameterized by  $\omega$  in the complex plane. The zero sets of the four invariants  $S, U, D$  and  $T$  give four curves partitioning the plane in sectors. Umbilics on the complement of these curves are generic.

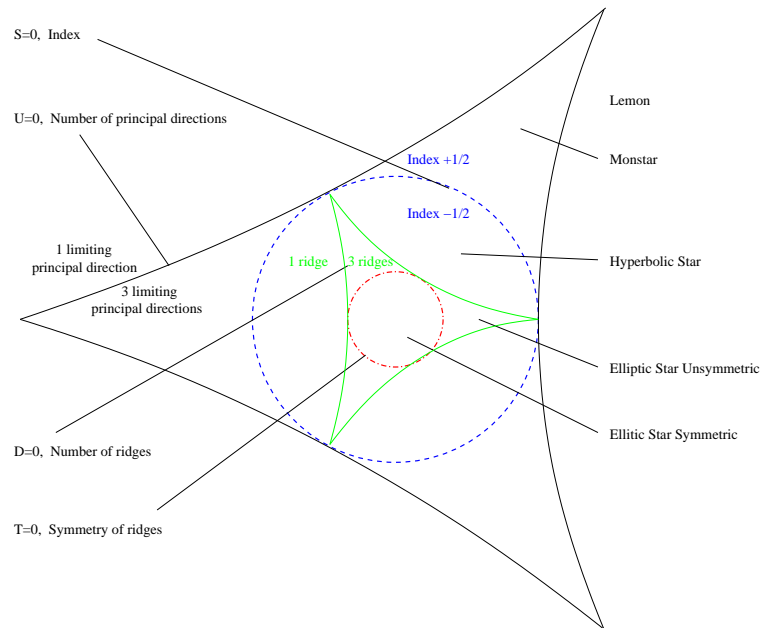


Figure 3.12: Umbilic classification in the complex plane

### 3.4.6 Summary of the global picture of ridges and umbilics on a generic surface

To summarize, a ridge point is distinguished by its color and its type. When displaying ridge curves, we shall adopt the following conventions:

- blue elliptic (hyperbolic) ridge curves are painted in blue (green),
- red elliptic (hyperbolic) ridges curves are painted in red (yellow).

At last, ridge curves displayed in black refer either to red or blue ridges.

Umbilic points can be considered as ridge points since they are in the closure of ridge curves. But from a topological standpoint, excluding umbilics, a ridge curve is a submanifold of  $S$  and one can distinguish the two cases:

**Definition. 8** For a closed and bounded surface, a ridge curve is called open if it is homeomorphic to the real line, and it is called closed if it is homeomorphic to a circle.

An open ridge has one or two points in its frontier which are umbilics. Hence an open ridge curve “connects” two umbilics or twice the same one.

To finish up this review, let us recall the following generic properties:

- a ridge curve contains an even number of turning points at which the ridge changes from elliptic to hyperbolic.
- Near an umbilic, open ridge curves connected to this umbilic are hyperbolic.
- The configuration of ridges of the same color at umbilics are the following:
  - either only 1 open ridge curve is connected to the umbilic which is called a 1-ridge umbilic;
  - or 3 different open ridges are connected at one end to the umbilic or, 1 open ridge is connected at both ends and another open ridge is connected at one end to the umbilic (cf. Fig. 3.13). This umbilic is called a 3-ridge umbilic.
- Ridges of the same color do not cross.
- Two ridges of different colors may cross at a so-called *purple point*.
- The index of an umbilic is  $\pm 1/2$ , this implies that the direction field is not orientable on a neighborhood of such points.

These notions are illustrated on the famous example of the ellipsoid on Figs. 3.14 and 3.15.

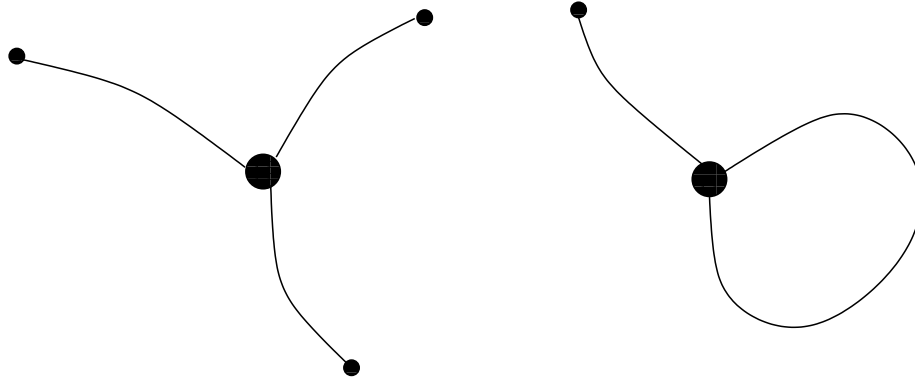


Figure 3.13: Two cases of 3-ridge umbilics: first with 3 different ridges, second with 2 different ridges connected to it. Points are umbilics, lines are ridges of the same color.

### 3.4.7 Illustrations

We illustrate the previous global structure theorems on the famous example of an ellipsoid with three different axes —Fig. 3.14, an implicit blend of two ellipsoids —Fig. 3.16, and a Bezier patch —Fig. 3.17. The figures are produced by the algorithm described in chapter 5, while the ridges of Fig. 3.17 are certified by the algorithm presented in chapter 7. The color conventions are: blue elliptic (hyperbolic) ridges are painted in blue (green), red elliptic (hyperbolic) ridges are painted in red (yellow). Intersections between ridges are the purple points.

On Fig. 3.14, the blue principal direction field is drawn —from which one infers that the normal is pointing outward so that the two principal curvatures are negative. The two elliptic ridges are closed curves without turning point. The four Lemon umbilics are the black dots, and they are linked by four separatrices —the yellow and green curves. The separatrices, which are curvature lines, are also ridges in that case. More generally, any line of symmetry is a line of curvature and a ridge ([Por01][p.162]). Notice also that the lines of curvatures which are not separatrices are all cycles. For each color, they are packed into a cylinder. But this is a non stable configuration since separatrices are umbilical connections, the cycles are not hyperbolic. The medial axis of the ellipsoid is a region homeomorphic to a disk, and is located in the symmetry plane of the two largest axes. This region looks like an ellipsis but is not so [Deg97]. The boundary of the medial axis projects onto the red ridge curve, and reciprocally on this example, every elliptic red ridge point corresponds to a point on the boundary of the medial axis.

Fig.3.16 is a blend between two ellipsoids defined by the following equation:

$$1 - \exp\left(-0.7\left(\frac{x^2}{0.15^2} + \frac{y^2}{0.25^2} + \frac{z^2}{0.35^2} - 1\right)\right) \quad (3.13)$$

$$- \exp\left(-0.7\left(\frac{(x-0.25)^2}{0.1^2} + \frac{(y-0.1)^2}{0.2^2} + \frac{(z-0.1)^2}{0.3^2} - 1\right)\right) = 0. \quad (3.14)$$

This model has six umbilics of index  $+1/2$  and two of index  $-1/2$ . Notice that this complies with the Euler characteristic. One can also observe purple points and turning points.

Figure 3.17 features ridges of a Bezier patch, one can observe 1 and 3-ridge umbilics. This surface is the graph of the degree 4 polynomial  $h(u, v)$  for  $(u, v) \in [0, 1]^2$ :

$$h(u, v) = 116u^4v^4 - 200u^4v^3 + 108u^4v^2 - 24u^4v - 312u^3v^4 + 592u^3v^3 - 360u^3v^2 \quad (3.15)$$

$$+ 80u^3v + 252u^2v^4 - 504u^2v^3 + 324u^2v^2 - 72u^2v - 56uv^4 + 112uv^3 - 72uv^2 + 16uv. \quad (3.16)$$

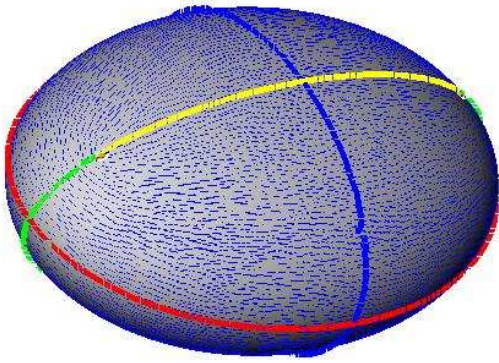


Figure 3.14: Umbilics, ridges, and principal blue foliation on the ellipsoid (10k points)

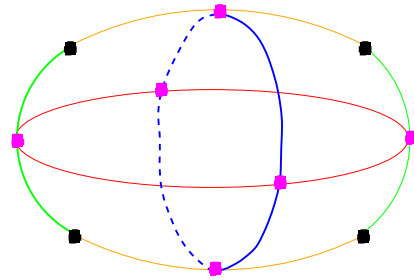


Figure 3.15: Schematic view of the umbilics and the ridges.

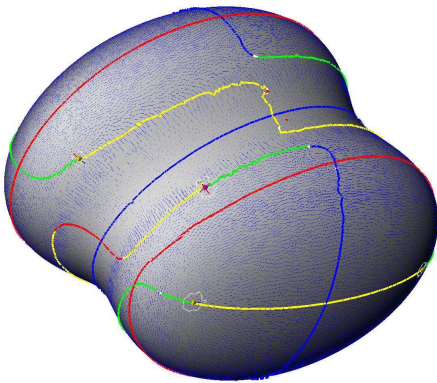


Figure 3.16: Implicit blending of two ellipsoids (40k points)

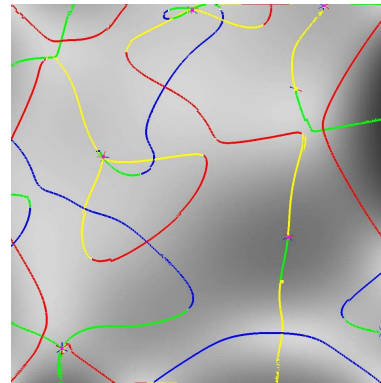


Figure 3.17: Ridges and umbilics on a Bezier patch (60k points)

## 3.5 Medial axis, skeleton, ridges

### 3.5.1 Medial axis of a smooth surface

The medial axis has an outstanding position in many communities and has been rediscovered several times. Example relevant citation are [Erd46, Hor83] in analysis, [Tho72, Mil80] in differential geometry, [Ser82, Ser88, BA91, BA92] in mathematical morphology. Since we just aim at presenting the local and global structure of the medial axis, we shall follow [BGG85, GK00], but the interested reader should also consult [Yom81].

Given a closed manifold  $S$  embedded in  $\mathbb{R}^3$ , the medial axis  $MA(S)$  consists of the points of the open set  $\mathbb{R}^3 \setminus S$  having two or more nearest points on  $S$ . A related notion is the skeleton of  $\mathbb{R}^3 \setminus S$ , which consists of the centers of maximal spheres included in  $\mathbb{R}^3 \setminus S$  —maximal for the inclusion amongst such spheres. For smoothly embedded manifolds, the closure of the medial axis is actually equal to the skeleton, which is why we just refer to the medial axis in the sequel. (Interestingly, applications such as surface reconstruction, which usually assume the surface to be reconstructed is smooth [AB99], do not distinguish between medial axis and skeleton.)

Having discussed the contact of a sphere with the surface, let us recall the classification of medial axis points and the corresponding *stratified* structure. While describing ridges, we actually cared more for the surface. For the medial axis, we change the perspective and care for the centers of the maximal spheres. When talking about a contact, one should therefore keep in mind that the corresponding sphere contributes its center to the medial axis.

Since we care for spheres intersecting the surface in an isolated point —otherwise the sphere is not contained in  $\mathbb{R}^3 \setminus S$ , the contact points must correspond to  $A_1^+$  and  $A_3^+$  singularities —refer to Def. 5 for the definition of the  $A_k^+$  types. Notice that an  $A_1^+$  singularity corresponds to a simple tangency. We shall drop the superscript and replace it by the *multiplicity* of the contact, that is  $A_1^k$  refers to a sphere having  $k$  separate  $A_1^+$  contacts. The medial axis points actually correspond to the following five cases:



- $A_1^4, A_1^3, A_1^2$  The sphere touches the surface at four, three or two points, and has a simple tangency at each contact point.  $A_1^4$  points are isolated points;  $A_1^3$  points lie on curves,  $A_1^2$  lie on sheets of the medial axis. Moreover, one has the following incidences. At an  $A_1^4$  point, six  $A_1^2$  sheets and four  $A_1^3$  curves meet. Along an  $A_1^3$  curve, three  $A_1^2$  sheets meet.
- $A_3^+$  The contact point is an elliptic ridge point. The corresponding medial axis points bound  $A_1^2$  sheets.
- $A_3^+ A_1$  The sphere has two contact points. The center of the sphere lies at the intersection between an  $A_1^3$  curve together with an  $A_3^+$  curve. This is where an  $A_1^2$  sheet vanishes.

An example consisting of a surface with two sheets is presented on Fig. 3.18. We describe it through a plane sweep from top to bottom. The top part consists of two sheets swept by two simple curves of roughly triangular and circular section. Then the inner contour vanishes so that we are left with the outer sheet which is roughly speaking a cylinder of triangular section. Then, section of the cylinder changes from triangular to elliptic. Eventually, the cylinder splits into two legs of elliptic sections. Near the top, the structure of the medial axis is that of a tetrahedron, with six  $A_1^2$  sheets and four  $A_1^3$  curves meeting. The boundary of each sheet consists of an  $A_3$  curve. When the section gets rounder, one  $A_2$  sheet vanishes at an  $A_3 A_1$  point.

There is an intuitive way to understand the preceding results, by counting separately the numbers of degrees of freedom and the number of constraints attached to a particular medial axis point. To see how, recall that a contact involves one sphere and one or more points on the surface. In terms of degrees of freedom (dof), a sphere yields four degrees of freedom, choosing a point on a surface is another two dof, and choosing a point on a curve drawn on a surface is one dof. In terms of constraints at the contact points, constraining a sphere to have an  $A_1$  contact imposes three constraints. (Indeed the tangent plane being set to that of the surface at  $p$ , we are left with the choice of the radius —which defines the pencil of spheres through the contact point.) Similarly, having an  $A_3$  contact imposes four degrees of freedom since the radius of the sphere has to be one of the principal curvatures. Let us now discuss the different cases:

- $A_1^2$  Having two contacts of order one imposes  $2 \cdot 3 = 6$  constraints. But choosing two points on  $S$  together with the contact spheres yields  $2 \cdot 2 + 4 = 8$  dof. One can expect  $A_1^2$  points to lie on sheets.
- $A_1^3$  Three  $A_1$  contacts define  $3 \cdot 3 = 9$  constraints, and  $3 \cdot 2 + 4 = 10$  dof.  $A_1^3$  points are expected to lie on curves.
- $A_1^4$  Four  $A_1$  yield  $4 \cdot 3 = 12$  constraints and  $4 \cdot 2 + 4 = 12$  dof. These medial axis points are expected to be isolated.
- $A_3$  Such a point yields 4 constraints. In terms of dof, we have two dof for the choice of the contact point, and three for the sphere with a radius equal to one of the principal radius of curvature.  $A_3$  contacts are therefore expected along curves.
- $A_3 A_1$  The contact points respectively yield  $4 + 3$  constraints. On the other hand, choosing one point along a curve, another on the surface, together with the dof of the sphere yield  $2 + 1 + 4$  dof. Such contacts are expected to be isolated.

### 3.5.2 Medial axis and ridges

Spheres centered on the boundary of the medial axis project onto elliptic ridge points of type  $A_3^+$  on the surface. But an elliptic ridge point can fail to be the contact of a point of the boundary of the MA in two cases: (i) if the limiting bitangent sphere crosses the surface away from the ridge point or (ii) if the surface is locally inside this sphere. (This latter case happens in elliptic regions for a positive minimum of  $k_2$  or a negative maximum of  $k_1$ ). In the first case, the sphere is not contained in  $\mathbb{R}^3 \setminus S$ , and in the second it is not maximal for inclusion.

Fig. 3.19 illustrated case (i), the lowest point is an elliptic ridge point but its bitangent sphere has a non local intersection with the curve. Fig. 3.14 illustrates case (ii), the blue elliptic ridge is the loci of negative maximum of  $k_1$ . The MA, which is an ellipsoid in the equatorial plane (spanned by the two longest principal axis of the ellipsoid), only gives birth to the red ridge (negative minimum of  $k_2$ ).



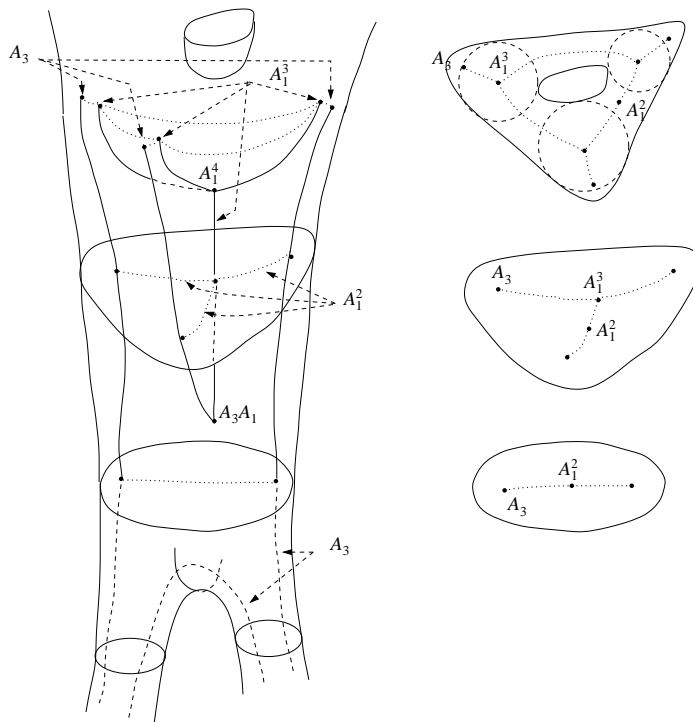


Figure 3.18: The stratified structure of the medial axis of a smooth surface

### 3.6 Topological equivalence between embedded surfaces

Having discussed delicate differential notions in the previous sections, we finish up with a seemingly simpler question: what is the right notion of equivalence for embedded surfaces of  $E^3$ , and what are sufficient conditions for two surfaces to be equivalent? Interestingly, the later question can be related to properties of the medial axis. We focus on surfaces embedded in  $E^3$ , orientable and without boundary, and which are either smooth —i.e. at least  $C^2$ — or piecewise linear.

#### 3.6.1 Homeomorphy, isotopy, ambient isotopy

A well known Theorem [Mas77][Thm 5.1] states that for surfaces, the genus characterizes the topology:

**Theorem. 7** *Two connected compact orientable surfaces without boundary are homeomorphic iff they have the same genus.*

Nevertheless, homeomorphy is not the relevant notion for topological equivalence of embedded surfaces. For example, a torus and a knotted torus are homeomorphic, while the two surfaces are obviously not equivalent as embedded surfaces of  $E^3$ . Intuitively, two surfaces are equivalent if one can continuously deform one into the other without introducing self-intersection. The natural notion is that of isotopy since it is an equivalence between embeddings. There are two slightly different notions: isotopy and ambient isotopy.

**Definition. 9** *Let  $S$  and  $S'$  be two surfaces embedded in  $E^3$ .*

- *$S$  and  $S'$  are isotopic if there is a continuous map  $F : S \times [0, 1] \rightarrow E^3$  such that  $F(., 0)$  is the identity of  $S$ ,  $F(S, 1) = S'$ , and for each  $t \in [0, 1]$ ,  $F(., t)$  is a homeomorphism onto its image.*
- *$S$  and  $S'$  are ambient isotopic if there is a continuous map  $F : E^3 \times [0, 1] \rightarrow E^3$  such that  $F(., 0)$  is the identity of  $E^3$ ,  $F(S, 1) = S'$ , and for each  $t \in [0, 1]$ ,  $F(., t)$  is a homeomorphism of  $E^3$ .*

In our study of compact surfaces embedded in  $E^3$ , the following theorem [Hir88][p.180] shows the equivalence of these two definitions, so we will merely speak of isotopy.

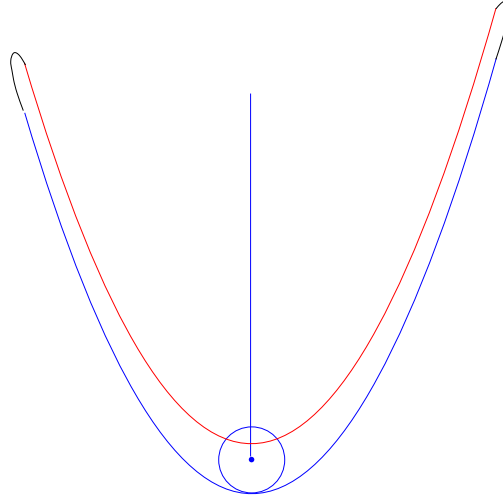


Figure 3.19: An extrema of curvature not image of the medial axis boundary

**Theorem. 8** Let  $S \subset M$  be a compact submanifold of  $M$  a manifold without boundary and  $F : S \times [0, 1] \rightarrow M$  an isotopy of  $S$ , then  $F$  extends to a ambient isotopy of  $M$ .

Isotopy between embedded surfaces is a topological characteristic of their embeddings, hence it does not interfere with the geometry. F. Chazal et al. [CCS04] give a purely topological condition for isotopy as well as applications to the concepts of medial axis and local feature size. They define the notion of topological thickening of a surface:

**Definition. 10** A topological thickening of  $S$  is a set  $M \subset E^3$  such that there exists a homeomorphism  $\Phi : S \times [0, 1] \rightarrow M$  satisfying  $\Phi(S \times \{1/2\}) = S \subset M$ .

The boundary of a topological thickening  $M$  of  $S$  thus is the union of  $\Phi(\partial S \times [0, 1])$  and two surfaces,  $\Phi(S, 0)$  and  $\Phi(S, 1)$ , which will be referred to as the sides of  $M$ . Another surface  $S'$  is said to separate the sides of  $M$  if one cannot go from one side to the other without crossing  $S'$  or leaving  $M$ . We are then able to state their main theorem and two corollaries:

**Theorem. 9** Suppose that  $S$  (resp.  $S'$ ) is included in a topological thickening  $M'$  of  $S'$  (resp.  $M$  of  $S$ ), and that  $S$  (resp.  $S'$ ) separates the sides of  $M'$  (resp.  $M$ ). Then  $S$  and  $S'$  are isotopic.

### 3.6.2 Geometric conditions for isotopy

Although isotopy is a topological property, sufficient conditions for isotopy can be obtained using geometric arguments, and in particular properties of the medial axis.

If  $S$  is smooth, for  $s \in S$ , the local feature size of  $s$  is defined as the Euclidean distance to the medial axis, that is  $\text{lfs}(s) = d(s, MA(S))$  —see [AB99]. (As observed in section 3.5, since the surface is smooth the medial axis is closed, so that the Euclidean distance is a minimum and not an infimum.) Moreover,  $\text{lfs}(S)$  is defined as the number  $\inf_{s \in S} d(s, MA(S))$ .  $S$  being at least  $C_2$ , one has  $\text{lfs}(S) > 0$  cf. [Fed59, Wol92]. The following is proved in [CCS04]:

**Corollary. 1** Let  $S$  and  $S'$  be compact orientable smooth surfaces without boundary.

- If each connected component of  $S$  (resp.  $S'$ ) encloses exactly one connected component of  $MA(S')$  (resp.  $MA(S)$ ), then  $S$  and  $S'$  are isotopic.
- If the Hausdorff distance  $H(S, S')$  between the two surfaces is such that  $H(S, S') < \min(\text{lfs}(S), \text{lfs}(S'))$ , then  $S$  and  $S'$  are isotopic.

Roughly speaking, one proves that  $S$  and  $S'$  are isotopic by first finding a neighborhood of  $S$  in  $E^3$  which contains  $S'$  and second deforming  $S'$  to  $S$  most of the time with the normal projection onto  $S$  in  $E^3$ .

Using the global bound  $\text{lfs}(S)$  and  $\varepsilon$ -neighborhoods, Sakkalis et al. [SP03] give a family of surfaces which are isotopic to  $S$ . Suppose  $S$  is smooth and oriented, for  $\rho \in \mathbb{R}$ ,  $S_\rho(\rho) = \{s + \rho n_s | s \in S\}$  is the offset surface of  $S$ . They show that for  $|\rho| < \text{lfs}(S)$  offset surfaces are smooth surfaces embedded in  $E^3$  and are isotopic to  $S$ . Moreover each point of the offset has a unique nearest point on  $S$ .

With the same kind of arguments, Amenta et al. [APR03] show the isotopy between a smooth surface and a piecewise linear approximation. More precisely, Amenta et al. [ACDL00] presented an algorithm to extract a piecewise linear surface  $T$  from the Delaunay triangulation of a  $\varepsilon$ -sample of  $S$ . The projection from  $T$  to its nearest point on  $S$  is a homeomorphism which is used to construct the isotopy. The advantage of this method is that the approximating surface needs not to stay in a  $\varepsilon$ -neighborhood globally defined.

### 3.7 Conclusion

We surveyed the notions of umbilics, lines of curvatures, foliations, ridges, medial axis, and topological equivalences for smooth embedded surfaces, with an emphasis on global structure theorems.

An important aspect which has been eluded is the dynamic case, that is the structure theorems valid if one replace a surface by say a one-parameter family of surfaces. Of particular interest in that case are the birth and death phenomena. These indeed feature transitions between patterns observed in the static case, and the time events between them are a measure of persistence of the objects involved. The reader is referred to [BG86, GK02, BGT96] [HGY<sup>+</sup>99][chap.7] for pointers in that direction concerning ridges and MA. Note that it does not make sense to study a single line of curvature dynamically. One has to consider the topology of the principal foliation instead, this is usually referred to as bifurcation theory, see [Tri02].

From a practical perspective, we expect this survey to provide incentives to develop certified algorithms for analysis and approximation of surface topology and geometry. In the following chapters, our algorithms for ridge extraction benefit from the theoretical results of this chapter.

### Acknowledgments

Abdelkrim Mebarki is acknowledged for producing the plots of Fig. 3.2 with his software `StreamLines_2`—to be released as a CGAL package.

## Chapter 4

# Estimating Differential Quantities using Polynomial fitting of Osculating Jets

This chapter addresses the point-wise estimation of differential properties of a smooth manifold  $S$  —a curve in the plane or a surface in  $3D$ — assuming a point cloud sampled over  $S$  is provided. The method consists of fitting the local representation of the manifold using a jet, and either interpolation or approximation. A jet is a truncated Taylor expansion, and the incentive for using jets is that they encode all local geometric quantities —such as normal, curvatures, extrema of curvature.

On the way to using jets, the question of estimating differential properties is recasted into the more general framework of multivariate interpolation / approximation, a well-studied problem in numerical analysis. On a theoretical perspective, we prove several convergence results when the samples get denser. For curves and surfaces, these results involve asymptotic estimates with convergence rates depending upon the degree of the jet used. For the particular case of curves, an error bound is also derived. To the best of our knowledge, these results are among the first ones providing accurate estimates for differential quantities of order three and more. On the algorithmic side, we solve the interpolation/approximation problem using Vandermonde systems. Experimental results for surfaces of  $\mathbb{R}^3$  are reported. These experiments illustrate the asymptotic convergence results, but also the robustness of the methods on general Computer Graphics models.

### 4.1 Introduction

#### 4.1.1 Estimating differential quantities

Several applications from Computer Vision, Computer Graphics, Computer Aided Design or Computational Geometry require estimating local differential quantities. Examples of such applications are surface segmentation, surface smoothing / denoising, surface reconstruction, shape design. In any case, the input consists of a point cloud or a mesh. Most of the time, estimating first and second order differential quantities, that is the tangent plane and curvature-related quantities, is sufficient. However, some applications involving shape analysis require estimating third order differential quantities [HGY<sup>+</sup>99, Por01].

Given these ubiquitous needs, a wealth of different estimators have been proposed in the vast literature of applied geometry [Pet01, GI04]. Most of these are adaptations to the discrete setting of smooth differential geometry results. For example, several definitions of normals, principal directions and curvatures over a mesh can be found in [Tau95, CW00]. Ridges of polyhedral surfaces as well as cuspidal edges of the focal sets are computed in [WB01]. Geodesics and discrete versions of the Gauss-Bonnet theorem are considered in [PS98].

Out of all these contributions, few of them address the question of the accuracy of the estimates proposed or that of their convergence when the mesh or the sample points get denser. This lack of sound theoretical analysis is however a major issue since discrete versions of smooth operators may not converge, or may converge to unexpected values. Examples of such phenomena are the surface area of a mesh which may not converge to that of the discretized surface [MT02], or the angular defect at a vertex of a triangulation which usually does not provide any information on the Gauss curvature of the underlying smooth surface [BCM02].

The estimation methods providing convergence guarantees are all concerned with first and second order differential quantities. In [AB99], an error bound is proved on the normal estimate to a smooth surface sampled according to a criterion involving the skeleton. The surface area of a mesh and its normal vector field versus those

of a smooth surface are considered in [MT02]. Asymptotic estimates for the normal and the Gauss curvature of a sampled surface for several methods are given in [MW00]. Based upon the normal cycle and restricted Delaunay triangulations, an estimate for the second fundamental form of a surface is developed in [CSM03].

Another striking fact about the estimation of first and second order differential quantities is that for plane curves, these quantities are often estimated using the osculating circle, while for surfaces, using osculating paraboloids is ubiquitous. Why not osculating parabolas for curves and osculating ellipsoids or hyperboloids for surfaces? Answering this question and developing estimation methods providing guarantees for third and higher order estimates motivates the following contributions.

### 4.1.2 Contributions and chapter overview

The main contribution of this chapter is to recast the problem of estimating differential properties to that of fitting the local representation of the manifold by a jet. A jet is a truncated Taylor expansion, and the incentive for using jets is that they encode all local geometric quantities —such as normal, curvatures, extrema of curvature. Accurate estimates of the coefficients of the jet therefore translate immediately to accurate estimates of differential quantities. Since the method proposed consists of performing a polynomial fitting, connections with the classical questions of interpolation and approximation deserve a careful discussion.

Interpolation is a well studied topics in numerical analysis. Most of the time however, the parameterization domain of interest is a subset of  $\mathbb{R}^n$ . In particular, convergence results on the coefficients of the Lagrange interpolation polynomial versus the Taylor expansion of a function are proved in [Coa66, CR72, QV94]. Our results differ from these in several concerns. On one hand, we are interested in interpolation *and* approximation over a manifold rather than a Euclidean domain. On the other hand, the afore-mentioned papers prove error bounds while we establish asymptotic error estimates. It should however be noticed that the dominant terms of these —as a function of the sampling density— are the same.

Regarding polynomial fitting of differential properties for a surface, our results are closely related to [MW00, Lemma 4.1]. In that article, a degree two interpolation is used and analyzed. We generalize this result for jets or arbitrary degree, under interpolation and approximation.

To complete the description, two comments are in order. First, it should emphasized that our focus is a local interpolation / approximation problem, that is we are *not* concerned with the convergence of the Lagrange interpolation polynomial to the height function on a whole given set. This problem requires specific conditions on the function and the position of the points, as illustrated by the Runge divergence phenomena [LS86, Chapter 2]. Therefore, our study is not to be confused with global fitting such as piecewise polynomial fitting encountered in CAD. Second, our focus is on the estimation of point-wise differential quantities and not the identification of loci of points exhibiting prescribed differential properties —examples of such loci are ridges or parabolic lines. While the former problem is local, the latter is global and therefore faces the issue of reporting loci with a global topological coherence.

The chapter is organized as follows. Fundamentals about jets and numerical issues are recalled in sections 4.2 and 4.3. The case of surfaces and curves are examined in sections 4.4 and 4.5. Finally, the overall algorithm together with experimental results are presented in sections 4.6 and 4.7.

## 4.2 Geometric pre-requisites

### 4.2.1 Curves and surfaces, height functions and jets

It is well known [dC76, Spi99a] that any regular embedded smooth<sup>1</sup> curve or surface can be locally written as the graph of a univariate or bivariate function with respect to any  $z$  direction that does not belong to the tangent space. We shall call such a function a *height function*. Taking an order  $n$  Taylor expansion of the height function over a curve yields:

$$f(x) = J_{B,n}(x) + O(x^{n+1}), \quad (4.1)$$

with

$$J_{B,n}(x) = B_0 + B_1x + B_2x^2 + B_3x^3 + \dots + B_nx^n. \quad (4.2)$$

---

<sup>1</sup>Regular means that the tangent space has dimension one/two for a curve/surface everywhere. Embedded forbids self-intersections. Smooth means as many times differentiable as we need, typically  $C^3$  or  $C^4$ .

Similarly for a surface:

$$f(x, y) = J_{B,n}(x, y) + O(\|(x, y)\|^{n+1}), \quad (4.3)$$

with

$$J_{B,n}(x, y) = \sum_{k=0}^n H_{B,k}(x, y), \quad H_{B,k}(x, y) = \sum_{j=0}^k B_{k-j,j} x^{k-j} y^j. \quad (4.4)$$

Notice that in Eq. (4.3), the term  $O(\|(x, y)\|^{n+1})$  stands for the remainder in Taylor's multivariate formula.

Borrowing to the jargon of singularity theory [BG92], the truncated Taylor expansion  $J_{B,n}(x)$  or  $J_{B,n}(x, y)$  is called a degree  $n$  jet, or  $n$ -jet. Since the differential properties of a  $n$ -jet match those of its defining curve/surface up to order  $n$ , the jet is said to have a  $n$  order contact with its defining curve or surface. This also accounts for the term *osculating jet*—although *osculating*<sup>2</sup> was initially meant for 2-jets. The degree  $n$ -jet of a curve involves  $n+1$  terms. For a surface, since there are  $i+1$  monomials of degree  $i$ , the  $n$ -jet involves  $N_n = 1 + 2 + \dots + (n+1) = (n+1)(n+2)/2$  terms. Notice that when the  $z$  direction used is aligned with the normal vector to the curve/surface, one has  $B_1 = 0$  or  $B_{1,0} = B_{0,1} = 0$ . The osculating  $n$ -jet encloses differential properties of the curve/surface up to order  $n$ , that is any differential quantity of order  $n$  can be computed from the  $n$ -jet. In particular, the tangent space can be computed from the 1-jet, the curvature related information can be obtained from the 2-jet,  $\dots$ . To clarify the presentation, we summarize as follows:

**Definition. 11** For a given point on a curve or surface and  $n \geq 1$ :

- given a coordinate system, the osculating  $n$ -jet is the Taylor expansion of the height function truncated at order  $n$ .
- the osculating  $n$ -jet is principal in a given coordinate system if the linear terms vanish (i.e. the  $z$ -axis is the normal direction of the manifold). Note that this is rather a property of the coordinate system which reads on the jet.
- an osculating conic/quadric is a conic/quadric whose 2-jet matches that of the curve/surface (independently of a given coordinate system).
- an osculating conic/quadric is degenerate if the quadratic form this conic/quadric is defined with is degenerate (that is the form does not have full rank).
- an osculating conic/quadric is principal if, in the given coordinate system, its  $n$ -jet is principal.

Degenerate osculating conics/quadrics are specific curves and surfaces since:

**Theorem. 10** [Ber87, Chapter 15] There are 9 Euclidean conics and 17 Euclidean quadrics.

**Observation. 5** The degenerate osculating conics to a smooth curve are parabola or lines. The degenerate osculating quadrics to a smooth surface are either paraboloids (elliptic, hyperbolic), parabolic cylinders, or planes.

Degenerate osculating conics and quadrics are therefore respectively 2 out of 9 conics and 4 out of 17 quadrics.

The Monge coordinate system of a curve is defined by its tangent and normal vectors. For a surface, the Monge coordinate system is such that the  $z$  axis is aligned with the normal and the  $x, y$  axis are aligned with the principal directions. Note that the  $n$ -jet is principal in the Monge coordinate system. The Monge form of the curve or surface at one of its points is the local Taylor expansion of the curve/surface in the Monge coordinate system. In this particular system, the height function is called the Monge form, and letting  $k_1, k_2$  stand for the principal curvatures, one has

$$f(x, y) = \frac{1}{2}(k_1 x^2 + k_2 y^2) + O(\|(x, y)\|^3). \quad (4.5)$$

From these observations, the question we ended paragraph 4.1.1 with can now be answered. By theorem 10 and observation 5, using a general conic/quadric or a degenerate one to approximate a curve or a surface does not make any difference. In both cases and up to order two, the local differential properties of the curve/surface, degenerate conic/quadric, or full rank conic/quadric are identical. All these local differential properties are enclosed in the 2-jet of the manifold. Yet, from a practical point of view, finding a conic/quadric requires more constraints than finding

<sup>2</sup>From the Latin *osculare*, to kiss.



a degenerate one since the latter reduces to a degree two polynomial fitting. Notice also that the normal direction to the manifold being a priori unknown, this polynomial fitting has to be performed in a coordinate system where the osculating jet is (in general) not principal.

As an example, consider Figure 4.1(a,b,c,d). Figure 4.1(a) features a curve  $C$  and an osculating conic<sup>3</sup>. In (b), the osculating circle is drawn, in (c), the osculating circle is replaced by the principal osculating parabola—whose symmetry axis is the normal to  $C$  and whose curvature matches that of  $C$ . At last, in (d) a general parabola locally approximates  $C$  in a coordinate system where the jet is not principal (its symmetry axis is not aligned with the normal to  $C$ ). This last case illustrates the setting we are working with in the sequel.

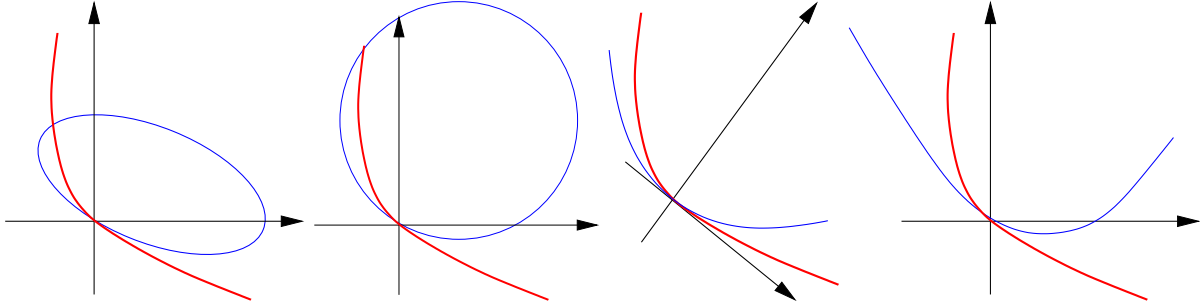


Figure 4.1: A curve and (a) an osculating ellipse, (b) its osculating circle (special case of osculating conic), (c) its principal degenerate conic, (d) an degenerate osculating conic: a parabola.

## 4.2.2 Interpolation, approximation and related variations

Our methodology to retrieve differential quantities consists of fitting the osculating jet of the manifold in a given coordinate system. The following variations need to be discussed in order to state our contributions precisely. The case of curves and surfaces being similar, our description focuses on surfaces. Assume we are given a set of  $N$  points  $p_i(x_i, y_i, z_i), i = 1, \dots, N$  in the neighborhood of a given point  $p$  on the surface processed. Point  $p$  itself may or may not be one of the  $N$  samples, and one can assume without loss of generality that  $p$  is located at the origin of the coordinate system used.

**Interpolation versus approximation.** Interpolating consists of finding a polynomial that fits exactly a set of data points. In our case and following Equation (4.3), let  $B$  index a coefficient of the jet of the surface, and  $A$  index a coefficient of the jet sought<sup>4</sup>. We aim at finding a degree  $n$  polynomial  $J_{A,n}$  such that

$$J_{A,n}(x_i, y_i) = f(x_i, y_i) = J_{B,n}(x_i, y_i) + O(\|(x_i, y_i)\|^{n+1}), \quad \forall i = 1, \dots, N. \quad (4.6)$$

Approximation, on the other hand, gives up on exactness, that is the graph of the polynomial sought may not contain the sample points. We shall focus on *least-square* approximation, which consists of minimizing the sum of the square errors between the value of the polynomial and that of the function. The quantity to be minimized is therefore

$$\sum_{i=1}^N (J_{A,n}(x_i, y_i) - f(x_i, y_i))^2. \quad (4.7)$$

The two problems can actually be written in the same matrix form. To see why, let us write the jets in the polynomial basis consisting of monomials  $x^i y^j$ . Examples of other bases that could be used are the Bezier-Bernstein basis or the Newton basis. We use the monomials since this basis is convenient for the asymptotic analysis but also the design of effective algorithms. Denote  $A$  the  $N_n$ -vector of the coefficients of the jet sought, that is

$$A = (A_{0,0}, A_{1,0}, A_{0,1}, \dots, A_{0,n})^t.$$

<sup>3</sup>A point worth noticing is the relative position of  $C$  and an osculating curve: the former usually crosses the latter at the intersection point. To see why, compare the order three Taylor expansions of the of two curves.

<sup>4</sup>As a mnemonic, the reader may want to remind that index  $A$  stands for the *Answer* to the fitting problem.

Denote  $Z$  the  $N$ -vector of the ordinates, i.e. with  $z_i = f(x_i, y_i)$ ,

$$Z = (z_1, z_2, \dots, z_N)^t = (J_{B,n}(x_i, y_i) + O(\|(x_i, y_i)\|^{n+1}))_{i=1, \dots, N}.$$

Equations (4.6) and (4.7) yield the following  $N \times N_n$  Vandermonde matrix

$$M = (1, x_i, y_i, x_i^2, \dots, x_i y_i^{n-1}, y_i^n)_{i=1, \dots, N}. \quad (4.8)$$

For the interpolation case, the number of points matches the number of parameters, so that matrix  $M$  is square and Eq. (4.6) can be written as  $MA = Z$ . For the approximation case,  $M$  is a rectangular  $N \times N_n$  matrix, and Eq. (4.7) is summarized as  $\min \|MA - Z\|_2$ .

Choosing between interpolation and approximation depends upon the problem tackled. For noisy datasets, approximation is the method of choice. Otherwise, the alternative depends of the relative values of the number of model parameters versus the number of available points. If the two match one-another, a natural choice is interpolation. In any case, fitting yields a linear system, so that numerical issues arise. Facing these difficulties is the topic of section 4.3.

**Mesh or mesh-less methods.** An important difference between local geometry estimation algorithms is whether or not they require some topological information—typically the connectivity of a mesh. Mesh-based methods are usually faster. Mesh-less techniques are more general and better suited for noisy datasets. A difficulty of the latter methods, however, is to select the relevant points used to perform the estimates. While one can always resort to heuristics of the  $k$ -nearest-neighbors type, user defined parameters should be avoided. This issue is addressed in section 4.6.

**One or two stages methods.** Fitting a 2-jet provides estimates of the tangent plane and the curvature related information. These steps can be carried out sequentially or simultaneously. Following the guideline of [SZ90], most of the methods already mentioned proceed sequentially. The provably good algorithm we propose proceeds simultaneously. Along its analysis, we also provide theoretical results on the accuracy of sequential methods.

### 4.2.3 Contributions revisited

Equipped with the language of jets, we can now state our contributions precisely. Consider Eqs. (4.6) and (4.7). We expect  $J_{A,n}$  and  $J_{B,n}$  to be equivalent in some sense. To specify this, we shall study the convergence properties of the coefficients of  $J_{A,n}$  when the points  $p_i$  converge to  $p$ . More precisely, assume that the coordinates of the  $p_i$  are given by  $p_i(x_i = a_i h, y_i = b_i h, z_i = f(x_i, y_i))$ . Parameters  $a_i$  and  $b_i$  are arbitrary real numbers, while  $h$  specifies that the  $p_i$  uniformly tend to the origin. We actually expect

$$A_{ij} = B_{ij} + O(r(h)).$$

Function  $r(h)$  describes the convergence rate or the precision of the fitting, and the main contribution of this chapter is to quantify  $r(h)$  for interpolation and approximation methods. This is done applying classical results of numerical analysis. These results are then translated for geometric quantities such as normal and curvatures. As we shall see, interpolation or approximation of the same degree yield the same convergence rate. The difficulties posed are also similar and are essentially to deal with singular matrices. This enables the design of an algorithm for the estimation of geometric quantities together with some knowledge about the quality of these estimates.

## 4.3 Numerical pre-requisites

In this section, we recall the fundamentals of the fitting methods used, namely interpolation and approximation, together with the numerical issues arising from the resolutions.

### 4.3.1 Interpolation

The interpolation fitting is based upon the Lagrange interpolation, that is the construction of a polynomial constrained to fit a set of data points. Although this problem is classical for the univariate case, the multivariate case is still an active research field from both the theoretical and computational points of view. We briefly review the univariate and multivariate basics of Lagrange interpolation.

**Univariate Lagrange interpolation.** Let  $X = \{x_0, \dots, x_n\}$  be  $n + 1$  distinct real values, the so-called *nodes*. Then, for any real function  $f$ , there is a unique polynomial  $P$  of degree  $n$  so that  $P(x_i) = f(x_i)$ ,  $\forall i = 0, \dots, n$ . Polynomial  $P$  is called the *Lagrange interpolation polynomial* of  $f$  at the nodes  $X$ . For any choice of distinct nodes, this polynomial exists and is unique, and in that case the Lagrange interpolation is said to be *poised*.

**Multivariate Lagrange interpolation.** Consider now the following bivariate problem. Let  $\Pi_n$  be the subspace of bivariate polynomials of total degree equal or less than  $n$ , whose dimension is  $N_n = \binom{n+2}{n}$ , and let  $X = \{x_1, \dots, x_N\}$  consist of  $N = N_n$  values in  $\mathbb{R}^2$  called nodes. (Notice that  $N$  is exactly the number of monomials found in the jet of Equation 4.3.) The Lagrange interpolation problem is said to be *poised* for  $X$  if for any function  $f : \mathbb{R}^2 \rightarrow \mathbb{R}$ , there exists a unique polynomial  $P$  in  $\Pi_n$  so that  $P(x_i) = f(x_i)$ ,  $\forall i = 1, \dots, N$ . It is intuitive and well known that this problem is *poised* iff the set of nodes  $X$  is not a subset of any algebraic curve of degree at most  $n$ , or equivalently the Vandermonde determinant formed by the interpolation equations does not vanish. As noticed in [SX95], the set of nodes for which the problem is not *poised* has measure zero, hence it is almost always *poised*.

However let us illustrate non-poised cases or degenerate configurations of nodes, together with almost degenerate configurations—a more precise definition will be given with the conditioning in section 4.3.3. Consider the two quadrics  $q_1(x, y, z) = 2x + x^2 - y^2 - z$  and  $q_2(x, y, z) = x^2 + y^2 - z$ , whose intersection curve  $I$  projects in the  $(x, y)$  plane to the conic  $C(x, y) = 0$  with  $C(x, y) = x - y^2$  (cf. Fig. 4.2). If one tries to interpolate a height function using points on  $I$ , uniqueness of the interpolant is not achieved since any quadric in the pencil of  $q_1$  and  $q_2$  goes through  $I$ . A similar example featuring the four one-ring and one two-ring neighbors of a point  $p$  is depicted on figure 4.3. Notice that being able to figure out such configurations is rather a strength than a weakness of the method since a surface is sought and, the amount of information available does not determine uniquely such a surface. A first fundamental difference between the univariate and multivariate cases is therefore the critical issue of choosing nodes so that the interpolation is *poised*.

In the particular case where the points lie on a regular square grid of the plane, the geometry of the configuration leads to the following remarks. On one hand, a non-poised degree  $n$  interpolation occurs if the points lie on  $n$  lines, since they define an algebraic curve of degree  $n$ . On the other hand, triangular lattices yield *poised* problems for every degree. These results and further extensions can be found in [GS00] and references therein.

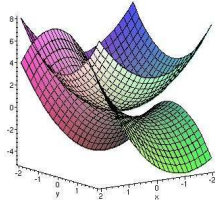


Figure 4.2: Two quadrics whose intersection curve  $I$  projects onto the parabola  $C : x = y^2$ . Interpolation points located on  $I$  do not uniquely define an interpolating height function.

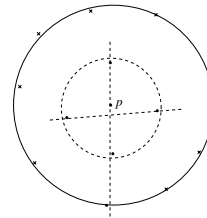


Figure 4.3: The Kite (almost) degenerate configuration—tangent plane seen from above: the 6 points used for a degree two interpolation are (almost) located on a conic, that is two intersecting lines.

### 4.3.2 Least square approximation

It is well known that the minimization problem of Eq. (4.7) has a unique solution iff the matrix  $M$  is of maximum rank  $N_n$ . In that case, the minimum value  $\rho$  is called the *residual* of the system, that is  $\rho = \min \|MA - Z\|_2$ . The important issue is again the rank of the matrix  $M$ . In terms of the relative values of  $N$  versus  $N_n$ , using too many points certainly smoothes out geometric features, but also makes rank deficient matrices less likely.

### 4.3.3 Numerical Issues

The difficulties of solving linear and least-squares systems consist of dealing with rank-deficient matrices. We now discuss these issues in more detail. Distances between matrices and matrix norms refer to the Euclidean norm.

**Singular systems and condition numbers.** To quantify degeneracies, we resort to a Singular Value Decomposition (SVD) [GvL83]. Denote  $\sigma_n, \dots, \sigma_1$  the singular values of  $M$  sorted in decreasing order. It is well known that

the least singular value of  $M$  is the distance from  $M$  to rank deficient matrices. The singular values also characterizes the sensitivity of the problem, that is the way errors on the input data induce errors on the computed solution. Notice that errors refer to the uncertainty attached to the input data and not to the rounding errors inherent to the floating point calculations. In our case, input data are the sample points, so that errors are typically related to the acquisition system —e.g. a laser range scanner.

To quantify the previous arguments, we resort to the *conditioning* or *condition number* of the system [GvL83, Hig96]. The conditioning is defined as a magnification factor which relates the afore-mentioned errors by the following rule  $\text{Error on solution} = \text{Error on input} \times \text{conditioning}$ . Denote

$$\kappa_2(M) = \|M\|_2 \|M^{-1}\|_2 = \sigma_n / \sigma_1$$

the condition number of the matrix  $M$ . The conditioning of the linear problem  $MX = Z$  and the least square problem  $\min \|MX - Z\|_2$  are respectively given by

$$\begin{cases} \text{linear square system:} & 2\kappa_2(M), \\ \text{least square system:} & 2\kappa_2(M) + \frac{\kappa_2(M)(\kappa_2(M)+1)\rho}{\|M\|_2 \|X\|_2} \text{ with } \rho = \|MX - Z\|_2 \text{ the residual.} \end{cases} \quad (4.9)$$

The following theorem provides precise error bounds:

**Theorem. 11** ([Hig96] p. 133 and 392) *Suppose  $X$  and  $\tilde{X}$  are the solutions of the problems*

$$\begin{cases} \text{linear square system:} & MX = Z \text{ and } (M + \Delta M)\tilde{X} = Z + \Delta Z, \\ \text{least square system:} & \min \|MX - Z\|_2 \text{ and } \min \|(M + \Delta M)\tilde{X} - (Z + \Delta Z)\|_2, \end{cases} \quad (4.10)$$

with  $\varepsilon$  a positive real value such that  $\|\Delta M\|_2 \leq \varepsilon \|M\|_2$ ,  $\|\Delta Z\|_2 \leq \varepsilon \|Z\|_2$ , and  $\varepsilon \kappa_2(M) < 1$ . Then one has:

$$\frac{\|X - \tilde{X}\|_2}{\|X\|_2} \leq \frac{\varepsilon}{1 - \kappa_2(M)\varepsilon} \text{ conditioning.} \quad (4.11)$$

In practice, if the conditioning is of order  $10^a$  and the relative error on the input is  $\varepsilon \approx 10^{-b}$  — with  $\varepsilon \kappa_2(M) < 1$ , then the relative error on the solution is of order  $10^{a-b}$ .

**Pre-conditioning the Vandermonde system.** As already discussed, a convenient way to solve Eqs. (4.6) and (4.7) consists of using the basis of monomials. One ends up with the Vandermonde matrix of Eq. (4.8), that can be solved with usual methods of linear algebra. Unfortunately, Vandermonde systems are known to be ill-conditioned due to the change of magnitude of the terms. We therefore pre-condition so as to improve the condition number. Assuming the  $\{x_i\}$ ,  $\{y_i\}$  are of order  $h$ , the pre-conditioning consists of performing a column scaling by dividing each monomial  $x_i^k y_i^l$  by  $h^{k+l}$ .

The new system is  $M'Y = MDY = Z$  with  $D$  the diagonal matrix  $D = (1, h, h, h^2, \dots, h^n, h^n)$ , so that the solution  $A$  of the original system is  $A = DY$ . The condition number used in the sequel is precisely  $\kappa(M')$ . (Notice it has the geometric advantage to be invariant under homothetic transformations of the input points.) Then the accuracy of the result can be estimated a posteriori, and almost degenerate cases hight-lighted by large conditioning.

**Alternatives for the interpolation case.** An alternative to the Vandermonde system consists of using the basis of Newton polynomials. Resolution of the system can be done using divided differences [Sau95], a numerically accurate yet instable method [Hig96].

## 4.4 Surfaces

### 4.4.1 Problem addressed

Let  $S$  be a surface and  $p$  be a point of  $S$ . Without loss of generality, we assume  $p$  is located at the origin and we aim at investigating differential quantities at  $p$ . Consider the height function  $f$  given by Equation (4.3) in any coordinate system whose  $z$  axis is not in the tangent plane. We shall interpolate  $S$  by a bivariate  $n$ -jet  $J_{A,n}(x,y)$  whose graph is denoted  $Q$ .

The normal to a surface given by Equation (4.3) is

$$n_S = (-B_{10}, -B_{01}, 1)^t / \sqrt{1 + B_{10}^2 + B_{01}^2}. \quad (4.12)$$

In order to characterize curvature properties, we resort to the Weingarten map  $A$  of the surface also called the shape operator, that is the tangent map of the Gauss map. (Recall that the first and second fundamental forms  $I, II$  and  $A$  satisfy  $II(v, v) = I(A(v), v)$  for any vector  $v$  of the tangent space.) The principal curvatures and principal directions are the eigenvalues (eigenvectors) of  $A$ , and the reader is referred to [dC76, Section 3.3]. If the  $z$  axis is aligned with the normal, the linear terms of Equation (4.3) vanish, and the second fundamental form reduces to the Hessian of the height function. Further simplifications are obtained in the Monge coordinate system, where  $I = Id_2$ , the Hessian is a diagonal matrix, and the principal curvatures are given by  $2B_{20}$  and  $2B_{02}$ .

#### 4.4.2 Polynomial fitting of the height function

We begin by an approximation result on the coefficients of the height function. We focus on the convergence rate given by the value of the exponent of parameter  $h$ .

**Proposition. 2** *Let  $\{(x_i, y_i)\}_{i=1, \dots, N}$  be a set of points of  $\mathbb{R}^2$  defining a poised polynomial interpolation or approximation problem of degree  $n$ , with  $x_i = O(h), y_i = O(h)$  ( $N = N_n$  for interpolation and  $N > N_n$  for approximation). Let  $J_{A,n}$  be the degree  $n$  polynomial solution of the problem associated to the function  $f$  that is, for interpolation*

$$J_{A,n}(x_i, y_i) = f(x_i, y_i), \quad \forall i = 1, \dots, N;$$

and for approximation

$$J_{A,n} = \arg \min \left\{ \sum_{i=1}^N (J_{A,n}(x_i, y_i) - f(x_i, y_i))^2 \right\}.$$

Then the coefficients  $B_{k-j,j}$  of degree  $k$  of the Taylor expansion of  $f$  are estimated by those of  $J_{A,n}$  up to accuracy  $O(h^{n-k+1})$ :

$$A_{k-j,j} = B_{k-j,j} + O(h^{n-k+1}) \quad \forall k = 0, \dots, n \quad \forall j = 0, \dots, k.$$

Moreover, if the origin is one of the chosen points and interpolation is used, then  $A_{0,0} = B_{0,0} = 0$ .

*Proof.* [Proof of Prop. 2, interpolation case.] Let  $K$  be the convex hull of the set  $\{(x_i, y_i)\}_{i=1, \dots, N}$ ,  $d_{max}$  be the diameter of  $K$  and  $d_{min}$  be the supremum of the diameter of disks inscribed in  $K$ . Also denote  $D^k$  is the differential of order  $k$ .

The result is a direct consequence of Theorem 2 of [CR72] or remark 3.4.2 of [QV94], which states that

$$\sup \{ \|D^k f(x, y) - D^k J_{A,n}(x, y)\|; (x, y) \in K \} = O(h^{n-k+1}). \quad (4.13)$$

Rephrasing it with our notations yields:

$$\begin{aligned} |B_{k-j,j} - A_{k-j,j}| &= \frac{1}{j!(k-j)!} |D^k (f - J_{A,n})_{(0,0)}(1, 0)^{k-j} (0, 1)^j| \\ &\leq \sup \{ \|D^k (f - J_{A,n})_{(0,0)}(\zeta_1, \dots, \zeta_k)\|; \zeta_i \in \mathbb{R}^2, \|\zeta_i\| \leq 1 \} \\ &\leq \|D^k (f - J_{A,n})_{(0,0)}\| \\ &\leq \sup \{ \|D^k f(x, y) - D^k J_{A,n}(x, y)\|; (x, y) \in K \}. \end{aligned}$$

For the particular case where the origin is one of the samples, notice that the equation involving the point  $(0, 0)$  is  $A_{0,0} = f(0, 0) = 0$ .  $\square$

As outlined by the proof, the constant hidden in the term  $O(h^{n-k+1})$  depends upon  $\sup \{ \|D^{n+1} f(x, y)\|; (x, y) \in K \}$ , and the geometry of  $K$ . In particular, the estimates are better when the ratio  $d_{max}/d_{min}$  is small, which intuitively means that the set  $K$  is not too “flat”.

For the approximation case, the result might be a consequence of the theorem 5 of [CR72] formulated in the Sobolev setting. But in order to meet its hypothesis, one must prove that the operator of discrete least square approximation is continuous, which is not straightforward. Alternatively, we give the following pedestrian proof.

*Proof.* [Proof of Prop. 2, approximation case.]

Using the notations introduced in section 4.2.2, consider the least-square system  $\min \|MA - Z\|_2$ . With the assumption that  $M$  is of rank  $N_n$ , the approximation is equivalent to the invertible linear system  $M^T M A = M^T Z$ . With the notation  $\Sigma_i^k = \sum_{i=1}^N x_i^k y_i^l$  and the assumption  $\|(x_i, y_i)\| = O(h)$ :

$$M^T Z = \begin{pmatrix} B_{0,0}\Sigma_0^0 + B_{1,0}\Sigma_0^1 + B_{0,1}\Sigma_1^0 + \dots & +B_{0,n}\Sigma_n^0 + O(h^{n+1}) \\ B_{0,0}\Sigma_0^1 + \dots & +B_{0,n}\Sigma_n^1 + O(h^{n+2}) \\ B_{0,0}\Sigma_0^0 + \dots & +O(h^{n+2}) \\ \vdots & \vdots \\ B_{0,0}\Sigma_n^0 + \dots & +O(h^{n+n+1}) \end{pmatrix}$$

$$M^T M = \begin{pmatrix} \Sigma_0^0 & \Sigma_0^1 & \Sigma_0^0 & \dots & \Sigma_n^0 \\ \Sigma_0^1 & \Sigma_0^2 & \Sigma_1^1 & \dots & \Sigma_n^1 \\ \Sigma_1^0 & \Sigma_1^1 & \Sigma_2^0 & \dots & \Sigma_{n+1}^0 \\ \vdots & \vdots & \vdots & \vdots & \vdots \\ \Sigma_n^0 & \Sigma_n^1 & \Sigma_{n+1}^0 & \dots & \Sigma_{2n}^0 \end{pmatrix}$$

Let  $D$  be  $\det(M^T M)$ , applying the Cramer's rule gives:

$$A_{j,k-j} = \det \begin{pmatrix} \Sigma_0^0 & \dots & B_{0,0}\Sigma_0^0 + B_{1,0}\Sigma_0^1 + B_{0,1}\Sigma_1^0 + \dots + B_{0,n}\Sigma_n^0 + O(h^{n+1}) & \dots & \Sigma_n^0 \\ \Sigma_0^1 & \dots & B_{0,0}\Sigma_0^1 + \dots + B_{0,n}\Sigma_n^1 + O(h^{n+2}) & \dots & \Sigma_n^1 \\ \Sigma_1^0 & \dots & B_{0,0}\Sigma_1^0 + \dots + O(h^{n+2}) & \dots & \Sigma_{n+1}^0 \\ \vdots & \vdots & \vdots & \vdots & \vdots \\ \Sigma_n^0 & \dots & B_{0,0}\Sigma_n^0 + \dots + O(h^{n+n+1}) & \dots & \Sigma_{2n}^0 \end{pmatrix} / D$$

Linear combinations of the columns gives:

$$A_{j,k-j} = \det \begin{pmatrix} \Sigma_0^0 & \dots & B_{j,k-j}\Sigma_{k-j}^j + O(h^{n+1}) & \dots & \Sigma_n^0 \\ \Sigma_0^1 & \dots & B_{j,k-j}\Sigma_{k-j}^{j+1} + O(h^{n+2}) & \dots & \Sigma_n^1 \\ \Sigma_1^0 & \dots & B_{j,k-j}\Sigma_{k-j+1}^j + O(h^{n+2}) & \dots & \Sigma_{n+1}^0 \\ \vdots & \vdots & \vdots & \vdots & \vdots \\ \Sigma_n^0 & \dots & B_{j,k-j}\Sigma_{k-j+n}^j + O(h^{n+n+1}) & \dots & \Sigma_{2n}^0 \end{pmatrix} / D$$

The numerator of this formula splits due to the multi-linearity of the determinant, and noticing that  $\Sigma_i^k = O(h^{k+1})$  gives  $A_{j,k-j} = B_{j,k-j} + O(h^{n-k+1})$ .  $\square$

With respect to the order of convergence, it is equivalent to performing the fitting in any coordinate system. Nevertheless, as noted above, the error estimates are better if the convex hull of the sample points is not too flat. Consequently, it means that for the best estimates one should take a coordinate system as close as possible to the Monge system. Using the previous proposition, the order of accuracy of a differential quantity is easily related to the degree of the interpolant and the order of this quantity. More precisely:

**Theorem. 12** *A polynomial fitting of degree  $n$  estimates any  $k^{\text{th}}$ -order differential quantity to accuracy  $O(h^{n-k+1})$ . In particular:*

- *the coefficients of the first fundamental form and the unit normal vector are estimated with accuracy  $O(h^n)$ , and so is the angle between the normal and the estimated normal.*
- *the coefficients of the second fundamental form and the shape operator are approximated with accuracy  $O(h^{n-1})$ , and so are the principal curvatures and directions (as long as they are well defined, i.e. away from umbilics).*

*Proof.* It is easily checked that the formula corresponding to the geometric quantities (as long as they are well defined) are  $C^1$  functions of the coefficients. The result follows from proposition 2 and lemma 1 below.  $\square$

**Lemma. 1** *Define a  $k^{\text{th}}$ -order differential quantity—for a curve or a surface—as a  $C^1$  function  $F$  of the coefficients of the  $k$ -jet of the height function. Also assume that a degree  $n$  fitting yields a precision  $A_j = B_j + O(h^{n+1-j})$ ,  $k = 1, \dots, n$  for a curve, and  $A_{k-j,j} = B_{k-j,j} + O(h^{n-k+1})$ ,  $j = 0, \dots, n$ ,  $k = 0, \dots, n$  for a surface.*

*Then, a polynomial fitting of degree  $n$  estimates a  $k^{\text{th}}$ -order differential quantity to accuracy  $O(h^{n-k+1})$ .*



*Proof.* The proof is the same for curves and surfaces, and we use the notations corresponding to a curve.

To begin with, we perform a substitution on the error terms in the expression of  $F$ :

$$F((A_i)_{i=0,\dots,k}) = F((B_i + O(h^{n-i+1}))_{i=0,\dots,k}) = F((B_i + O(h^{n-k+1}))_{i=0,\dots,k}).$$

Since  $F((B_i)_{i=0,\dots,k})$  is a  $C^1$  function, and denoting  $DF_p$  the differential of  $F$  at point  $p$ , an order one Taylor formula yields:

$$\begin{aligned} F((B_i + O(h^{n-k+1}))_{i=0,\dots,k}) &= F((B_i)_{i=0,\dots,k}) + DF_{(B_i + uO(h^{n-k+1}))_{i=0,\dots,k}}(O(h^{n-k+1}), \dots, O(h^{n-k+1}))^t, u \in ]0, 1[ \\ &= F((B_i)_{i=0,\dots,k}) + O(h^{n-k+1}). \end{aligned}$$

□

The previous theorem generalizes [MW00, Lemma 4.1] where 2-jet interpolations only are studied. The  $O(h^n)$  bound on the normal should also be compared to the estimate of the normal vector using specific Voronoi centers called poles considered in [AB99]. The error bound proved there is equivalent to  $2\varepsilon$  with  $\varepsilon$  the sampling density of the surface. Letting lfs stand for *local feature size*, setting  $h = \varepsilon \text{lfs}$  and assuming lfs is bounded from above, the estimation stemming from a polynomial fitting therefore yields more accurate results for the tangent plane, and also provides information on higher order quantities.

### 4.4.3 Influence of normal accuracy on higher order estimates

Following the guideline initiated in [SZ90] several algorithms first estimate the normal to the surface and then proceed with Hessian of the height function. We analyze the error incurred by the latter as a function of the accuracy on the former. We denote  $\theta$  the angle between the normal  $n_S$  to the surface and the normal  $n_Q$  estimated by the two-stages method. In order to simplify calculations, we assume that  $n_Q$  is aligned with the  $z$ -axis and  $n_S$  is in the  $(x, z)$ -plane, so that  $f(x, y) = B_{10}x + B_{20}x^2 + B_{11}xy + B_{02}y^2 + O(\|(x, y)\|^3)$ , with  $B_{10} = -\tan \theta$ . Expressed in the same coordinate system, the interpolant—a 2-jet to simplify calculations—reads as  $J_{A,2}(x, y) = A_{20}x^2 + A_{11}xy + A_{02}y^2$ .

**Proposition. 3** *If a small error  $\theta$  is done on the estimated normal, a 2-jet interpolation gives the Gauss curvature with a linear error with respect to  $\theta$ :*

$$k_Q - k_S = \theta O(h^{-1}) + O(h) + O(\theta^2).$$

*Proof.* The system of equations for the interpolation is:

$$A_{2,0}x_i^2h + A_{1,1}x_iy_i + A_{0,2}y_i^2 = B_{1,0}x_i + B_{2,0}x_i^2 + B_{1,1}x_iy_i + B_{0,2}y_i^2 + O(\|(x_i, y_i)\|^3) \quad i = 1, \dots, 3.$$

Let  $D$  be the determinant:  $D = \det(x_i^2, x_iy_i, y_i^2)_{i=1,\dots,3}$ , Cramer's rule gives:

$$\begin{aligned} A_{2,0} &= \det(B_{1,0}x_i + B_{2,0}x_i^2 + B_{1,1}x_iy_i + B_{0,2}y_i^2 + O(\|(x_i, y_i)\|^3), x_iy_i, y_i^2)_{i=1,\dots,3}/D \\ &= B_{1,0}O(h^{-1}) + B_{2,0} + O(h). \end{aligned}$$

Similar calculations gives:  $A_{1,1} = B_{1,0}O(h^{-1}) + B_{1,1} + O(h)$ , and  $A_{0,2} = B_{1,0}O(h^{-1}) + B_{0,2} + O(h)$ . The Gaussian curvature of  $Q$  is then:

$$\begin{aligned} k_Q &= \frac{4A_{2,0}A_{0,2} - A_{1,1}^2}{1 + A_{1,0}^2} \\ &= 4A_{2,0}A_{0,2} - A_{1,1}^2 \\ &= 4(B_{1,0}O(h^{-1}) + B_{2,0} + O(h))(B_{1,0}O(h^{-1}) + B_{0,2} + O(h)) - (B_{1,0}O(h^{-1}) + B_{1,1} + O(h))^2 \\ &= 4B_{2,0}B_{0,2} - B_{1,1}^2 + B_{1,0}O(h^{-1}) + B_{1,0}^2O(h^{-2}) + O(h) \\ &= 4B_{2,0}B_{0,2} - B_{1,1}^2 + \tan \theta O(h^{-1}) + \tan^2 \theta O(h^{-2}) + O(h). \end{aligned}$$

The Gaussian curvature of  $S$  is

$$k_S = \frac{4B_{2,0}B_{0,2} - B_{1,1}^2}{(1 + B_{1,0}^2)^2} = \frac{4B_{2,0}B_{0,2} - B_{1,1}^2}{(1 + \tan^2 \theta)^2} = (4B_{2,0}B_{0,2} - B_{1,1}^2) \cos^4 \theta.$$

Thus the error on the curvature is:

$$\begin{aligned} k_Q - k_S &= (4B_{2,0}B_{0,2} - B_{1,1}^2) \cos^4 \theta + \tan \theta O(h^{-1}) + \tan^2 \theta O(h^{-2}) + O(h) \\ &= \theta O(h^{-1}) + O(h) + O(\theta^2). \end{aligned}$$

□

For a fixed  $h$ , the curvature error is a linear function of the angle between the normals. The term  $\theta O(h^{-1})$  shows that if  $\theta$  is fixed, the smaller  $h$  the worse the accuracy. Hence estimating the normal deserves specific care.

## 4.5 Plane Curves

All the results proved for surfaces in the previous section can also be proved for curves, and we omit them. Instead, for the interpolation case, we prove an error bound between the coefficients of the curve and those of the jet.

### 4.5.1 Problem addressed

Let  $C$  be a curve, and consider the height function  $f$  following Equation (4.1) in any coordinate system whose  $y$  axis is not tangent to the curve and, whose origin is on the curve (this implies that  $B_0 = 0$ ). We shall fit  $C$  by a  $n$ -jet  $J_{A,n}(x)$ . As already mentioned, there are  $n + 1$  unknown coefficients  $A_i$ , we assume  $N$  data points  $P_i(x_i = a_i h, y_i = f(x_i))$  are given, where  $N = n + 1$  for interpolation fitting. Notice again that parameter  $h$  specifies the uniform convergence of these data points to the origin. The fitting equations are:

$$y_i = f(x_i) = J_{B,n}(x_i) + O(x_i^{n+1}) = J_{A,n}(x_i).$$

Since curve  $C$  is given by Equation (4.1), the normal and the curvature of  $C$  at the origin are given by

$$n_C = (-B_1, 1)^t / \sqrt{1 + B_1^2}, \quad k_C = 2B_2 / (1 + B_1^2)^{\frac{3}{2}}. \quad (4.14)$$

Moreover, in the Monge coordinate system  $-B_1 = 0$ , these expressions simplify to  $n_C = (0, 1)^t$  and  $k_C = 2B_2$ .

### 4.5.2 Error bounds for the interpolation

The equivalent of Prop. 2 for curves gives the magnitude of the accuracy of the interpolation. We can actually be more precise and provide error bounds depending upon the function interpolated and the position of the interpolation points.

**Proposition. 4** Consider a degree  $n$  ( $n \geq 1$ ) interpolation problem for a curve  $y = f(x)$ . Let  $h$  be a positive number so that the interpolation point abscissa lie in the interval  $[-h, h]$ , and  $c = \sup_{x \in [-h, h]} |f^{(n+1)}(x)|$ . Then for  $k = 0, \dots, n$ :

$$|A_k - B_k| \leq \frac{h^{n-k+1} c}{k!(n-k+1)!}.$$

*Proof.* This result is a simple application of the analysis of the Lagrange interpolation remainder which can be found in [EK66]. Let  $R_n(x) = f(x) - J_A(x)$ , theorem 1 p.289 states that  $\forall k = 0, \dots, n$  and  $\forall x \in [-h, h]$ :

$$R_n^{(k)}(x) = \prod_{j=0}^{n-k} (x - \xi_j) \frac{f^{(n+1)}(\eta)}{(n+1-k)!}$$

with  $x, \xi_j, \eta \in [-h, h]$ .

For  $x = 0$ , this leads to:

$$\begin{aligned} |R_n^{(k)}(0)| &= |k!A_k - k!B_k| \leq \frac{h^{n-k+1} c}{(n-k+1)!} \\ |A_k - B_k| &\leq \frac{h^{n-k+1} c}{k!(n-k+1)!} \end{aligned}$$

□

Here is an application of the previous result. Let  $\theta$  denote the angle between the normal and the estimated normal. We have  $\sin(\theta) = \|n_Q \wedge n_C\| = |A_1 - B_1| / \sqrt{(1 + A_1^2)(1 + B_1^2)} \leq |A_1 - B_1|$ . It is found that

$$\theta \leq \arcsin\left(\frac{h^n c}{n!}\right).$$

## 4.6 Algorithm

The fitting algorithm to estimate the differential properties at a point  $p$  consists of (i)collecting the  $N$  points used for the fitting. (Recall that a  $n$ -jet involves  $N_n = (n + 1)(n + 2)/2$  coefficients, so that when interpolating (approximating) we assume  $N = N_n$  ( $N > N_n$ )). (ii)solving the linear system (iii)recovering the differential properties.

We examine in turn the details of these three steps.

### 4.6.1 Collecting $N$ neighbors

**The mesh case.** Although no topological information is required by the fitting method, the connectivity information of a mesh can be used as follows. We sequentially visit the one-ring neighbors, two-ring neighbors, and so on until  $N$  points have been collected. Let  $R_1, \dots, R_k$  be the  $k$  rings of neighbors necessary to collect  $N$  neighbors. All the points of the  $k - 1$  first rings are used. The complement up to  $N$  points is chosen arbitrarily out of the  $k$ th ring.

**The point-cloud case.** The normal at  $p$  is first estimated, and the neighbors of  $p$  are further retrieved from a power diagram in the estimated tangent plane [BF02] —a provably good procedure if the samples are dense enough. If the number of neighbors collected is less than  $N$ , we recursively collect the neighbors of the neighbors.

Collecting the points therefore boils down to estimating the tangent plane. One solution is to construct the Voronoi diagram of the point set and use these Voronoi vertices called *poles* [AB99]. Poles yield an accurate estimate of the normal vector but require a global construction.

An alternative is to resort to the algorithm of section 4.4, and solve a degree one interpolation problem —which requires three points and is well poised as soon as the three points are not collinear. Geometrically, the closer the three points to being aligned, the more unstable the tangent plane estimate. To see how one can get around this difficulty, denote  $q$  the nearest neighbor of  $p$ . Also, let  $r$  be the sample point so that the circum-radius  $r_{circ}$  of the triangle  $pqr$  is minimum. The estimated normal at  $p$  is the normal to the plane through  $pqr$ . Intuitively, minimizing the circum-radius  $r_{circ}$  prevents two difficulties: on one hand triangles with a large angle (near to  $\pi$ ) exhibit a large circum-circle and are discarded; on the other hand, triangles involving a third point  $r$  which is not a *local* neighbor of  $p$  cannot minimize  $r_{circ}$  and are also discarded. A more formal argument advocating the choice of the triangle with minimum  $r_{circ}$  is provided in [She02b], where it is shown that the worst error on the approximation of the gradient of a bivariate function by a linear interpolant precisely involves  $r_{circ}$ .

### 4.6.2 Solving the fitting problem

The next stage consists of choosing the  $z$  direction to work with. Since the tangent plane has not been estimated, we use a principal component analysis to compute a rough estimate of the normal with the collected points. The polynomial fitting can be done in any coordinate system whose  $z$  axis is not tangent to the surface. Hence at least one of the three axes of the world coordinate system matches this requirement. A natural choice is to select the coordinate axis whose angle with the rough estimated normal is minimum. Another choice is that of a coordinate system for which the  $z$  axis is the rough estimated normal. This choice may increase the ratio  $d_{max}/d_{min}$  and improve the results as explained in section 4.4, but this requires the calculation of a non trivial coordinate transformation. The improvement of this latter choice has not been studied experimentally since the first alternative performs well enough to confirm the theoretical orders of convergence —cf. section 4.7.1. For the chosen coordinates, we fill the Vandermonde matrix. The matrix is further pre-conditioned as explained in section 4.3.3, with  $h$  the average value of the norms  $\|(x_i, y_i)\|$ . The corresponding system is solved using a Singular Value Decomposition. Practically, we use the SVD of the Gnu Scientific Library, available from <http://sources.redhat.com/gsl>.

As pointed out in section 4.3.3, the instability of the system is provided by the condition number. Whenever degenerate configurations are detected, one can proceed as follows. For the approximation strategy, one can either

keep the same degree and increase the number of points used, or reuse the same points with a lower degree. These changes are likely to provide a non singular matrix  $M$ . In the worst-case, a degree one fitting must be possible since then only three linearly independent points are required! For the interpolation, things are a bit more involved since reducing the interpolation degree requires discarding some points. Selecting the subset yielding the best conditioning is a challenging problem [Las99, Hig96]. Notice also that for the approximation case, one can always retrieve a solution from an under-constrained least-square problem by choosing, e.g., the solution vector of least norm.

### 4.6.3 Retrieving differential quantities

We have already mentioned how to compute the normal. For the second order information, we compute the Weingarten map of the surface [dC76, Section 3.3]. Its eigenvalues (eigenvectors) provide the principal curvatures (directions) of the surface. For a parameterized surface given as a height function, one ends up with the formula given on Table 4.1. Notice that a basis of the tangent space associated to the parameterization  $X(u, v) = (u, v, h(u, v))$  consists of the two vectors  $X_u = (1, 0, h_u)^t$  and  $X_v = (0, 1, h_v)^t$ . A Gram-Schmidt orthonormalization of the basis  $\{X_u, X_v\}$  gives another basis  $\{Y, Z\}$  of the tangent space. The diagonalization of the symmetric matrix representing the Weingarten map in the basis  $\{Y, Z\}$  provides the expression of the principal curvature directions with respect to the  $\{Y, Z\}$  orthonormal basis. Note that the sign of principal curvatures and hence the definition of minimal and maximal directions rely on the orientation of the normal. As long as our experimental study is performed on meshes of oriented surfaces, it is straightforward to find a global and coherent orientation of the normals.

$$\begin{aligned} e &= 1 + a_1^2 & l &= \frac{2a_3}{\sqrt{a_1^2 + 1 + a_2^2}} \\ f &= a_2 a_1 & m &= \frac{a_4}{\sqrt{a_1^2 + 1 + a_2^2}} \\ g &= 1 + a_2^2 & n &= \frac{2a_5}{\sqrt{a_1^2 + 1 + a_2^2}} \end{aligned} \quad A = - \begin{pmatrix} e & f \\ f & g \end{pmatrix}^{-1} \begin{pmatrix} l & m \\ m & n \end{pmatrix}$$

Table 4.1: Computing the matrix  $A$  of the Weingarten map of  $h(u, v) = a_1 u + a_2 v + a_3 u^2 + a_4 uv + a_5 v^2$  in the basis  $\{X_u, X_v\}$

## 4.7 Experimental study

We present results along two lines. First, we illustrate the convergence theorems proved in section 4.4. Second, we present illustrations on standard computer graphics models.

### 4.7.1 Convergence estimates on a graph

**Setup.** We illustrate the convergence properties with the smooth height fields  $f(u, v) = 0.1e^{2u+v-v^2}$  and  $g(u, v) = 4u^2 + 2v^2$  defined over the parametric domain  $(u, v) \in [-0.5, 0.5]^2$ —see Figs. 4.4 and 4.5. At selected points on the graphs of  $f$  and  $g$ , we study the angle between the normals—more precisely its sine  $\sin(n, \tilde{n})$ , and the relative errors on principal curvatures. The values output by our algorithm are compared against the exact values computed analytically with arbitrary precision under Maple, and we report both average and maximum errors over sample points. More precisely, the graph of  $f$  or  $g$  are sampled with points  $p_i(x_i, y_i, f(x_i, y_i))$  where the  $(x_i, y_i)$  lies on a randomly perturbed triangulated square grid of side  $h$ . The triangulation is randomly perturbed to avoid simple degenerate configurations such as points lying on lines. The perturbation for the point  $(u, v)$  of the regular grid is the point  $(x, y)$  with  $x = u + \delta h$ ,  $y = v + \delta' h$  and  $\delta, \delta'$  random numbers in  $[0, 0.9]$ . The connectivity of the graph is that of the triangulated grid. Notice also that since calculations are carried out on a surface patch parameterized over a square grid, the direction chosen for the polynomial fitting is the  $z$  direction near the origin, and either the  $x$  or  $y$  directions at the periphery of the domain.

The convergence properties are illustrated (i)with respect to the discretization step  $h$  of the grid—for a given fitting degree  $n$  (ii)with respect to the fitting degree  $n$ —for a given discretization step  $h$ . We compare the convergence properties of the interpolation and approximation schemes, for fitting degrees ranging from one to nine. To quantify the observations, notice that according to theorem 12, the error  $\delta$  on a  $k^{\text{th}}$ -order differential quantity is

$O(h^{n-k+1})$ , hence

$$\delta \approx c h^{n-k+1} \Leftrightarrow \log(1/\delta) \approx \log(1/c) + (n-k+1)\log(1/h) \quad (4.15)$$

$$\Leftrightarrow \frac{\log(1/\delta)}{\log(1/h)} \approx \frac{\log(1/c)}{\log(1/h)} + (n-k+1). \quad (4.16)$$

**Convergence with respect to  $h$ .** To highlight the convergence properties with respect to the size of the neighborhood, we consider sequences of meshes with  $h \rightarrow 0$ , more precisely  $h$  ranges from  $2^{-2}$  to  $2^{-6}$ . The results for  $f$  and  $g$  being alike, we focus on the exponential  $f$ .

Curves of Figs. 4.6 to 4.11 show the average convergence behavior as the size of the neighborhood decreases. For a given degree and following equation (4.15), curves of figures 4.6 to 4.11 should be lines of slope  $(n-k+1)$ . The behavior is more regular for the approximation case, and the estimate is also better: a gain of about a digit can be observed between  $k_{max}$  estimates of figures 4.10 and 4.11.

**Convergence with respect to the interpolation degree.** For the convergence with respect to the interpolation degree —with  $h$  fixed, we present results for the polynomial  $g$  (cf. Fig. 4.12 to 4.17). Conclusions are similar for  $f$  (cf. Fig. 4.18 to 4.23), but it should however be noticed that since the graph of  $g$  is more curvy than that of  $f$ , a finer grid is required. (The higher the degree the more points required by the fitting ... and we compute local quantities!) To be precise, we ran experiments with  $h = 2^{-5}$  for  $f$  and  $h = 2^{-7}$  for  $g$ .

Curves of figures 4.12 and 4.13 show the convergence as a function of the degree of the fitted polynomial for a fixed neighborhood size. According to Eq. (4.16), curves of these figures should be lines of unit slope, with a vertical shift of one unit between normal and curvatures errors since curvature is a  $2^{nd}$  order quantity whereas normal is  $1^{st}$  order. The gap between the average values and the maximal values is greater for interpolation than for approximation. The other charts provide the conditioning and the least singular value. Interpolation fitting is always more ill-conditioned than approximation, and closer to a degenerate problem (the least singular value is the distance of the matrix system to singular matrices). The particular case of a degree 7 approximation reveals to be badly conditioned due to the regular connectivity of the mesh used to find the neighbors: there is only one more point than for the degree 7 interpolation fitting.

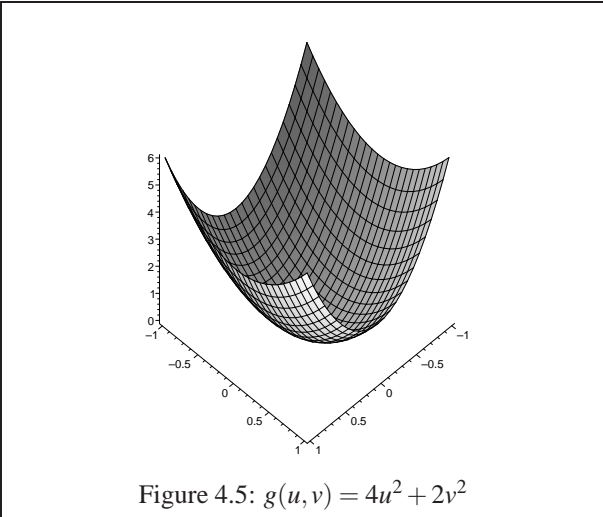
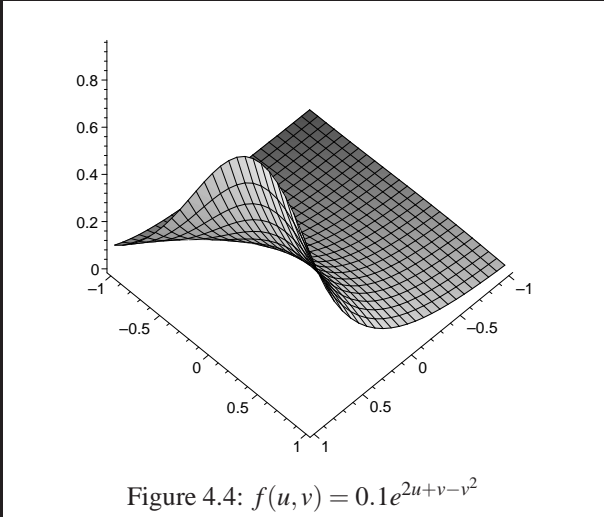
## 4.7.2 Illustrations

We depict differential informations on several models. When principal directions are displayed, blue and red respectively correspond to  $k_{min}$  and  $k_{max}$  —that is  $k_{min} \leq k_{max}$ —, assuming the surface normal points to the outside. To display patches of osculating  $n$ -jets, it is sufficient to select a rectangular domain in parameter space, sample it with a grid, and plot the corresponding mesh.

Consider the mesh models of the elliptic paraboloid  $z = 2x^2 + y^2$  —16k points, Fig. 4.24—, and the surface of revolution  $z = 0.1 \sin(10\sqrt{x^2 + y^2})$  —8k points, Fig. 4.25. The arrangement of curvature lines provides informations on umbilical points —where principal directions are not defined since  $k_{min} = k_{max}$ . On the paraboloid, it is easy to follow curvature lines and see how they turn around an umbilic. The surface of revolution provides an example of two parabolic lines (where the principal curvature  $k_{max}$  vanishes), that is a curve along which the Gauss curvature  $K_{Gauss}$  vanishes. This specific line splits the surface into elliptic ( $K_{Gauss} > 0$ ) and hyperbolic regions ( $K_{Gauss} < 0$ ). This model also illustrates a line of umbilical points where minimum and maximum principal directions swap each over.

For a standard example from Computer Graphics, consider the Michelangelo's David of Fig. 4.26. On this model of 95922 pts, the principal curvatures provide meaningful information for shape perception<sup>5</sup>. To finish up, we illustrate the robustness of the method. Figure 4.27 displays random patches on the Mechanic model, a 12,500 points model reconstructed from the output of a range scanner. In spite of the coarse sampling, patches and principal directions provide faithful information. In a similar vein, approximation fitting with large neighborhoods Fig. 4.28 features a noisy triangulation of a graph. In spite of the severe level of noise, surface patches *average* the available information. On Fig. 4.29, a noisy triangulation of an ellipsoid, 15k points, principal directions are enough precise to recognize an umbilic.

<sup>5</sup>See also [HCV52, p197] as well as [HGY<sup>+</sup>99].





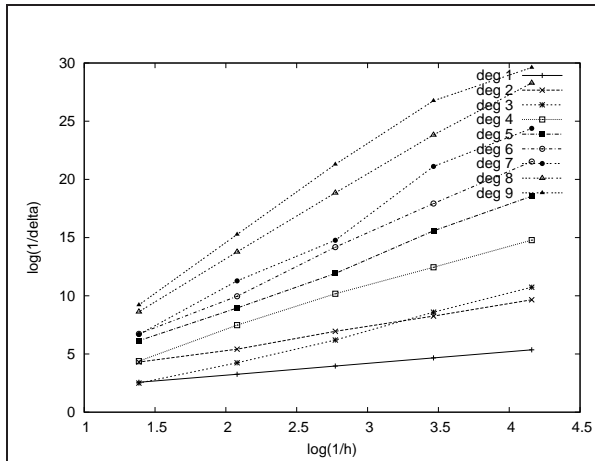


Figure 4.6: Exponential model: Convergence of the normal estimate with respect to  $h$ , interpolation fitting

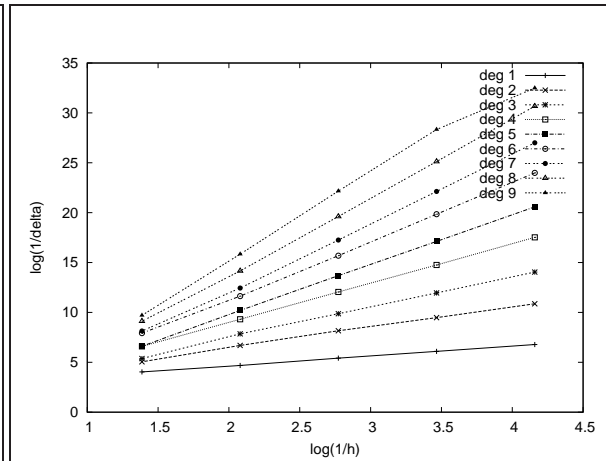


Figure 4.7: Exponential model: Convergence of the normal estimate with respect to  $h$ , approximation fitting

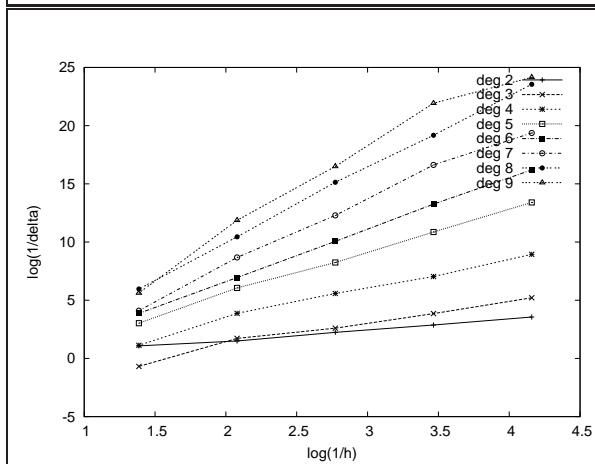


Figure 4.8: Exponential model: Convergence of the  $k_{min}$  estimate with respect to  $h$ , interpolation fitting

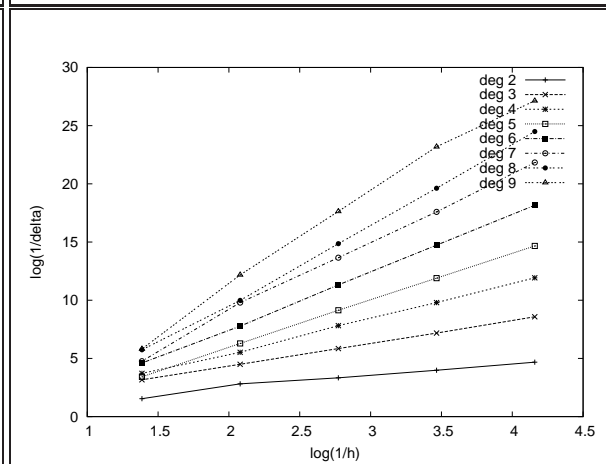


Figure 4.9: Exponential model: Convergence of the  $k_{min}$  estimate with respect to  $h$ , approximation fitting

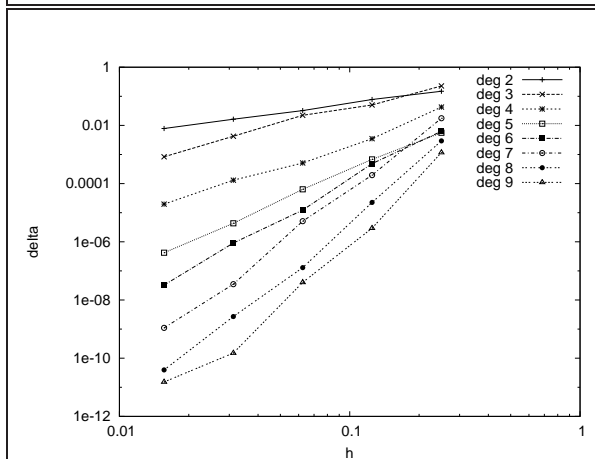


Figure 4.10: Exponential model: Convergence of the  $k_{max}$  estimate with respect to  $h$ , interpolation fitting

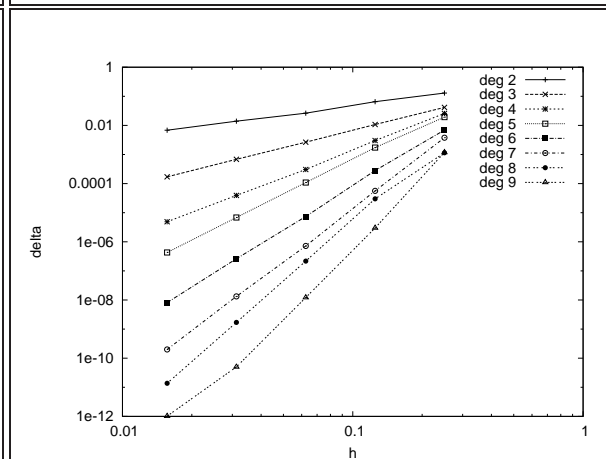


Figure 4.11: Exponential model: Convergence of the  $k_{max}$  estimate with respect to  $h$ , approximation fitting

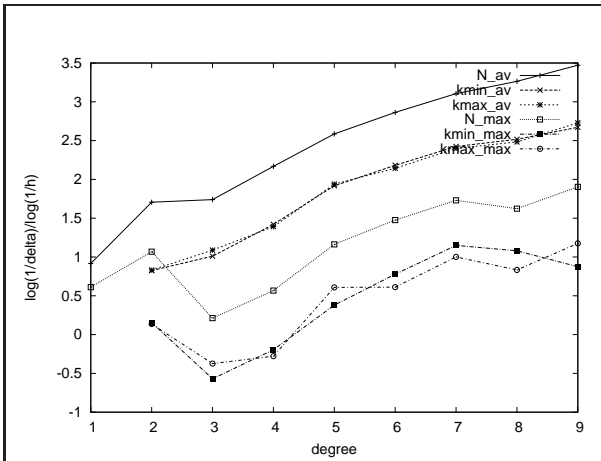


Figure 4.12: Polynomial model: Convergence of normal and curvature estimates with respect to the degree of the interpolation fitting

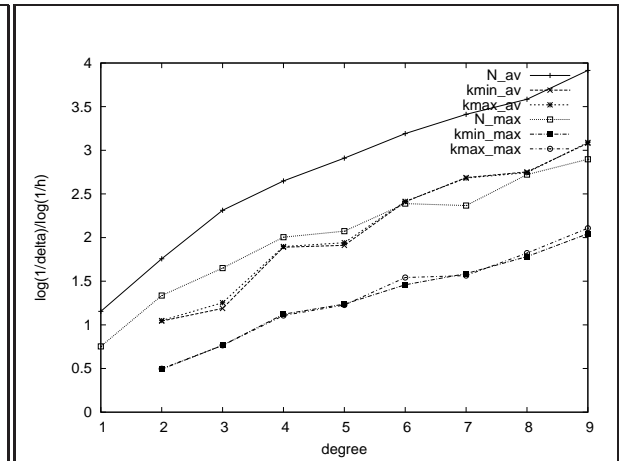


Figure 4.13: Polynomial model: Convergence of normal and curvature estimates with respect to the degree of the approximation fitting

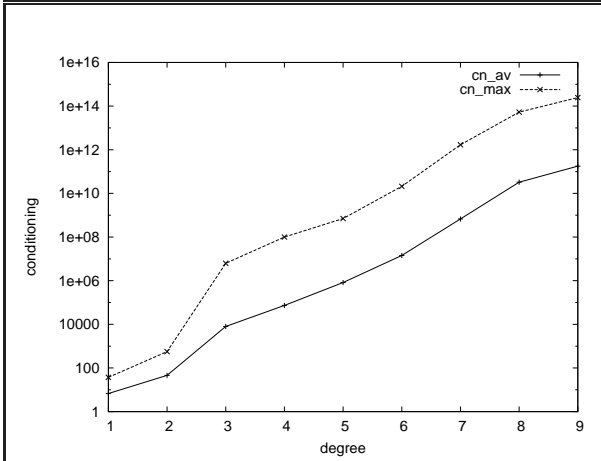


Figure 4.14: Polynomial model: Conditioning with respect to the degree of the interpolation fitting

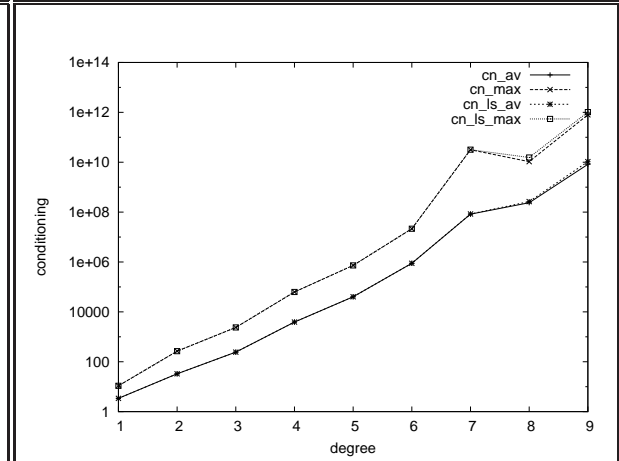


Figure 4.15: Polynomial model: Conditioning with respect to the degree of the approximation fitting

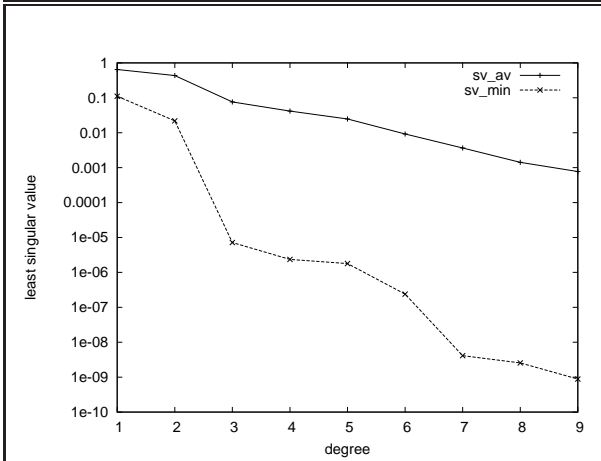


Figure 4.16: Polynomial model: Least singular value with respect to the degree of the interpolation fitting

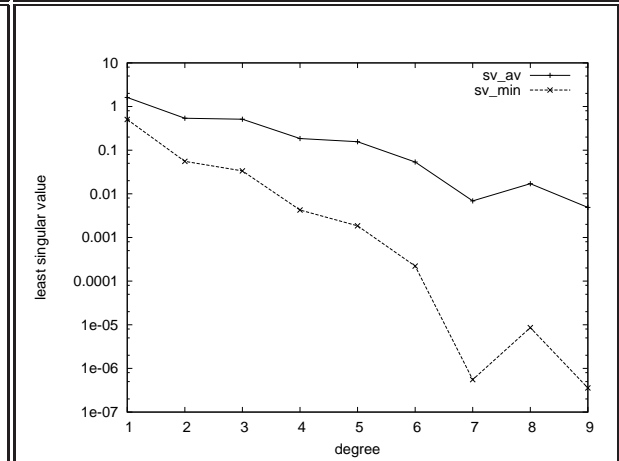


Figure 4.17: Polynomial model: Least singular value with respect to the degree of the approximation fitting

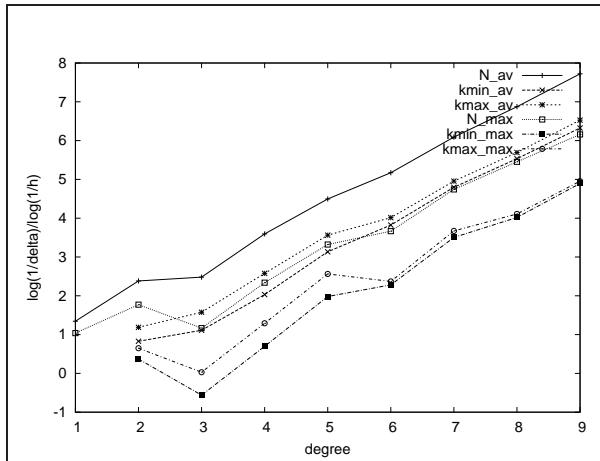


Figure 4.18: Exponential model: Convergence of normal and curvature estimates with respect to the degree of the interpolation fitting

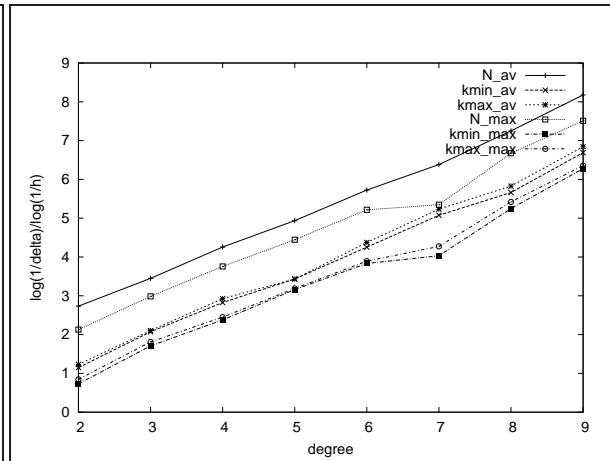


Figure 4.19: Exponential model: Convergence of normal and curvature estimates with respect to the degree of the approximation fitting

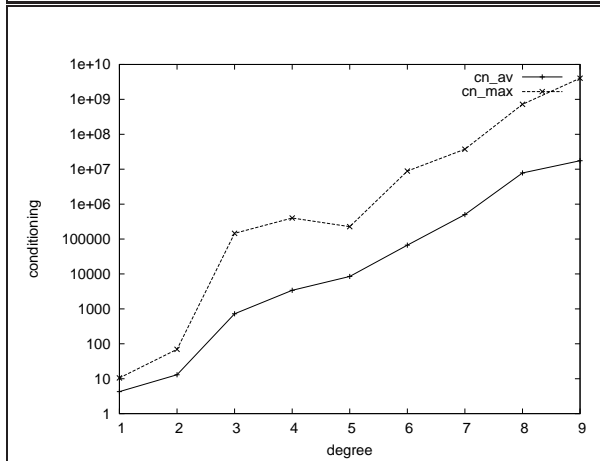


Figure 4.20: Exponential model: Conditioning with respect to the degree of the interpolation fitting

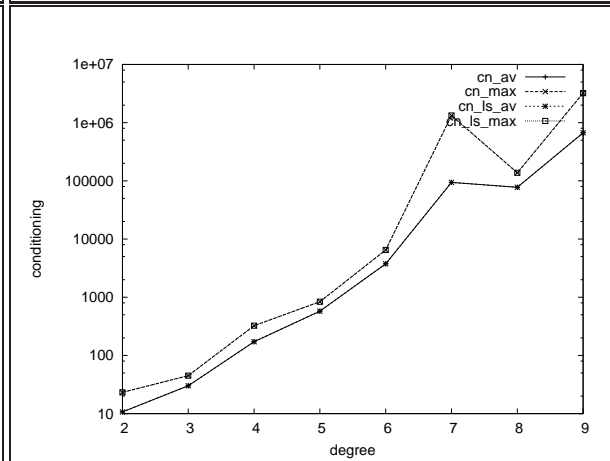


Figure 4.21: Exponential model: Conditioning with respect to the degree of the approximation fitting

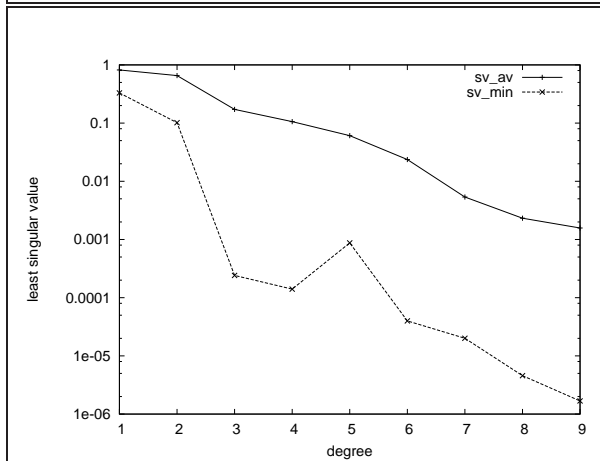


Figure 4.22: Exponential model: Least singular value with respect to the degree of the interpolation fitting

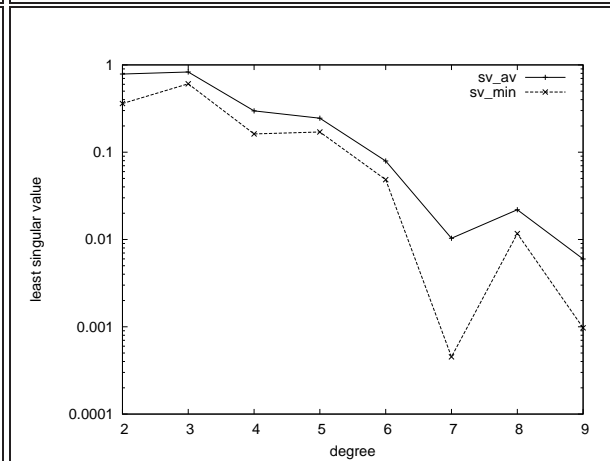


Figure 4.23: Exponential model: Least singular value with respect to the degree of the approximation fitting

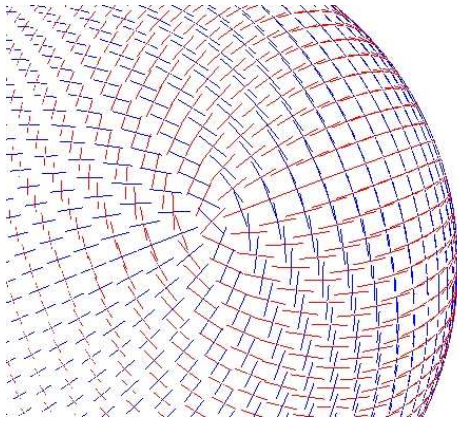


Figure 4.24: Elliptic paraboloid

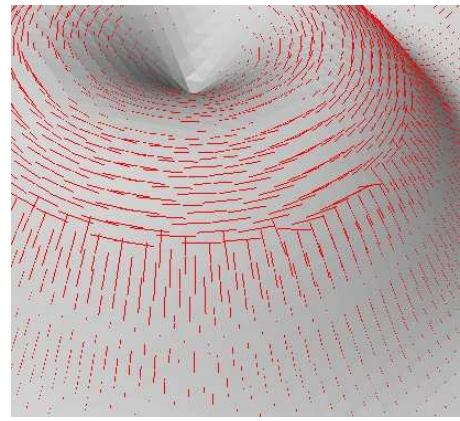


Figure 4.25: Surface of revolution

Figure 4.26: Michelangelo's David: principal directions associated with  $k_{max}$  scaled by  $k_{min}$



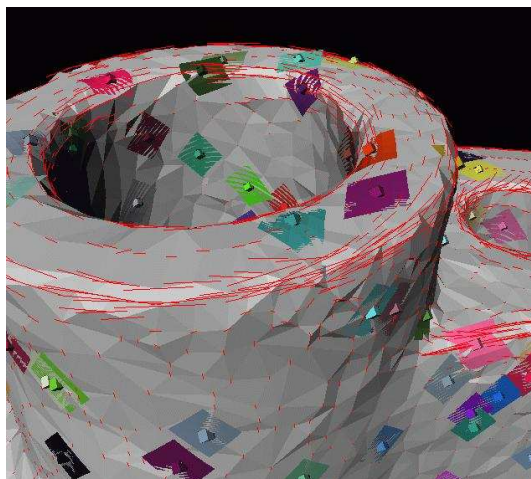


Figure 4.27: Mechanic: closeup

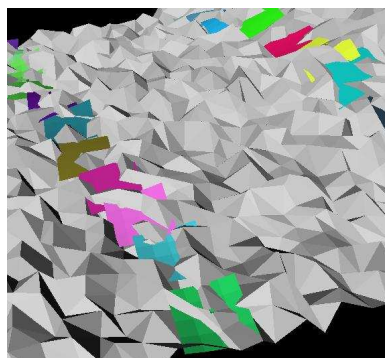
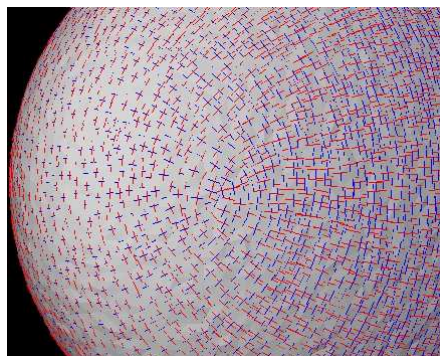
Figure 4.28:  $f(u, v) = u + 3v + e^{2u+v-v^2}$  with noise

Figure 4.29: Principal directions on a noisy ellipsoid

## 4.8 Conclusion

Estimating differential quantities is of prime importance in many applications from Computer Vision, Computer Graphics, Computer Aided Design or Computational Geometry. This importance accounts for the many different differential estimators one can find in the vast literature of applied geometry. Unfortunately, few of these have undergone a precise theoretical analysis. Another striking fact is that estimates of second order differential quantities are always computed using degenerate conics/quadratics without even mentioning the classification of Euclidean conics/quadratics.

The main contribution of the chapter is to bridge the gap between the question of estimating differential properties of arbitrary order and multivariate interpolation and approximation. In making this connection, the use of jets —truncated Taylor expansions— is advocated. Precise asymptotic convergence rates are proved for curves and surfaces, both for the interpolation and approximation schemes. To the best of our knowledge, these results are among the first ones providing accurate estimates for differential quantities of order three and more. Experimental results for surfaces of  $\mathbb{R}^3$  are reported. These experiments illustrate the asymptotic convergence results, but also the robustness of the methods on general Computer Graphics models.

**Acknowledgments.** P. Chenin is acknowledged for pointing out Ref. [EK66].

## Chapter 5

# Topology driven algorithms for ridge extraction on meshes

Given a smooth surface, a ridge is a curve along which one of the principal curvatures has an extremum along its curvature line. Ridges are curves of *extremal* curvature and therefore encode important informations used in segmentation, registration, matching and surface analysis. Surprisingly, no method developed so far to report ridges from a mesh approximating a smooth surface comes with a careful analysis, which entails that one does not know whether the ridges are reported in a coherent fashion. To bridge this gap, we make the following contributions.

First, we present a careful analysis of the orientation issues arising when one wishes to report the ridges associated to the two principal curvatures separately. The analysis highlights the subtle interplay between ridges, umbilics, and curvature lines. Second, given a triangulation  $T$  approximating a smooth generic surface  $S$ , we present sufficient conditions on  $T$  together with a generic algorithm reporting an isotopic approximation of the ridges. Third, we develop a heuristic algorithm to process a mesh when no information on an underlying smooth surface is known. Fourth, for coarse models, we provide a filtering mechanism retaining the most stable ridges only. Fifth, we present experimental results of the heuristic algorithm for smooth surfaces as well as coarse models. Our running times improve of at least one order of magnitude those of state-of-the-art methods.

The common point of these contributions is to exploit the topological patterns of ridges on smooth generic surfaces recalled in chapter 3. These contributions also pave the way to the first certified algorithm for ridge extraction on polynomial parametric surfaces, developed in the next chapters.

## 5.1 Introduction

### 5.1.1 Ridges of a smooth surface

Differential properties of surfaces embedded in  $\mathbb{R}^3$  are a fascinating topic per se, and have long been of interest for artists and mathematicians, as illustrated by the parabolic lines drawn by Felix Klein on the Apollo of Belvedere [HCV52], and also by the developments reported in [Koe90]. Beyond these noble considerations, the recent development of laser range scanners and medical images shed light on the importance of being able to analyze discrete datasets consisting of point clouds in 3D or medical images —grids of 3D voxels. Whenever the datasets processed model piecewise smooth surfaces, a precise description of the models naturally calls for differential properties. In particular, applications such as shape matching [HGY<sup>+</sup>99], surface analysis [HGY<sup>+</sup>99], or registration [TG95, PAT00] require the characterization of high order properties and in particular the characterization of curves of *extremal* curvatures, which are precisely the so-called *ridges*.

Chapter 3 surveys theoretical analysis of ridges, so we just recall basic definitions below. A ridge consists of the points where one of the principal curvatures has an extremum along its curvature line. Since each point which is not an umbilic has two different principal curvatures, a point potentially belongs to two different ridges. Denoting  $k_1$  and  $k_2$  the principal curvatures —we shall always assume that  $k_1 \geq k_2$ , a ridge is called blue (red) if  $k_1$  ( $k_2$ ) has an extremum. Moreover, a ridge is called *elliptic* if it corresponds to a maximum of  $k_1$  or a minimum of  $k_2$ , and is called *hyperbolic* otherwise. Ridges witness extrema of principal curvatures and their definition involves derivatives of curvatures, whence third order differential quantities. Moreover, the classification of ridges as elliptic or hyperbolic involves fourth order differential quantities, so that the precise definition of ridges requires



$C^4$  differentiable surfaces. Therefore, the calculation of ridges from a mesh approximating a smooth surface poses difficult problems, which are of three kinds.

**Numerical difficulties.** It is well known that parabolic curves of a smooth surface correspond to points where the Gauss curvature vanishes. Similarly, ridges are witnessed by the zero crossings of the so-called extremality coefficients, denoted  $b_0$  ( $b_3$ ) for blue (red) ridges, which are the derivatives of the principal curvatures along their respective curvature lines. Algorithms reporting ridges need to estimate  $b_0$  and  $b_3$ . Estimating these coefficients depends on the particular type of surface processed—implicitly defined, parameterized, discretized by a mesh—and is numerically a difficult task. Notice though, that the estimation of these quantities is independent from the combinatorial processing of ridges.

**Orientation difficulties.** Since coefficients  $b_0$  and  $b_3$  are derivatives of principal curvatures, they are third-order coefficients in the Monge form of the surface—the Monge form is the Taylor expansion of the surface expressed as a height function in the particular frame defined by the principal directions. But like all odd term of the Monge form, their sign depends upon the orientation of the principal frame used. Tracking the sign change of functions whose sign depends on the particular orientation of the frame in which they are expressed poses a problem. In particular, tracking a zero-crossing of  $b_0$  or  $b_3$  along a line-segment imposes to find a coherent orientation of the principal frame at the segment endpoints. Given two principal vectors at the segment endpoints, one way to find such an orientation consists of orienting the directions so that they make an acute angle, whence the name of *Acute Rule* or A.R. for short. The A.R. is implicitly used in [Mor90, Mor96, TG95, OBS04], but surprisingly, none of these papers addresses the question of specifying conditions guaranteeing the decisions made are correct. As we shall see, such analysis highlights the interplay between foliations, ridges and umbilics. (A principal foliation is the collection of lines of curvature associated to either principal curvature.)

**Topological difficulties.** The last difficulty is of topological nature and stems from the complex patterns made on generic surfaces by ridges and umbilics. As an illustration, consider a generic closed surface of genus zero—a topological sphere. Each such surface has at least four umbilics, each being traversed by either one or three ridges. For precise relationship between ridges and umbilics, the reader is referred to [Por01] as well as to section 3.4. Reporting ridges therefore requires reporting and classifying umbilics, an issue not addressed, to the best of our knowledge, by any paper tackling the issue of reporting ridges. This issue is illustrated in Figs. 3.14 and 3.15 for the particular case of the ellipsoid.

Another difficulty of topological nature is the interference of red and blue ridges at the so-called purple points. Given that each point of a smooth surface (which is not an umbilic) potentially belongs to two different ridges—one for each principal curvature, ridges near purple points must be handled with care. This difficulty requires again an orientation procedure such as the A.R. already mentioned.

## 5.1.2 Previous work

To the best of our knowledge, the only algorithm taking into account the topology of ridges at umbilics is described by Morris [Mor90, Mor96]. This method applies to parameterized surfaces and uses heuristics to orient edges and report umbilics, so that no guarantee is provided. For algebraic surfaces, Bogaeovski et al. [BLBK03] use a formal computation to determine the equation of a surface whose intersection with the original surface gives the ridges. For implicit surfaces, Thirion [Thi96] applies a marching line algorithm to the Gaussian extremality. However, the behavior of the algorithm near umbilics is not specified, and the Gaussian extremality  $E_g = b_0 b_3$  used to avoid orienting with the acute rule disconnects red and blue ridges at their intersections—5.2(c).

All other methods do not address the problem of topology, but focus on identifying a subset of the ridges and filtering methods. The connection between the medial axis and ridges is used by M.Hisada et al. [HBK02]. (Notice though that the projection of the medial axis boundary misses all hyperbolic ridges, and may also miss elliptic ones.) The connection with the focal surfaces is considered in [WB01] and [LA98]. Methods using only the estimation of curvatures on meshes are derived by Ohtake et al [OB01] or Stylianou et al [SF00]. Ohtake et al. [OBS04] use implicit surface fitting of a mesh to extract ridge-valley lines. The curvature tensor and the derivatives of curvatures of a mesh vertex are defined as the analytically computed values of the projection of the vertex on the fitted surface.

### 5.1.3 Contributions and chapter overview

Following the previous discussion, given a mesh  $T$  providing an approximation of a smooth compact oriented generic surface  $S$ , we aim at using  $T$  so as to report the ridges of  $S$ . (We implicitly assume  $S$  and  $T$  are isotopic [ACDL00, APR03, CCS04].) We make the following contributions.

In section 5.2, we specify the topological difficulties arising when reporting ridges, and introduce the Acute Rule. In section 5.3, we define *compliant* triangulations amenable to an isotopic extraction of ridges, and develop a generic algorithm. The algorithm is generic since two routines are assumed to compute the Monge coefficients of the surface at any point, and to report umbilic patches. In section 5.4, we develop a heuristic algorithm to process a mesh when no information on an underlying smooth surface is known. In section 5.5, we develop a filtering mechanism to report the most stable ridges of a coarse mesh. Finally, experimental results are provided in section 5.6.

## 5.2 Ridge topology and orientation issues

In this section, we introduce formally the problem addressed. Readers not familiar with ridges are referred to section 3.4 as well as to [HGY<sup>+</sup>99]. The set of ridges is composed of simple curves either closed and free of umbilic called *closed ridges*, or open curves connecting umbilics called *open ridges*. Hence reporting ridges means reporting umbilics and these ridge curves with the correct connectivity. As our aim is to report blue and red ridges separately, we focus on the set  $R_S^b$  of blue ridges of  $S$ .

### 5.2.1 Problem addressed

Assume we are given a triangle mesh  $T$  and an homeomorphism  $\Phi$  from  $T$  to  $S$ . As indicated in Fig. 5.1, we aim at reporting the *pull-back* of the set  $R_S^b$  of ridges of  $S$  onto  $T$ . More precisely, we aim at reporting a set  $R_T^b$  of polygonal curves on  $T$  corresponding to this pull-back. Given such a polyline, each pair of consecutive points is called a *ridge segment*. Let us consider on  $S$  ( $T$ ) the ridge set  $R_S^b$  ( $R_T^b$ ), together with the topology induced by  $\mathbb{R}^3$ .

**Definition. 12** *The set  $R_T^b$  is an isotopic approximation of the blue ridges of  $S$  if the push-forward of  $R_T^b$  ( $\Phi(R_T^b)$ ) is isotopic to  $R_S^b$  on  $S$ , or equivalently the pull-back of  $R_S^b$  ( $\Phi^{-1}(R_S^b)$ ) is isotopic to  $R_T^b$  on  $T$ .*

As suggested by the previous definition, we shall use the following abuses of terminology. When saying that “an edge is crossed by a ridge” or “a triangle contains an umbilic” we shall mean “the push-forward of the edge is crossed by a ridge” or “the push-forward of the triangle contains an umbilic”. Equivalently, this also means that “an edge is crossed by the pull-back of a ridge” or “a triangle contains the pull-back of an umbilic”.

Before proceeding, a comment is in order. We do not consider purple points —intersection between ridges of different colors— because the topology of the blue and red sets of ridges are processed separately. The incentive for ignoring purple points is that red and blue ridges are independent since functions  $b_0$  and  $b_3$  are so. Incidentally, this assumption alleviates the constraint of reporting the correct topology of ridges around purple points, as depicted in Fig. 5.2.

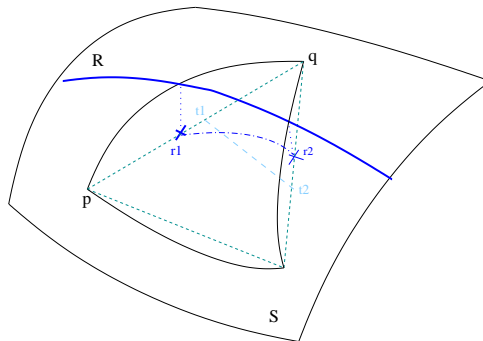


Figure 5.1: A ridge  $R$  on a smooth surface, its pull-back  $[r_1, r_2]$  on an inscribed triangulated surface, and a straight ridge segment  $[t_1, t_2]$  isotopic to this pull-back in the triangle  $pqs$

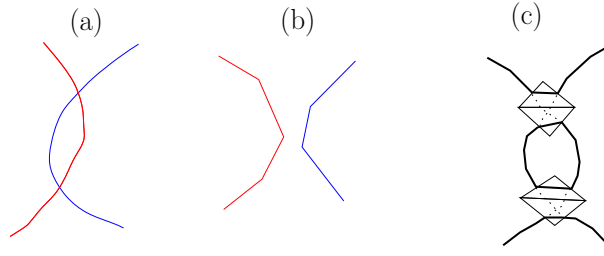


Figure 5.2: (a) Two ridges of different colors (b) Blue / red ridges reported independently: the topology of each ridge is respected, but that of the union is not (c) Ridges reported simultaneously by the Gaussian extremality: ridges are disconnected at purple points. No ridge point is detected when both red and blue ridges cross the same edge

### 5.2.2 Orientation and crossings

Consider a mesh  $T$  approximating of a smooth compact oriented generic surface  $S$  as explained in the previous section. The main issue tackled is to understand which properties  $T$  must have in order for one to report the ridges of  $S$  faithfully. We first recall the following:

**Observation. 6** *At any point of a smooth oriented surface  $S$  which is not an umbilic, orienting the principal directions at a vertex is equivalent to choosing a unit maximal principal vector, and there are two such orientations. (The minimal principal vector is then uniquely defined to be the unit vector so that the basis (maximal vector; minimal vector, normal) is direct.) Orienting the principal directions of an edge of a triangulation  $T$  whose endpoints lie on  $S$  means orienting them at its two vertices, and there are four possibilities.*

Consider now a simple curve  $C$  homeomorphic to the line-segment  $[0, 1]$  drawn on  $S$ . If  $C$  does not contain any umbilic one can define along  $C$  two continuous unit vector fields (opposite of one another) which orient the maximum direction field along  $C$ . Once a unit maximum vector has been chosen at one endpoint of  $C$ , we call the orientation induced by the corresponding vector field at the other endpoint the *orientation by continuity*. Replacing  $C$  by the push-forward of an edge yields the following:

**Definition. 13** *The orientation of the principal directions of an edge is called correct (erroneous) if it coincides with (differs from) one of the two orientations by continuity (of its push-forward on  $S$ ).*

As already noticed, a blue ridge point is witnessed by the zero crossing of a bivariate function  $b_0$ . More precisely, consider a curve oriented by continuity and crossing transversally a blue ridge, then the function  $b_0$  along the curve vanishes at the crossing point and undergoes a sign change. Since we are given a triangulation  $T$  of  $S$ , using an idea reminiscent from Marching Lines and Marching cubes, it is natural to seek the zero crossings of function  $b_0$  along the edges of  $T$ . But in our case however, function  $b_0$  depends on the orientation of the principal directions and by the above observation there are four possible orientations for the edge. Having discussed these orientation issues, we finally raise the observation used to track the blue ridge crossings with the sign of  $b_0$ :

**Observation. 7** *Let  $C$  be the push-forward of an edge  $[p, q]$ . Assume that the orientation of the principal directions of the edge is correct, no ridge crossing occurs at  $p$  or  $q$  and that at a crossing point the ridge and the curve  $C$  are transverse. Then the number of blue ridge crossings on  $C$  is odd (even) iff  $b_0(p)b_0(q) < 0$  ( $b_0(p)b_0(q) > 0$ ). If moreover, there is at most one blue ridge crossing on  $C$  then a ridge crosses  $C$  only once iff  $b_0(p)b_0(q) < 0$ .*

### 5.2.3 Gaussian extremality

An attempt to avoid the orientation procedure has been done by J.P. Thirion [Thi96] with the introduction of the Gaussian extremality. This function is defined at non-umbilical points by  $E_g = b_0 b_3$ . As both  $b_0$  and  $b_3$  change sign if the orientation is changed, the Gaussian extremality remains independent of the orientation. A sign change of this function along an edge means that an odd number of ridges is crossing the edge, but it does not allow to know the color of these ridges. If one could find a mesh so that each edge crosses at most one ridge regardless the color, it would be possible to recover the topology of uncolored ridges correctly. Unfortunately, the existence of a crossing between red and blue ridges in a triangle implies that one of its edge is crossed by at least two ridges (cf. Fig. 5.2(c)). In conclusion, the Gaussian extremality does not specify the color of the ridge, and consequently is unable to preserve the topology of ridges near purple points.

### 5.2.4 Acute rule

Consider an edge  $e$  of the mesh  $T$ . In the case of a dense mesh  $T$ , and whenever the vertices of  $e$  are close on  $S$ , one expects the maximal principal directions at the vertices of  $e$  to be nearly aligned —at least far from umbilics, which motivates the following:

**Definition. 14 (Acute Rule)** *Orienting an edge with the acute rule consists of choosing maximal principal vectors at the two vertices so that they make an acute angle in the ambient space  $\mathbb{R}^3$ .*

Note that this rule is well defined as soon as the maximal principal directions are not at right angle. The deviation of the maximal principal direction along a curvature line on the surface has two components which are extrinsic (the normal curvature) and intrinsic (the geodesic curvature). The denser the mesh, the shorter the edges of the triangulation and the smaller the extrinsic deviation. But the situation is different for the geodesic curvature. In particular, the geodesic curvature is arbitrarily large near umbilics as illustrated on Fig. 5.4, so that the acute rule is likely to yield erroneous orientations there. For these reasons, in developing a generic algorithm, we shall process differently the vicinity of umbilics (the so-called *umbilic patches*) and the complement of these patches.

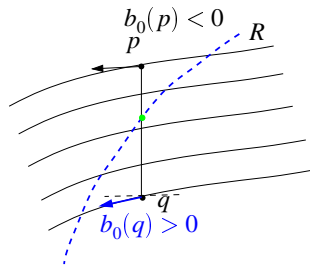


Figure 5.3: The A.R. gives a correct orientation.

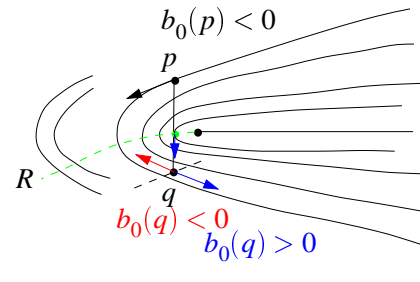


Figure 5.4: The A.R. gives an erroneous orientation near an umbilic —of index  $1/2$  here.

## 5.3 A generic algorithm

### 5.3.1 Compliant triangulations

We aim at designing an algorithm able to report an isotopic approximation of ridges as specified by definition 12. Since ridges are reported on the triangulation  $T$ , this triangulation shall fulfill some conditions. We thus define *compliant* triangulations, together with a generic algorithm in such a way that for a compliant triangulation, the generic algorithm will report an isotopic approximation of ridges. Since blue and red ridges are handled separately by the same process, we focus on blue ones and unless stated differently, “ridge” refers to “blue ridge” in the sequel.

To begin with, and following a well established trend to keep the description of the algorithm tractable without having to consider degenerate situations, we shall require genericity conditions. Note that these hypothesis are not restrictive in practice since they can be simulated during the processing (see the proof of theorem 13).

**Hypothesis. 1 (Genericity hypothesis.)** *The vertices and edges of  $T$  are assumed to meet the following generic conditions :*

**S1** *no ridge goes through a vertex of  $T$ .*

**S2** *ridges intersect edges transversally.*

Second, we specify conditions on the density of the triangulation  $T$ . To specify these conditions, we consider separately regions around umbilics and their complement on the surface. The rationale for doing so is that to provide guarantees on ridge crossings, we need correct orientations. But the A.R. is used for orientation and as discussed in section 5.2.4, it is not reliable near umbilics. Therefore, we apply two different strategies to umbilical regions inside which orientation is not certified, and to the rest of the surface where a correct orientation of edges is given.

Let us first discuss the case of umbilics. First, we require umbilic patches to be disjoint, which is natural since umbilics on generic surfaces are isolated. The orientation of edges inside patches is not certified, hence we cannot seek crossings inside a patch and have to infer the topology of ridges inside the patch from the patch boundary. This leads to the assumptions that (i) the topology inside a patch is as simple as possible (ii) one can find a correct orientation for edges on the boundary of the patch and each such boundary edge is crossed at most once by a given ridge. To substantiate these hypothesis, recall that generically, an umbilic is either a one ridge umbilic, or a three ridges umbilic (cf. section 3.4). Also recall that the three tangents to ridges connected to a three ridge umbilic are distinct. For a small enough topological disk around an umbilic, the configurations of ridges expected are therefore those depicted in Fig. 5.5. This formally leads to hypothesis D2.

Let us now consider the complement of the umbilic patches on the surface. Since, we are detecting ridge crossings along edges by observation 7, we assume each edge is crossed by at most one ridge. We wish we could assume that an edge has at most one ridge crossing witnessed by a sign change of the extremality coefficient. However, such an assumption is not realistic—if the ridge is almost tangent to the edge (Fig. 5.6) it crosses it twice. Hence we require instead that if one counts the number of crossings modulo 2 on the edge then the topology of this ridge is not modified. Finally, we require that no whole ridge is included in a triangle.

A triangulation meeting these hypothesis is called a *compliant* triangulation. More formally, we define five density hypothesis, namely D0 for the orientation property, D1 and D2 for umbilics, D3 and D4 for the complement of umbilic patches:

**Hypothesis. 2 (Density hypothesis.)**

**D0** *Triangulation  $T$  is such that outside umbilic patches, the A.R. correctly orients edges.*

**D1** *Umbilic patches  $U_i$  are disjoint.*

**D2** *A patch  $U_i$  of an umbilic  $u_i$  is such that (cf. fig. 5.5)*

- (a)  *$U_i$  does not contain a whole ridge,*
- (b) *ridges not connected to  $u_i$  do not cross the boundary of  $U_i$ ,*
- (c) *a ridge connected to  $u_i$  only once crosses exactly one edge of the boundary of  $U_i$ ,*
- (d) *a ridge connected to  $u_i$  twice crosses exactly two edges of the boundary of  $U_i$ .*

**D3** *All edges outside and on the boundary of the patches cross at most one ridge. If an edge crosses the ridge more than once, the topology is not modified if the number of crossing is counted modulo 2 (That is, if the number of crossings is odd the edge is processed as it were crossing the ridge once, and if the number of crossings is even the edge is processed as it were not crossing the ridge).*

**D4** *A triangle of  $T - \cup_i U_i$  does not contain a whole ridge.*

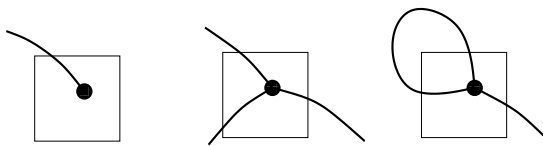


Figure 5.5: The only allowed configuration of ridges near an umbilic: first figure for a 1-ridge umbilic patch, second and third figures for a 3-ridge umbilic patch.

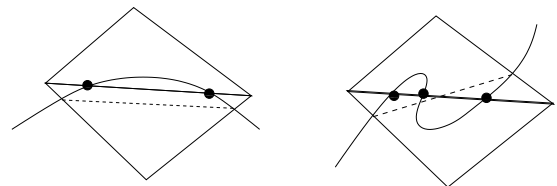


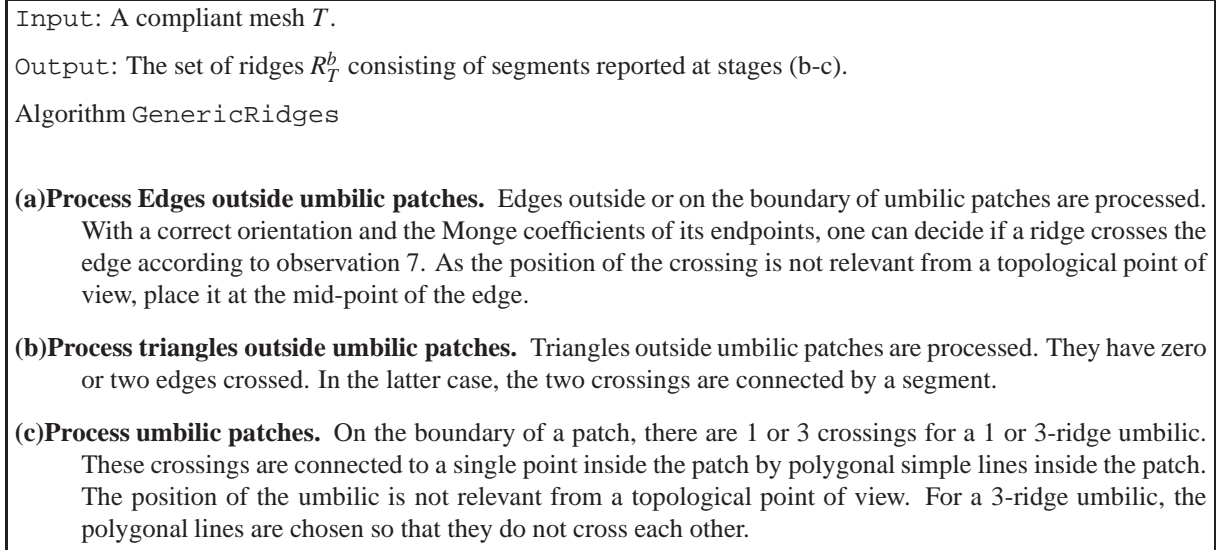
Figure 5.6: A double crossing simplifying to no crossing and three crossings simplifying to a single one

### 5.3.2 Generic algorithm

Based upon the previous hypothesis, algorithm `GenericRidges`—Fig. 5.7— processes separately umbilic regions and their complement. The algorithm requires, as a preprocessing, (i) estimations of the differential quantities at vertices of the mesh  $T$  and (ii) the identification of umbilic patches. The algorithm is generic in the sense that it performs combinatorial decisions which are independent from the method of the preprocessing, but only depend on the result of this preprocessing.

**Theorem. 13** *For a compliant triangulation, the algorithm `GenericRidges` reports an isotopic approximation of ridges as specified by definition 12.*



Figure 5.7: Algorithm `GenericRidges`

*Proof. Simulation of genericity hypothesis.* If S1 is not satisfied, a ridge goes through a vertex  $v_0$  of  $T$  and then  $b_0(v_0) = 0$ . To avoid the description of this particular case and a specific processing, one gives to  $b_0$  an arbitrary value  $\varepsilon > 0$  with  $\varepsilon < \min\{|b_0(v)|, v \text{ vertex of } V, b_0(v) \neq 0\}$ . This just shifts the ridge slightly away from the vertex  $v_0$  without any modification of the topology. If S2 is not satisfied, a ridge crosses an edge at a point  $p$  and stays on the same side of this edge in a neighborhood of  $p$ . Since only the values of  $b_0$  at endpoints of the edge are checked, the processing ignores such a crossing. Hence the processing is equivalent to slightly shift the ridge away from the edge without any modification of the topology. In other words, a non-transverse intersection is processed as if there was no intersection at all.

*Topology outside umbilic patches.* First, for edges outside and on the boundary of umbilic patches, due to hypothesis S1, S2 and D3, observation 7 gives the number of ridge crossings modulo 2. Moreover, from a topological point of view, hypothesis D3 allows one to assume that an edge is crossed at most once by at most one ridge. Once these crossings are detected, one processes the triangles outside patches. Second, outside patches there is no umbilic, this means that a ridge cannot end inside a triangle. Hence a triangle has 0 or 2 ridge crossings. If two crossings occur, then the same ridge is crossing the triangle and it is correct to represent it topologically by a segment connecting the mid-points of two crossed edges. A closed ridge cannot be included neither in a triangle (D4) nor a patch (D2a) and cannot cross the boundary of any patch (D2b). Any closed ridge is thus crossing some edges outside patches and hence is completely reported at this stage of the detection. All open ridges are also detected but not completely reported. Indeed umbilic patches are disjoint (D1) and an open ridge crosses the boundary of the patch(es) it is connected to (D2c-d). Hence any open ridge crosses at least one edge outside patches and two edges on the patch(es) it is connected to. Any open ridge is thus witnessed by at least two ridge segments outside patches.

*Topology inside umbilic patches.* Third, one has to connect open ridges inside patches. Hypothesis D2 implies that the boundary of a patch has either one edge with one ridge crossing or three such edges. This distinguishes patches containing a 1-ridge umbilic or a 3-ridge umbilic. If the patch contains a 1-ridge umbilic, the open ridge connected to this umbilic cross the only edge with a ridge crossing of the boundary of the patch (hypothesis D2c). It is thus correct to represent it topologically by a simple polygonal line connecting the mid-point of the edge to some interior point standing for the umbilic. If the patch contains a 3-ridge umbilic, the open ridges connected to this umbilic must cross the boundary of the patch (D2c-d) and it can only happen at the three crossings detected on the boundary. It is thus correct to represent the ridge topology in this patch by three disjoint polygonal simple lines connecting the mid-points of the edges to a single point inside the patch standing for the umbilic.

Finally, note  $R_T^b$  the set of all polygonal lines defined inside and outside patches. The pull-back of any ridge of  $R_S^b$  is reported on  $T$  by a simple polygonal curve of  $R_T^b$ . The set  $R_T^b$  is isotopic to the pull-back of  $R_S^b$ .  $\square$



## 5.4 A Heuristic to process a triangle mesh

Assume we are given a triangle mesh  $T$  providing a piecewise-linear approximation of  $S$  as an inscribed mesh—that is the vertices of  $T$  belong to  $S$ . Triangulation  $T$  might have been reconstructed from a point cloud [AB99, ACDL00, BC00] or might be the output of a meshing algorithm such as Chew’s algorithm [Che93, BO03]. Even though no information on the surface underlying the mesh (if any) is known, one can design an algorithm following the framework of the generic algorithm of section 5.3.2. If the mesh does comply with hypothesis Hyp. 2, then the output will be correct. As we shall see, the heuristic algorithm performs satisfactorily on practical examples.

Following this guideline, we instantiate the generic algorithm with two heuristic routines to compute the Monge coefficients, and report umbilic patches. We also develop a geometric rule to tag ridges as elliptic or hyperbolic.

### 5.4.1 Computing the Monge coefficients using polynomial fitting

We estimate differential quantities using a local polynomial fitting described and analyzed in [CP05a]. The polynomial used is of degree 3 or 4 depending on the method used to identify ridge types—see section 5.4.4. Convergence properties and numerical degeneracies of the polynomial fitting are proved and discussed in the aforementioned article.

### 5.4.2 Detection of umbilics and patches

We want to detect patches of triangles of  $T$  containing an umbilic. The method combines a minimization and an index computation on the neighborhood of each triangle of  $T$ . The size of the neighborhood is the only parameter of the algorithm. This method is a heuristic without guaranty, nevertheless it gives satisfaction in practice (cf. section 5.6).

**Finding patches around triangles.** Given a triangle  $t$ , we aim at defining a collection of triangles around it so that this collection defines a topological disk on the triangulation  $T$ . To do so, the most natural way consists of using the successive rings of triangles around  $t$ . Let us define the 0-ring neighbors of a triangle as the triangle itself. The  $k$ -th ring neighbors is defined recursively by adding to the  $(k-1)$ -th ring neighbors the triangles incident to one edge of this set. However, the  $k$ -th ring neighbors may not form a topological disk as indicated in Fig. 5.8.

To get around this difficulty and starting from the patch consisting of the triangle  $t$ , we iteratively construct a patch  $P$  by the following algorithm. Each triangle incident to one or two edges of the boundary of  $P$  is placed into a priority queue—the *grade* being the distance between the centroid of this triangle to that of  $t$ . Then, patch  $P$  is enlarged with the triangle  $t'$  having the least grade provided  $P \cup t'$  remains a topological disk. If triangle  $t'$  is stitched to the patch, its neighbors are inserted in the queue—if they are not already in it. The process stops as soon as the least distance is more than some threshold.

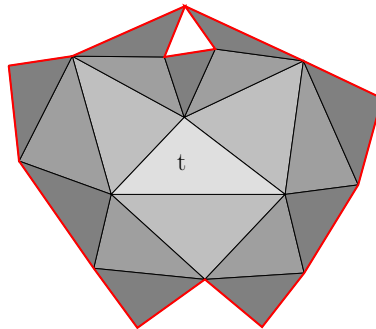


Figure 5.8: The third-ring triangles of the triangle  $t$  do not form a topological disk.

We aim at identifying disjoint patches of the mesh  $T$  containing generic umbilics of index  $\pm 1/2$  (cf. section 3.4). Notice that on a smooth surface, the function  $k_1 - k_2$  is always positive, and vanishes at umbilics only. To use this criterion, we define the value of  $k_1 - k_2$  for a triangle as the arithmetic mean of the values at its vertices. The detection proceeds in three steps:

1. Compute a patch around each triangle;

2. Select the patch of a triangle  $t$  if the function  $k_1 - k_2$  has its minimum at  $t$  amongst all the triangles of the patch;
3. Compute the index of the principal directions on the contour of the patches of triangles selected in step 2.

Given a triangle  $t$ , the first step consists of aggregating the successive rings of triangles around  $t$  while making sure that any new addition retains a topological disk. This step is parameterized by a positive number defining the *size* of the patch, which is defined as a multiple of the greatest grade of the one-ring triangles. The second step is straightforward. The third step requires following the contour of each patch, orienting the maximal principal directions with the A.R. , and computing the index by adding the angle deviations of the corresponding maximal principal vectors. Theoretically, the computation of the index of a direction field at a point on a manifold needs the use of a chart [BG88, chap.7,p.260]. Here, we assume that the projection on the tangent plane of the studied vertex is a chart, the index is computed for principal vectors projected on this plane. We then keep only triangle patches with an index  $\pm 1/2$ .

From a theoretical perspective, if the triangulated surface  $T$  is inscribed in a smooth generic closed surface, then the sum of indices of umbilics equals the Euler characteristic of the surface.

The Monge coefficients of the umbilical triangle (defined as the arithmetic mean of that of its vertices) should be close to those of the umbilic it is identified to. Hence we can use them to decide further knowledge of the umbilic type. For example, the sign of  $S = (b_0 - b_2)b_2 - b_1(b_1 - b_3)$  which is a third order quantity should also give the index of the umbilic. It is likely to be less accurate than our computation of step 3 which uses only second order quantities. Other invariants of third order decide the type 1-ridge or 3-ridge and the symmetry of ridges at the umbilic —see [Por01] and chapter 3.

### 5.4.3 Processing edges outside umbilic patches

We use the acute rule as specified by definition 14 in section 5.2.4. Since umbilics are identified, the A.R. is expected to give a correct orientation for edges outside or on the boundary of patches. A blue ridge crossing  $r$  along an edge  $[p, q]$  is detected if  $b_0(p)b_0(q) < 0$ . The position of  $r$  along the edge can be computed by linear interpolation:

$$r = \frac{|b_0(q)|p + |b_0(p)|q}{|b_0(q)| + |b_0(p)|} \quad (5.1)$$

We associate to the point  $r$  the differential quantities interpolated as above from the vertices  $p$  and  $q$ . For example the type elliptic or hyperbolic of  $r$  is given by the sign of  $P_1(r)$  (cf. section 3.4).

Ridge points are reported along edges of the triangulation, and two consecutive points define a ridge segment.

### 5.4.4 Tagging ridge segments

Once a ridge segment has been reported, one may classify it as elliptic or hyperbolic. As recalled in section 3.4 —see Fig. 3.6 for the geometric interpretation of ridge types, this can be done using the quantity  $P_1$  defined by Eq. (3.6), which involves 4th order differential coefficients. If the signs of  $P_1$  agree at both endpoints, the ridge segment is tagged accordingly. If not, the ridge segment is tagged as containing a turning point. In this section, we provide a geometric tagging rule using third order differential quantities only —a procedure likely to be more stable than the one using 4th order coefficients. Notice that ridges connected to umbilics are hyperbolic, so that our tagging rule is mainly concerned with ridges outside umbilic patches.

Consider an edge along which the sign of  $b_0$  changes. As illustrated in Fig. 5.10, the knowledge of the principal directions at the edge endpoints together with the location of the ridge point  $r$  falls short of providing enough information to state the ridge type.

In [OBS04] the following heuristic is used. The principal vectors  $u_1$  and  $u_2$  at the endpoints  $v_1$  and  $v_2$  are chosen according to the A.R. . Note  $b_0^u(v)$  the value of  $b_0$  at the vertex  $v$  and with the principal vector  $u$ . The ridge crossing is tagged as elliptic if  $b_0^{u_1}(v_1)(u_1 \cdot (v_2 - v_1)) > 0$  and  $b_0^{u_2}(v_2)(u_2 \cdot (v_1 - v_2)) > 0$ . This rule takes into account the principal directions at the endpoints of the edge but not local information on the ridge itself. This method implicitly assumes that orienting the principal direction with a vector making a acute angle with the edge leads the curvature line towards the ridge. As an example, the rule fails at vertex  $v_2$  of Fig. 5.9 and vertex  $v_1$  on Fig. 5.10(a). Such a situation is likely to occur when an edge is almost parallel to the ridge.

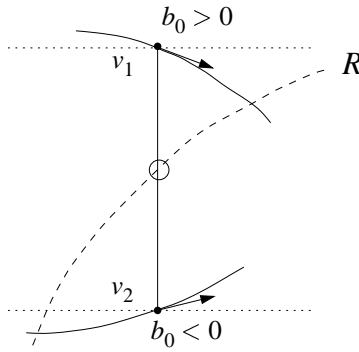


Figure 5.9: Tagging a ridge point as elliptic or hyperbolic: information at edge endpoints is not sufficient.

As an alternative, we propose not to tag a ridge point but a ridge segment providing more geometric knowledge. Consider a triangle crossed by a ridge segment  $[r_1, r_2]$ . The idea is to use the direction information given by  $[r_1, r_2]$  to distinguish between the two types — see Fig. 5.11. The sign of  $b_0$  for a maximal principal vector pointing towards the ridge segment  $[r_1, r_2]$  for the triangle is defined as the sign appearing at least at two vertices. If this sign is positive then there is a maximum of  $k_1$  and the ridge is elliptic else it is hyperbolic. Let  $(v_1, v_2, v_3)$  be a triangle,  $r_1$  and  $r_2$  the ridge points on the edges  $[v_1, v_2]$  and  $[v_1, v_3]$ . As  $S$  is oriented, assume  $(v_1, v_2, v_3)$  is direct. Then the sign of  $b_0(v_1)$  for an orientation pointing toward the ridge segment  $[r_1, r_2]$  is that of:

$$\text{sign}(b_0^{u_1}(v_1)) \det(u_1, r_2 - r_1, n)$$

with  $u_1$  any of the two orientations of  $d_1(v_1)$  and  $b_0^{u_1}(v_1)$  the value of  $b_0$  at the vertex  $v_1$  with the orientation  $u_1$ . The sign of  $b_0(v_2)$  (resp.  $b_0(v_3)$ ) for an orientation pointing toward the ridge segment  $[r_1, r_2]$  is that of:

$$-\text{sign}(b_0^{u_2}(v_2)) \det(u_2, r_2 - r_1, n) \quad (\text{resp. } -\text{sign}(b_0^{u_3}(v_3)) \det(u_3, r_2 - r_1, n))$$

with  $u_2$  (resp.  $u_3$ ) any of the two orientations of  $d_1(v_2)$  (resp.  $d_1(v_3)$ ).

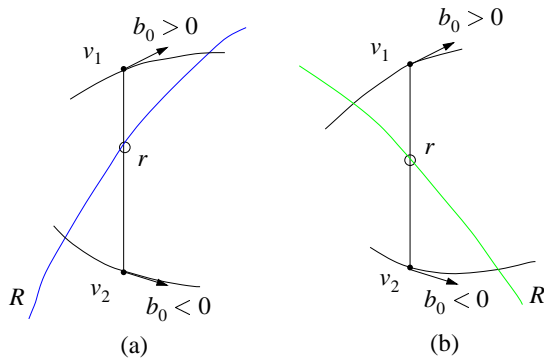


Figure 5.10: An elliptic (left), and an hyperbolic (right) ridge crossing an edge of the triangulation  $T$

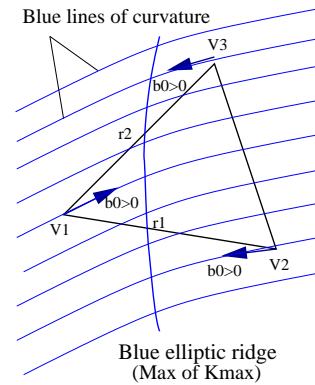


Figure 5.11: Determining the type of a ridge segment using third order properties

## 5.5 Filtering sharp ridges and crest lines

For real world applications dealing with coarse meshes, or meshes featuring degenerate regions or sharp features, one cannot expect a configuration of umbilics and ridges matching that of a smooth generic surface. For example, if the principal curvatures are constant — which is the case on a plane or a cylinder, then all points are ridge points. In this context, an appealing notion is that of *sharp* ridge or *prominent* ridge. Since ridges are witnessed by zero crossings of  $b_0$  and  $b_3$ , one can expect erroneous detections as long as these coefficients remain small. In order to select the most prominent ridge points, we can focus on points where the variation of the curvature is fast along the curvature line.

**Observation. 8** *At a ridge point, according to the equation 3.6, the second derivative of  $k_1$  along its curvature line satisfies  $k_1''(0) = P_1/(k_1 - k_2)$ .*

Using the previous observation, one can define the *sharpness of a ridge* as the integral of the absolute value of  $P_1/(k_1 - k_2)$  along the ridge. As the second derivative of the curvature is homogeneous to the inverse of the cube of a length, the sharpness is homogeneous to the inverse of the square of a length. Multiplying the sharpness by the square of the model size gives a threshold and an associated sharpness-filter which are scale independent. It should be noticed this filter is different from the *strength of a ridge segment* as defined in [OBS04], which is the integral of the curvature along the line.

As an alternative to ridges, some applications focus on the so-called crest-lines [PAT00]. A crest line is an elliptic ridge which is a maximum of  $\max(|k_1|, |k_2|)$ , and one may see these lines as the visually most salient curves on a surface. (Notice that these lines do not cross each other and avoid umbilics.) Filtering ridge points using observation 8 retains more information than focusing on crest lines since hyperbolic ridges might be sharp also.

## 5.6 Illustration

In this section, we illustrate the algorithm developed in section 5.4. We assume the surface is given in discretized form as a mesh.

**Smooth surfaces.** The experimental setup faces two difficulties. First, finding compact generic  $C^4$  surfaces of complex geometry and topology is a challenging task by itself. On one hand, subdivision surfaces do not exhibit such smoothness properties. On the other hand, algebraic surfaces often exhibit symmetries and or singularities. A promising class of such surfaces might be the manifold-based construction developed by Ying et al. [YZ04]. We shall report experiments on these surfaces upon availability of their code. Second, given such a surface, the patterns made by umbilics and ridges are usually unknown—the only complete descriptions we are aware of can be found in [Por01]. Consequently, we illustrate the algorithm on two surfaces whose ridges are known (the standard ellipsoid, and a Bezier patch whose ridges are certified by algebraic methods (see chapter 7), and on the blend of two ellipsoids. The discretization of the Bezier patch is achieved by a regular triangular grid on the parameter space. Implicit surfaces are meshed with the algorithm described in Boissonnat et al. [BO03].

The first test surface is the ellipsoid of Fig.3.14, where the algorithm reports perfectly the well-known patterns of umbilics and ridges.

The second test surface, Figure 5.13, is a triangulated Bezier surface whose control points are

$$\begin{pmatrix} [0, 0, 0] & [1/4, 0, 0] & [2/4, 0, 0] & [3/4, 0, 0] & [4/4, 0, 0] \\ [0, 1/4, 0] & [1/4, 1/4, 1] & [2/4, 1/4, -1] & [3/4, 1/4, -1] & [4/4, 1/4, 0] \\ [0, 2/4, 0] & [1/4, 2/4, -1] & [2/4, 2/4, 1] & [3/4, 2/4, 1] & [4/4, 2/4, 0] \\ [0, 3/4, 0] & [1/4, 3/4, 1] & [2/4, 3/4, -1] & [3/4, 3/4, 1] & [4/4, 3/4, 0] \\ [0, 4/4, 0] & [1/4, 4/4, 0] & [2/4, 4/4, 0] & [3/4, 4/4, 0] & [4/4, 4/4, 0] \end{pmatrix}$$

Alternatively, this surface can be expressed as the graph of the degree 4 polynomial  $h(u, v)$  for  $(u, v) \in [0, 1]^2$ :

$$h(u, v) = 116u^4v^4 - 200u^4v^3 + 108u^4v^2 - 24u^4v - 312u^3v^4 + 592u^3v^3 - 360u^3v^2 + 80u^3v + 252u^2v^4 - 504u^2v^3 + 324u^2v^2 - 72u^2v - 56uv^4 + 112uv^3 - 72uv^2 + 16uv.$$

The whole configuration of ridges and umbilics matches the correct topology computed and certified by the algorithm of chapter 7. Zoom views, Figure 5.14, allow one to follow ridges in the neighborhood of 3-ridge umbilics. Turning points and different ridge types can also be observed.

The third test surface is a blend between two ellipsoids displayed on Fig.5.15 and defined by the following equation:

$$1 - \exp(-0.7(\frac{x^2}{0.15^2} + \frac{y^2}{0.25^2} + \frac{z^2}{0.35^2} - 1)) - \exp(-0.7(\frac{(x-0.25)^2}{0.1^2} + \frac{(y-0.1)^2}{0.2^2} + \frac{(z-0.1)^2}{0.3^2} - 1)) = 0$$

The umbilic detection algorithm gives good results for a size of the patch around a vertex 2 or 3 times the size of its 1-ring. Indeed, the greater the patch, the fewer the number of points collected with the minimization step. More

importantly, the boundary of large patches are not too close from umbilics, which as explained in section 5.2.4 favors a correct orientation with the A.R. outside patches. As an example on this surface, 14 points are detected by the minimization algorithm—using a patch size 3 times the 1-ring size, while six umbilics of index  $+1/2$  and two of index  $-1/2$  are reported by the index computation. Notice that this complies with the Euler characteristic. On this model, apart from isolated ridge segments of erroneous type, the ridges reported look convincing but we cannot claim the result is correct since the configurations of ridges for this surface is unknown.

The complexity of the algorithm is linear with respect to the number of vertices. The whole process on a 2GHz PC takes 7 seconds for the ellipsoid, 25s for the Bezier surface and 20s for the ellipsoid blend.

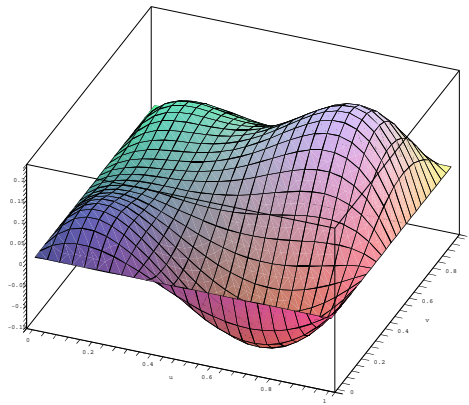


Figure 5.12: Plot of the degree 4 Bezier surface

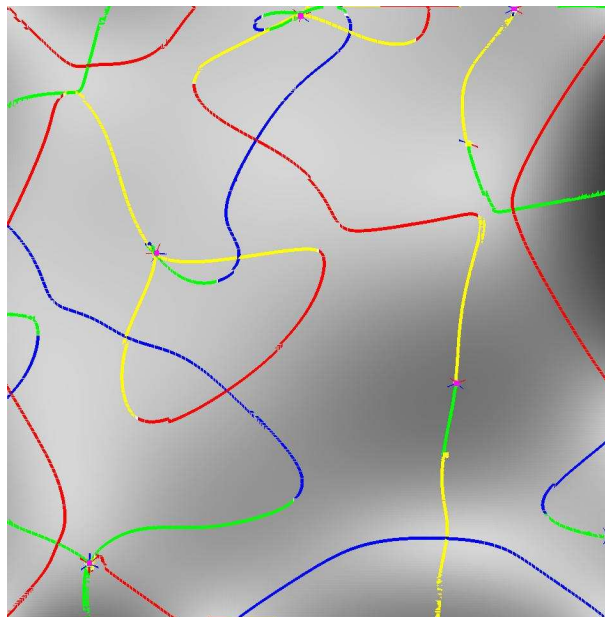


Figure 5.13: Ridges and umbilics on a triangulated model of the Bezier surface (60k points), view from above

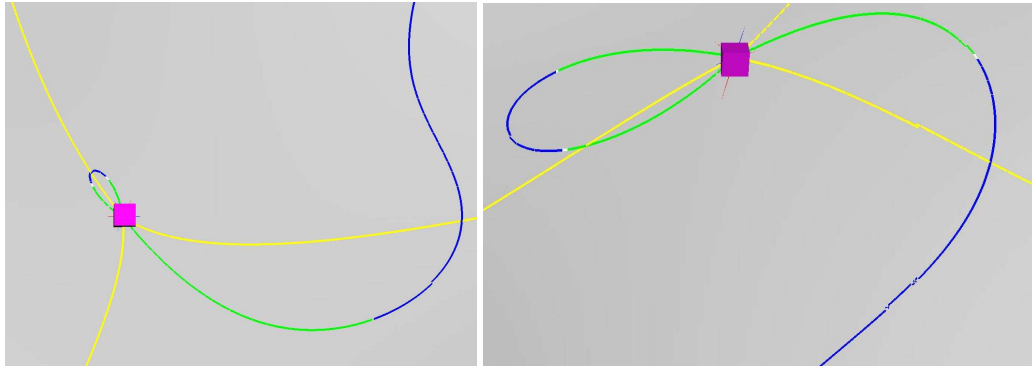


Figure 5.14: Zoom view on two 3-ridge umbilics

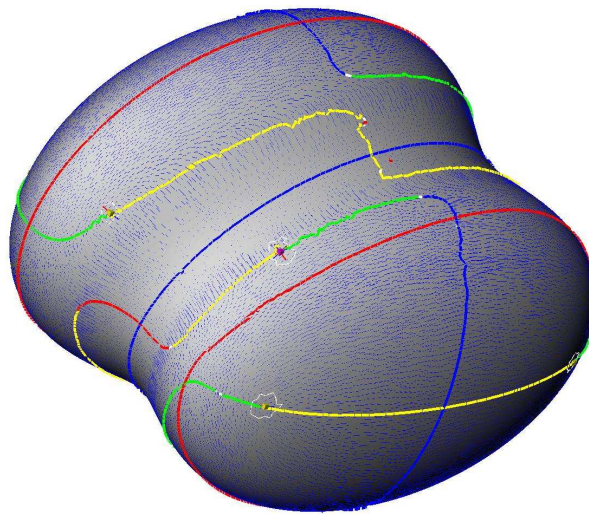


Figure 5.15: Ridges and umbilics on the implicit blending of two ellipsoids (40k points)

**Coarse meshes.** Figure 5.16 features a coarse mesh of a mechanical part with first all crests lines, second crest lines filtered with their strength and third filtered with their sharpness. This example is especially interesting since it features flat and cylindrical regions. Each point on such region has constant thus critical principal curvatures and is therefore a ridge point. The whole configuration of crests is very noisy. The strength-filtered crest lines [OBS04] avoid the planar regions but remains in cylindrical ones. The sharpness-filter discards these spurious elements in cylindrical regions too, and retains only the crests appearing on salient features of the model. This example also calls for a comment on methods aiming at reporting ridges after having performed an interpolation / approximation of the model. Again, if the model features flat or cylindrical regions, such algorithms report many insignificant ridges—that would also have to be filtered. The whole process of this mesh takes 10 seconds on a 2GHz PC.

Figure 5.17 features the David model (380k pts) processed in 2 minutes. The sharpness filter is used, but the strength filter gives similar results on this model more generic than the mechanical one. Notice that our running time improves the results of [OBS04] of at least one order of magnitude and that the result is quite similar even for a smaller model.

## 5.7 Conclusion

Given a mesh discretizing a smooth surface, this chapter presents the first algorithm for extracting an isotopic approximation of the ridges of the smooth surface on the discretization. The algorithm exploits the patterns made by ridges and umbilics on generic surfaces, and dissociates the processing near umbilics and on the rest of the surface. The algorithm is generic since the calculation of extremality coefficients and the separation of umbilics are deferred to routines that may depend from the type of smooth surface discretized by the mesh.



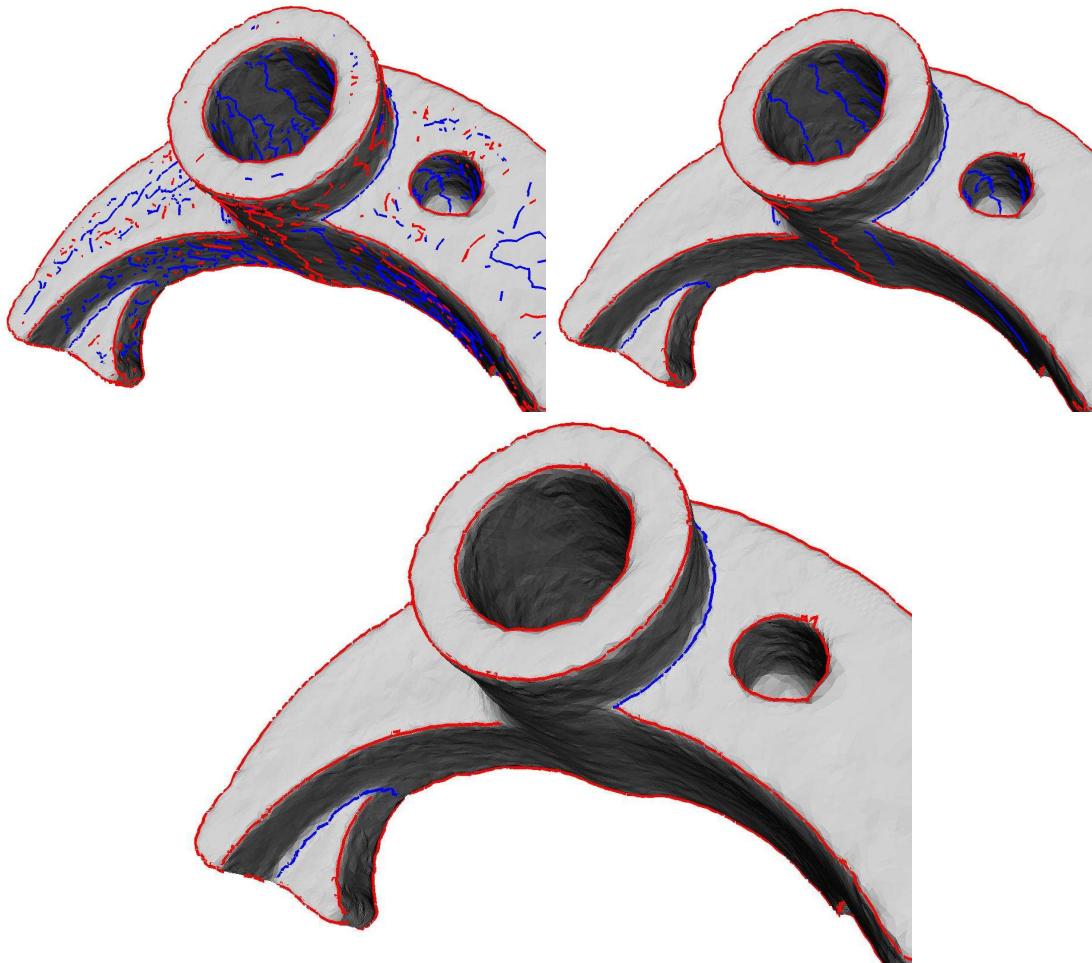


Figure 5.16: Mechanical part (37k pts): (a) All crest lines, (b) crests filtered with the strength and (c) crests filtered with the sharpness. Notice that any point on a flat or cylindrical part lies on two ridges, so that the noise observed on the top two Figs. is unavoidable. It is however easily filtered out with the sharpness on the bottom figure.

For meshes approximating smooth surfaces —without access to any analytical information on the surface, we provide heuristics. We also present a geometric rule to tag ridges as elliptic or hyperbolic —which has the advantage of using third order properties only, and a filtering procedure retaining the most stable ridges. For meshes discretizing smooth surface whose ridges are known, experiments show that our heuristic algorithm recovers the correct topology of ridges and umbilics. For meshes computed from scans by a surface reconstruction algorithm, experiments show that our algorithm recovers the ridges of state-of-the-art methods (which use global fitting), while improving running times of at least one order of magnitude and providing a more efficient filtering method.

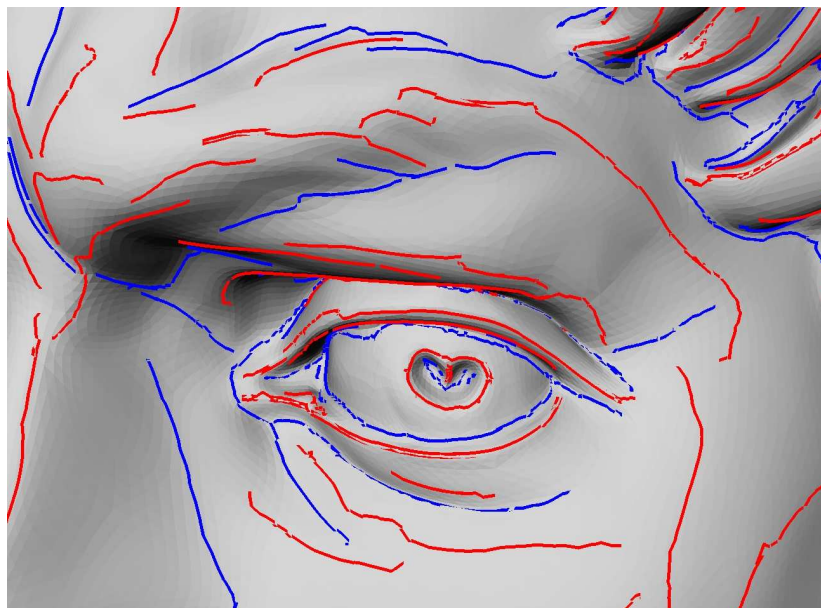
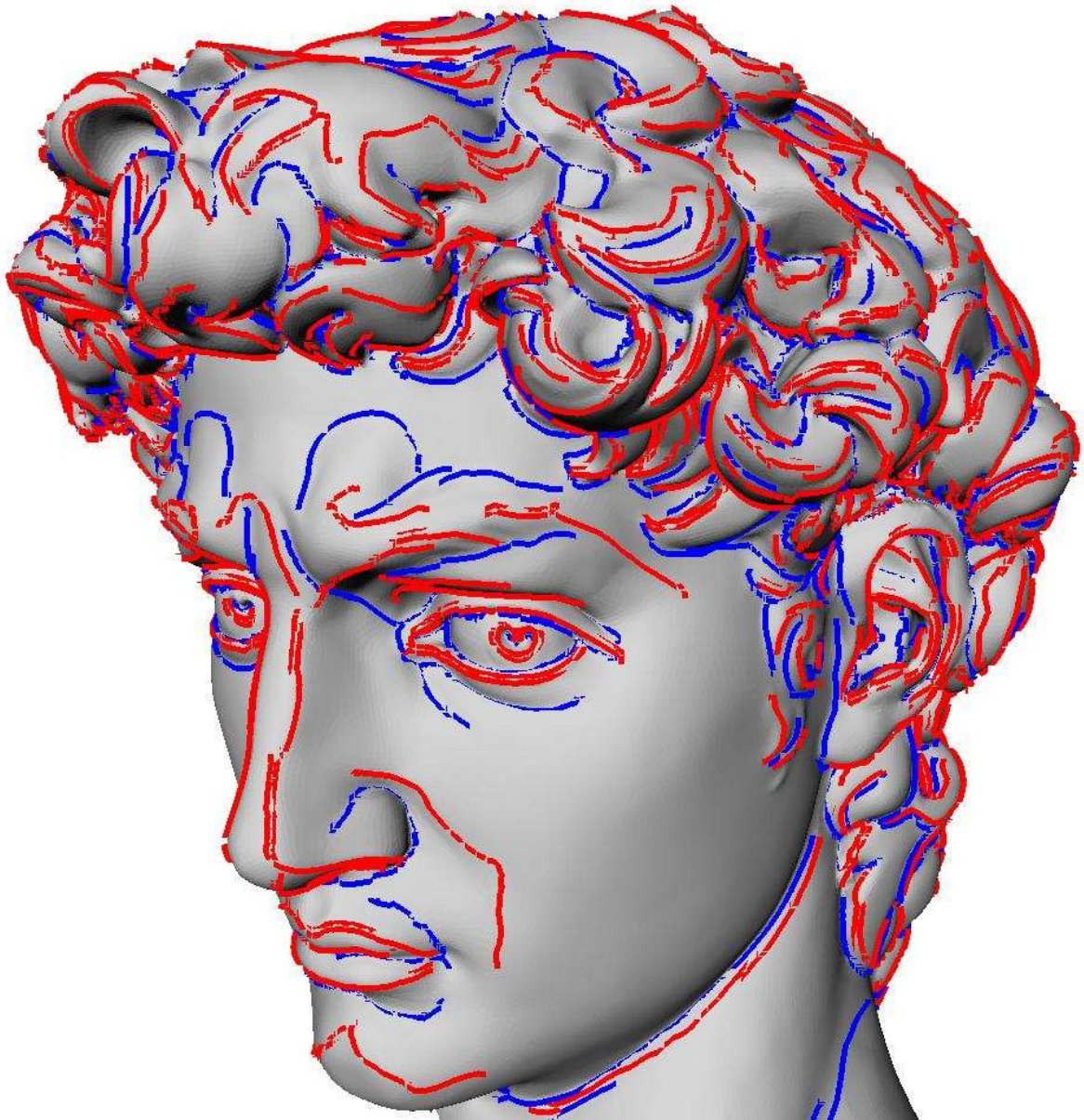


Figure 5.17: Filtered crest lines on a 380k pts model



## Chapter 6

# The implicit structure of ridges of a smooth parametric surface

As seen in the previous chapter, ridge extraction algorithms need of a local orientation procedure of principal directions. Consequently, the extraction is conducted locally and no global equation of ridges is defined.

On the way to developing certified algorithms independent from local orientation procedures, we study ridges of a parametric surface. For this special case, we are able to describe ridges as an implicit curve in the parametric domain and analyze its singularities. Algorithms exploiting the structure of  $P$  for polynomial surfaces are developed in the next chapter.

## 6.1 Introduction

### 6.1.1 Contributions and chapter overview

Let  $\Phi(u, v)$  be a smooth parameterized surface over a domain  $\mathcal{D} \subset \mathbb{R}^2$ . Recall that we qualify blue and red the ridges associated to the maximal and the minimal principal curvatures. We make the following two contributions. First, we exhibit the implicit equation  $P = 0$  of the singular curve  $\mathcal{S}$  encoding all ridges of the surface (blue and red), and show how to recover the colors from factors of  $P$ . Second, we derive a zero dimensional system coding the so-called turning points, from which elliptic and hyperbolic ridge sections of the two colors can be identified. Both contributions exploit properties of the Weingarten map of the surface and require computer algebra.

The chapter is organized as follows. Preliminary differential lemmas are proved in section 6.2. The implicit equation for ridges is derived in section 6.3. The system for turning points and the determination of ridge types are stated in section 6.4. Corollaries for polynomial parametric surfaces and an illustration of the effectiveness of the main theorem on a bidegree (4,4) Bezier surface is given in section 6.5. Symbolic computations performed with Maple are provided in section 6.6.

### 6.1.2 Notations

**Ridges.** The derivation of the implicit equation  $P = 0$  of all ridges of a surface exploits properties of the Weingarten map and of the Monge form of the surface. Properties of the Monge form, i.e. of the expression of the surface as a height function in a coordinate frame associated to the principal directions are recalled in chapter 3.4. We just point out the main notations and some key conventions.

At any point of the surface, the maximal (minimal) principal curvature is denoted  $k_1$  ( $k_2$ ), and its associated direction  $d_1$  ( $d_2$ ). Anything related to the maximal (minimal) curvature is qualified blue (red), for example we shall speak of the blue curvature for  $k_1$  or the red direction for  $d_2$ . A ridge associated with  $k_1$  is defined by the equation  $b_0 = 0$ , with  $b_0$  is the directional derivative of the principal curvature  $k_1$  along its curvature line. Similarly, ridges associated to  $k_2$  are defined by  $b_3 = 0$ . Since we shall make precise statements about ridges, it should be recalled that ridges through umbilics are open i.e. umbilics are excluded.



**Differential calculus.** Let  $f(u, v) : \mathcal{D} \subset \mathbb{R}^2 \rightarrow \mathbb{R}$  be a continuously differentiable function. The derivative of  $f$  with respect to variable  $u$  denoted  $f_u$ , and the gradient of  $f$  is denoted  $df = (f_u, f_v)$ . A point in  $\mathcal{D}$  is *singular* if the gradient  $df$  vanishes, else it is *regular*.

**Misc.** The inner product of two vectors  $x, y$  is denoted  $\langle x, y \rangle$ , the norm of  $x$  is  $\|x\| = \langle x, x \rangle^{1/2}$  and the exterior product is  $x \wedge y$ .

## 6.2 Manipulations involving the Weingarten map of the surface

Let  $\Phi$  be the parameterization of class  $C^k$  for  $k \geq 4$ . Principal directions and curvatures of the surface are expressed in terms of second order derivatives of  $\Phi$ . More precisely, the matrices of the first and second fundamental forms in the basis  $(\Phi_u, \Phi_v)$  of the tangent space are

$$I = \begin{pmatrix} e & f \\ f & g \end{pmatrix} = \begin{pmatrix} \langle \Phi_u, \Phi_u \rangle & \langle \Phi_u, \Phi_v \rangle \\ \langle \Phi_u, \Phi_v \rangle & \langle \Phi_v, \Phi_v \rangle \end{pmatrix},$$

$$II = \begin{pmatrix} l & m \\ m & n \end{pmatrix} = \begin{pmatrix} \langle N_n, \Phi_{uu} \rangle & \langle N_n, \Phi_{uv} \rangle \\ \langle N_n, \Phi_{uv} \rangle & \langle N_n, \Phi_{vv} \rangle \end{pmatrix}, \quad \text{with } N = \Phi_u \wedge \Phi_v, \quad N_n = \frac{N}{\|N\|}.$$

To compute the principal directions and curvatures, one resorts to the Weingarten map, whose matrix in the basis  $(\Phi_u, \Phi_v)$  is given by  $W = (w_{ij}) = I^{-1}II$ . The Weingarten map is a self-adjoint operator<sup>1</sup> of the tangent space [dC76]. The principal directions  $d_i$  and principal curvatures  $k_i$  are the eigenvectors and eigenvalues of the matrix  $W$ . Observing that  $\|N\|^2 = \det I$ , matrix  $W$  can also be written as follows—an expression of special interest for polynomial surfaces:

$$W = \frac{1}{(\det I)^{3/2}} \begin{pmatrix} A & B \\ C & D \end{pmatrix}. \quad (6.1)$$

Recall that a parameterized surface is called *regular* if the tangent map of the parameterization (the Jacobian) has rank two everywhere. Since the first fundamental form is the restriction of the inner product of the ambient space to the tangent space, one has:

**Observation. 9** *If  $\Phi$  is a parameterized surface which is regular, the quadratic form  $I$  is positive definite.*

In the following, the surface is assumed regular, thus  $\det(I) \neq 0$ .

### 6.2.1 Principal curvatures.

The characteristic polynomial of  $W$  is

$$P_W(k) = k^2 - \text{tr}(W)k + \det(W) = k^2 - (w_{11} + w_{22})k + w_{11}w_{22} - w_{12}w_{21}.$$

Its discriminant is

$$\Delta(k) = (\text{tr}(W))^2 - 4\det(W) = (w_{11} + w_{22})^2 - 4(w_{11}w_{22} - w_{12}w_{21}) = (w_{11} - w_{22})^2 + 4w_{12}w_{21}.$$

A simplification of this discriminant leads to the definition of the following function, denoted  $p_2$ :

$$p_2 = (\det I)^3 \Delta(k) = (A - D)^2 + 4BC$$

The principal curvatures  $k_i$ , with the convention  $k_1 \geq k_2$ , are the eigenvalues of  $W$ , that is:

$$k_1 = \frac{A + D + \sqrt{p_2}}{2(\det I)^{3/2}} \quad k_2 = \frac{A + D - \sqrt{p_2}}{2(\det I)^{3/2}}. \quad (6.2)$$

A point is called an *umbilic* if the principal curvatures are equal. One has:

**Lemma. 2** *The two following equivalent conditions characterize umbilics:*

<sup>1</sup>A self-adjoint map  $L$  over a vector space  $V$  with a bilinear form  $\langle \cdot, \cdot \rangle$  is a linear map such that  $\langle Lu, v \rangle = \langle u, Lv \rangle$ , for all  $u, v \in V$ . Such a map can be diagonalized in an orthonormal basis of  $V$ .

1.  $p_2 = 0$
2.  $A = D$  and  $B = C = 0$ .

*Proof.* Since  $\det(I) \neq 0$ , one has  $p_2 = 0 \Leftrightarrow \Delta(k) = 0$ , hence 1. characterizes umbilics. Condition 2. trivially implies 1. To prove the converse, assume that  $p_2 = 0$  i.e. the Weingarten map has a single eigenvalue  $k$ . This linear map is self-adjoint hence diagonalizable in an orthogonal basis, and the diagonal form is a multiple of the identity. It is easily checked that the matrix remains a multiple of the identity in any basis of the tangent space, in particular in the basis  $(\Phi_u, \Phi_v)$ , which implies condition 2.  $\square$

### 6.2.2 Principal directions.

Let us focus on the maximum principal direction  $d_1$ . A vector of direction  $d_1$  is an eigenvector of  $W$  for the eigenvalue  $k_1$ . Denote:

$$W - k_1 Id = \begin{pmatrix} w_{11} - k_1 & w_{12} \\ w_{21} & w_{22} - k_1 \end{pmatrix}. \quad (6.3)$$

At non umbilic points, the matrix  $W - k_1 Id$  has rank one, hence either  $(-w_{12}, w_{11} - k_1) \neq (0, 0)$  or  $(-w_{22} + k_1, w_{21}) \neq (0, 0)$ . Using the expression of  $W$  given by Eq. 6.1, up to a normalization factor of  $(\det I)^{3/2}$ , a non zero maximal principal vector can be chosen as either

$$v_1 = 2(\det I)^{3/2}(-w_{12}, w_{11} - k_1) = (-2B, A - D - \sqrt{p_2}) \text{ or } w_1 = 2(\det I)^{3/2}(-w_{22} + k_1, w_{21}) = (A - D + \sqrt{p_2}, 2C). \quad (6.4)$$

For the minimal principal direction  $d_2$  one chooses  $v_2 = (-2B, A - D + \sqrt{p_2})$  and  $w_2 = (A - D - \sqrt{p_2}, 2C)$ .

**Lemma. 3** *One has the following relations:*

$$\begin{aligned} v_1 = (0, 0) &\Leftrightarrow (B = 0 \text{ and } A \geq D), \\ v_2 = (0, 0) &\Leftrightarrow (B = 0 \text{ and } A \leq D), \\ w_1 = (0, 0) &\Leftrightarrow (C = 0 \text{ and } A \leq D), \\ w_2 = (0, 0) &\Leftrightarrow (C = 0 \text{ and } A \geq D). \end{aligned}$$

*Proof.* The proofs being equivalent, we focus on the first one. One has:

$$v_1 = (0, 0) \Leftrightarrow \begin{cases} B = 0 \\ A - D = \sqrt{(A - D)^2 + 4BC} \end{cases} \Leftrightarrow \begin{cases} B = 0 \\ A - D = \sqrt{(A - D)^2} \end{cases} \Leftrightarrow \begin{cases} B = 0 \\ A - D \geq 0 \end{cases}$$

$\square$

A direct consequence of lemma 3 is the following:

**Observation. 10** 1. *The two vector fields  $v_1$  and  $w_1$  vanish simultaneously exactly at umbilics. The same holds for  $v_2$  and  $w_2$ .*

2. *The equation  $\{v_1 = (0, 0) \text{ or } v_2 = (0, 0)\}$  is equivalent to  $B = 0$ .*

## 6.3 Implicitly defining ridges

In this section, we prove the implicit expression  $P = 0$  of ridges. Before diving into the technicalities, we first outline the method.

### 6.3.1 Problem

In characterizing ridges, a first difficulty comes from the fact that the sign of an extremality coefficient ( $b_0$  or  $b_3$ ) is not well defined. Away from umbilics, denoting  $d_1$  the principal direction associated to  $k_1$ , there are two unit opposite vectors  $y_1$  and  $-y_1$  orienting  $d_1$ . That is, one can define two extremality coefficients  $b_0(y_1) = \langle \nabla k_1, y_1 \rangle$  and  $b_0(-y_1) = \langle \nabla k_1, -y_1 \rangle = -b_0(y_1)$ . Therefore, the sign of  $b_0$  is not well defined. In particular, notice that tracking the zero crossings of  $b_0$  in-between two points of the surface requires using coherent orientation of the principal direction  $d_1$  at these endpoints, a problem usually addressed using the acute rule (see chap. 5). Notice however the equation  $b_0 = 0$  is not ambiguous. A second difficulty comes from umbilics where  $b_0$  is not defined since  $k_1$  is not smooth—that is  $\nabla k_1$  is not defined.



### 6.3.2 Method outline

Principal curvatures and directions read from the Weingarten map of the surface. At each point which is not an umbilic, one can define two vector fields  $v_1$  or  $w_1$  which are collinear with  $d_1$ , with the additional property that one (at least) of these two vectors is non vanishing. Let  $z$  stand for one of these non vanishing vectors. The nullity of  $b_0 = \langle \nabla k_1, y_1 \rangle$  is equivalent to that of  $\langle \nabla k_1, z \rangle$  —that is the normalization of the vector along which the directional derivative is computed does not matter.

Using  $v_1$  and  $w_1$ , the principal maximal vectors defined in the previous section, we obtain two independent equations of blue ridges. Each has the drawback of encoding, in addition to blue ridge points, the points where  $v_1$  (or  $w_1$ ) vanishes. As a consequence of observation 10, the conjunction of these two equations defines the set of blue ridges union the set of umbilics. The same holds for red ridges and the minimal principal vector fields  $v_2$  ad  $w_2$ . One has to note the symmetry between the equations for blue and red ridges in lemma 4. Eventually, combining the equation for blue ridges with  $v_1$  and the equation for red ridges with  $v_2$  gives the set of blue ridges union the set of red ridges union the set of zeros of  $v_1 = 0$  or  $v_2 = 0$ . This last set is also  $B = 0$  (observation 10), hence dividing by  $B$  allows to eradicate these spurious points and yields the equation  $P = 0$  of blue ridges together with red ridges. One can think of this equation as an improved version of the Gaussian extremality  $E_g = b_0 b_3$  defined in [Thi96].

Our strategy cumulates several advantages: (i)blue and red ridges are processed at once, and the information is encoded in a single equation (ii)orientation issues arising when one is tracking the zero crossings of  $b_0$  or  $b_3$  disappear. The only drawback is that one loses the color of the ridge. But this color is recovered with the evaluation of the sign of factors of the expression  $P$ .

### 6.3.3 Precisions of vocabulary

In the statement of the results, we shall use the following terminology. Umbilic points are points where both principal curvatures are equal. A ridge point is a point which is not an umbilic, and is an extremum of a principal curvature along its curvature line. A ridge point is further called a blue (red) ridge point is a an extrema of the blue (red) curvature along its line. A ridge point may be both blue and red, in which case it is called a purple point.

### 6.3.4 Implicit equation of ridges

**Lemma. 4** *For a regular surface, there exist differentiable functions  $a, a', b, b'$  which are polynomials with respect to  $A, B, C, D$  and  $\det I$ , as well as their first derivatives, such that:*

1. *the set of blue ridges union  $\{v_1 = 0\}$  has equation  $a\sqrt{p_2} + b = 0$ ,*
2. *the set of blue ridges union  $\{w_1 = 0\}$  has equation  $a'\sqrt{p_2} + b' = 0$ ,*
3. *the set of blue ridges union the set of umbilics has equation  $\begin{cases} a\sqrt{p_2} + b = 0 \\ a'\sqrt{p_2} + b' = 0 \end{cases}$*
4. *the set of red ridges union  $\{v_2 = 0\}$  has equation  $a\sqrt{p_2} - b = 0$ ,*
5. *the set of red ridges union  $\{w_2 = 0\}$  has equation  $a'\sqrt{p_2} - b' = 0$ ,*
6. *the set of red ridges union the set of umbilics has equation  $\begin{cases} a\sqrt{p_2} - b = 0 \\ a'\sqrt{p_2} - b' = 0 \end{cases}$*

Moreover,  $a, a', b, b'$  are defined by the equations:

$$a\sqrt{p_2} + b = \langle \text{Numer}(dk_1), v_1 \rangle \quad a'\sqrt{p_2} + b' = \langle \text{Numer}(dk_1), w_1 \rangle . \quad (6.5)$$

*Proof.* The principal curvatures are not differentiable at umbilics since the denominator of  $dk_i$  contains  $\sqrt{p_2}$ . But away from umbilics, the equation  $\langle dk_1, v_1 \rangle = 0$  is equivalent to  $\langle \text{Numer}(dk_1), v_1 \rangle = 0$ . This equation is rewritten as  $a\sqrt{p_2} + b = 0$ , the explicit expressions of  $a$  and  $b$  being given in section 6.6. This equation describes the set of blue ridge points union the set where  $v_1$  vanishes. A similar derivation yields the second claim. Finally, the third claim follows from observation 10.

Results for red ridges are similar and the reader is referred to section 6.6 for the details.  $\square$

**Lemma. 5** 1. If  $p_2 = 0$  then  $a = b = a' = b' = 0$ .

$$2. \text{ The set of purple points has equation } \begin{cases} a = b = a' = b' = 0 \\ p_2 \neq 0 \end{cases}$$

*Proof.* 1. If  $p_2 = 0$ , one has  $A = D$  and  $B = C = 0$ . Substituting these conditions in the expressions of  $a, a', b, b'$  gives the result, computations are sketched in section 6.6.

2. Let  $p$  be a purple point, it is a ridge point and hence not an umbilic, then  $p_2 \neq 0$ . The point  $p$  is a blue and a red ridge point, hence it satisfies all equations of lemma 4. If  $a \neq 0$  then equations 1. and 4. imply  $\sqrt{p_2} = -b/a = b/a$  hence  $b = 0$  and  $\sqrt{p_2} = 0$  which is a contradiction. Consequently,  $a = 0$  and again equation 1. implies  $b = 0$ . A similar argument with equation 2. and 5. gives  $a' = b' = 0$ .

The converse is trivial: if  $a = b = a' = b' = 0$  then equations 3. and 6. imply that the point is a purple point or an umbilic. The additional condition  $p_2 \neq 0$  excludes umbilics.  $\square$

The following definition is a technical tool to state the next theorem in a simple way. The meaning of the function  $Sign_{ridge}$  introduced here will be clear from the proof of the theorem. Essentially, this function describes all the possible sign configurations for  $ab$  and  $a'b'$  at a ridge point.

**Definition. 15** The function  $Sign_{ridge}$  takes the values

$$\begin{aligned} -1 & \text{ if } \begin{cases} ab < 0 \\ a'b' \leq 0 \end{cases} \quad \text{or} \quad \begin{cases} ab \leq 0 \\ a'b' < 0 \end{cases}, \\ +1 & \text{ if } \begin{cases} ab > 0 \\ a'b' \geq 0 \end{cases} \quad \text{or} \quad \begin{cases} ab \geq 0 \\ a'b' > 0 \end{cases}, \\ 0 & \text{ if } ab = a'b' = 0. \end{aligned}$$

**Theorem. 14** The set of blue ridges union the set of red ridges union the set of umbilics has equation  $P = 0$  with  $P = (a^2 p_2 - b^2)/B$ , and one also has  $P = -(a^2 p_2 - b^2)/C = 2(a'b - ab')$ . For a point of this set  $\mathcal{P}$ , one has:

- If  $p_2 = 0$ , the point is an umbilic.
- If  $p_2 \neq 0$  then:
  - if  $Sign_{ridge} = -1$  then the point is a blue ridge point,
  - if  $Sign_{ridge} = +1$  then the point is a red ridge point,
  - if  $Sign_{ridge} = 0$  then the point is a purple point.

*Proof.* To form the equation of  $\mathcal{P}$ , following the characterization of red and blue ridges in lemma 4, and the vanishing of the vector fields  $v_1$  and  $v_2$  in lemma 3, we take the product of equations 1. and 3. of lemma 4. The equivalence between the three equations of  $\mathcal{P}$  is proven with the help of Maple, see section 6.6.

To qualify points on  $\mathcal{P}$ , first observe that the case  $p_2 = 0$  has already been considered in lemma 5. Therefore, assume  $p_2 \neq 0$ , and first notice the following two simple facts:

- The equation  $(a^2 p_2 - b^2)/B = 0$  for  $\mathcal{P}$  implies that  $a = 0 \Leftrightarrow b = 0 \Leftrightarrow ab = 0$ . Similarly, the equation  $-(a^2 p_2 - b^2)/C = 0$  for  $\mathcal{P}$  implies that  $a' = 0 \Leftrightarrow b' = 0 \Leftrightarrow a'b' = 0$ .
- If  $ab \neq 0$  and  $a'b' \neq 0$ , the equation  $ab' - a'b = 0$  for  $\mathcal{P}$  implies  $b/a = b'/a'$ , that is the signs of  $ab$  and  $a'b'$  agree.

These two facts explain the introduction of the function  $Sign_{ridge}$  of definition 15. This function enumerates all disjoint possible configurations of signs for  $ab$  and  $a'b'$  for a point on  $\mathcal{P}$ . One can now study the different cases with respect to the signs of  $ab$  and  $a'b'$  or equivalently the values of the function  $Sign_{ridge}$ .

**Assume**  $Sign_{ridge} = -1$ .

–*First case:*  $ab < 0$ . The equation  $(a^2 p_2 - b^2)/2B = 0$  implies that  $(a\sqrt{p_2} + b)(a\sqrt{p_2} - b) = 0$ . Since  $\sqrt{p_2} > 0$ , one must have  $a\sqrt{p_2} + b = 0$  which is equation 1 of lemma 4. From the second simple fact, either  $a'b' < 0$  or  $a'b' = 0$ .

- For the first sub-case  $a'b' < 0$ , equation  $(a'^2 p_2 - b'^2)/C = 0$  implies  $(a'\sqrt{p_2} + b')(a'\sqrt{p_2} - b') = 0$ . Since  $\sqrt{p_2} > 0$ , one must have  $a'\sqrt{p_2} + b' = 0$  which is equation 2 of lemma 4.
- For the second sub-case  $a'b' = 0$ , one has  $a' = b' = 0$  and the equation 2 of lemma 4 is also satisfied. (Moreover, equation 5 is also satisfied which implies that  $w_2 = 0$ ).

In both cases, equations 1 and 2 or equivalently equation 3 are satisfied. Since one has excluded umbilics, the point is a blue ridge point.

–*Second case:*  $ab = 0$ . One has  $a'b' < 0$  the study is similar to the above.  $ab = 0$  implies equation 1 and  $a'b' < 0$  implies equation 2 of lemma 4. The point is a blue ridge point.

**Assume**  $Sign_{ridge} = 1$ .

This case is the exact symmetric of the previous, one only has to exchange the roles of  $a, b$  and  $a', b'$ .

**Assume**  $Sign_{ridge} = 0$ .

The first simple fact implies  $a = b = a' = b' = 0$  and lemma 5 identifies a purple point.  $\square$

As shown along the proof, the conjunctions  $<, =$  and  $=, <$  in the definition of  $Sign_{ridge} = -1$  correspond to the blue ridge points where the vector fields  $w_2$  and  $v_2$  vanish. The same holds for  $Sign_{ridge} = 1$  and  $w_1$  and  $v_1$ . One can also observe that the basic ingredient of the previous proof is to transform an equation with a square root into a system with an inequality. More formally:

**Observation. 11** For  $x, y, z$  real numbers and  $z \geq 0$ , one has:

$$x\sqrt{z} + y = 0 \iff \begin{cases} x^2 z - y^2 = 0 \\ xy \leq 0 \end{cases} \quad (6.6)$$

### 6.3.5 Singular points of $\mathcal{P}$

Having characterized umbilics, purple points and ridges in the domain  $\mathcal{D}$  with implicit equations, an interesting question is to relate the properties of these equations to the classical differential geometric properties of these points.

In particular, recall that generically (with the description of surfaces with Monge patches and contact theory recalled in chapter 3.4), umbilics of a surface are either 1-ridge umbilics or 3-ridge umbilics. This means that there are either 1 or 3 non-singular ridge branches passing through an umbilic. The latter are obviously singular points of  $\mathcal{P}$  since three branches of the curve are crossing at the umbilic. For the former ones, it is appealing to believe they are regular points since the tangent space to the ridge curve on the surface at such points is well defined and can be derived from the cubic of the Monge form [HGY<sup>+</sup>99]. Unfortunately, one has:

**Proposition. 5** Umbilics are singular points of multiplicity at least 3 of the function  $P$  (i.e. the gradient and the Hessian of  $P$  vanish).

*Proof.* Following the notations of Porteous [Por01], denote  $P_k$ ,  $k = 1, \dots, 3$  the  $k$ th times linear form associated with  $P$ , that is  $P_k = [\partial P / (\partial u^{k-i} \partial v^i)]_{i=0, \dots, k}$ . Phrased differently,  $P_1$  is the gradient,  $P_2$  is the vector whose three entries encodes the Hessian of  $P$ , etc. To show that the multiplicity of an umbilic of coordinates  $(u_0, v_0)$  is at least three, we need to show that  $P_1(u_0, v_0) = [0, 0]$ ,  $P_2(u_0, v_0) = [0, 0, 0]$ . We naturally do not know the coordinates of umbilics, but lemma 2 provides the umbilical conditions. The proof consists of computing derivatives and performing the appropriate substitutions under Maple, and is given in section 6.6.  $\square$

We can go one step further so as to relate the type of the cubic  $P_3$  —the third derivative of  $P$ — to the number of non-singular ridge branches at the umbilic.

**Proposition. 6** The classification of an umbilic as 1-ridge or 3-ridges from  $P_3$  goes as follows:

- If  $P_3$  is elliptic, that is the discriminant of  $P_3$  is positive ( $\delta(P_3) > 0$ ), then the umbilic is a 3-ridge umbilic and the 3 tangent lines to the ridges at the umbilic are distinct.
- If  $P_3$  is hyperbolic ( $\delta(P_3) < 0$ ) then the umbilic is a 1-ridge umbilic.

*Proof.* Since the properties of interest here are local ones, studying ridges on the surface or in the parametric domain is equivalent because the parameterization is a local diffeomorphism. More precisely the parameterization  $\Phi$  maps a curve passing through  $(u_0, v_0) \in \mathcal{D}$  to a curve passing through the umbilic  $p_0 = \Phi(u_0, v_0)$  on the surface  $S = \Phi(\mathcal{D})$ . Moreover, the invertible linear map  $d\Phi_{(u_0, v_0)}$  maps the tangent to the curve in  $\mathcal{D}$  at  $(u_0, v_0)$  to the tangent at  $p_0$  to its image curve in the tangent space  $T_{p_0}S$ .

Having observed the multiplicity of umbilics is at least three, we resort to singularity theory. From [AVGZ82, Section 11.2, p157], we know that a cubic whose discriminant is non null is equivalent up to a linear transformation to the normal form  $y(x^2 \pm y^2)$ . Moreover, a function having a vanishing second order Taylor expansion and its third derivative of this form is diffeomorphic to the same normal form. Therefore, whenever the discriminant of  $P_3$  is non null, up to a diffeomorphism, the umbilic is a so called  $D_4^\pm$  singularity of  $P$ , whose normal form is  $y(x^2 \pm y^2)$ . It is then easily seen that the zero level set consists of three non-singular curves through the umbilic with distinct tangents which are the factor lines of the cubic. For a  $D_4^-$  singularity ( $\delta(P_3) > 0$ ), these 3 curves are real curves and the umbilic is a 3-ridge. For a  $D_4^+$  singularity  $\delta(P_3) < 0$ , only one curve is real and the umbilic is a 1-ridge.  $\square$

Note that the classifications of umbilics with the Monge cubic  $C_M$  and the cubic  $P_3$  do not coincide. Indeed if  $C_M$  is elliptic, it may occur that two ridges have the same tangent. In such a case, the cubic  $P_3$  is not elliptic since  $\delta(P_3) = 0$ .

Since purple points correspond to the intersection of two ridges, one has:

**Proposition. 7** *Purple points are singular points of multiplicity at least 2 of the function  $P$  (i.e. the gradient of  $P$  vanish).*

*Proof.* It follows from the equation  $P = 2(a'b - ab')$  that  $dP = 2(d(a')b + a'd(b) - d(a)b - ad(b))$ . At purple points one has  $a = a' = b = b' = 0$  hence  $dP = 0$ .  $\square$

## 6.4 Implicit system for turning points and ridge type

In this section, we define a system of equations that encodes turning points. Once these turning points identified, we show how to retrieve the type (elliptic or hyperbolic) of a ridge from a sign evaluation.

### 6.4.1 Problem

Going one step further in the description of ridges requires distinguishing between ridges which are maxima or minima of the principal curvatures. Following the classical terminology recalled in chapter 3.4, a blue (red) ridge changes from a maxima to a minima at a blue (red) turning point. These turning points are witnessed by the vanishing of the second derivative of the principal curvature along its curvature line. As recalled in chapter 3.4 —see [HGY<sup>+</sup>99] for the details, from the parameterization of a principal curvature along its curvature line —Eq. 3.6, a turning point is witnessed by the vanishing of the coefficient  $P_1$  ( $P_2$ ) for blue (red) ridges. Since we are working from a parameterization, denoting  $Hess$  the Hessian matrix of either principal curvature, we have:

**Observation. 12** *A blue turning point is a blue ridge point where  $Hess(k_1)(d_1, d_1) = 0$ . Similarly, a red turning point is a red ridge point with  $Hess(k_2)(d_2, d_2) = 0$ .*

Generically, turning points are not purple points, however we shall provide conditions identifying these cases. Even less generic is the existence of a purple point which is also a blue and a red turning point, a situation for which we also provide conditions.

Once turning points have been found, reporting elliptic and hyperbolic ridge sections is especially easy. For ridges through umbilics, since ridges at umbilics are hyperbolic, and the two types alternate at turning points, the task is immediate. For ridges avoiding umbilics, one just has to test the sign of  $Hess(k_1)(d_1, d_1)$  or  $Hess(k_2)(d_2, d_2)$  at a ridge points, and then propagate the alternation at turning points.

### 6.4.2 Method outline

We focus on blue turning points since the method for red turning points is similar. As already pointed out, we do not have a global expression of the blue direction  $d_1$ , but only the two blue vector fields  $v_1$  and  $w_1$  vanishing on some curves going through umbilics. Consequently, we have to combine equations with these two fields to get a global expression of turning points. A blue ridge point is a blue turning point iff  $Hess(k_1)(d_1, d_1) = 0$ . This last

equation is equivalent to  $\text{Numer}(\text{Hess}(k_1))(v_1, v_1) = 0$  when the vector field  $v_1$  does not vanish. The same holds for the equation  $\text{Numer}(\text{Hess}(k_1))(w_1, w_1) = 0$  and the solutions of  $w_1 = (0, 0)$ . As a consequence of observation 10, the conjunction of these two equations defines the set of blue turning points.

The drawback of distinguishing the color of the turning points is that equations contain a square root. Combining the equations for blue and red turning points gives an equation  $Q = 0$  without square roots. The intersection of the corresponding curve  $\mathcal{Q}$  with the ridge curve  $\mathcal{P}$  and sign evaluations allow to retrieve all turning points and their color.

### 6.4.3 System for turning points

**Lemma. 6** *For a regular surface, there exist differentiable functions  $\alpha, \alpha', \beta, \beta'$  which are polynomials with respect to  $A, B, C, D$  and  $\det I$ , as well as their first and second derivatives, such that:*

1.  $\text{Numer}(\text{Hess}(k_1))(v_1, v_1) = \alpha\sqrt{p_2} + \beta$ .
2.  $\text{Numer}(\text{Hess}(k_1))(w_1, w_1) = \alpha'\sqrt{p_2} + \beta'$ .
3. A blue ridge point is a blue turning point iff  $\begin{cases} \alpha\sqrt{p_2} + \beta = 0 \\ \alpha'\sqrt{p_2} + \beta' = 0 \end{cases}$
4.  $\text{Numer}(\text{Hess}(k_2))(v_2, v_2) = \alpha\sqrt{p_2} - \beta$ .
5.  $\text{Numer}(\text{Hess}(k_2))(w_2, w_2) = \alpha'\sqrt{p_2} - \beta'$ .
6. A red ridge point is a red turning point iff  $\begin{cases} \alpha\sqrt{p_2} - \beta = 0 \\ \alpha'\sqrt{p_2} - \beta' = 0 \end{cases}$

*Proof.* Calculations for points 1-2-4-5 are performed with Maple cf. section 6.6. Blue turning points are blue ridge points on  $\mathcal{P}$  where  $\text{Hess}(k_1)(d_1, d_1) = 0$ . This equation is not defined at umbilics where principal curvatures are not differentiable. Nevertheless, including umbilics and points where  $v_1$  vanishes, this equation is equivalent to  $\text{Numer}(\text{Hess}(k_1))(v_1, v_1) = 0$ . This equation is rewritten as  $\alpha\sqrt{p_2} + \beta = 0$  and yields point 1. The same analysis holds for  $w_1$  and yields point 2. Point 3. is a consequence of observation 10. Results for red turning points are similar and the reader is referred to section 6.6 for the details.  $\square$

The following definition is a technical tool to state the next theorem in a simple way. As we shall see along the proof, this function describes all the possible sign configurations for  $\alpha\beta$  and  $\alpha'\beta'$  at a turning point.

**Definition. 16** *The function  $\text{Sign}_{\text{turn}}$  takes the values*

$$\begin{aligned} -1 & \text{ if } \begin{cases} \alpha\beta < 0 \\ \alpha'\beta' \leq 0 \end{cases} \quad \text{or} \quad \begin{cases} \alpha\beta \leq 0 \\ \alpha'\beta' < 0 \end{cases}, \\ +1 & \text{ if } \begin{cases} \alpha\beta > 0 \\ \alpha'\beta' \geq 0 \end{cases} \quad \text{or} \quad \begin{cases} \alpha\beta \geq 0 \\ \alpha'\beta' > 0 \end{cases}, \\ 0 & \text{ if } \alpha\beta = \alpha'\beta' = 0. \end{aligned}$$

**Theorem. 15** *Let  $Q$  be the smooth function which is a polynomial with respect to  $A, B, C, D$  and  $\det I$ , as well as their first and second derivatives defined by*

$$Q = (\alpha^2 p_2 - \beta^2)/B^2 = (\alpha'^2 p_2 - \beta'^2)/C^2 = 2(\alpha'\beta - \alpha\beta')/(D - A). \quad (6.7)$$

The system  $\begin{cases} P = 0 \\ Q = 0 \end{cases}$  encodes turning points in the following sense. For a point, solution of this system, one has:

- If  $p_2 = 0$ , the point is an umbilic.
- If  $p_2 \neq 0$  then:

- if  $Sign_{ridge} = -1$  and  $Sign_{turn} \leq 0$  then the point is a blue turning point,
- if  $Sign_{ridge} = +1$  and  $Sign_{turn} \geq 0$  then the point is a red turning point,
- if  $Sign_{ridge} = 0$  then the point is purple point and in addition
  - \* if  $Sign_{turn} = -1$  then the point is also a blue turning point,
  - \* if  $Sign_{turn} = +1$  then the point is also a red turning point,
  - \* if  $Sign_{turn} = 0$  then the point is also a blue and a red turning point.

*Proof.* Following lemma 6, we form the equation of  $Q$  by taking the products of 1. and 4. in the lemma. Equalities of equation 6.7 are performed with Maple cf. section 6.6.

The case  $p_2 = 0$  has already been considered in lemma 5. Assume that  $p_2 \neq 0$ , and first notice the following two simple facts:

- The equation  $(\alpha^2 p_2 - \beta^2)/B^2 = 0$  for  $\mathcal{Q}$  implies that  $\alpha = 0 \Leftrightarrow \beta = 0 \Leftrightarrow \alpha\beta = 0$ . Similarly, the equation  $(\alpha'^2 p_2 - \beta'^2)/C^2 = 0$  for  $\mathcal{Q}$  implies that  $\alpha' = 0 \Leftrightarrow \beta' = 0 \Leftrightarrow \alpha'\beta' = 0$ .
- If  $\alpha\beta \neq 0$  and  $\alpha'\beta' \neq 0$ , the equation  $2(\alpha'\beta - \alpha\beta')/(D - A) = 0$  for  $\mathcal{Q}$  implies  $\beta/\alpha = \beta'/\alpha'$ , that is the signs of  $\alpha\beta$  and  $\alpha'\beta'$  agree.

These two facts explain the introduction of the function  $Sign_{turn}$  of definition 16. This function enumerates all disjoint possible configurations of signs for  $\alpha\beta$  and  $\alpha'\beta'$  for a point on  $\mathcal{Q}$ . The analysis of the different cases is similar to that of the proof of theorem 14, the basic ingredient being observation 11.  $\square$

**Observation. 13** *Note that in the formulation of equation 6.7 there are solutions of the system ( $P = 0$  and  $Q = 0$ ) which are not turning points nor umbilics. These points are characterized by ( $Sign_{ridge} = -1$  and  $Sign_{turn} = +1$ ) or ( $Sign_{ridge} = +1$  and  $Sign_{turn} = -1$ ). This drawback is unavoidable since equations avoiding the term  $\sqrt{p_2}$  cannot distinguish colors.*

**Observation. 14** *The following holds:*

- $p_2 = 0$  implies  $\alpha = \alpha' = \beta = \beta' = 0$
- $\alpha = \alpha' = \beta = \beta' = 0$  are singularities of  $Q$  of multiplicity at least 2.

To test if a blue ridge segment between two turning points is a maxima or a minima requires the evaluation of the sign of  $\alpha\sqrt{p_2} + \beta$  or  $\alpha'\sqrt{p_2} + \beta'$ , which cannot vanish simultaneously.

## 6.5 Polynomial surfaces

A fundamental class of surface used in Computer Aided Geometric Design consist of Bezier surfaces and splines. In this section, we state some elementary observations on the objects studied so far, for the particular case of polynomial parametric surfaces. Notice that the parameterization can be general, in which case  $\Phi(u, v) = (x(u, v), y(u, v), z(u, v))$ , or can be a height function  $\Phi(u, v) = (u, v, z(u, v))$ .

### 6.5.1 About $W$ and the vector fields

Using Eq. 6.1, we first observe that if  $\Phi$  is a polynomial then the coefficients  $A, B, C$  and  $D$  are also polynomials—this explains the factor  $(\det I)^{3/2}$  in the denominator of  $W$  in equation 6.1. For example

$$\begin{aligned} A &= (\det I)^{3/2} w_{11} = (\det I)^{3/2} \frac{g^l - fm}{\det I} = \sqrt{\det I} (g < N/\sqrt{\det I}, \Phi_{uu} > - f < N/\sqrt{\det I}, \Phi_{uv} >) \\ &= g < N, \Phi_{uu} > - f < N, \Phi_{uv} > . \end{aligned}$$

Thus, in the polynomial case, the equation of ridges is algebraic. Hence the set of all ridges and umbilics is globally described by an algebraic curve. The function  $Q$  is also a polynomial so that turning points are described by a polynomial system.

An interesting corollary of lemma 3 for the case of polynomial surfaces is the following:

**Observation. 15** *Given a principal vector  $v$ , denote  $Z_v$  the zero set of  $v$  i.e. the set of points where  $v$  vanishes. For a polynomial surface, the sets  $Z_{v_1}, Z_{w_1}, Z_{v_2}, Z_{w_2}$  are semi-algebraic sets.*



### 6.5.2 Degrees of expressions

As a corollary of Thm. 14 and 15, one can give upper bounds for the total degrees of expressions with respect to that of the parameterization. Distinguishing the cases where  $\Phi$  is a general parameterization or a height function (that is  $\Phi(u, v) = (u, v, h(u, v))$ ) with  $h(u, v)$  and denoting  $d$  the total degree of  $\Phi$ , table 6.1 gives the total degrees of  $A, B, C, D, \det I, P$  and  $Q$ .

Note that in the case of a height function,  $P$  is divided by its factor  $\det I^2$ , and  $Q$  is divided by its factor  $\det I$  (cf. section 6.6).

Polynomials	General parameterization	Height function
$A, B, C, D$	$d_1 = 5d - 6$	$d_{1_h} = 3d - 4$
$\det I$	$d_2 = 4d - 4$	$d_2 = 4d - 4$
$P$	$5d_1 + 2d_2 - 2 = 33d - 40$	$5d_{1_h} - 2 = 15d - 22$
$Q$	$10d_1 + 4d_2 - 4 = 66d - 80$	$10d_{1_h} + 3d_2 - 4 = 42d - 56$

Figure 6.1: Total degrees of polynomials

### 6.5.3 An example

Theorem 14 is effective and allows one to report certified ridges of polynomial parametric surfaces without resorting to local orientation procedures.

Without engaging into the algebraic developments carried out in the next chapter, we just provide an illustration of ridges for a degree four Bezier surface defined over the domain  $\mathcal{D} = [0, 1] \times [0, 1]$ . This surface, already studied in the former chapter (see Fig. 5.12), can be expressed as the graph of the total degree 8 polynomial  $h(u, v)$  for  $(u, v) \in [0, 1]^2$ :

$$h(u, v) = 116u^4v^4 - 200u^4v^3 + 108u^4v^2 - 24u^4v - 312u^3v^4 + 592u^3v^3 - 360u^3v^2 + 80u^3v + 252u^2v^4 - 504u^2v^3 + 324u^2v^2 - 72u^2v - 56uv^4 + 112uv^3 - 72uv^2 + 16uv.$$

The computation of the implicit curve has been performed using Maple 9.5 (see section 6.6). It is a bivariate polynomial  $P(u, v)$  of total degree 84, of degree 43 in  $u$ , degree 43 in  $v$  with 1907 terms and coefficients with up to 53 digits. Figure 6.2 displays ridges on the parametric domain  $\mathcal{D}$ , there are 17 purple points (black dots) and 8 umbilics (green dots), 3 of which are 3-ridge and 5 are 1-ridge. More information on this example and other examples are provided in the next chapter.

## 6.6 Maple computations

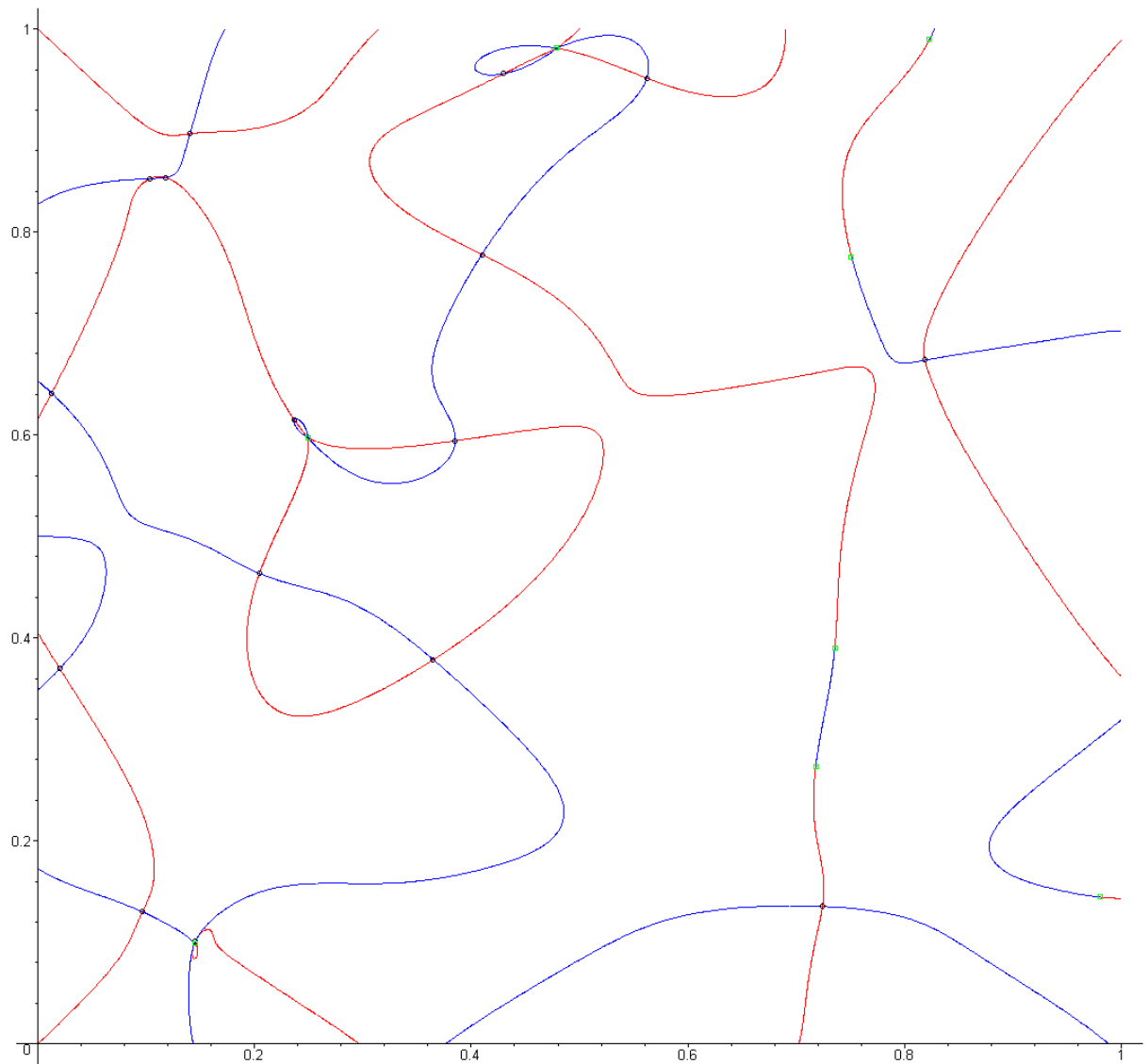
The Maple computations are provided for convenience. The corresponding Maple worksheet is available from the authors' web pages.

### 6.6.1 Principal directions, curvatures and derivatives

```
> v1 := [-2*B(u, v), A(u, v) - DD(u, v) - sqrt(p2(u, v))];
> w1 := [A(u, v) - DD(u, v) + sqrt(p2(u, v)), 2*C(u, v)];
> v2 := [-2*B(u, v), A(u, v) - DD(u, v) + sqrt(p2(u, v))];
> w2 := [A(u, v) - DD(u, v) - sqrt(p2(u, v)), 2*C(u, v)];
> k1 := (A(u, v) + DD(u, v) + sqrt(p2(u, v))) / (2*detI(u, v)^(3/2));
> k2 := (A(u, v) + DD(u, v) - sqrt(p2(u, v))) / (2*detI(u, v)^(3/2));
```

$$\begin{aligned} v1 &:= [-2B(u, v), A(u, v) - DD(u, v) - \sqrt{p2(u, v)}] \\ w1 &:= [A(u, v) - DD(u, v) + \sqrt{p2(u, v)}, 2C(u, v)] \\ v2 &:= [-2B(u, v), A(u, v) - DD(u, v) + \sqrt{p2(u, v)}] \\ w2 &:= [A(u, v) - DD(u, v) - \sqrt{p2(u, v)}, 2C(u, v)] \\ k1 &:= 1/2 \frac{A(u, v) + DD(u, v) + \sqrt{p2(u, v)}}{(\det I(u, v))^{3/2}} \\ k2 &:= 1/2 \frac{A(u, v) + DD(u, v) - \sqrt{p2(u, v)}}{(\det I(u, v))^{3/2}} \end{aligned}$$

First derivatives

Figure 6.2: The certified plot of  $\mathcal{P}$  (1024×1024 pixels)

```

> k1u:=diff(k1,u);k1un:=numer(k1u):
> k1v:=diff(k1,v):k1vn:=numer(k1v):
> k2u:=diff(k2,u):k2un:=numer(k2u):
> k2v:=diff(k2,v):k2vn:=numer(k2v):
> dk1n:=[k1un, k1vn]:
> dk2n:=[k2un, k2vn]:

```

$$k1u := 1/2 \left( \frac{\partial}{\partial u} A(u,v) + \frac{\partial}{\partial u} DD(u,v) + 1/2 \frac{\frac{\partial}{\partial u} p^2(u,v)}{\sqrt{p^2(u,v)}} \right) (detl(u,v))^{-3/2} - 3/4 \frac{(A(u,v) + DD(u,v) + \sqrt{p^2(u,v)}) \frac{\partial}{\partial u} detl(u,v)}{(detl(u,v))^{5/2}}$$

Second derivatives

```

> k1uu:=diff(k1,u$2):k1uun:=numer(k1uu):
> k1uv:=diff(k1,u,v):k1uvn:=numer(k1uv):
> k1vv:=diff(k1,v$2):k1vvn:=numer(k1vv):
> k2uu:=diff(k2,u$2):k2uun:=numer(k2uu):
> k2uv:=diff(k2,u,v):k2uvn:=numer(k2uv):
> k2vv:=diff(k2,v$2):k2vvn:=numer(k2vv):

```

## 6.6.2 Ridges

Blue and red equations with respect to the vector fields  $v_1, v_2, w_1, w_2$ .

```

> subs_sqrtp2:=sqrt(p2(u,v)) = sqrtp2, p2(u,v)^(3/2)= p2(u,v)*sqrtp2;
> b0v1:=subs( subs_sqrtp2, expand(linalg[dotprod](dk1n,v1, 'orthogonal') )):
> b0w1:=subs( subs_sqrtp2, expand(linalg[dotprod](dk1n,w1, 'orthogonal') )):
> b3v2:=subs( subs_sqrtp2, expand(linalg[dotprod](dk2n,v2, 'orthogonal') )):
> b3w2:=subs( subs_sqrtp2, expand(linalg[dotprod](dk2n,w2, 'orthogonal') )):
> b0v1a:=coeff(b0v1, sqrtp2, 1):b0v1b:=coeff(b0v1, sqrtp2, 0):
> b0w1a:=coeff(b0w1, sqrtp2, 1):b0w1b:=coeff(b0w1, sqrtp2, 0):
> b3v2a:=coeff(b3v2, sqrtp2, 1):b3v2b:=coeff(b3v2, sqrtp2, 0):
> b3w2a:=coeff(b3w2, sqrtp2, 1):b3w2b:=coeff(b3w2, sqrtp2, 0):

```

$$\text{subs\_sqrtp2} := \left\{ (p2(u,v))^{3/2} = p2(u,v)\text{sqrtp2}, \sqrt{p2(u,v)} = \text{sqrtp2} \right\}$$

Identities between b0 with (v1,w1) and b3 with (v2,w2).

```

> [b3v2a-b0v1a, b0v1b+b3v2b, b3w2a-b0w1a, b0w1b+b3w2b];
[0,0,0,0]

```

Definition of a,b,abis,bbis

```

> subs_p2:= p2(u,v)=(A(u,v)-DD(u,v))^2+4*B(u,v)*C(u,v);
> a:=expand(subs(subs_p2, b0v1a));
> b:=expand(subs(subs_p2, b0v1b));
> abis:=expand(subs(subs_p2, b0w1a));
> bbis:=expand(subs(subs_p2, b0w1b));

```

$$\text{subs\_p2} := \left\{ p2(u,v) = (A(u,v) - DD(u,v))^2 + 4B(u,v)C(u,v) \right\}$$

$$\begin{aligned}
a := & -4B(u,v) \det I(u,v) \frac{\partial}{\partial u} A(u,v) - 4B(u,v) \det I(u,v) \frac{\partial}{\partial u} DD(u,v) \\
& + 6B(u,v) \left( \frac{\partial}{\partial u} \det I(u,v) \right) A(u,v) + 6B(u,v) \left( \frac{\partial}{\partial u} \det I(u,v) \right) DD(u,v) + 4 \det I(u,v) \left( \frac{\partial}{\partial v} DD(u,v) \right) A(u,v) \\
& - 4 \det I(u,v) \left( \frac{\partial}{\partial v} DD(u,v) \right) DD(u,v) - 4 \det I(u,v) \left( \frac{\partial}{\partial v} B(u,v) \right) C(u,v) - 4 \det I(u,v) B(u,v) \frac{\partial}{\partial v} C(u,v) \\
& + 6 \left( \frac{\partial}{\partial v} \det I(u,v) \right) (DD(u,v))^2 - 6 \left( \frac{\partial}{\partial v} \det I(u,v) \right) A(u,v) DD(u,v) + 12 \left( \frac{\partial}{\partial v} \det I(u,v) \right) B(u,v) C(u,v)
\end{aligned}$$

$$\begin{aligned}
b := & 6B(u,v) \left( \frac{\partial}{\partial u} \det I(u,v) \right) (DD(u,v))^2 + 24 (B(u,v))^2 \left( \frac{\partial}{\partial u} \det I(u,v) \right) C(u,v) \\
& - 8 (B(u,v))^2 \det I(u,v) \frac{\partial}{\partial u} C(u,v) - 4 \det I(u,v) \left( \frac{\partial}{\partial v} DD(u,v) \right) (A(u,v))^2 \\
& + 6B(u,v) \left( \frac{\partial}{\partial u} \det I(u,v) \right) (A(u,v))^2 - 12 \left( \frac{\partial}{\partial v} \det I(u,v) \right) (DD(u,v))^2 A(u,v) \\
& - 4 \det I(u,v) \left( \frac{\partial}{\partial v} DD(u,v) \right) (DD(u,v))^2 + 6 \left( \frac{\partial}{\partial v} \det I(u,v) \right) DD(u,v) (A(u,v))^2 \\
& - 4B(u,v) \det I(u,v) A(u,v) \frac{\partial}{\partial u} A(u,v) \\
& + 4B(u,v) \det I(u,v) \left( \frac{\partial}{\partial u} A(u,v) \right) DD(u,v) + 4B(u,v) \det I(u,v) A(u,v) \frac{\partial}{\partial u} DD(u,v) \\
& - 4B(u,v) \det I(u,v) DD(u,v) \frac{\partial}{\partial u} DD(u,v) - 8B(u,v) \det I(u,v) \left( \frac{\partial}{\partial u} B(u,v) \right) C(u,v) \\
& - 12B(u,v) \left( \frac{\partial}{\partial u} \det I(u,v) \right) A(u,v) DD(u,v) - 8 \det I(u,v) \left( \frac{\partial}{\partial v} A(u,v) \right) B(u,v) C(u,v) \\
& + 8 \det I(u,v) \left( \frac{\partial}{\partial v} DD(u,v) \right) A(u,v) DD(u,v) - 8 \det I(u,v) \left( \frac{\partial}{\partial v} DD(u,v) \right) B(u,v) C(u,v) \\
& + 4 \det I(u,v) A(u,v) \left( \frac{\partial}{\partial v} B(u,v) \right) C(u,v) + 4 \det I(u,v) A(u,v) B(u,v) \frac{\partial}{\partial v} C(u,v) \\
& - 4 \det I(u,v) DD(u,v) \left( \frac{\partial}{\partial v} B(u,v) \right) C(u,v) - 4 \det I(u,v) DD(u,v) B(u,v) \frac{\partial}{\partial v} C(u,v) \\
& + 24 \left( \frac{\partial}{\partial v} \det I(u,v) \right) DD(u,v) B(u,v) C(u,v) + 6 \left( \frac{\partial}{\partial v} \det I(u,v) \right) (DD(u,v))^3
\end{aligned}$$

Ridge equation, identities

```

> curveb0b3v:=simplify( subs( subs_p2, (a^2*p2(u,v)-b^2)/B(u,v) ) ):
> curveb0b3w:=simplify( subs( subs_p2, (abis^2*p2(u,v)-bbis^2)/(-C(u,v)) ) ):
> curveb0b3vw:=simplify( 2*(abis*b-a*bbis) ):
> [curveb0b3v-curveb0b3w,curveb0b3v-curveb0b3vw];

```

$$[0,0]$$

Final result: ridge has 170 terms of the form 5 times a term amongst A,B,C,DD and twice detI and derivatives

```

> ridge:=simplify( curveb0b3vw/content( curveb0b3vw ) ):
> [whattype(ridge), nops(ridge), op(1,ridge)];

```

$$[\text{' + '}, 170, -36 (B(u,v))^3 \left( \frac{\partial}{\partial u} \det I(u,v) \right)^2 (C(u,v))^2]$$

Umbilics are points on  $P=0$  of multiplicity  $t$  least 3

```

> list_diff:= diff(B(u, v), u)=B[u](u,v), diff(C(u, v), u)=C[u](u,v), diff(B(u, v),
v)=B[v](u,v), diff(C(u, v), v)=C[v](u,v), diff(A(u, v), u)=A[u](u,v), diff(DD(u, v),
u)=DD[u](u,v), diff(A(u, v), v)=A[v](u,v), diff(DD(u, v), v)=DD[v](u,v) :
> umb_cond:=A(u,v)=DD(u,v), B(u,v)=0, C(u,v)=0 ;
> ridge_sub:=subs( list_diff, courbe):
> ridge_gradient:=[diff(ridge_sub, u), diff(ridge_sub, v)]:
> ridge_gradient_sub:=simplify(subs( list_diff, ridge_gradient)):
> ridge_gradient_umb:=simplify(subs(umb_cond, ridge_gradient_sub));
> ridge_hessien:=[ diff(op(1,ridge_gradient_sub), u), diff(op(1,ridge_gradient_sub),
v), diff(op(2,ridge_gradient_sub), v)]:
> ridge_hessien_sub:=simplify(subs(list_diff, ridge_hessien)):
> ridge_hessien_umb:=simplify(subs( umb_cond, ridge_hessien_sub));

```

$$\text{umb\_cond} := \{A(u,v) = DD(u,v), C(u,v) = 0, B(u,v) = 0\}$$

$$\text{ridge\_gradient\_umb} := [0,0]$$

$$\text{ridge\_hessien\_umb} := [0,0,0]$$

### 6.6.3 Turning points

```

> subs_sqrtp2bis:=sqrt(p2(u,v)) =sqrtp2, p2(u,v)^(3/2)= p2(u,v)*sqrtp2,p2(u,v)^(5/2)=
p2(u,v)^2*sqrtp2:
> hessk1v1:=subs( subs_sqrtp2bis, expand(k1uun*v1[1]^2+k1lvn*v1[1]*v1[2]+k1vvn*v1[2]^2)):
> hessk1w1:=subs( subs_sqrtp2bis, expand(k1uun*w1[1]^2+k1lvn*w1[1]*w1[2]+k1vvn*w1[2]^2)):
> hessk2v2:=subs( subs_sqrtp2bis, expand(k2uun*v2[1]^2+k2uvn*v2[1]*v2[2]+k2vvn*v2[2]^2)):
> hessk2w2:=subs( subs_sqrtp2bis, expand(k2uun*w2[1]^2+k2uvn*w2[1]*w2[2]+k2vvn*w2[2]^2)):
> hessk1v1a:=coeff(hessk1v1, sqrtp2, 1):hessk1v1b:=coeff(hessk1v1, sqrtp2, 0):
> hessk1w1a:=coeff(hessk1w1, sqrtp2, 1):hessk1w1b:=coeff(hessk1w1, sqrtp2, 0):
> hessk2v2a:=coeff(hessk2v2, sqrtp2, 1):hessk2v2b:=coeff(hessk2v2, sqrtp2, 0):
> hessk2w2a:=coeff(hessk2w2, sqrtp2, 1):hessk2w2b:=coeff(hessk2w2, sqrtp2, 0):

```

Identities

```

> [hessk1v1a-hessk2v2a, hessk1v1b+hessk2v2b, hessk1w1a-hessk2w2a, hessk1w1b+hessk2w2b];

```

$$[0,0,0,0]$$

Definition of alpha, beta, alphabis, betabis: one has  $\text{hessk1v1} = a*\sqrt{p2(u,v)} + b$ ;  $\text{hessk2v2} = a*\sqrt{p2(u,v)}$

-b

alpha, beta, alphabis, betabis are fct of A,B,C,DD, detI and first and second derivatives

```

> alpha:=simplify( subs( subs_p2, hessk1v1a ) ):
> alphabis:=simplify( subs( subs_p2, hessk1w1a ) ):
> beta:=simplify( subs( subs_p2, hessk1v1b ) ):
> betabis:=simplify( subs( subs_p2, hessk1w1b ) ):
> [nops(alpha), nops(beta)];

```

$$[216, 371]$$

turn, turn-B and turn-C are fct of A,B,C,D,DetI and first and second derivatives

```

> turn_B:=expand( subs( subs_p2, alpha^2*p2(u,v)-beta^2 ) /B(u,v)^2 ):
> turn_C:=expand( subs( subs_p2, alphabis^2*p2(u,v)-betabis^2 ) /C(u,v)^2 ):
> turn_AD:= simplify( 2*(alphabis*beta-alpha*betabis)/(-A(u, v)+DD(u, v)) ):

```

Equivalence of equations

```

> [turn_B-turn_C, turn_B-turn_AD];

```

$$[0,0]$$

Final equation, in each term of turn, there are 10 terms amongst A,B,C,D and 4 times DetI and 4first derivatives (2\*first derivative=2nd derivative)

```

> turn:=simplify( turn_AD/ content(turn_AD) ):
> [whattype(turn), nops(turn), op(1, turn)];

```

$$[\text{' + '}, 17302, -96 (\det I(u,v))^4 (A(u,v))^2 \left( \frac{\partial}{\partial \xi \partial (v,2)} B(u,v) \right) (C(u,v))^3 \left( \frac{\partial}{\partial u} DD(u,v) \right) \left( \frac{\partial}{\partial v} B(u,v) \right) (DD(u,v))^2]$$

## 6.7 Conclusion

This chapter sets the implicit equation  $P = 0$  of the singular curve encoding all ridges of a smooth parametric surface. From a mathematical standpoint, a corollary of this result shows that ridges of polynomial surfaces are polynomial objects. From an algorithmic perspective, this result paves the alley for the development of certified algorithms reporting ridges without resorting to local orientation procedures. For algebraic surfaces, such algorithms are developed in the next chapter.

## Chapter 7

# Topologically certified approximation of umbilics and ridges on polynomial parametric surfaces

In the context of polynomial parametric surfaces, we make two contributions for the computation of ridges. First, by instantiating to the polynomial setting the global structure theorem of ridge curves proved in the former chapter, we develop the first certified algorithm to produce a topological approximation of the curve  $\mathcal{P}$  encoding all the ridges of the surface. The algorithm exploits the singular structure of  $\mathcal{P}$  —umbilics and purple points, and reduces the problem to solving zero dimensional systems using Gröbner basis. Second, for cases where the zero-dimensional systems cannot be practically solved, we develop a certified plot algorithm at any fixed resolution. These contributions are respectively illustrated for Bezier surfaces of degree four and five.

### 7.1 Introduction

#### 7.1.1 Previous work

Up to our knowledge, no algorithm reporting ridges in a certified fashion has been developed as of today. Most contributions deal with sampled surfaces known through a mesh, and a complete review of these contributions can be found in chapter 5. In the following, we focus on contributions related to parametric surfaces.

**Reporting umbilics.** Umbilics of a surface are always traversed by ridges, so that reporting ridges faithfully requires reporting umbilics. To do so, Morris [Mor90] minimizes the function  $k_1 - k_2$ , which vanishes exactly at umbilics. Meakawa et al. [MWP96] define a polynomial system whose roots are the umbilics. This system is solved with the *rounded interval arithmetic projected polyhedron method*. This algorithm uses specific properties of the Bernstein basis of polynomials and interval arithmetic. The domain is recursively subdivided and a set of boxes containing the umbilics is output, but neither existence nor uniqueness of an umbilic in a box is guaranteed.

**Reporting ridges.** The only method dedicated to parametric surfaces we are aware of is that of Morris [Mor90, Mor96]. The parametric domain is triangulated and zero crossings are sought on edges. Local orientation of the principal directions are needed but only provided with a heuristic. This enables to detect crossings assuming (i) there is at most one such crossing on an edge (ii) the orientation of the principal directions is correct. As this simple algorithm fails near umbilics, these points are located first and crossings are found on a circle around the umbilic.

#### 7.1.2 Contributions and chapter overview

Consider a parameterized surface  $\Phi(u, v)$ , the parameterization being *polynomial* with rational coefficients. Let  $\mathcal{P}$  be the curve encoding the ridges of  $\Phi(u, v)$ . We aim at studying  $\mathcal{P}$  on the compact box domain  $\mathcal{D} = [a, b] \times [c, d]$ . We know from chapter 6 that curve  $\mathcal{P}$  is a singular curve defined by a polynomial  $P$  with rational coefficients. Ideally, we would like to produce a topologically certified approximation of  $\mathcal{P}$ . Given a real algebraic curve, the standard way to approximate it consists of resorting to the Cylindrical Algebraic Decomposition (CAD). Running the CAD requires computing singular points and critical points of the curve —points with a horizontal tangent.



Theoretically, these points are defined by zero-dimensional systems. Practically, because of the high degree of the polynomials involved, the calculations may not go through. Replacing the bottlenecks of the CAD by a resolution method adapted to the singular structure of  $\mathcal{P}$ , we make two contributions:

1. First, we develop an algorithm producing a graph  $\mathcal{G}$  embedded in the domain  $\mathcal{D}$ , which is isotopic to the curve  $\mathcal{P}$  of ridges in  $\mathcal{D}$ . The key points are twofold:
  - (a) no generic assumption is required, i.e. several critical or singular points may have the same horizontal projection;
  - (b) no computation with algebraic numbers is involved.

If singular and critical points can be computed—in a reasonable amount of time, the method is effective.

2. Second, if singular or critical points cannot be computed in a reasonable amount of time, we develop a certified plot algorithm at any fixed resolution: we subdivide  $\mathcal{D}$  into *pixels*, a pixel being lit iff the curve intersects it.

The chapter is organized as follows. Notations are presented in section 7.2. The pre-requisites on ridges are recalled in section 7.3. Section 7.4 provides a note on methods for approximating implicit plane curves. Section 7.5 presents the main algebraic tools used by our algorithms, these algebraic methods are further explained in appendix 7.11. The main difficulties of CAD based algorithms are discussed in section 7.6. Certified topological approximation and the certified plot are developed in sections 7.7 and 7.8, and illustrated in section 7.9.

## 7.2 Notations

For a bivariate function  $f(u, v)$ , the partial derivatives are denoted with indices, for example  $f_{uv} = \frac{\partial^2 f}{\partial u \partial v}$ . The quadratic form induced by the second derivatives is denoted  $f_2(u, v) = f_{uu}u^2 + 2f_{uv}uv + f_{vv}v^2$ . The discriminant of this form is denoted  $\delta(f_2) = f_{uv}^2 - f_{uu}f_{vv}$ . The cubic form induced by the third derivatives is denoted  $f_3(u, v) = f_{uuu}u^3 + 3f_{uuv}u^2v + 3f_{uvv}uv^2 + f_{vvv}v^3$ . The discriminant of this form is denoted  $\delta(f_3) = 4(f_{uuu}f_{uvv} - f_{uuv}^2)(f_{uuv}f_{vvv} - f_{uvv}^2) - (f_{uuu}f_{vvv} - f_{uuv}f_{uvv})^2$ .

Let  $f$  be a real bivariate polynomial and  $\mathcal{F}$  the real algebraic curve defined by  $f$ . A point  $(u, v) \in \mathbb{C}^2$  is called

- a singular point of  $\mathcal{F}$  if  $f(u, v) = 0$ ,  $f_u(u, v) = 0$  and  $f_v(u, v) = 0$ ;
- a critical point of  $\mathcal{F}$  if  $f(u, v) = 0$  and  $f_u(u, v) = 0$  and  $f_v(u, v) \neq 0$  (such a point has an horizontal tangent);
- a regular point of  $\mathcal{F}$  if  $f(u, v) = 0$  and it is neither singular nor critical.

If the domain  $\mathcal{D}$  of study is a subset of  $\mathbb{R}^2$ , by *fiber* we refer to a cross section of this domain at a given ordinate or abscissa.

## 7.3 The implicit structure of ridges, and study points

### 7.3.1 Implicit structure of the ridge curve

As shown in chapter 6, the ridge curve  $\mathcal{P}$  is defined by the bivariate polynomial  $P(u, v)$ . In that chapter, we also introduce polynomials  $a$ ,  $b$ ,  $a'$  and  $b'$ , together with  $Sign_{ridge}$ ,  $p_2$ , which are functions of the curvatures of the surface and their first derivatives. These functions characterize the singularities and the colors of  $\mathcal{P}$  in the following sense

**Theorem. 16** *Consider a smooth parametric surface whose parameterization is denoted  $\Phi(u, v)$ . There exists polynomial functions  $P$ ,  $p_2$  and  $Sign_{ridge}$  so that the set of blue ridges union the set of red ridges union the set of umbilics has equation  $P = 0$ . In addition, for a point of this set  $\mathcal{P}$ , one has:*

- If  $p_2 = 0$ , the point is an umbilic.
- If  $p_2 \neq 0$  then:
  - if  $Sign_{ridge} = -1$  then the point is a blue ridge point,
  - if  $Sign_{ridge} = +1$  then the point is a red ridge point,

- if  $\text{Sign}_{\text{ridge}} = 0$  then the point is a purple point.

Following the theoretical study performed in chapter 6, the only assumption made is that the surface admits generic ridges in the sense that real singularities of  $\mathcal{P}$  satisfy the following conditions:

- Real singularities of  $\mathcal{P}$  are of multiplicity at most 3.
- Real singularities of multiplicity 2 are called purple points. They satisfy the system  $S_p = \{a = b = a' = b' = 0, \delta(P_2) > 0, p_2 \neq 0\}$ . In addition, two real branches of  $\mathcal{P}$  are passing through a purple point.
- Real singularities of multiplicity 3 are called umbilics. They satisfy the system  $S_u = \{p_2 = 0\} = \{p_2 = 0, P = 0, P_u = 0, P_v = 0\}$ . In addition, if  $\delta(P_3)$  denote the discriminant of the cubic of the third derivatives of  $P$  at an umbilic, one has:
  - if  $\delta(P_3) > 0$ , then the umbilic is called a 3-ridge umbilic and three real branches of  $\mathcal{P}$  are passing through the umbilic with three distinct tangents;
  - if  $\delta(P_3) < 0$ , then the umbilic is called a 1-ridge umbilic and one real branch of  $\mathcal{P}$  is passing through the umbilic.

As we shall see in section 7.7, these conditions are checked during the processing of the algorithm.

### 7.3.2 Study points and zero dimensional systems

As recalled in introduction, the most demanding task to certify to topology of a real algebraic curve consists of isolating its real singular and critical points. For our problem, the singular and critical points of  $\mathcal{P}$  have a well known structure which can be exploited. More precisely: we successively isolate umbilics, purple points and critical points. As a system defining one set of these points also include as solution the points of the previous system, we use a localization method to simplify the calculations (see theorem 9). The points reported at each stage are characterized as roots of a zero-dimensional system—a system with a finite number of complex solutions, together with the number of half-branches of the curve connected to each point. In addition, points on the border of the domain of study need a special care. This setting leads to the definition of *study points*:

**Definition. 17** *Study points are points in  $\mathcal{D}$  which are*

- *real singularities of  $\mathcal{P}$ , denoted  $S_u \cup S_p$ , with  $S_u = S_{1R} \cup S_{3R}$  and*
  - $S_{1R} = \{p_2 = P = P_u = P_v = 0, \delta(P_3) < 0\}$  (1-ridge umbilics)
  - $S_{3R} = \{p_2 = P = P_u = P_v = 0, \delta(P_3) > 0\}$  (3-ridges umbilics)
  - $S_p = \{a = b = a' = b' = 0, \delta(P_2) > 0, p_2 \neq 0\} = \{a = b = a' = b' = 0, \delta(P_2) > 0\} \setminus S_u$  (purple points)
- *real critical points of  $\mathcal{P}$  in the  $v$ -direction (i.e. points with a horizontal tangent which are not singularities of  $\mathcal{P}$ ) defined by the system*

$$S_c = \{P = P_u = 0, P_v \neq 0\}$$
 (critical points);
- *intersections of  $\mathcal{P}$  with the left and right sides of the box  $\mathcal{D}$  satisfying the system*

$$S_b = \{P(a, v) = 0, v \in [c, d]\} \cup \{P(b, v) = 0, v \in [c, d]\}.$$
*Such a point may also be critical or singular.*

## 7.4 Note on methods for approximating implicit plane curves

In this section, we review classical methods aiming at computing an approximation  $\mathcal{G}$  of a plane curve  $\mathcal{P} = \{P = 0\}$ . Algorithms providing topological guarantees in the non-singular case use interval analysis or some additional knowledge on the function  $P$ . The singular case is completely handled only for algebraic curves. Our description of these algorithms assumes some familiarity with the notion of *local feature size* [AB99], and isotopic approximation [APR03].

Let  $P : D \subset \mathbb{R}^2 \rightarrow \mathbb{R}$  be a continuously differentiable function. Assume the 0-level set of  $P$  defines a curve  $\mathcal{P} = \{(u, v) \in \mathbb{R}^2; P(u, v) = 0\}$  with potentially some isolated singularities. The purpose is to give a description of the curve  $\mathcal{P}$ . This description can simply be a subset of  $D$  enclosing  $\mathcal{P}$  or a piecewise linear graph  $\mathcal{G}$ . From a topological point of view, one expects  $\mathcal{G}$  to be isotopic to  $\mathcal{P}$ . From a geometrical point of view, one expects  $\mathcal{P}$  and  $\mathcal{G}$  to be close for some distance.

### 7.4.1 Marching cubes and relatives

The Marching cube algorithm discretizes the domain  $D$  with a regular square grid. An intersection between the curve  $\mathcal{P}$  and an edge of a cell is detected if the sign of  $P$  changes at the vertices. The approximation  $\mathcal{G}$  is defined from intersections along edges.

The main advantage of the methods is to require a mere evaluation of  $P$ . The drawbacks are that the connection of intersection points in a grid cell can be ambiguous, and that some parts of the curve can be merged or missed since the sign change test counts the number of intersection points modulo two. If the curve has no singularity and one has a lower bound on the local feature size of the curve, these two problems can be overcome and a graph  $\mathcal{G}$  isotopic to  $\mathcal{P}$  can eventually be found. It is indeed sufficient to increase the precision of the grid so as to match the bound on  $lfs$ . But then, one faces the question of adaptability since many grid cells are not intersected by the curve. Continuation methods, which consist of tracing the connected components from seed points, can overcome this problem but they need at least one starting point on each connected component.

### 7.4.2 Interval analysis

Interval analysis consists of using inclusion functions computing lower and upper bounds on the functions manipulated. The simplest idea is to recursively subdivide the domain  $D$  in regions and evaluate  $f$  on these regions with an inclusion function. Regions where 0 does not belong to the interval evaluation of the function are certified not to be intersected by the curve. On the other hand, regions where 0 belongs to the evaluation may or may not be intersected by the curve, depending on how sharp the evaluation has been done.

This method has been improved to certify the topology of  $\mathcal{P}$ . The idea consists of adding the requirement that on each region intersected by the curve, the curve is the graph of a function [Sny92, PV04]. This requires controlling the gradient of  $P$  on each region with another inclusion function. On such a region, the portion of  $\mathcal{P}$  is approximated by polygonal lines and a graph  $\mathcal{G}$  is constructed. The method defines a set of boxes certified to enclose all parts of the curve, and a quad-tree based recursive subdivision adapts the search to the curve.

If the curve has no singularity, the method provides a stopping criteria for the subdivision process, and certifies that  $\mathcal{G}$  is isotopic to  $\mathcal{P}$ . Moreover, some conditions may be added to the subdivision criteria to provide a better geometric approximation [LOF02].

Unfortunately, even in the polynomial case, calculations with inclusion functions are prohibitive for high degree polynomials. Additionally, singular curves cannot be handled since the gradient of the function vanishes at singular points—the curve cannot be locally defined by a graph.

### 7.4.3 Restricted Delaunay diagrams

These algorithms [Che93, BO03] use properties of Delaunay and Voronoi diagram. Given samples located on the curve, the graph  $\mathcal{G}$  is defined as the Delaunay diagram restricted to the curve (the restricted Delaunay diagram consists of Delaunay edges whose dual Voronoi edges intersect the curve  $\mathcal{P}$ ). If a lower bound on the local feature size is known, these methods guarantee that upon termination, the graph  $\mathcal{G}$  is isotopic to  $\mathcal{P}$ , and that  $\mathcal{G}$  is in a  $\epsilon$ -neighborhood of  $\mathcal{P}$ .

The main advantage of these methods is to use a simple predicate—reporting whether a line-segment intersects the curve. Moreover, adaptive versions of the algorithm guarantee that locally, the sizes of simplices match the local feature size.

However, curves with singularities are not handled, and the lower bound on  $lfs$  is difficult (if not impossible) to compute in practice. To overcome the computation of the  $lfs$ , an alternative criteria is proposed in [CDRR04] requiring the computation of the critical points of the curve with respect to a given direction of projection.

### 7.4.4 Using Morse theory

If the singularities of the function  $P$  are known and non-degenerate, classical and stratified Morse theory can be used [BCSV04]. A triangulation of the ambient space is constructed so that the 0-level set of the piecewise linear interpolation of  $P$  is isotopic to  $\mathcal{P}$ . Eventually this 0-level set is meshed and a bound on the Hausdorff distance between the two curves is derived.

## 7.5 Some Algebraic tools for our method

In this section, we sketch the two algebraic methods ubiquitously called by our algorithms. More details are provided in appendix 7.11.

### 7.5.1 Zero dimensional systems

In our algorithms, we will need to represent solutions of zero-dimensional systems depending on two or more variables. We use the so called Rational Univariate Representation of the roots [Rou99], which can be viewed as a univariate equivalent to the studied system.

Given a zero-dimensional system  $I = \langle p_1, \dots, p_s \rangle$  where the  $p_i \in \mathbb{Q}[X_1, \dots, X_n]$ , a Rational Univariate Representation of  $V(I)$  has the following shape :  $f_t(T) = 0, X_1 = \frac{g_{t,X_1}(T)}{g_{t,1}(T)}, \dots, X_n = \frac{g_{t,X_n}(T)}{g_{t,1}(T)}$ , where  $f_t, g_{t,1}, g_{t,X_1}, \dots, g_{t,X_n} \in \mathbb{Q}[T]$  ( $T$  is a new variable). It is uniquely defined w.r.t. a given polynomial  $t$  which separates  $V(I)$  (injective on  $V(I)$ ), the polynomial  $f_t$  being necessarily the characteristic polynomial of  $m_t$  (the multiplication operator by the polynomial  $t$ ) in  $\mathbb{Q}[X_1, \dots, X_n]/I$  [Rou99]. The RUR defines a bijection between the roots of the system  $I$  and those of  $f_t$  preserving the multiplicities and the real roots :

$$\begin{array}{ccc} V(I)(\cap \mathbb{R}) & \approx & V(f_t)(\cap \mathbb{R}) \\ \alpha = (\alpha_1, \dots, \alpha_n) & \rightarrow & t(\alpha) \\ (X_1(\alpha) = \frac{g_{t,X_1}(t(\alpha))}{g_{t,1}(t(\alpha))}, \dots, X_n(\alpha) = \frac{g_{t,X_n}(t(\alpha))}{g_{t,1}(t(\alpha))}) & \leftarrow & t(\alpha) \end{array}$$

There exists several ways for computing a RUR. One can use the strategy from [Rou99] which consists of computing a Gröbner basis of  $I$  and then to perform linear algebra operations to compute a separating element as well as the full expression of the RUR. The Gröbner basis computation can also be replaced by the generalized normal form from [MT05b]. There exists more or less certified alternatives such as the Geometrical resolution [GLS01] (it is probabilistic since the separating element is randomly chosen and its validity is not checked, one also loses the multiplicities of the roots) or resultant based strategies such as [KOR05].

### 7.5.2 Univariate root isolation

This second tool is used to analyze fibers i.e. cross sections of  $\mathcal{D}$  at a given ordinate or abscissa, and requires isolating roots of univariate polynomials whose coefficients are rational numbers or intervals. The method uses the Descartes rule and is fully explained in [RZ03]. The algorithm is based on a recursive subdivision of the initial interval. If exact computations with rationals are performed, the algorithm is proved to terminate—but such computations may be costly. However, the structure of our problem is such that certifications can be achieved using interval arithmetic rather than an exact arithmetic. To see how, given a polynomial  $P = \sum_{i=0}^n a_i u^i$  with rational coefficients, assume we are given intervals  $[l_i, r_i]$  enclosing the coefficients  $a_i$ . Representing a rational number by an interval amounts to approximating the number, and we shall assume the intervals' widths can be made arbitrarily small. The specifications of the algorithm [RZ03] in the case of polynomials with intervals as coefficients are the following :

- Input :
  - $P_{\varepsilon_1} = \sum_{i=0}^n [l_i, r_i] u^i$  a univariate polynomial with intervals  $[l_i, r_i]$  of width less than  $\varepsilon_1$  as coefficients. Notice that  $P_{\varepsilon_1}$  can be seen as a family of polynomials parameterized by the choice of a  $(n+1)$ -uple  $(a_i)_{i=0..n}$  with  $a_i \in [l_i, r_i]$ ;
  - $[a, b]$  an interval for the variable  $u$ ;
  - a precision  $\varepsilon_2$  for the interval arithmetic computations. (This is the precision used to represent the intervals' boundaries.)
- Output :
  - a list  $L_i$  of intervals with rational bounds containing a unique real root of  $P_{\varepsilon_1}$  (that is any polynomial of the family has a unique real root in each of these intervals);
  - a list  $L_e$  of interval with rational bounds where no decision was possible—i.e. the Descartes rule of sign cannot be applied because signs of interval coefficients are not defined;
  - all the elements of  $L_i$  and  $L_e$  are intervals contained in  $]a, b[$ ;

- a real root of  $P_{\varepsilon_1}$  in  $]a, b[$  is represented by an interval of  $L_i$  or  $L_e$ ;

According to [RZ03],  $L_e$  is not empty only in one of the following situations :

- there exists a polynomial in the family of polynomial  $P_{\varepsilon_1}$  which has a multiple root in  $]a, b[$ ;
- the precision  $\varepsilon_2$  of the interval arithmetic used for the computation is not sufficient;

In the present chapter, we need to solve two kinds of problems : isolating all the solutions of a polynomial with rational coefficients; and isolating all the simple roots of a polynomial whose coefficients are intervals —of arbitrary length, knowing intervals which separate the multiple roots from the simple ones.

In the first case, the square free part of the polynomial is computed so that it has no multiple root. Hence both problems become equivalent if we use interval arithmetics: we need to isolate all roots of  $P$  on the interval  $[a, b]$  containing no multiple roots of  $P$ . This can straightforwardly be done running the previous algorithm for  $P_{\varepsilon_1}$ . If the list  $L_e$  is empty we are done, otherwise the algorithm is run for  $P_{\varepsilon_1/2}$  and  $\varepsilon_2/2$ . The termination of this process is proved in [RZ03].

### 7.5.3 About square-free polynomials

Many computations suppose that the considered polynomials are square-free, replacing them, when needed, by their square-free part. In our algorithms, we use interpolation based algorithms (multi-modular, Hensel lifting, etc.) in the univariate case as well as in the bivariate case (default strategy in most computer algebra systems). One key advantage of such methods is that they detect quickly that a polynomial is square-free by solving a simpler problem (univariate problem in the bivariate case, computation modulo a prime number in the univariate case). In particular, this first part of the computation can be used to test if a polynomial is square-free or not.

In the univariate case for example, if a polynomial is square-free modulo a prime number which does not divide its leading coefficient, then it is square-free.

Thus, using algorithms based on interpolation strategies, the overall cost of the computations for testing if a polynomial is square-free (or to compute its square-free part when it is not) is negligible compared to the rest. (With a standard variant using the Euclidean algorithm, one would perform, in average,  $O(d^2)$  binary operations,  $d$  being the degree of the polynomial.)

In the few cases where the computation of a square-free part is non trivial, the computing time for interpolation based methods is, in average, proportional to the size of the result and polynomial in the size (degree and coefficients sizes) of the input. For example, in the univariate case, a naive variant will run Euclid's algorithm modulo some prime numbers ( $O(d^2)$  binary operations for a polynomial of degree  $d$ ) until the product of these prime numbers exceeds the size of the coefficients in the result and finally will recover the result using the Chinese remainder theorem). Since the non trivial cases are few, these computations do not represent a blocking step in the whole algorithms of the present chapter.

## 7.6 On the difficulty of approximating algebraic curves

The standard way to approximate algebraic curves is to resort to the CAD (Cylindrical Algebraic Decomposition). In this section, we recall the main steps of such strategies to approximate  $\mathcal{P}$  and discuss the major difficulties of algorithms like [GVN02]. In section 7.7 we will show how to keep track of the specific implicit structure of ridges (see chap. 6) to optimize the process.

The CAD has been introduced in [Col75]. Basically, a CAD adapted to a set of multivariate polynomials is a partition of the ambient space ( $\mathbb{R}^n$  if the polynomials depends on  $n$  variables) into cells (connected subsets with a trivial topology) where the signs of the considered polynomials are all constant. Such a general method can be adapted to compute a graph reporting the topology of 2-D or 3-D curves —see respectively [GVN02] and [GLMT04]. The following give the basic principles of the method.

Given any implicit curve  $P(u, v) = 0$ , one consider  $P$  as a univariate polynomial in  $u$  (or  $v$ ) and study the values of  $v$  (or  $u$ ) for which the number of roots of  $P$  varies. When  $v$  varies, a root of  $P$  may "go to infinity" or become singular. The first case corresponds to the values of  $v$  for which the leading coefficient of  $P$  vanishes and the second case to the values of  $v$  for which the discriminant with respect to  $u$  vanishes ( $v$ -coordinates of singular points and critical points with respect to the projection on the  $v$ -axis). Both sets of values can be expressed as the (real) roots of a univariate polynomial  $c(v)$  which can be explicitly computed from  $P$ . When restricted to a cylinder between



the fibers over two consecutive real roots of  $c(v)$ ,  $P(u, v) = 0$  has the topology of a trivial covering. Using the CAD to approximate an algebraic curve requires mainly three stages.

In the following, we consider there is no (horizontal) asymptotes: no roots to the leading coefficient with respect to the variable  $u$ . A change of coordinate is always able to transform the curve in such a configuration and anyways, as we will see later, one can easily avoid such an assumption when studying the curve in a compact box.

**First stage.** Produce the  $v$ -coordinates of the singular points and the critical points with respect to the projection on the  $v$ -axis. These  $v$ -coordinates are the real roots  $\alpha_1, \dots, \alpha_s$  of the discriminant of  $P$  w.r.t.  $u$ , denoted by  $Crit_u$ .

**Second stage.** Consists of building the fiber above each  $v$ -coordinate of critical and singular points. This calculation involves polynomials whose coefficients are algebraic numbers, so as to isolate the solutions in each fiber and at least discriminate the multiple points from the simple points. More formally, this requires solving:

- **L-1a.** Report the simple real roots of  $P(u, \alpha_i)$ ,  $i = 1..s$ ;
- **L-1b.** Report the multiple real roots of  $P(u, \alpha_i)$ ,  $i = 1..s$  and their multiplicity;

Note that the  $u$ -coordinates of the critical and singular points are the multiple roots of the polynomials  $P(u, \alpha_i)$ .

**Third stage.** Finally, the connection phase consists of connecting points from fibers. This requires:

- Finding the real roots of  $P(u, \beta_i)$ ,  $i = 0..s$ ,  $\beta_i$  being any arbitrary point in  $] \alpha_i, \alpha_{i+1} [$ , with the convention  $\alpha_0 = -\infty$  and  $\alpha_{s+1} = +\infty$ .
- Finding the number of half branches which connect to the real roots of  $P(u, \alpha_i)$ ,  $i = 1..s$  in order to connect each real root of  $P(u, \beta_i)$ ,  $i = 0..s$ , to a real root of  $P(u, \alpha_i)$ ,  $i = 0..s$  and to a real root of  $P(u, \alpha_{i+1})$ ,  $i = 0..s$ .

These three stages face four major difficulties.

**Computing the discriminant  $Crit_u$ .** For large polynomials, the first difficulty comes from the calculation of the discriminant with respect to  $u$ , which may be unpractical. In section 7.7, we shall face this difficulty by sequentially reporting study points independently and thus decreasing strongly the degrees of the involved polynomials.

**Isolating the roots of  $P(u, \alpha_i)$ .** The second difficulty comes from the isolation of the roots of  $P(u, \alpha_i)$ ,  $\alpha_i$  being a real root of  $Crit_u$  and the computation of their multiplicities. Since  $\alpha_i$  is an algebraic number, there are three main ways to certify such a computation:

- (i) use an approximated representation of the real algebraic numbers involved such as floating point numbers or intervals. It then becomes possible to isolate some of the simple real roots of  $P(u, \alpha_i)$ . Managing correctly the precision of the approximations as well as the numerical errors during the computations, one can hope being able to isolate all the simple real roots of  $P(u, \alpha_i)$ . However, we are not aware of any general implementation of this strategy.
- (ii) use an exact representation of the real algebraic numbers involved – for example an interval and a polynomial to refine it to an arbitrary precision, or Thom's coding of the roots– and apply classical algorithms with the induced arithmetic such as Sturm-habicht sequences and sub-resultants algorithms for computing the roots of  $P(u, \alpha_i)$  [BPR03] for details. For large problems, the size of the polynomials involved and the cost of exact arithmetic over real algebraic numbers prevents this solution from being practical.
- (iii) solve the zero-dimensional system  $P(u, v) = 0, Crit_u(v) = 0$ . This third strategy computes directly the 2D representation of the singular and critical points. On the one hand, the basic computations may be more difficult, but in the other hand, the operations using real algebraic numbers are simple to perform (only evaluates polynomial at real algebraic numbers). In other words, one may increase the number of arithmetic operations but decrease their cost.



**Genericity assumption.** In order to avoid difficult computations in the cases where it is not possible to compute the multiplicities of the roots at the second stage of the previous algorithm or to perform computations using the strategy (ii), most recent algorithms such as [GVN02] or [GLMT04] suppose that the curve is in *generic position* w.r.t. the coordinate system —which means that each fiber  $P(u, \alpha_i) = 0$  contains a unique critical or singular point. This implies that each polynomial  $P(u, \alpha_i)$  has one and only one multiple root. In such a situation, points of consecutive fibers corresponding to  $\alpha_i, \alpha_{i+1}$  are easily connected through points in an intermediate witness fiber [GVN02]. (One-to-one connections are made between regular points, and one is left with connections between the unique critical point of each fiber  $\alpha_i, \alpha_{i+1}$  with the remaining points of the intermediate fiber.)

The genericity hypothesis can be met through a linear change of variables. The algorithm described in [GVN02] or [GLMT04] provides such a generic position for the curve and this eases the computation of the roots of  $P(u, \alpha_i)$ . In our case, the studied curves are usually in generic position and, anyways, it is also true that a randomly chosen linear change of coordinates will put the curve in generic position with a probability one. But checking deterministically that a curve is in generic position may be more costly than all the other operations and is required if we pretend to implement a certified algorithm. For example, in [GVN02] such a test requires the computation of some principal Sturm-Habicht coefficients of  $P$  with respect to  $u$  which is mainly as costly as using strategy (ii) for computing the fibers over the  $\alpha_i$ .

Moreover, one can choose not to fully certify the *generic position* (by performing a random linear change of variables) and thus use strategy (i) to compute the fibers  $P(u, \alpha_i) = 0$ . This is suggest by [GVN02] but the way it is done is again not certified since they use a purely numerical function (`fsolve` from MAPLE software), which can not make the distinction between a cluster of 3 simple roots and a triple point.

In addition, replacing a variable by a linear form in a huge bivariate polynomial may be a difficult task. The sizes of the coefficients increases so that all the computations except perhaps those involving real algebraic numbers become more difficult.

All the above problems are illustrated by the example from section 7.9 :

- we were not able to perform the generic position test;
- we were not able to compute the roots of some  $P(u, \alpha_i)$  even under the generic position assumption —in which case  $P(u, \alpha_i)$  has exactly one multiple root which allows to use several optimization tricks.

## 7.7 Certified topological approximation

In this section, we circumvent the difficulties of the CAD and develop a certified algorithm to compute the topology of  $\mathcal{P}$ .

### 7.7.1 Output specification

**Definition. 18** Let  $\mathcal{G}$  be a graph whose vertices are points of  $\mathcal{D}$  and edges are non-intersecting straight line-segments between vertices. Let the topology on  $\mathcal{G}$  be induced by that of  $\mathcal{D}$ . We say that  $\mathcal{G}$  is a topological approximation of the ridge curve  $\mathcal{P}$  on the domain  $\mathcal{D}$  if  $\mathcal{G}$  is ambient isotopic to  $\mathcal{P} \cap \mathcal{D}$  in  $\mathcal{D}$ .

More formally, there exists a function  $F : \mathcal{D} \times [0, 1] \longrightarrow \mathcal{D}$  such that:

- $F$  is continuous;
- $\forall t \in [0, 1], F_t = F(., t)$  is an homeomorphism of  $\mathcal{D}$  onto itself;
- $F_0 = Id_{\mathcal{D}}$  and  $F_1(\mathcal{P} \cap \mathcal{D}) = \mathcal{G}$ .

Note that homeomorphic approximation is weaker and our algorithm using a cylindrical decomposition technique actually gives isotopy. In addition, our construction allows to identify singularities of  $\mathcal{P}$  to a subset of vertices of  $\mathcal{G}$  while controlling the error on the geometric positions. We can also color edges of  $\mathcal{G}$  with the color of the ridge curve it is isotopic to. Once this topological sketch is given, one can easily compute a more accurate geometrical picture.

### 7.7.2 Method outline

Taking the square free part of  $P$ , we can assume  $P$  is square free. We can also assume  $\mathcal{P}$  has no part which is a horizontal segment —parallel to the  $u$ -axis. Otherwise this means that a whole horizontal line is a component of  $P$ . In other words, the content of  $P$  with respect to  $u$  is a polynomial in  $v$  and we can study this factor separately and divide  $P$  by this factor. Eventually, to get the whole topology of the curve, one has to merge the components.

#### The algorithm

Our algorithm consists of the following five stages:

1. **Isolating study points.** Study points are isolated in  $2D$  with rational univariate representations (RUR). Study points within a common fiber are identified.
2. **Regularization of the study boxes.** The boxes of study points are reduced so as to have the right number of intersections between their border and  $\mathcal{P}$ . This number is 6 for 3-ridge umbilic, 2 for 1-ridge umbilic, 4 for a purple, 2 for others. Moreover, boxes are reduced so as to have crossings on the top and bottom sides only. Define the number of branches coming from the top and the bottom.
3. **Computing regular points in study fibers.** In each fiber of a study point, the  $u$ -coordinates of intersection points with  $\mathcal{P}$  other than study points are computed.
4. **Adding intermediate rational fibers.** Add rational fibers between study points fibers and isolate the  $u$ -coordinates of intersection points with  $\mathcal{P}$ .
5. **Performing connections.** This information is enough to perform the connections. Consider the cylinder between two consecutive fibers, the number of branches connected from above the lower fiber is the same than the number of branches connected from below the higher fiber. Hence there is only one way to perform connections with non-intersecting straight segments.

#### Key points with respect to CAD based algorithms

Our algorithm avoids the difficulties of CAD methods, and the following comments are in order.

**Zero-dimensional systems versus the discriminant  $Crit_u$ .** Instead of computing the  $v$ -coordinates of all critical and singular points at once, as done by the CAD, study points are sequentially computed directly in  $2D$ , together with the information required to derive the graph  $\mathcal{G}$ .

**Isolating the roots of  $P(u, \alpha_i)$ .** The isolation of roots of polynomials whose coefficients are algebraic numbers does not arise since study points are isolated in  $2D$  in the first place. We only use the isolation of simple roots of polynomial whose coefficients are intervals. However, we do need to characterize the presence of multiple study points in the same fibers, an information required by the connection process.

**The connection phase without genericity assumption.** Algorithms derived from the CAD have problems to perform the proper connection between consecutive fibers if these fibers contain more than one critical or singular point. We alleviate this limitation using the information on the number of half-branches connected to the point. This number is equal to 6 for a 3-ridge umbilic, 4 for a purple point and 2 otherwise. These informations are sufficient to build the approximation  $\mathcal{G}$ .

**Complexity-wise.** The advantage of the strategy is to iteratively split the problem into simpler ones, and to solve the sub-problems directly in  $2D$ . The main drawback of the method may be the arithmetic asymptotic complexity upper bounds of some of the tools we use to compute and certify the solutions of zero-dimensional systems (see section 7.11).

Let  $F$  be a set of polynomials,  $\mindeg(F)$  (resp.  $\maxdeg(F)$ ) the minimal (resp. maximal) degree of a polynomial which belongs to  $F$ . According to [Laz83], in the case of two variables, a Gröbner basis for a Degree ordering has at most  $\mindeg(F) + 1$  polynomials of degree less than  $2\maxdeg(F) - 1$  so that modern strategies like [Fau02] will compute it in a polynomial time. In short, the algorithm is faster than inverting a matrix whose number of columns is bounded by the number of possible monomials while the number of rows is bounded by the number of

polynomials. Since all the other algorithms we use are also polynomial (RUR, isolation, etc.) in their input, the full strategies we use are still polynomial.

We would like to point out that we need to compute, certify and provide numerical approximations with an arbitrary precision of the real roots of huge systems. Up to our knowledge, the tools we used are, at least in practice, the most efficient ones with such specifications.

### 7.7.3 Step 1. Isolating study points

The method to identify these study points is to compute a RUR of the system defining them. Details of the method are exposed in section 7.11.

The less the number of solutions of a system, the easier the computation of the RUR. Hence, we use a localization method to decompose the computation of the different types of study points —see section 7.11.5. More precisely, we sequentially solve the following systems:

1. The system  $S_u$  from which the sets  $S_{1R}$  and  $S_{3R}$  are distinguished by evaluating the sign of  $\delta(P_3)$ .
2. The system  $S_p$  for purple points.
3. The system  $S_c$  for critical points.
4. The system  $S_b$  for border points, that is intersections of  $\mathcal{P}$  with the left and right sides of the box  $\mathcal{D}$ . Solving this system together with one of the previous identifies border points which are also singular or critical.

Selecting only points belonging to  $\mathcal{D}$  reduces to adding inequalities to the systems and is well managed by the RUR. According to 7.11.5, solving such systems is equivalent to solving zero-dimensional systems without inequalities when the number of inequations remains small compared to the number of variables.

The RUR of the study points provides a way to compute a box around each study point  $q_i$  which is a product of two intervals  $[u_i^1; u_i^2] \times [v_i^1; v_i^2]$  (see section 7.11). The intervals can be as small as desired.

The computation of the RUR of one of these systems begins with testing if the polynomial  $v$  is separating for the system (see 7.11 for the definition of a separating element). Note that if it is so, the solution points are in generic position with respect to the projection on the  $v$ -axis, that is each fiber of a point contains no other point of this system. In any case, we compute the square-free part of the minimal or characteristic polynomial of the multiplication by  $v$  modulus the ideal generated by the system (nothing to do when  $v$  is separating since it is the first polynomial of the RUR) : its roots are exactly all the  $v$ -coordinates of the solutions of the system.

Until now, we only have separate informations on the different systems. In order to identify study points having the same  $v$ -coordinate, we need to cross these informations. First we compute isolation intervals for all the  $v$ -coordinates of all the study points together, denote  $I$  this list of intervals. If two study points with the same  $v$ -coordinate are solutions of two different systems, the gcd of polynomials enable to identify them:

- Initialize the list  $I$  with all the isolation intervals of all the  $v$ -coordinates of the different systems.
- Let  $A$  and  $B$  be the square free polynomials defining the  $v$ -coordinates of two different systems, and  $I_A, I_B$  the lists of isolation intervals of their roots. Let  $C = \gcd(A, B)$  and  $I_C$  the list of isolation intervals of its roots. One can refine the elements of  $I_C$  until they intersect only one element of  $I_A$  and one element of  $I_B$ . Then replace these two intervals in  $I$  by the single interval which is the intersection of the three intervals. Do the same for every pair of systems.
- $I$  then contains intervals defining different real numbers in one-to-one correspondence with the  $v$ -coordinates of the study points. It remains to refine these intervals until they are all disjoint.

Second, we compare the intervals of  $I$  and those of the 2d boxes of the study points. Let two study points  $q_i$  and  $q_j$  be represented by  $[u_i^1; u_i^2] \times [v_i^1; v_i^2]$  and  $[u_j^1; u_j^2] \times [v_j^1; v_j^2]$  with  $[v_i^1; v_i^2] \cap [v_j^1; v_j^2] \neq \emptyset$ . One cannot, a priori, decide if these two points have the same  $v$ -coordinate or if a refinement of the boxes will end with disjoint  $v$ -intervals. On the other hand, with the list  $I$ , such a decision is straightforward. The boxes of the study points are refined until each  $[v_i^1; v_i^2]$  intersects only one interval  $[w_i^1; w_i^2]$  of the list  $I$ . Then two study points intersecting the same interval  $[w_i^1; w_i^2]$  are in the same fiber.

Finally, one can refine the  $u$ -coordinates of the study points with the same  $v$  coordinate until they are represented with disjoint intervals since, thanks to localizations, all the computed points are distinct.

#### Checking genericity conditions of section 7.3.1.

First, real singularities shall be the union of purple and umbilical points, this reduces to compare the systems for singular points and for purple and umbilical points. Second, showing that  $\delta(P_3) \neq 0$  for umbilics and  $\delta(P_2) > 0$  for purple points reduces to sign evaluation of polynomials at the roots of a system (see section 7.11.5).

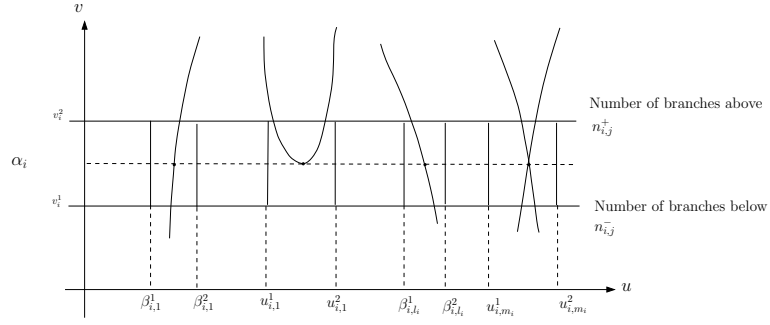


Figure 7.1: Notations for a fiber involving several critical/singular points:  $u_{i,j}^{1(2)}$  are used for study points,  $\beta_{i,j}^{1(2)}$  for simple points.

### 7.7.4 Step 2. Regularization of the study boxes

At this stage, we have computed all the  $v$ -coordinates  $\alpha_1, \dots, \alpha_s$  of all the study points  $\{q_{i,j}, i = 1 \dots s, j = 1 \dots m_i\}$  by means of isolating intervals  $[v_i^1; v_i^2], i = 1 \dots s$ . We have isolated  $u$ -coordinates of the  $m_i$  study points in each fiber  $\alpha_i$  by the intervals  $[u_{i,j}^1; u_{i,j}^2], j = 1 \dots m_i$  and we know (section 7.7.3) the number of branches which should be connected to each of them.

Note that an intersection (in  $\mathcal{D}$ ) of  $\mathcal{P}$  with a fiber  $v = v_0$  which is not a study point is a regular point of  $\mathcal{P}$ . Hence, the  $u$ -coordinate of this point is a simple root of the univariate polynomial  $P(u, v_0)$ . The first additional computation we need to do is to ensure that for each fiber  $P(u, \alpha_i) = 0$  the isolating boxes of the study points do not contain any regular point. It is sufficient to count the number of intersection points between  $\mathcal{P}$  and the border of the isolating box to detect if the box contains or not a regular point : such a computation remains to solve 4 univariate polynomials with rational coefficients and can be done efficiently using the algorithm from section 7.5.2. Precisely, if the study point is a critical point, the isolating box contains no regular point if and only if the number of points in the computed intersection is 2 (2 for a 1-ridge, 6 for a 3-ridge, 4 for a purple, 2 for a non-critical nor singular border point). If the box contains a regular point, one use the RUR to refine the isolating box and perform again the test : after a finite number of steps, each study point will be represented by an isolating box which do not contain any regular point.

In addition, reducing boxes if necessary, we can also assume the intersections on the border of the isolation boxes only occur on the top or the bottom sides of the boxes (that is the sides parallel to the  $u$ -axis). This allows to compute the number of half-branches connected to the top and to the bottom of each study point. For the special case of border points, one has to compute the number of branches inside the domain  $\mathcal{D}$  only.

### 7.7.5 Step 3. Computing regular points in study fibers

We now compute the regular points in each fiber  $P(u, \alpha_i) = 0$ . Computing the regular points of each fiber is now equivalent to computing the roots of the polynomials  $P(u, \alpha_i)$  outside the intervals representing the  $u$ -coordinates of the study points (which contain all the multiple roots of  $P(u, \alpha_i)$ ).

Denote  $[u_{i,j}^1; u_{i,j}^2], j = 1 \dots m_i$  the intervals representing the  $u$ -coordinates of the study points on the fiber of  $\alpha_i$  and  $[v_i^1; v_i^2]_\varepsilon$  an interval of length  $\varepsilon$  containing (strictly)  $\alpha_i$  and no other  $\alpha_j, j \neq i$ . Substituting  $v$  by  $[v_i^1; v_i^2]_\varepsilon$  in  $P(u, v)$  gives a univariate polynomial with intervals as coefficients we denote  $P(u, [v_i^1; v_i^2]_\varepsilon)$ . We apply the algorithm 7.5.2 for the polynomial  $P(u, [v_i^1; v_i^2]_\varepsilon)$  and on the domain  $\cup_{j=1}^{m_i} [u_{i,j}^1; u_{i,j}^2]$ . We know that for every  $v_i \in [v_i^1; v_i^2]_\varepsilon$  the polynomial  $P(u, v_i)$  has no multiple roots on this domain. Hence the algorithm will return intervals  $[\beta_{i,j}^1; \beta_{i,j}^2], j = 1 \dots l_i$  such that for  $\varepsilon$  sufficiently small and  $\forall v_i \in [\alpha_i]_\varepsilon$ , each root of  $P(u, v_i)$  belonging to  $[a, b] \setminus \cup_{j=1}^{m_i} [u_{i,j}^1; u_{i,j}^2]$  is contained in a unique  $[\beta_{i,j}^1; \beta_{i,j}^2]$ .

We have isolated, along each fiber, a collection of points  $s_{i,j}, i = 1 \dots s, j = 1, \dots, m_i + l_i$ , which are either study points or regular points of  $\mathcal{P}$ . Each such point is isolated in a box i.e. a product of intervals and comes with two integers  $(n_{i,j}^+, n_{i,j}^-)$  denoting the number of branches in  $\mathcal{D}$  connected from above and from below.

### 7.7.6 Step 4. Adding intermediate rational fibers

Consider now an intermediate fiber, i.e. a fiber associated with  $v = \delta_i, i = 1 \dots s - 1$ , with  $\delta_i$  a rational number in-between the intervals of isolation of two consecutive values  $\alpha_i$  and  $\alpha_{i+1}$ . If the fibers  $v = c$  or  $v = d$  are not

fibers of study points, then they are added as fibers  $\delta_0$  or  $\delta_s$ .

Getting the structure of such fibers amounts to solving a univariate polynomial with rational coefficients, which is done using the algorithm described in section 7.5.2. Thus, each such fiber also comes with a collection of points for which one knows that  $n_{i,j}^+ = n_{i,j}^- = 1$ . Again, each such point is isolated in a box.

### 7.7.7 Step 5. Performing connections

We thus obtain a full and certified description of the fibers: all the intersection points with  $\mathcal{P}$  and their number of branches connected. We know, by construction, that the branches of  $\mathcal{P}$  between fibers have empty intersection. The number of branches connected from above a fiber is the same than the number of branches connected from below the next fiber. Hence there is only one way to perform connections with non-intersecting straight segments. More precisely, vertices of the graph are the centers of isolation boxes, and edges are line-segments joining them.

Notice that using the intermediate fibers  $v = \delta_i$  is compulsory if one wishes to get a graph  $\mathcal{G}$  isotopic to  $\mathcal{P}$ . If not, whenever two branches have common starting points and endpoints, the embedding of the graph  $\mathcal{G}$  obtained is not valid since two arcs are identified.

The algorithm is illustrated on Fig. 7.2. In addition

- If a singular point box have width  $\delta$ , then the distance between the singular point and the vertex representing it is less than  $\delta$ .
- One can compute the sign of the function  $Sign_{ridge}$  defined in 7.3.1 for each regular point of each intermediate fiber. This defines the color of the ridge branch it belongs to. Then one can assign to each edge of the graph the color of its end point which is on an intermediate fiber.

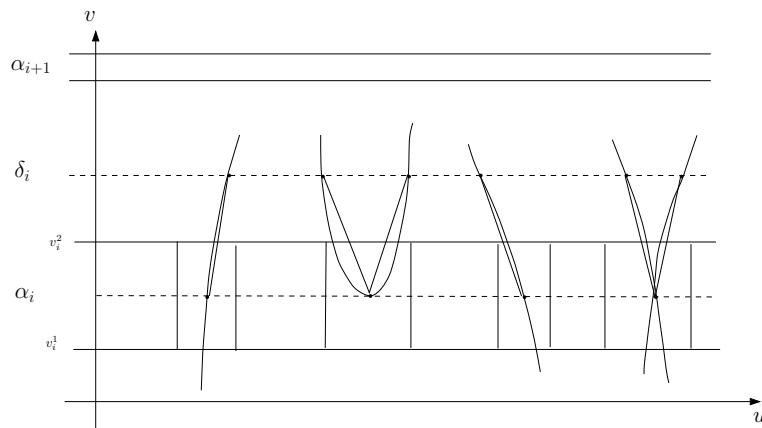


Figure 7.2: Performing connections

## 7.8 Certified plot

In this section, we develop an algorithm to provide information of  $\mathcal{P}$  when some of the calculations required to certify the topology do not succeed. The information we provide consists of intersections between rational fibers in the study box and the curve. These intersections are used to define the so-called *certified plot*. Notice that if some calculations succeed –in particular those of umbilics and purple points, then, the isolation boxes of these singularities can be superimposed to the certified plot.

For simplicity, we suppose that  $P$  is irreducible, that  $P(u, v) = 0$  has no isolated points, which is true under our genericity conditions of section 7.3.1, and that the studied domain is  $[0, 1] \times [0, 1]$ . In addition, we denote by  $n'$  an integer such that there does not exist a connected component of  $P(u, v) = 0$  which is embedded in a product of intervals of length less than  $1/n'$ .

**Certified plot with  $n'$  known.** To specify the plot, we make the following:

**Definition. 19** Given an integer  $n$  with  $n > n'$ , consider the  $n \times n$  decomposition of the bounded domain  $[0, 1] \times [0, 1]$  into pixels, i.e. products of intervals of length  $1/n$ :  $\{[\frac{i}{n}; \frac{i+1}{n}] \times [\frac{j}{n}; \frac{j+1}{n}] \mid i = 0 \dots n-1, j = 0 \dots n-1\}$ . Also assume each pixel has a binary attribute: lit or not.

This  $n \times n$  decomposition is called the certified plot of  $\mathcal{P}$  at resolution  $n$  if a pixel is lit if and only if  $\mathcal{P}$  intersects the pixel. (Note that the intersection may occur only on the border or even on a corner of the pixel).

The method reduces to finding intersections between the curve  $\mathcal{P}$  and horizontal and vertical fibers defining the pixels. The algorithm processing horizontal fibers is presented on Fig. 7.3. The same algorithm is used to process the vertical lines, i.e. computations are applied to polynomials  $P(i/n, v)$ .

For each  $i = 0 \dots n$ :

1. Compute the square free part of  $P(u, i/n)$ .
2. Isolate its roots with intervals of length less than  $1/n$ . (As recalled in section 7.5.2, the algorithm terminates with  $L_e = \emptyset$  since the square free part has been taken.) Let  $L_i = \{I_j \mid j = 1 \dots m_i\}$  be the set of these intervals.
3. For each  $j = 1 \dots m_i$ 
  - (a) If  $I_j$  does not intersect a fiber in the other direction, there exists  $k = 0 \dots n-1$  such that  $I_j \subset [\frac{k}{n}; \frac{k+1}{n}]$ . The pixels containing this segment are lit (if  $0 < i < n$  these are  $[\frac{k}{n}; \frac{k+1}{n}] \times [\frac{i-1}{n}; \frac{i}{n}]$  and  $[\frac{k}{n}; \frac{k+1}{n}] \times [\frac{i}{n}; \frac{i+1}{n}]$ , else only one of these is in the studied domain).
  - (b) If  $I_j$  intersects the fiber  $u = k/n$  ( $k = 0 \dots n-1$ ) in the other direction then
    - if  $P(k/n, i/n) \neq 0$  then its sign enable to refine  $I_j$  such that it does not intersect the fiber and one lights pixels as in step 3a—that is, we light the pixel to the right or the left of  $u = k/n$ .
    - if  $P(k/n, i/n) = 0$  then one lights the pixels containing the point  $(k/n, i/n)$  (if this point is not on the border of the domain, there are 4 such pixels).

Figure 7.3: Processing horizontal fibers  $P(u, i/n)$

**Certified plot with  $n'$  unknown.** If  $n'$  is not known, one can choose an arbitrary  $n$  and apply the same strategy : only components which are embedded into products of intervals of length  $< 1/n$  may not be represented.

## 7.9 Illustrations

We illustrate our algorithms for Bezier surfaces of degree four and five respectively. In both cases, the study domain is the domain  $\mathcal{D} = [0, 1] \times [0, 1]$ .

### 7.9.1 Certified topology for ridges in generic position

Given a parameterized surface, recall that certifying the topology of ridges requires going through three stages. First, the polynomial  $P$  is computed using Maple. Second, the zero-dimensional systems defining the study points are solved, together with the intersections between  $\mathcal{P}$  and the fibers of study points and intermediate fibers. Third, the connections between all these points are performed so as to produce the embedded graph  $\mathcal{G}$  isotopic to  $\mathcal{P}$ .

We illustrate this process on the Bezier surface whose control points are

$$\begin{pmatrix} [0, 0, 0] & [1/4, 0, 0] & [2/4, 0, 0] & [3/4, 0, 0] & [4/4, 0, 0] \\ [0, 1/4, 0] & [1/4, 1/4, 1] & [2/4, 1/4, -1] & [3/4, 1/4, -1] & [4/4, 1/4, 0] \\ [0, 2/4, 0] & [1/4, 2/4, -1] & [2/4, 2/4, 1] & [3/4, 2/4, 1] & [4/4, 2/4, 0] \\ [0, 3/4, 0] & [1/4, 3/4, 1] & [2/4, 3/4, -1] & [3/4, 3/4, 1] & [4/4, 3/4, 0] \\ [0, 4/4, 0] & [1/4, 4/4, 0] & [2/4, 4/4, 0] & [3/4, 4/4, 0] & [4/4, 4/4, 0] \end{pmatrix}$$

Alternatively, this surface can be expressed as the graph of the total degree 8 polynomial  $h(u, v)$  for  $(u, v) \in [0, 1]^2$ :

$$\begin{aligned} h(u, v) = & 116u^4v^4 - 200u^4v^3 + 108u^4v^2 - 24u^4v - 312u^3v^4 + 592u^3v^3 - 360u^3v^2 + 80u^3v + 252u^2v^4 - 504u^2v^3 \\ & + 324u^2v^2 - 72u^2v - 56uv^4 + 112uv^3 - 72uv^2 + 16uv. \end{aligned}$$



The computation of the implicit curve has been performed using Maple 9.5 —see the previous chapter, and requires less than one minute. It is a bivariate polynomial  $P(u, v)$  of total degree 84, of degree 43 in  $u$ , degree 43 in  $v$  with 1907 terms and coefficients with up to 53 digits.

The study points  $S_u$ ,  $S_p$  and  $S_c$  were computed using the softwares FGB and RS (<http://fgbrs.lip6.fr>). These systems being in shape position —cf appendix 7.11.3, the RUR can be computed as shown in [Rou99]. Alternatively, Gröbner basis can be computed first using [Fau99] or [Fau02]. We tested both methods and the computation time for the largest system  $S_c$  does not exceed 5 minutes. Table 7.1 gives the main characteristics of these systems.

Figure 7.4 displays the topological approximation graph of the ridge curve in the parametric domain  $\mathcal{D}$  computed with the algorithm of section 7.7. The surface and its ridges are displayed on Fig. 7.5. To avoid occlusion problems of lifted ridge segments by the surface, we lifted on the surface the points lit by the algorithm from section 7.8 rather than the ridge segments of Fig. 7.4.

There are 19 critical points (black dots), 17 purple points (pink dots) and 8 umbilics, 3 of which are 3-ridge (green) and 5 are 1-ridge (yellow). Figure 7.6 displays on the left two close-ups of the bottom left 3-ridge umbilic, and on the right a more readable sketch. One can recognize an unsymmetric umbilic, that is a 3-ridge umbilic where the three blue branches are followed by the three red ones round the umbilic. The other 3-ridge umbilics are symmetric, that is branches alternate colors round the umbilic.

System	# of roots $\in \mathbb{C}$	# of roots $\in \mathbb{R}$	# of real roots $\in \mathcal{D}$
$S_u$	160	16	8
$S_p$	749	47	17
$S_c$	1432	44	19

Table 7.1: characteristics of zero dimensional systems

On this example, the discriminant with respect to  $u$  has degree 3594 in  $v$  and coefficients with up to 3418 digits. CAD based strategies require solving polynomials of degree 43 with coefficients in a field extension defined by an irreducible polynomial of degree 1431 with coefficient of 1071 digits. Up to our knowledge, none of the best existing software or libraries can perform such a computation in a reasonable time.

## 7.9.2 Certified plot

We provide a certified plot of the ridges for the degree 5 Bezier surface defined by the height function

$$\begin{aligned}
 h'(u, v) = & -587u^4v^3 - 0.15u - 0.5v - 469.5u^4v^4 + 1835u^3v^3 + 353.3u^5v^4 - 213.55u^5v^5 - 1627u^3v^2 + 407.5u^3v \\
 & - 1642u^2v^3 + 1222u^2v^2 - 304u^2v + 0.5u^2 + 1.8v^2 - 1.4u^3 - 2.5v^3 + 465uv^3 - 308uv^2 + 76.5uv \\
 & + 1.5u^4 + 808u^4v^2 - 205.5u^4v - 401.5u^3v^4 + 826u^2v^4 + 1.1v^4 - 309.75uv^4 - 68.4u^5v^3 - 0.51u^5 \\
 & + 0.09v^5 - 96.9u^5v^2 + 26.1u^5v + 452.75u^4v^5 - 213.3u^3v^5 - 101.9u^2v^5 + 76.2uv^5 + 0.05.
 \end{aligned}$$

The ridge curve has total degree 110 and 3245 terms, it requires about 15 minutes to be computed with Maple. The system for umbilics has been computed and there are 9 solutions in the domain  $\mathcal{D}$ . The informations to build a topological approximation cannot be obtained in reasonable time, hence we only provide a certified plot. Figure 7.7 displays this certified plot and umbilics on the domain  $\mathcal{D}$ , this  $512 \times 512$  resolution plot is computed in less than one minute. Figure 7.8 displays the certified plot lifted on the surface.

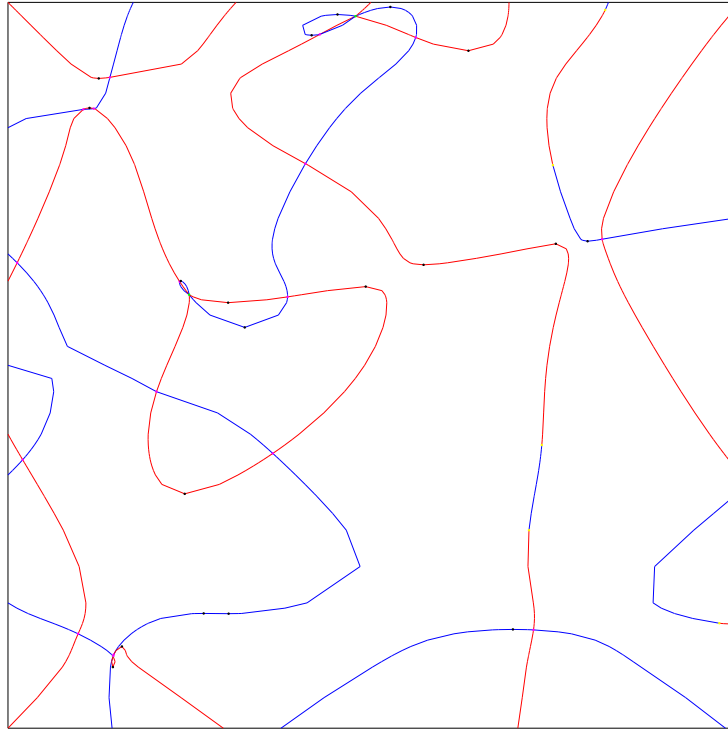


Figure 7.4: Isotopic approximation of the ridge curve with 3-ridge umbilics (green), 1-ridge umbilics (yellow), purple points (pink) and critical points (black).

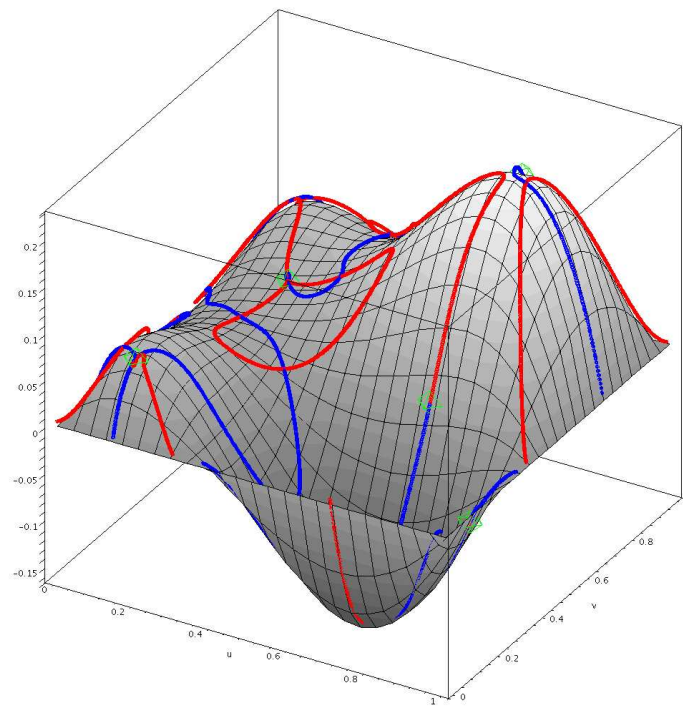


Figure 7.5: Plot of the degree 4 bivariate Bezier surface with ridges and umbilics

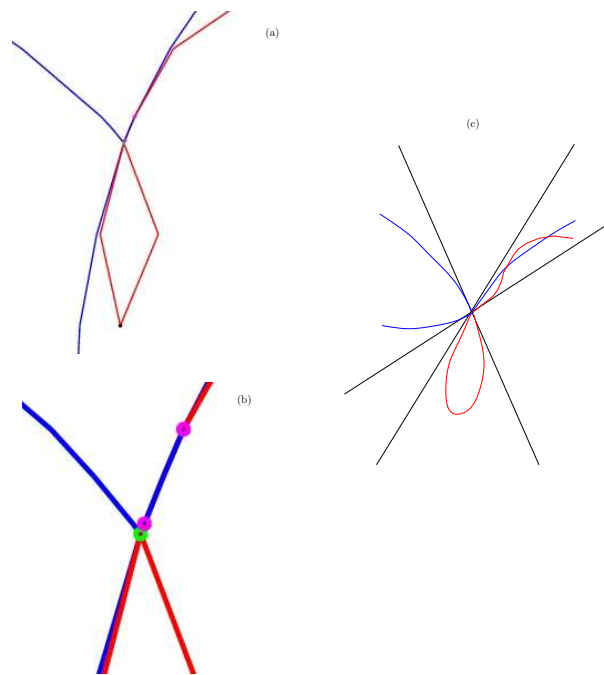


Figure 7.6: Close-up on the unsymmetrical umbilic of Fig. 7.4 —bottom left umbilic: (a,b)zooms of the isotopic approximation (c)corresponding arrangement of ridges

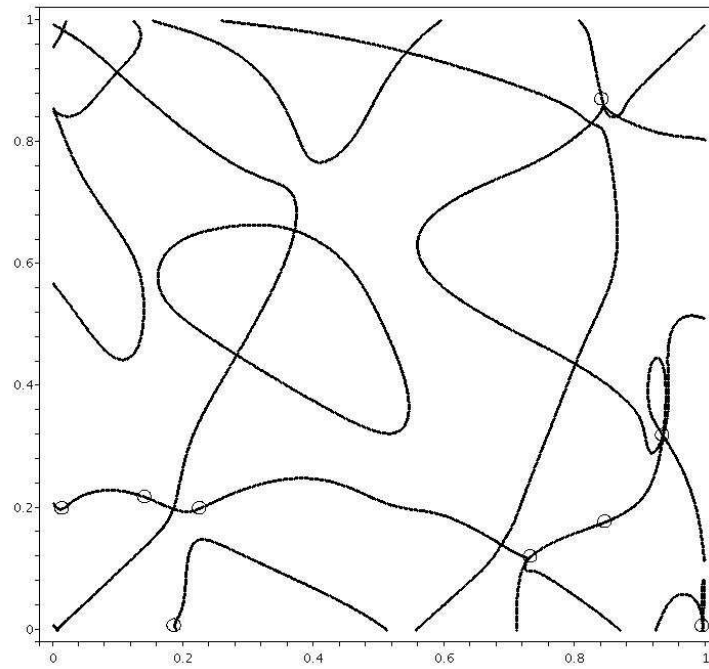


Figure 7.7: Certified plot of the degree 5 Bezier surface ridges with umbilics (circles) in the parametric domain.

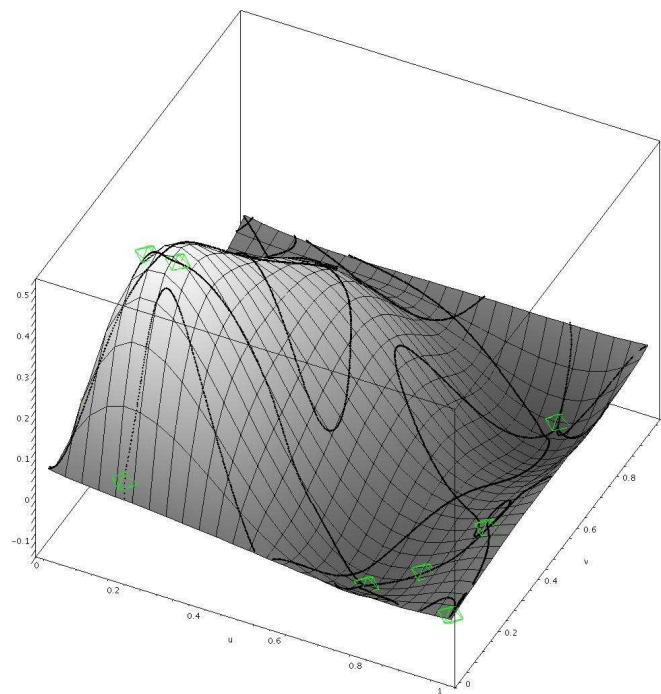


Figure 7.8: Certified plot of the degree 5 Bezier surface ridges with umbilics lifted on the surface.

## 7.10 Conclusion

This chapter develops two algorithms to investigate the ridges of parametric algebraic surfaces. The first one reports a topologically certified approximation of the ridges, and is the first one to achieve such a guarantee. For the practical cases where the resolution of the systems characterizing singular and critical points cannot be performed, the second one computes a certified plot at any fixed resolution. These algorithms are computationally demanding in terms of algebra. They are in a sense complementary to the heuristic ones developed in chapter 5, which are working directly on a triangulation of the surface, and provide a fast way to report non certified results.

The method developed for the computation of the topology of the ridges can be generalized for other algebraic curves. It gives an alternative to usual algorithms based on the CAD.

**Acknowledgments.** Jean-Pierre Merlet is acknowledged for fruitful discussions.

## 7.11 Appendix: Algebraic pre-requisites

In this section, we summarize some basic results about Gröbner bases and their applications to solving zero-dimensional systems (systems with a finite number of complex roots). The reader may refer to [CLO92],[BPR03].

Lets denote by  $\mathbb{Q}[X_1, \dots, X_n]$  the ring of polynomials with rational coefficients and unknowns  $X_1, \dots, X_n$  and  $S = \{P_1, \dots, P_s\}$  any subset of  $\mathbb{Q}[X_1, \dots, X_n]$ . A point  $x \in \mathbb{C}^n$  is a zero of  $S$  if  $P_i(x) = 0 \quad \forall i = 1 \dots s$ . The ideal  $I = \langle P_1, \dots, P_s \rangle$  generated by  $P_1, \dots, P_s$  is the set of polynomials in  $\mathbb{Q}[X_1, \dots, X_n]$  constituted by all the combinations  $\sum_{k=1}^R P_k U_k$  with  $U_k \in \mathbb{Q}[X_1, \dots, X_n]$ . Since every element of  $I$  vanishes at each zero of  $S$ , we denote by  $V(S) = V(I) = \{x \in \mathbb{C}^n \mid p(x) = 0 \quad \forall p \in I\}$  (resp.  $V_{\mathbb{R}}(S) = V_{\mathbb{R}}(I) = V(I) \cap \mathbb{R}^n$ ) the set of complex (resp. real) zeroes of  $S$ .

### 7.11.1 Gröbner bases

A Gröbner basis of  $I$  is a computable generator set of  $I$  with good algorithmical properties (as described below) and defined with respect to a monomial ordering. In this paper, one will use the following orderings:

- *lexicographic order* : (Lex)

$$X_1^{\alpha_1} \dots X_n^{\alpha_n} <_{\text{Lex}} X_1^{\beta_1} \dots X_n^{\beta_n} \Leftrightarrow \exists i_0 \leq n \quad , \quad \begin{cases} \alpha_i = \beta_i, & \text{for } i = 1, \dots, i_0 - 1, \\ \alpha_{i_0} < \beta_{i_0} \end{cases} \quad (7.1)$$

- *degree reverse lexicographic order* (DRL) :

$$X_1^{\alpha_1} \dots X_n^{\alpha_n} <_{\text{DRL}} X_1^{\beta_1} \dots X_n^{\beta_n} \Leftrightarrow X^{((\sum_k \alpha_k), -\alpha_n, \dots, -\alpha_1)} <_{\text{Lex}} X^{((\sum_k \beta_k), -\beta_n, \dots, -\beta_1)} \quad (7.2)$$

Lets define the mathematical object ‘‘Gröbner’’:

**Definition. 20** For any  $n$ -uple  $\mu = (\mu_1, \dots, \mu_n) \in \mathbb{N}^n$ , let denote by  $X^\mu$  the monomial  $X_1^{\mu_1} \dots X_n^{\mu_n}$ . If  $<$  is an admissible (compatible with the multiplication) monomial ordering and  $P = \sum_{i=0}^r a_i X^{\mu^{(i)}}$  any polynomial in  $\mathbb{Q}[X_1, \dots, X_n]$ , we define:  $\text{LM}(P, <) = \max_{i=0 \dots r} \mu^{(i)}$  (leading monomial of  $P$  w.r.t.  $<$ ),  $\text{LC}(P, <) = a_i$  with  $\text{LM}(P, <) = X^{\mu^{(i)}}$  (leading coefficient of  $P$  w.r.t.  $<$ ) and  $\text{LT}(P, <) = \text{LC}(P, <) \text{LM}(P, <)$  (leading term of  $P$  wrt  $<$ ).

**Definition. 21** A set of polynomials  $G$  is a Gröbner basis of an ideal  $I$  wrt to a monomial ordering  $<$  if for all  $f \in I$  there exists  $g \in G$  such that  $\text{LM}(g, <)$  divides  $\text{LM}(f, <)$ .

Given any admissible monomial ordering  $<$  one can easily extend the classical Euclidean division to *reduce* a polynomial  $p$  by another one or, more generally, by a set of polynomials  $F$ , performing the reduction wrt to each polynomial of  $F$  until getting an expression which can not be reduced anymore. Lets denote such a function by  $\text{Reduce}(p, F, <)$  (reduction of the polynomial  $p$  wrt  $F$ ). Unlike in the univariate case, the result of such a process is not canonical except if  $F = G$  is a Gröbner basis:

**Theorem. 17** Let  $G$  be a Gröbner basis of an ideal  $I \subset \mathbb{Q}[X_1, \dots, X_n]$  for a fixed ordering  $<$ .

- a polynomial  $p \in \mathbb{Q}[X_1, \dots, X_n]$  belongs to  $I$  if and only if  $\text{Reduce}(p, G, <) = 0$ ,
- $\text{Reduce}(p, G, <)$  does not depend on the order of the polynomials in the list  $G$ , thus, this is a canonical reduced expression modulo  $I$ .

Gröbner bases are computable objects. The most popular method for computing them is Buchberger’s algorithm ([BCL82, Buc85]). It has several variants and it is implemented in most of general computer algebra systems like Maple or Mathematica. The computation of Gröbner bases using Buchberger’s original strategies has to face to two kind of problems :

- (A) arbitrary choices : the order in which are done the computations has a dramatic influence on the computation time; Precisely, one compute  $G$  by increasing the set of initial polynomials, adding so called  $S$ -polynomials ( $\text{spol}_{<}(p, q) = \frac{\text{COF}_{<}(p, q)}{\text{LT}(p)} p - \frac{\text{COF}_{<}(p, q)}{\text{LT}(q)} q$ ,  $\text{COF}_{<}(p, q) = \text{LCM}(\text{LT}_{<}(p), \text{LT}_{<}(q))$  where LCM stands for ‘‘least common multiple’’) until all the possible  $S$ -polynomials of polynomials of  $G$  reduce to 0 modulo  $G$  ( $\text{Reduce}(\text{spol}_{<}(p, q), G, <) = 0$ ).



- (B) useless computations : the original algorithm spends most of its time in computing 0 (at each step, most of the new  $S$ -polynomials do reduce to zero in a naive algorithm).

For problem (A), J.C. Faugère proposed ([Fau99] - algorithm  $F_4$ ) a new generation of powerful algorithms ([Fau99]) based on the intensive use of linear algebra techniques. In short, the arbitrary choices are left to computational strategies related to classical linear algebra problems (matrix inversions, linear systems, etc.). For problem (B), J.C. Faugère proposed ([Fau02]) a new criterion for detecting useless computations

We pay a particular attention to Gröbner bases computed for elimination orderings since they provide a way of "simplifying" the system (an equivalent system with a structured shape). For example, a lexicographic Gröbner basis of a zero dimensional system (when the number of complex solutions is finite) has always the following shape (if we suppose that  $X_1 < X_2 \dots < X_n$ ):

$$\left\{ \begin{array}{l} f(X_1) = 0 \\ f_2(X_1, X_2) = 0 \\ \vdots \\ f_{k_2}(X_1, X_2) = 0 \\ f_{k_2+1}(X_1, X_2, X_3) = 0 \\ \vdots \\ f_{k_{n-1}+1}(X_1, \dots, X_n) = 0 \\ \vdots \\ f_{k_n}(X_1, \dots, X_n) = 0 \end{array} \right. .$$

(when the system is not zero dimensional some of the polynomials may be identically null). A well known property is that the zeros of the smallest (w.r.t.  $<$ ) non null polynomial define the Zariski closure (classical closure in the case of complex coefficients) of the projection on the coordinate's space associated with the smallest variables.

More generally, an admissible ordering  $<$  on the monomials depending on variables  $[X_1, \dots, X_n]$  is an ordering which eliminates  $X_{d+1}, \dots, X_n$  if  $X_i < X_j \forall i = 1 \dots d, j = d+1 \dots n$ . The lexicographic ordering is a particular elimination ordering.

**Definition. 22** Given two monomial orderings  $<_U$  (w.r.t. the variables  $U_1, \dots, U_d$ ) and  $<_X$  (w.r.t. the variables  $X_{d+1}, \dots, X_n$ ) one can define an ordering which "eliminates"  $X_{d+1}, \dots, X_n$  by setting the so called block ordering  $<_{U,X}$  as follows : given two monomials  $m$  and  $m'$ ,  $m <_{U,X} m'$  if and only if  $m|_{U_1=1, \dots, U_d=1} <_X m'|_{U_1=1, \dots, U_d=1}$  or  $(m|_{U_1=1, \dots, U_d=1} = m'|_{U_1=1, \dots, U_d=1} \text{ and } m|_{X_{d+1}=1, \dots, X_n=1} <_U m'|_{X_{d+1}=1, \dots, X_n=1})$ .

Two important applications of elimination theory are the "projections" and "localizations". In the following, given any subset  $\mathcal{V}$  of  $\mathbb{C}^d$  ( $d$  is an arbitrary positive integer),  $\overline{\mathcal{V}}$  is its Zariski closure, say the smallest subset of  $\mathbb{C}^d$  containing  $\mathcal{V}$  which is the zero set of a system of polynomial equations.

**Proposition. 8** Let  $G$  be a Gröbner basis of an ideal  $I \subset \mathbb{Q}[U, X]$  w.r.t. any ordering  $<$  which eliminates  $X$ . Then  $G \cap \mathbb{Q}[U]$  is a Gröbner basis of  $I \cap \mathbb{Q}[U]$  w.r.t. to the ordering induced by  $<$  on the variables  $U$ ; Moreover, if  $\Pi_U : \mathbb{C}^n \longrightarrow \mathbb{C}^d$  denotes the canonical projection on the coordinates  $U$ ,  $V(I \cap \mathbb{Q}[U]) = V(G \cap \mathbb{Q}[U]) = \overline{\Pi_U(V(I))}$ .

**Proposition. 9** Let  $I \subset \mathbb{Q}[X]$ ,  $f \in \mathbb{Q}[X]$  and  $T$  be a new indeterminate, then  $\overline{V(I) \setminus V(f)} = V((I + \langle Tf - 1 \rangle) \cap \mathbb{Q}[X])$ . If  $G' \subset \mathbb{Q}[X, T]$  is a Gröbner basis of  $I + \langle Tf - 1 \rangle$  with respect to  $<_{X,T}$  then  $G' \cap \mathbb{Q}[X]$  is a Gröbner basis of  $I : f^\infty := (I + \langle Tf - 1 \rangle) \cap \mathbb{Q}[X]$  w.r.t.  $<_X$ . The variety  $\overline{V(I) \setminus V(f)}$  and the ideal  $I : f^\infty$  are usually called the localization of  $V(I)$  and  $I$  by  $f$ .

### 7.11.2 Zero-dimensional systems

Zero-dimensional systems are polynomial systems with a finite number of complex solutions. This specific case is fundamental for many engineering applications. The following theorem shows that we can detect easily that a system is zero dimensional or not by computing a Gröbner basis for any monomial ordering :

**Theorem. 18** Let  $G = \{g_1, \dots, g_l\}$  be a Gröbner basis for any ordering  $<$  of any system  $S = \{P_1, \dots, P_s\} \in \mathbb{Q}[X_1, \dots, X_n]^s$ . The two following properties are equivalent :

- For all index  $i = 1 \dots n$ , there exists a polynomial  $g_j \in G$  and a positive integer  $n_j$  such that  $X_i^{n_j} = LM(g_j, <)$ ;

- The system  $\{P_1 = 0, \dots, P_s = 0\}$  has a finite number of solutions in  $\mathbb{C}^n$ .

If  $S$  is zero-dimensional, then, according to theorem 18, only a finite number of monomials  $m \in \mathbb{Q}[X_1, \dots, X_n]$  are not reducible modulo  $G$ , meaning that  $\text{Reduce}(m, G, <) = m$ . Mathematically, a system is zero-dimensional if and only if  $\mathbb{Q}[X_1, \dots, X_n]/I$  is a  $\mathbb{Q}$ -vector space of finite dimension. This vector space can fully be characterized when knowing a Gröbner basis:

**Theorem. 19** Let  $S = \{p_1, \dots, p_s\}$  be a set of polynomials with  $p_i \in \mathbb{Q}[X_1, \dots, X_n] \ ; \forall i = 1 \dots s$ , and suppose that  $G$  is a Gröbner basis of  $\langle S \rangle$  with respect to any monomial ordering  $<$ . Then :

- $\mathbb{Q}[X_1, \dots, X_n]/I = \{\text{Reduce}(p, G, <) \ ; \ p \in \mathbb{Q}[X_1, \dots, X_n]\}$  is a vector space of finite dimension;
- $\mathcal{B} = \{t = X_1^{e_1} \dots X_n^{e_n} \ ; \ (e_1, \dots, e_n) \in \mathbb{N}^n \mid \text{Reduce}(t, G, <) = t\} = \{w_1, \dots, w_D\}$  is a basis of  $\mathbb{Q}[X_1, \dots, X_n]/I$  as a  $\mathbb{Q}$ -vector space;
- $D = \#\mathcal{B}$  is exactly the number of complex zeroes of the system  $\{P = 0, \ \forall P \in S\}$  counted with multiplicities.

Thus, when a polynomial system is known to be zero-dimensional, one can switch to linear algebra methods to get informations about its roots. Once a Gröbner basis is known, a basis of  $\mathbb{Q}[X_1, \dots, X_n]/I$  can easily be computed (Theorem 19) so that linear algebra methods can be applied for doing several computations.

For any polynomial  $q \in \mathbb{Q}[X_1, \dots, X_n]$  the decomposition  $\vec{q} = \text{Reduce}(q, G, <) = \sum_{i=1}^D a_i w_i$  is unique (theorem 17) and we denote by  $\vec{q} = [a_1, \dots, a_D]$  the representation of  $\vec{q}$  in the basis  $\mathcal{B}$ . For example, the matrix w.r.t.  $\mathcal{B}$  of the linear map  $m_q: \left( \begin{array}{ccc} \mathbb{Q}[X_1, \dots, X_n]/I & \longrightarrow & \mathbb{Q}[X_1, \dots, X_n]/I \\ \vec{p} & \longmapsto & \vec{p}\vec{q} \end{array} \right)$  can explicitly be computed (its columns are the vectors  $\vec{q}w_i$ ) and one can then apply the following well-known theorem:

**Theorem. 20** (Stickelberger) The eigenvalues of  $m_q$  are exactly the  $q(\alpha)$  where  $\alpha \in V_{\mathbb{C}}(S)$ .

According to Theorem 20, the  $i$ -th coordinate of all  $\alpha \in V_{\mathbb{C}}(S)$  can be obtained from  $m_{X_i}$  eigenvalues but the issue of finding all the coordinates of all the  $\alpha \in V_{\mathbb{C}}(S)$  from  $m_{X_1}, \dots, m_{X_n}$  eigenvalues is not explicit nor straightforward (see [AS98] for example) and difficult to certify.

### 7.11.3 The Rational Univariate Representation

The Rational Univariate Representation [Rou99] is, with the end-user point of view, the simplest way for representing symbolically the roots of a zero-dimensional system without losing information (multiplicities or real roots) since one can get all the information on the roots of the system by solving univariate polynomials.

Given a zero-dimensional system  $I = \langle p_1, \dots, p_s \rangle$  where the  $p_i \in \mathbb{Q}[X_1, \dots, X_n]$ , a Rational Univariate Representation of  $V(I)$  has the following shape :  $f_t(T) = 0, X_1 = \frac{g_{t,X_1}(T)}{g_{t,1}(T)}, \dots, X_n = \frac{g_{t,X_n}(T)}{g_{t,1}(T)}$ , where  $f_t, g_{t,1}, g_{t,X_1}, \dots, g_{t,X_n} \in \mathbb{Q}[T]$  ( $T$  is a new variable). It is uniquely defined w.r.t. a given polynomial  $t$  which separates  $V(I)$  (injective on  $V(I)$ ), the polynomial  $f_t$  being necessarily the characteristic polynomial of  $m_t$  (see above section) in  $\mathbb{Q}[X_1, \dots, X_n]/I$  [Rou99]. The RUR defines a bijection between the roots of  $I$  and those of  $f_t$  preserving the multiplicities and the real roots :

$$\begin{array}{ccc} V(I)(\cap \mathbb{R}) & \approx & V(f_t)(\cap \mathbb{R}) \\ \alpha = (\alpha_1, \dots, \alpha_n) & \rightarrow & t(\alpha) \\ \left( \frac{g_{t,X_1}(t(\alpha))}{g_{t,1}(t(\alpha))}, \dots, \frac{g_{t,X_n}(t(\alpha))}{g_{t,1}(t(\alpha))} \right) & \leftarrow & t(\alpha) \end{array}$$

For computing a RUR one has to solve two problems :

- finding a separating element  $t$ ;
- given any polynomial  $t$ , compute a RUR-Candidate  $f_t, g_{t,1}, g_{t,X_1}, \dots, g_{t,X_n}$  such that if  $t$  is a separating polynomial, then the RUR-Candidate is a RUR.

According to [Rou99], a RUR-Candidate can explicitly be computed when knowing a suitable representation of  $\mathbb{Q}[X_1, \dots, X_n]/I$  :

- $f_t = \sum_{i=0}^D a_i T^i$  is the characteristic polynomial of  $m_t$ . Lets denote by  $\overline{f}_t$  its square-free part.

- for any  $v \in \mathbb{Q}[X_1, \dots, X_n]$ ,  $g_{t,v} = g_{t,v}(T) = \sum_{i=0}^{d-1} \text{Trace}(m_{v_i}) H_{d-i-1}(T)$ ,  $d = \deg(\overline{f_t})$  and  $H_j(T) = \sum_{i=0}^j a_i T^{i-j}$

In [Rou99], a strategy is proposed for computing a RUR for any system (a RUR-Candidate and a separating element), but there are special cases where it can be computed differently. When  $X_1$  is separating  $V(I)$  and when  $I$  is a radical ideal, the system is said to be in *shape position*. In such cases, the shape of the lexicographic Gröbner basis is always the following :

$$\begin{cases} f(X_1) = 0 \\ X_2 = f_2(X_1) \\ \vdots \\ X_n = f_n(X_1) \end{cases} \quad (7.3)$$

As shown in [Rou99], if the system is in shape position,  $g_{X_1,1} = f'_{X_1}$  and we have  $f_{X_1} = f$  and  $f_i(X_1) = g_{X_1, X_i}(X_1)/g_{X_1,1}(X_1) \bmod f$ . Thus the RUR associated with  $X_1$  and the lexicographic Gröbner basis are equivalent up to the inversion of  $g_{X_1,1} = f'_{X_1}$  modulo  $f_{X_1}$ . In the rest of the paper we call this object a RR-Form of the corresponding lexicographic Gröbner basis. The RUR is well known to be much smaller than the lexicographic Gröbner basis in general (this may be explained by the inversion of the denominator) and thus will be our privileged object. Note that it is easy to check that a system is in shape position once knowing a RUR-Candidate (and so to check that  $X_1$  separates  $V(I)$ ): it is necessary and sufficient that  $f_{X_1}$  is square-free.

We thus can multiply the strategies for computing a symbolic solution : one can compute the RR-Form Gröbner directly using [Fau99] or [Fau02] for example or by change of ordering like in [FGLM93] or a RUR using the algorithm from [Rou99].

#### 7.11.4 From formal to numerical solutions

Computing a RUR reduces the resolution of a zero-dimensional system to solving one polynomial in one variable ( $f_t$ ) and to evaluating  $n$  rational fractions ( $\frac{g_{t,X_i}(T)}{g_{t,1}(T)}$ ,  $i = 1 \dots n$ ) at its roots (note that if one simply want to compute the number of real roots of the system there is no need to consider the rational coordinates). The next task is thus to compute all the real roots of the system (and only the real roots), providing a numerical approximation with an arbitrary precision (set by the user) of the coordinates.

The isolation of the real roots of  $f_t$  can be done using the algorithm proposed in [RZ03] : the output will be a list  $l_{f_t}$  of intervals with rational bounds such that for each real root  $\alpha$  of  $f_t$ , there exists a unique interval in  $l_{f_t}$  which contains  $\alpha$ . The second step consists in refining each interval in order to ensure that it does not contain any real root of  $g_{t,1}$ . Since  $f_t$  and  $g_{t,1}$  are co-prime this computation is easy and we then can ensure that the rational functions can be evaluated using interval arithmetics without any cancellation of the denominator. This last evaluation is performed using multi-precision arithmetics (MPFI package - [RR05]). As we will see in the experiments, the precision needed for the computations is poor and, moreover, the rational functions defined by the RUR are stable under numerical evaluation, even if their coefficients are huge (rational numbers), and thus this part of the computation is still efficient. For increasing the precision of the result, it is only necessary to decrease the length of the intervals in  $l_{f_t}$  which can easily be done by bisection or using a certified Newton's algorithm. Note that it is quite simple to certify the sign of the coordinates : one simply have to compute some gcds and split, when necessary the RUR.

#### 7.11.5 Signs of polynomials at the roots of a system

Computing the sign of given multivariate polynomials  $\{q_1, \dots, q_l\}$  at the real roots of a zero-dimensional system may be important for many applications and this problem is not solved by the above method. Instead of "plugging" straightforwardly the formal coordinates provided by the RUR into the  $q_i$ , we better extend the RUR by computing rational functions which coincide with the  $q_i$  at the roots of  $I$ . This can theoretically simply be done by using the general formula from [Rou99] :  $h_{t,j} = \sum_{i=0}^{D-1} \text{Trace}(m_{q_j^i}) H_{D-i-1}(T)$ . One can directly compute the  $\text{Trace}(m_{q_j^i})$  reusing the computations already done if the (classical) RUR (without additional constraints) has already been computed and show that as soon as  $l$  is small (at least smaller than the number of variables), it is not more costly to compute the extended RUR than the classical one.

## Chapter 8

# Conclusion

In this thesis, two topics of the geometry of surfaces have been addressed: the local estimation of differential properties of a smooth surface from a discretization, and the computation of the global structure of ridges of a smooth surface.

Regarding the local estimations of differential quantities, our method uses local polynomial fitting and applies to meshes and points clouds. The method is analyzed with synthetic data, and the asymptotic error estimates proved are the best known so far. Although our estimation method mimics the smooth setting, hence does not define discrete concepts, it enables the estimation of differential quantities of any order. When the fitting is conducted with an approximation scheme, we have experimentally observed that the method has a good behavior with noisy data.

Another approach to the estimation problem from discrete data is proposed by discrete differential geometry. The idea is to define differential quantities on the discrete object and develop a purely discrete theory parallel to the smooth one. Then the problem of convergence of the discrete quantities for a sequence of discretization of a smooth surface can be addressed. Results have been obtained for the normal field, area, geodesics [MT02, HPW05], mean and gauss curvature with a variational formulation [PP93], curvature tensor with a measure formulation [CSM03]. All these contributions are based on meshes, and point cloud data are not considered. Convergence theorems are only available for first or second order differential quantities.

As the interest for point cloud data is growing, a major issue would be to understand how far differential geometry and statistical analysis can help. One has to take into account irregular sampling density, anisotropy and noise. For example, the influence of the neighborhood of a point to be considered for the estimation is not well understood [LP05]. An analysis of surface normal estimation in noisy point cloud data is proposed in [MN03]. Voting techniques propagate informations in local neighborhoods to determine the reliability of each individual information. Normal or curvature tensor voting are well designed to identify noise and discontinuities, hence can handle piecewise smooth objects [TM02].

Regarding the computation of global structures on surfaces, we focus on reporting the topology and a geometric approximation of ridges. Two kinds of data have been analyzed: a mesh discretizing a smooth surface and a parametric surface.

First, for a mesh discretizing a smooth surface, we present the first certified algorithm for extracting the ridges of the smooth surface with guaranteed topology. The algorithm exploits the patterns made by ridges and umbilics on generic surfaces, and dissociates the processing near umbilics and on the rest of the surface. The algorithm is generic since the calculation of local differential quantities and the separation of umbilics are deferred to routines that may depend from the type of smooth surface discretized by the mesh. For meshes approximating smooth surfaces —without access to any analytical information on the surface, we provide heuristics. For meshes discretizing smooth surfaces whose ridges are known, experiments show that our heuristic algorithm recovers the correct topology of ridges and umbilics. For meshes computed from scans by a surface reconstruction algorithm, experiments show that our algorithm recovers the ridges of state-of-the-art methods (which use global fitting), while improving running times of at least one order of magnitude and providing a more efficient filtering method.

Second, for parametric surfaces, we derive the implicit equation of the singular curve encoding the ridges in the parametric domain. We also analyze its singularities and provide methods to identify the different types of ridges. This formulation of the problem avoids the difficulties of the local orientation of the principal directions of curvature. Hence it enables a global approach to ridge extraction on parametric surfaces. Finally, these results on the structure of ridges are exploited for the special case of polynomial parametric surfaces. As classical com-

puter algebra tools were unable to process our large equations, we took advantage of the geometrical information derived. We develop a specific algorithm based on rational univariate representation of zero dimensional systems, and root isolation of univariate polynomials. This strategy avoids the costly computations with algebraic numbers. Indeed, our method only requires computations on polynomials with rational coefficients. The algorithm reports a topologically certified approximation of the ridges, and is the first one to achieve such a guarantee. Once the topology is computed, a more precise geometrical approximation can easily be obtained. Another algorithm computes a certified plot at any fixed resolution : it is less costly in terms of computations but does not provide topological guarantees. The results for parametric surfaces are directly applicable to Bezier surfaces ubiquitous in CAD. It is worth noting that the method developed for the computation of the topology of the ridges can be generalized for other algebraic curves, provided the number of real branches going through singularities can be computed efficiently.

In conclusion, we give several efficient and certified algorithms for the extraction of ridges. The methods apply to discrete as well as smooth data and, different levels of certification are available to satisfy the user requirements.

The interest for the analysis and the computation of global geometric properties is not new. For example, many contributions have been done so far for the visualization of vector fields with topological informations [DH94, Tri02]. Nevertheless, most of these contributions are addressed in Euclidean domains and not on surfaces. In addition, only heuristics are proposed, but algorithms providing topological guarantees or accuracy analysis are missing.

In a discrete setting vector fields on surfaces are analyzed with discrete Hodge decomposition [PP03], or Morse-Smale decomposition [EHZ01] via the *simulation of differentiability paradigm*. When one wants to study a global differential property from a discretization, the first step is to analyze its stability and understand its generic patterns. Such a method proved to be successful for the ridge extraction as well as for the medial axis. Reporting the homotopy type of the medial axis has been addressed in [CL05] guided by results of stability [eRS04]. For surfaces, the principal curvature foliations are of special interest, they may be used to quadrangulate the surface and optimize approximation [ACSD<sup>+</sup>03]. However, no certified methods are available to compute the topology of such foliations.

Given this panorama, there is an obvious need of cooperative research between mathematicians and computer scientists to set a common framework able to address and solve problems of applied geometry.

# Bibliography

- [AB99] Nina Amenta and Marshall Bern. Surface reconstruction by Voronoi filtering. *Discrete Comput. Geom.*, 22(4):481–504, 1999.
- [ACDL00] N. Amenta, S. Choi, T. K. Dey, and N. Leekha. A simple algorithm for homeomorphic surface reconstruction. In *Proc. 16th Annu. ACM Sympos. Comput. Geom.*, pages 213–222, 2000.
- [ACSD<sup>+</sup>03] Pierre Alliez, David Cohen-Steiner, Olivier Devillers, Bruno Levy, and Mathieu Desbrun. Anisotropic polygonal remeshing. *ACM Transactions on Graphics*, 2003. SIGGRAPH '2003 Conference Proceedings.
- [AK04] Nina Amenta and Yong Joo Kil. Defining point-set surfaces. *ACM Trans. Graph.*, 23(3):264–270, 2004.
- [APR03] N. Amenta, T. Peters, and A. Russell. Computational topology: ambient isotopic approximation of 2-manifolds. *Theoretical Computer Science*, 305:3–15, 2003.
- [Arn92] V.I. Arnold. *Catastrophe theory (3rd Ed.)*. Springer, 1992.
- [AS98] Auzinger and Stetter. An elimination algorithm for the computation of all zeros of a system of multivariate polynomial equations. *Int. Series of Numerical Math.*, 86:11–30, 1998.
- [AVGZ82] V. Arnold, A. Varchenko, and S. Goussein-Zadé. *Singularités des applications différentiables – Volume I*. Mir, 1982.
- [BA91] Jonathan W. Brandt and V. Ralph Algazi. Computing a stable, connected skeleton from discrete data. In *Proceedings of the 1991 IEEE Computer Society Conference on Computer Vision and Pattern Recognition*, pages 666–667, IEEE Service Center, Piscataway, NJ, USA (IEEE cat n 91CH2983-5), 1991. IEEE.
- [BA92] J. W. Brandt and V. R. Algazi. Continuous skeleton computation by Voronoi diagram. *CVGIP: Image Understanding*, 55(3):329–338, 1992.
- [Ban67] T. F. Banchoff. Critical points and curvature for embedded polyhedra. *J. Diff. Geom.*, 1:245–256, 1967.
- [BC00] Jean-Daniel Boissonnat and Frédéric Cazals. Smooth surface reconstruction via natural neighbour interpolation of distance functions. In *Proc. 16th Annu. ACM Sympos. Comput. Geom.*, pages 223–232, 2000.
- [BC01] J.-D. Boissonnat and F. Cazals. Natural neighbor coordinates of points on a surface. *Comput. Geom. Theory Appl.*, 19:155–173, 2001.
- [BCL82] B. Buchberger, G.-E. Collins, and R. Loos. *Computer Algebra Symbolic and Algebraic Computation*. Springer-Verlag, second edition edition, 1982.
- [BCM02] V. Borrelli, F. Cazals, and J-M. Morvan. On the angular defect of triangulations and the pointwise approximation of curvatures. In *Curves and Surfaces*, St Malo, France, 2002. INRIA Research Report RR-4590.
- [BCM03] V. Borrelli, F. Cazals, and J-M. Morvan. On the angular defect of triangulations and the pointwise approximation of curvatures. *Comput. Aided Geom. Design*, 20, 2003.



- [BCSV04] J.-D. Boissonnat, D. Cohen-Steiner, and G. Vegter. Meshing an implicit surface with certified topology. In *ACM STOC*, 2004.
- [Ber87] M. Berger. *Geometry (vols. 1-2)*. Springer-Verlag, 1987.
- [BF02] J.-D. Boissonnat and J. Flotto. A local coordinate system on a surface. In *ACM symposium on Solid modeling*, Saarbrücken, 2002.
- [BG86] J. Bruce and P. Giblin. Growth, motion and 1-parameter families of symmetry sets. *Proc. R. Soc. Edinb., Sect. A*, 104, 1986.
- [BG88] M. Berger and B. Gostiaux. *Differential geometry: Manifolds, Curves and Surfaces*. Springer, 1988.
- [BG92] J.W. Bruce and P.J. Giblin. *Curves and singularities (2nd Ed.)*. Cambridge, 1992.
- [BGG85] J. Bruce, P. Giblin, and C. Gibson. Symmetry sets. *Proc. Roy Soc Edinburgh Sect. A*, 101, 1985.
- [BGT96] J. Bruce, P. Giblin, and F. Tari. Ridges, crests and sub-parabolic lines of evolving surfaces. *Int. J. Computer Vision*, 18(3):195–210, 1996.
- [BLBK03] I. A. Bogaevski, V. Lang, A. G. Belyaev, and T. L. Kunii. Color ridges on implicit polynomial surfaces. In *GraphiCon 2003, Moscow, Russia*, 2003.
- [BO03] J.-D. Boissonnat and S. Oudot. Provably good surface sampling and approximation. In *Symp. on Geometry Processing*, 2003.
- [BPR03] S. Basu, R. Pollack, and M.-F. Roy. *Algorithms in real algebraic geometry*, volume 10 of *Algorithms and Computations in Mathematics*. Springer-Verlag, 2003.
- [BS05] Alexander I. Bobenko and Yuri B. Suris. Discrete differential geometry. consistency as integrability. Technical Report math.DG/0504358, Mathematics arXiv, 2005.
- [Buc85] B. Buchberger. *Gröbner bases : an algorithmic method in polynomial ideal theory*. Recent trends in multidimensional systems theory. Reider ed. Bose, 1985.
- [CCL03] Frédéric Cazals, Frédéric Chazal, and Thomas Lewiner. Molecular shape analysis based upon the morse-smale complex and the connolly function. In *Proc. 19th Annu. ACM Sympos. Comput. Geom.*, pages 237–246, 2003.
- [CCS04] F. Chazal and D. Cohen-Steiner. A condition for isotopic approximation. In *ACM Symposium on Solid Modeling*, 2004.
- [CDRR04] Siu-Wing Cheng, Tamal K. Dey, Edgar A. Ramos, and Tathagata Ray. Sampling and meshing a surface with guaranteed topology and geometry. In *SCG '04: Proceedings of the twentieth annual symposium on Computational geometry*, pages 280–289, New York, NY, USA, 2004. ACM Press.
- [CdVL05] Éric Colin de Verdière and Francis Lazarus. Optimal system of loops on an orientable surface. *Discrete and Computational Geometry*, 33(3):507–534, March 2005.
- [Che93] L. P. Chew. Guaranteed-quality mesh generation for curved surfaces. In *Proc. 9th Annu. ACM Sympos. Comput. Geom.*, pages 274–280, 1993.
- [CL05] F. Chazal and A. Lieutier. The lambda medial axis. *Graphical Models*, To Appear, 2005.
- [Cla97] F.H. Clarke. *Nonsmooth Analysis and Control Theory*. Springer, 1997.
- [CLO92] D. Cox, J. Little, and D. O’Shea. *Ideals, varieties, and algorithms an introduction to computational algebraic geometry and commutative algebra*. Undergraduate texts in mathematics. Springer-Verlag New York-Berlin-Paris, 1992.
- [Coa66] C. Coatmelec. Approximation et interpolation des fonctions différentielles de plusieurs variables. *Ann. Sci. Ecole Norm. Sup.*, 83, 1966.
- [Col75] G.E. Collins. Quantifier elimination for real closed fields by cylindrical algebraic decomposition. *Springer Lecture Notes in Computer Science 33*, 33:515–532, 1975.

- [CP05a] F. Cazals and M. Pouget. Estimating differential quantities using polynomial fitting of osculating jets. *Computer Aided Geometric Design*, 22(2), 2005. Conference version: Symp. on Geometry Processing 2003.
- [CP05b] Frédéric Cazals and Marc Pouget. Smooth surfaces, umbilics, lines of curvatures, foliations, ridges and the medial axis: selected topics. *Int. J. of Computational Geometry and Applications*, 15(5):511–536, 2005.
- [CR72] P.G. Ciarlet and P.-A. Raviart. General lagrange and hermit interpolation in  $r^n$  with applications to the finite element method. *Arch. Rational Mesh. Engrg.*, 46:177–199, 1972.
- [CSM03] D. Cohen-Steiner and J.-M. Morvan. Restricted delaunay triangulations and normal cycle. In *ACM Symposium on Computational Geometry*, 2003.
- [CW00] P. Csàkány and A.M. Wallace. Computation of local differential parameters on irregular meshes. In Springer, editor, *Mathematics of Surfaces*. R. Cipolla and R. Martin Eds, 2000.
- [D'A91] E. F. D'Azevedo. Optimal triangular mesh generation by coordinate transformation. *SIAM J. Sci. Statist. Comput.*, 12(4):755–786, 1991.
- [Dam04] J. Damon. On the smoothness and geometry of boundaries associated to skeletal structures ii: Geometry in the blum case. *Compositio Mathematica*, 140(6), 2004.
- [dC76] M. de Carmo. *Differential Geometry of Curves and Surfaces*. Prentice Hall, Englewood Cliffs, NJ, 1976.
- [Deg97] W. L. F. Degen. The cut locus of an ellipsoid. *Geometriae Dedicata*, 67(2), 1997.
- [DH94] T. Delmarcelle and L. Hesselink. The topology of symmetric, second-order tensor fields. In *IEEE Visualization Proceedings*, pages 104–145, 1994.
- [DMSB00] M. Desbrun, M. Meyer, P. Schröder, and A. Barr. Discrete differential-geometry operators in  $nD$ , 2000. Preprint, The Caltech Multi-Res Modeling Group.
- [DZ02] T. K. Dey and W. Zhao. Approximate medial axis as a voronoi subcomplex. In *ACM Sympos. Solid Modeling and Applications*, 2002.
- [EHZ01] Herbert Edelsbrunner, John Harer, and Afra Zomorodian. Hierarchical morse complexes for piecewise linear 2-manifolds. In *ACM SoCG*, 2001.
- [EK66] E. Isaacson and H.B. Keller. *Analysis of numerical methods*. John Wiley & Sons, 1966.
- [ELZ00] Herbert Edelsbrunner, D. Letscher, and Afra Zomorodian. Topological persistence and simplification. In *Proc. 41st Annu. IEEE Sympos. Found. Comput. Sci.*, pages 454–463, 2000.
- [Erd46] P. Erdős. On the hausdorff dimension of some sets in euclidean space. *Bull. Am. Math. Soc.*, 52, 1946.
- [eRS04] F. Chazal et R. Soufflet. Stability and finiteness properties of medial axis and skeleton. *J. of Control and Dynamical Systems*, 10(2), 2004.
- [Fau99] J.-C. Faugère. A new efficient algorithm for computing gröbner bases ( $f_4$ ). *Journal of Pure and Applied Algebra*, 139(1-3):61–88, June 1999.
- [Fau02] Jean-Charles Faugère. A new efficient algorithm for computing gröbner bases without reduction to zero  $f_5$ . In *International Symposium on Symbolic and Algebraic Computation Symposium - ISSAC 2002, Villeneuve d'Ascq, France, Jul 2002*.
- [Fed59] H. Federer. Curvature measures. *Trans. Amer. Math. Soc.*, 93:418–491, 1959.
- [FGLM93] J.C. Faugère, P. Gianni, D. Lazard, and T. Mora. Efficient computation of zero-dimensional gröbner basis by change of ordering. *Journal of Symbolic Computation*, 16(4):329–344, Oct. 1993.
- [Fid97] Márta Fidrich. *Analyse multiéchelle des invariants, Application à l'imagerie médicale volumique*. Thèse de sciences, université Paris XI, Orsay, 1997.

- [For98] R. Forman. Morse theory for cell complexes. *Advances in Mathematics*, 134:90–145, 1998.
- [GI04] J. Goldfeather and V. Interrante. A novel cubic-order algorithm for approximating principal direction vectors. *ACM Trans. Graph.*, 23(1):45–63, 2004.
- [GK00] P. Giblin and B. Kimia. A formal classification of 3d medial axis points and their local geometry. In *Computer Vision and Pattern Recognition*, Hilton Head, South Carolina, USA, 2000.
- [GK02] P. Giblin and B. Kimia. Transitions of the 3d medial axis under a one-parameter family of deformations. *ECCV*, 1, 2002.
- [GLMT04] G. Gattellier, A. Labrouzy, B. Mourrain, and J.-P. T  court. Computing the topology of 3-dimensional algebraic curves. In *Computational Methods for Algebraic Spline Surfaces*, pages 27–44. Springer-Verlag, 2004.
- [GLS01] M. Giusti, G. Lecerf, and B. Salvy. A gr  bner free alternative for solving polynomial systems. *Journal of Complexity*, 17(1):154–211, 2001.
- [GS91] C. Gutierrez and J Sotomayor. *Lines of Curvature and Umbilical Points on Surfaces*. IMPA, 1991.
- [GS00] M. Gasca and T. Sauer. Polynomial interpolation in several variables. *Advances in Comp. Math.*, 12(4), 2000.
- [GvL83] G. Golub and C. van Loan. *Matrix Computations*. Johns Hopkins Univ. Press, Baltimore, MA, 1983.
- [GVN02] L. Gonzalez-Vega and I. Necula. Efficient topology determination of implicitly defined algebraic plane curves. *Computer Aided Geometric Design*, 19(9), 2002.
- [HBK02] M. Hisada, A. Belyaev, and T. L. Kunii. A skeleton-based approach for detection of perceptually salient features on polygonal surfaces. In *Computer Graphics Forum*, volume 21, pages 689–700, 2002.
- [HCV52] D. Hilbert and S. Cohn-Vossen. *Geometry and the Imagination*. Chelsea, 1952.
- [HGY<sup>+</sup>99] P. W. Hallinan, G. Gordon, A.L. Yuille, P. Giblin, and D. Mumford. *Two-and Three-Dimensional Patterns of the Face*. A.K.Peters, 1999.
- [Hig96] N.J. Higham. *Accuracy and Stability of Numerical Algorithms*. SIAM, 1996.
- [Hir88] M.W. Hirsch. *Differential Topology*. Springer-Verlag, 1988.
- [Hor83] L. Hormander. *The analysis of linear partial differential operators - I*. Springer, 1983.
- [Hor94] L. Hormander. *Notions of convexity*. Birkhauser, 1994.
- [HPW05] Klaus Hildebrandt, Konrad Polthier, and Max Wardetzky. On the convergence of metric and geometric properties of polyhedral surfaces. Technical Report 05-24, ZIB Preprint, 2005.
- [Koe90] J.J. Koenderink. *Solid Shape*. MIT, 1990.
- [KOR05] J. Keyser, K Ouchi, and M. Rojas. The exact rational univariate representation for detecting degeneracies. In *DIMACS Series in Discrete Mathematics and Theoretical Computer Science*. AMS Press, 2005. To appear.
- [LA98] G. Luk  cs and L. Andor. Computing natural division lines on free-form surfaces based on measured data. In M. Daehlen, T. Lyche, and L. Schumaker, editors, *Mathematical Methods for Curves and Surfaces II*, pages 319–326. Vanderbilt University Press, 1998.
- [Las99] M. Lassak. Parallelotopes of maximum volumes in a simplex. *Disc. Comp. Geometry*, 21, 1999.
- [Laz83] D. Lazard. Gr  bner bases, gaussian elimination, and resolution of systems of algebraic equations. In *EUROCAL' 83 European Computer Algebra Conference*, volume 162 of *LNCS*, pages 146–156. Springer, 1983.

- [Lev03] D. Levin. Mesh-independent surface interpolation. *Geometric Modeling for Scientific Visualization*, 2003.
- [LF99] S.K. Lodha and R. Franke. Scattered data techniques for surfaces. In *Dagstuhl '97, Scientific Visualization*, pages 181–222. IEEE Computer Society, 1999.
- [Lie03] A. Lieutier. Any open bounded subset of  $\mathbb{R}^n$  has the same homotopy type than its medial axis. In *ACM Solid Modeling*, 2003.
- [LLT03] Thomas Lewiner, Hélio Lopes, and Geovan Tavares. Optimal discrete Morse functions for 2-manifolds. *Computational Geometry: Theory and Applications*, 26(3):221–233, 2003.
- [LOF02] H. Lopes, J.B. Oliveira, and L.H. Figueiredo. Robust adaptive polygonal approximation of implicit curves. *Computers and Graphics*, 26(6), 2002.
- [LP05] C. Lange and K. Polthier. Anisotropic fairing of point sets. *Special Issue of CAGD*, 2005.
- [LS86] P. Lancaster and K. Salkauskas. *Curve and surface fitting: an introduction*. Academic, 1986.
- [Mas77] W. S. Massey. *Algebraic Topology: An Introduction*, volume 56 of *Graduate Texts in Mathematics*. Springer-Verlag, 1977.
- [MBF92] O. Monga, S. Benayoun, and O. Faugeras. From partial derivatives of 3D volumic images to ridge lines. In *IEEE Conference on Vision and Pattern Recognition (CVPR)*, Urbana Champaign, Juin 1992.
- [Mil80] D. Milman. The central function of the boundary of a domain and its differentiable properties. *J. Geom.*, 14, 1980.
- [MLD94] O. Monga, R. Lengagne, and R. Deriche. Extraction of the zero-crossings of the curvature derivative in volumic 3D medical images: a multi-scale approach. In *Proc. of IEEE Conference on Computer Vision and Pattern Recognition*, pages 852–855, 1994.
- [MN03] N.J. Mitra and A. Nguyen. Estimating surface normals in noisy point cloud data. In *ACM SoCG*, San Diego, USA, 2003.
- [Mor] J.-M. Morvan. On generalized curvatures. In preparation.
- [Mor90] R. Morris. *Symmetry of curves and the geometry of surfaces: two explorations with the aid of computer graphics*. PhD thesis, Univ. of Liverpool, 1990.
- [Mor96] R. Morris. The sub-parabolic lines of a surface. In Glen Mullineux, editor, *Mathematics of Surfaces VI, IMA new series 58*, pages 79–102. Clarendon Press, Oxford, 1996.
- [MT02] J-M. Morvan and B. Thibert. Smooth surface and triangular mesh : Comparison of the area, the normals and the unfolding. In *ACM Symposium on Solid Modeling and Applications*, 2002.
- [MT05a] B. Mourrain and J.P. Tecourt. Computing the topology of real algebraic surfaces. In *MEGA 2005, Effective Methods in Algebraic Geometry*, 2005.
- [MT05b] B. Mourrain and P. Trébuchet. Generalized normal forms and polynomial system solving. In *Proceedings of the International Symposium on Symbolic and Algebraic Computation*, 2005. To appear.
- [MW00] D. Meek and D. Walton. On surface normal and Gaussian curvature approximations given data sampled from a smooth surface. *Computer-Aided Geometric Design*, 17:521–543, 2000.
- [MWP96] T. Maekawa, F. Wolter, and N. Patrikalakis. Umbilics and lines of curvature for shape interrogation. *Computer Aided Geometric Design*, 13:133–161, 1996.
- [Nik01] I. Nikolaev. *Foliations on Surfaces*. Springer, 2001.
- [OB01] Y. Ohtake and A. Belyaev. Automatic detection of geodesic ridges and ravines on polygonal surfaces. *The Journal of Three Dimensional Images*, 15(1):127–132, 2001.

- [OBS04] Y. Ohtake, A. Belyaev, and H-P. Seidel. Ridge-valley lines on meshes via implicit surface fitting. In *ACM Siggraph*, 2004.
- [PAT00] X. Pennec, N. Ayache, and J.-P. Thirion. Landmark-based registration using features identified through differential geometry. In I. Bankman, editor, *Handbook of Medical Imaging*. Academic Press, 2000.
- [Pet01] S. Petitjean. A survey of methods for recovering quadrics in triangle meshes. *ACM Computing Surveys*, 34(2), 2001.
- [Por71] I. Porteous. The normal singularities of a submanifold. *J. Diff. Geom.*, 5:543–564, 1971.
- [Por83] I. Porteous. The normal singularities of surfaces in  $\mathbb{R}^3$ . In *Proc. Symp. Pure Math. (40, Part 2)*, pages 379–393, 1983.
- [Por01] I. Porteous. *Geometric Differentiation (2nd Edition)*. Cambridge University Press, 2001.
- [PP93] U. Pinkall and K. Polthier. Computing discrete minimal surfaces and their conjugates. *Experimental Mathematics*, 2(1):15–36, 1993.
- [PP03] K. Polthier and E. Preuss. Identifying vector fields singularities using a discrete hodge decomposition. *Visualization and Mathematics III*, eds: H.C. Hege, K. Polthier, Springer Verlag, 2003.
- [PS98] K. Polthier and M. Schmies. Straightest geodesics on polyhedral surfaces. In *Mathematical Visualization*, H.C. Hege, K. Polthier Editors, 1998.
- [PV04] S. Plantinga and G. Vegter. Isotopic approximation of implicit curves and surfaces. In *Symposium on Geometric Processing*, pages 251–260, 2004.
- [QV94] A. Quarteroni and A. Valli. *Numerical Approximation of Partial Differential Equations*. Springer, 1994.
- [Rou99] F. Rouillier. Solving zero-dimensional systems through the rational univariate representation. *Journal of Applicable Algebra in Engineering, Communication and Computing*, 9(5):433–461, 1999.
- [RR05] N. Revol and F. Rouillier. Motivations for an arbitrary precision interval arithmetic and the mpfi library. *Reliable Computing*, 11:1–16, 2005.
- [RZ03] F. Rouillier and P. Zimmermann. Efficient isolation of polynomial real roots. *Journal of Computational and Applied Mathematics*, 162(1):33–50, 2003.
- [Sau95] T. Sauer. Computational aspects of multivariate polynomial interpolation. *Advances in Comp. Math.*, 3(3), 1995.
- [Ser82] J. Serra. *Image Analysis and Mathematical Morphology*. Academic Press, London, UK, 1982.
- [Ser88] J. Serra, editor. *Image Analysis and Mathematical Morphology, volume 2: Theoretical Advances*. Academic Press, New York, 1988.
- [SF00] G. Stylianou and G. Farin. Crest line extraction from 3d triangulated meshes. *NSF/DoE Lake Tahoe Workshop on Hierarchical Approximation and Geometrical Methods for Scientific Visualization*, 2000.
- [SF04] Georgios Stylianou and Gerald Farin. Crest lines for surface segmentation and flattening. *IEEE Transactions on Visualization and Computer Graphics*, 10(5):536–544, 2004.
- [She02a] J. R. Shewchuk. What is a good linear element? interpolation, conditioning, and quality measures. In *Eleventh International Meshing Roundtable*, pages 115–126, 2002.
- [She02b] Jonathan R. Shewchuk. What is a good linear element? interpolation, conditioning, and quality measures. In *11th International Meshing Roundtable*, Ithaca, New York, USA, 2002.
- [Sny92] J. M. Snyder. Interval analysis for computer graphics. In *Proceedings of the 19th annual conference on Computer graphics and interactive techniques*, pages 121–130. ACM Press, 1992.



- [SP03] T. Sakkalis and T. Peters. Ambient isotopic approximations for surface reconstruction and interval solids. In *ACM Symposium on Solid Modeling*, 2003.
- [Spi99a] M. Spivak. *A comprehensive introduction to Differential Geometry (Third Ed.)*. Publish or Perish, 1999.
- [Spi99b] M. Spivak. *A Comprehensive Introduction to Differential Geometry*, volume 3. Publish or Perish, 1999.
- [SX95] T. Sauer and Yuan Xu. On multivariate lagrange interpolation. *Math. Comp.*, 64, 1995.
- [SZ90] P. Sander and S. Zucker. Inferring surface trace and differential structure from 3-D images. *IEEE Trans. Pattern Analysis and Machine Intelligence*, 12(9):833–854, 1990.
- [Tau95] G. Taubin. Estimating the tensor of curvature of a surface from a polyhedral approximation. In *Fifth International Conference on Computer Vision*, 1995.
- [TG95] J.-P. Thirion and A. Gourdon. Computing the differential characteristics of iso-intensity images. *Computer Vision and Image Understanding*, 61(2):190–202, 1995.
- [Thi96] J.-P. Thirion. The extremal mesh and the understanding of 3d surfaces. *International Journal of Computer Vision*, 19(2):115–128, August 1996.
- [Tho72] R. Thom. Sur le cut-locus d’une variété plongée. *J. Differ. Geom.*, 6, 1972.
- [TM02] Chi-Keung Tang and Gerard Medioni. Curvature-augmented tensor voting for shape inference from noisy 3d data. *IEEE Transactions on Pattern Analysis and Machine Intelligence*, 24(6):858–864, 2002.
- [Tri02] X. Tricoche. *Vector and Tensor Field Topology Simplification, Tracking, and Visualization*. Universität Kaiserslautern, 2002.
- [WB01] K. Watanabe and A.G. Belyaev. Detection of salient curvature features on polygonal surfaces. In *Eurographics*, 2001.
- [Wol92] F. E. Wolter. Cut locus and medial axis in global shape interrogation and representation. Technical Report 92-2, MIT, Dept. Ocean Engg., Design Lab, Cambridge, MA 02139, USA, January 1992.
- [Yom81] Y. Yomdin. On the general structure of a generic central set. *Compositio Math*, 43, 1981.
- [YZ04] Lexing Ying and Denis Zorin. A simple manifold-based construction of surfaces of arbitrary smoothness. *ACM Trans. Graph.*, 23(3):271–275, 2004.



## Summary

This research work relates to the geometrical aspects of mathematics and computer sciences. It is motivated by applications such as computer aided design, medical imaging, scientific computations and simulations or also virtual reality and multimedia. More precisely, this thesis proposes an analysis of some local as well as global topics of the geometry of surfaces.

From a local point of view, the problem is the estimation of the normal, the curvatures and quantities of higher order from points sampled on a smooth surface. A method of estimation using polynomial fitting is studied: the properties of convergence are established and an algorithm is proposed and implemented.

From a global point of view, we analyze the lines of extreme curvature on surfaces, called ridges. For a surface discretized by a mesh, precise sampling conditions are given, and if they are fulfilled, an algorithm reporting a certified topological approximation of the ridges is developed. In the case of a parameterized surface, we show that the ridges have a global implicit structure, and we characterize the singularities of this curve in the parametric domain with zero-dimensional systems. For a polynomial parameterization, these equations are also polynomial, and specific methods of computer algebra are developed to compute the topology of the singular curve of the ridges.

## Résumé

Ce travail de recherche porte sur les aspects géométriques des mathématiques et de l'informatique. Il est fortement motivé par des applications telles que la conception assistée par ordinateur, l'imagerie médicale, le calcul scientifique et la simulation ou encore la réalité virtuelle et le multimédia. Plus précisément, cette thèse propose une analyse de la géométrie des surfaces tant d'un point de vue local que global.

Tout d'abord, étant donnée une surface lisse connue via un échantillonnage, nous étudions le problème de l'estimation des quantités différentielles locales: normale, courbures et quantités d'ordre supérieur. Une méthode d'estimation utilisant un ajustement polynomial est développée: les propriétés de convergence sont établies et un algorithme est proposé et implémenté.

D'un point de vue global, nous analysons les lignes d'extrême de courbure sur une surface, appelées ridges. Pour le cas d'une surface discrétisée par un maillage, des conditions précises d'échantillonnage sont données, et sous ces hypothèses, un algorithme produisant une approximation topologiquement certifiée des ridges est développé. Dans le cas d'une surface paramétrée, nous établissons que les ridges ont une structure implicite globale, et étudions les singularités de la courbe associée dans le domaine de paramétrage en termes de systèmes zero-dimensionnels. Pour une paramétrisation polynomiale, ces équations sont aussi polynomiales et des méthodes spécifiques de calcul formel sont développées pour calculer la topologie de la courbe singulière des ridges.